STUDIA

UNIVERSITATIS BABEŞ-BOLYAI

Chemia

CLUJ-NAPOCA 2002

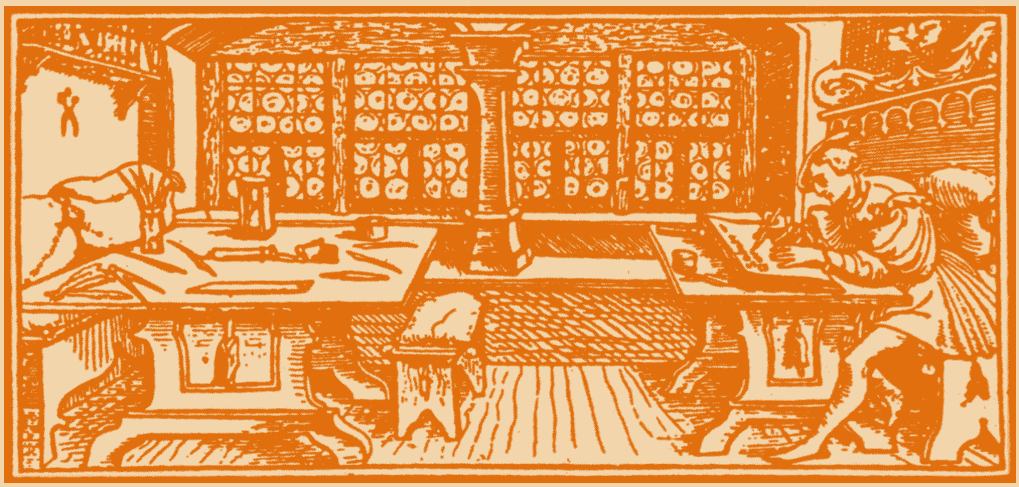

1-2

Anul XLVII **2002**

STUDIA
UNIVERSITATIS BABEŞ-BOLYAI
CHEMIA
1-2

EDITORIAL OFFICE: Gh. Bilaşcu no. 24, 3400 Cluj-Napoca, Romania ✦ Phone 0264-40.53.52

SUMAR - SOMMAIRE - CONTENTS - INHALT

Academician Ionel Haiduc at His 65th Anniversary 3

A. PĂTRUŢ, A. NICOARĂ, D. MĂRGINEAN, A Challenge for Chemistry: Very Large Inorganic Molecules Penetrate the Mesoscopic Realm..... 13

LUIZA GĂINĂ, CASTELIA CRISTEA, I. SILBERG, T. LOVASZ, C. DELEANU, SILVIA UDREA, Solvent Effects in ^{1}H-RMN Spectrum of 3-formyl-10-methyl-phenothiazine 41

D. PORUMB, CASTELIA CRISTEA and IOAN SILBERG, The Synthesis of New Phenothiazine Componds by the Thiation of Diphenylamino Derivatives 45

CERASELA AFLOROAEI, M. VLASSA, An Improved Synthesis of 1,7-dioxa-4,10 – diazacyclododecane 51

CERASELA AFLOROAEI, M. VLASSA, Application of Phase Transfer Catalysis in Acridine Series VIII[1]. Synthesis of 9-(1,2,3-triazol-1-yl) Acridines 55

ERIKA KOZMA, IOAN CRISTEA, Study of Acetylation on terpinen-4-ol. Synthesis of the 4-terpinenyl-acetate 61

CLAUDIA GEMA MUREŞANU, GABRIELA CRISTINA BUCŞA, I. BÂLDEA, Kinetics and Mechanism of p-xylene Oxidation by Ce(IV) in Aqueous Acidic Medium..... 67

SIMONA BUNGĂU, I. BÂLDEA, L. COPOLOVICI, Determination of Some Aminoacids from Pharmaceutical Products by Using a Kinetic Method Based on a Clock Landolt-Type System of Redox Reactions 75

C. CORMOŞ, Ş. AGACHI, Modeling and Simulation of 3-aminopropionitrile Synthesis Using Dedicated Software Packages 85

SIMONA FUNAR-TIMOFEI, GEORGETA SIMU, EUGENIA SĂRĂNDAN, Study of Lipophilicity of Some 4,4 –diaminobenzanilide Based Direct Dyse in the Cellulose Dyeing. 93

ALINA GHEORGHE, OCTAVIA GHEORGHE, C. STRĂTULĂ, MIHAELA PETRE, Chlorhidric Acid Removal from Reaction Effluent in Making Acetochlor 103

D. MIHĂESCU, F. OPREA, Hydrogen Gas Separation System Optimisation in Hydrotreating Plants 111

A. V. MARTINIUC, LUC CINOTTI, V. BOCOŞ-BINȚINȚAN, LUMINIȚA UNGUREAN, Positron Emission Tomography (PET) – Principles and General Characteristics 121

MIRCEA V. DIUDEA, Cluj Polynomials 131

SIMONA BUNGĂU, LUCIAN COPOLOVICI, GAVRIL NIAC and IOAN BALDEA, Kinetic Determination of B_1, B_2 And B_6 Vitamins 141

V. BOCOŞ-BINȚINȚAN, C.L.P. THOMAS, A.H. BRITTAIN, Characterization of the Chemical Warfare Agent Simulant Methyl Salicylate by Ion Mobility Spectrometry/Mass Spectrometry (IMS/MS) at Ambient Temperature 149

J. BÓDIS, J.A. LERCHER, Reductive Amination of Methyl Ethyl Ketone over Supported Group VIII Noble Metal Catalysts. 161

J. BÓDIS, G. MULLER, J. KORNATOWSKI, J.A. LERCHER, Adsorption of Ammonia and Pyridine on CoAPO-5 Single Crystals Studied by *In Situ* FT-IR Micro-Spectroscopy 169

L. OPREAN, L. DAVID, V. ZAHARIA, A. COMŞA, R. OPREAN, Synthesis and Structural Studies of Some Metal Coordination Compounds with [1,2,4]-triazole Derivative as Ligand 179

ANAMARIA TEREC, LUMINIȚA MUNTEAN, ŞTEFANIA TOTOS, NICULINA BOGDAN, CARMEN FLORIAN, D. MĂRGINEANU, S. MAGER, I. GROSU, Synthesis and Stereochemistry of Some New 2,4-substituted–1,3–dioxanes 187

LUMINIȚA MUNTEAN, MIRELA BALOG, CARMEN FLORIAN, ANAMARIA TEREC, I. GROSU, S. MAGER, D. MĂRGINEANU, Synthesis and Stereochemistry of Some New 1,3-dioxane Derivatives of α, β-unsaturated Aldehydes 195

I. SILAGHI-DUMITRESCU, LUMINIȚA SILAGHI-DUMITRESCU, Electronic Structure of Hypervalent Organoarsenic Bromo Derivatives 203

RECENZII - BOOK REVIEWS

Planar Chromatography, A Retrospective View for the Third Millennium, Ed. Sz. Nyiredy, Springer, Budapest, 2001, 614 p. (CONSTANTIN MĂRUȚOIU) 213

Academician Ionel Haiduc at his 65th anniversary

Born in Cluj on May 9th, 1937, Ionel Haiduc distinguished himself from the very beginning of his years in school as an exceptional personality, dedicated for study, with a remarkable capacity of interrelating a huge amount of knowledge and an unusual scientific curiosity.

He graduated in 1959 the Faculty of Chemistry of the University of Cluj (where he was admitted in 1954 without admission examination) with the best marks to all exams.

In 1964, he obtained the equivalent of a PhD in chemistry at the M.V. Lomonosov Institute of Fine Chemical Technology in Moscow under a guidance of the Academician K.A.Andrianov.

All the scientific life of Acad. Ionel Haiduc was developed at the Faculty of Chemistry of the University of Cluj, from 1959 until the present time. Full professor at the age of 36, he completed his formation as a researcher, in U.S.A., between 1966 and 1972, during three post doctoral stages.

It is very difficult to summarize the monumental contribution of Acad. Ionel Haiduc to the fields of inorganic and organometallic chemistry; his scientific work is covered by 9 books (published in Romanian, Polish, English and Greek), 23 chapters in collective volumes and 319 papers (as shown in the list of publications).

His brilliant career received a fully deserved recognition. The Romanian Academy offered him the “Gh. Spacu” prize in 1974 and elected him as corresponding member in 1990 and as titular member in 1991. Between 1990 and 1993 he was the Rector of “Babes-Bolyai” University of Cluj-Napoca and the vice-president of National Conference of Rectors. He is now president of the Cluj-branch of the Romanian Academy and member of the Praesidium of the same institution. In 2000 the President of Romania decorated him with “Steaua Romaniei”.

A creative mind, born to be a leader, prof. Ionel Haiduc was always connected to the different aspects of the chemists’ community life. Like a member of many academic bodies, he participated to elaboration and implementation of policies and managerial decisions in science, fighting for quality in the academic life.

The exceptional value of prof. Ionel Haiduc was also internationally recognized: elected as member of the editorial scientific board of 7 journals, member of IUPAC, of the International Council of Main Group Chemists and of the Alliance of the Universities for Democracy, he was also invited as visiting professor in USA, Brazil, Spain, Germany and Mexico. In 1999 the Hungarian Academy of Sciences, Debrecen branch offered him the "Pro Colaboratione" award. In 2001 he received the “Gauss” award, offered by the Humboldt Foundation and in 2002 he was elected as member in Academia Europea.

With his scientific horizon, his sense of humor and his kindness, he was a perfect ambassador of the Romanian school of chemistry.

At his 65th anniversary, the whole community of Romanian chemists presents to prof. Ionel Haiduc the very best wishes of long and fruitful life, many successes in the years to come and express their appreciation for his entire work.

THE EDITORIAL BOARD

Prof. Ionel Haiduc
Faculty of Chemistry and Chemical Engineering
"Babes-Bolyai" University Cluj-Napoca, Romania

LIST OF PUBLICATIONS (in the last 5 years)

BOOKS

9. Ionel Haiduc and Frank T. Edelmann
Supramolecular Organometallic Chemistry
Wiley-VCH, Weinheim, New York, 1999 (470 pag.)

ARTICLES

2002

319. Vasile Bercean, Crina Crainic, Ionel Haiduc, Mary F. Mahon, Kieran C. Molloy, Monica M. Venter and Paul J. Wilson
The structural chemistry of organotin derivatives of 5-mercapto-3-phenyl-1,3,4-thiadiazoline-2-thione: supramolecular structures involving intermolecular Sn···S, N-H···S or S···S interactions
J. Chem. Soc., Dalton Trans., 2002, Advance article DOI:10.1039/b109726a

318. José S. Casas, Eduardo E. Castellano, Javier Ellena, Ionel Haiduc, Agustín Sánchez, Radu F. Semeniuc and José Sordo:
Supramolecular self-assembly in the crystal structures of methylmercury xanthates, MeHgS(S)COR, R = Et, ^{i}Pr and CH_2Ph
Inorganica Chimica Acta 2002, **329** (1) 71-78.

317. Ionel Haiduc and Lai Yoong Goh
Reactions of bis(thiophosphoryl)disulfanes and bis(thiophosphinyl)disulfanes with metal species: an alternative, convenient route to metal complex and organometallic dithiophosphates and dithiophosphinates
Coord. Chem. Rev. 2002, **224** (1/2) 151-170.

2001

316. Ioan Silaghi-Dumitrescu, Gabriela Cretiu, Luminita Silaghi-Dumitescu, Ionel Haiduc, Alfredo Toscano and Raymundo Cea-Olivares
Crystal, molecular and electronic structure of 9,9'-bis(trimethylsilyl)fluorene
Rev. Roumaine Chim. 2001, **45** (4) 31-37.

315. Mircea Banciu, Eduardo E. Castellano, Javier Ellena, Ionel Haiduc, Constantin Draghici and Alexandru T. Balaban,
Serendipitous formation of 2,3,7-triphenylcyclopenta[c]pyran from 1,2-diphenylethanedione ("benzil") and cyclopentadiene
New J. Chem. 2001, **25**, 1472-1474.

314. Lai Yoong Goh, Zhiqiang Weng, Weng Lee Leong, Ionel Haiduc, Kong Mun Lo and Richard C.S. Wong
Chemistry of cyclopentadienyl tricarbonylchromium dimer. Cleavage of bis(thiophosphoryl)disulfanes. Syntheses and X-ray crystal structures of $CpCr(CO)_2(S_2P(OR)_2)$, $CpCr(S_2P(OR)_2)_2$ and $Cr(S_2P(OR)_2)_3$ (R = ^{i}Pr)
J. Organomet. Chem. 2001, **631**, 67-75.

313. Ionel Haiduc and Julio Zukerman-Schpector
Supramolecular self-assembly through seconday bonds in organotellurium chemistry
Phosphorus, Sulfur & Silicon 2001, **171**, 171-185.

312. Julio Zukerman-Schpector and Ionel Haiduc
Diorganotellurium(IV) dihalides and secondary bonding; revisiting the coordination polyhedra
Phosphorus, Sulfur & Silicon *2001*, **171**, 73-112.

311. William C. Herndon and Ionel Haiduc
Contrasting bonding modes of copper(I), silver(I) and gold(I) in dithioimidodiphosphinato metallacycles, $Ph_3P{\cdot}M(SPh_2P)_2N$ (M = Cu, Ag, Au)
J. Mol. Struct. *2001*, **598** (2/3) 127-131.

310. Andrea Deák, Lajos Radics, Alajos Kálmán, László Párkányi and Ionel Haiduc
Heptacoordinate dimethyltin(IV) cupferronato complexes. X-Ray and solid-state NMR structural analysis. Hydrogen bond supramolecular self-assembly
Eur. J. Inorg. Chem. *2001* (11) 2849-2856.

309. Ioana Pavel, Francisco Cervantes-Lee, Keith H. Pannell and Ionel Haiduc
Supramolecular self-assembly involving cooperative use of dative coordinate, secondary and hydrogen bonding in solid $[Me_3Sn(\mu\text{-}OH)SnMe_3(\mu\text{-}OH)SnMe_3]^+Br^-$
Inorg. Chem. Commun. *2001*, **4** (10) 530-533.

308. Jose S. Casas, Alfonso Castineiras, Ionel Haiduc, Agustin Sanchez, Radu F. Semeniuc and Jose Sordo
New organotin xanthates $R_2Sn(S_2COR')_2$ and R_3SnS_2COR' (R = Me, Ph and R' = Me, CH_2Ph). Molecular structure of bis(O-methyldithiocarbonato)diphenyltin (IV), $Ph_2Sn(S_2COMe)_2$
Syn. React. Inorg. Metal-Org. Chem. *2001*, **31** (5) 725-736.

307. J. Zukerman-Schpector, I. Haiduc, R.L. Camillo, J.V. Comasseto, R.L.O.R. Cunha and I. Caracelli
Acetonyldichloro[(Z)-2-chloro-2-phenylvinyl]tellurium(IV), helical chains of metal complexes
Acta Crystallogr. *2001*, **C 57**, 749-750.

306. A. Deák, A Kálmán, L. Párkányi and I. Haiduc
Hydrogen-bonded hexagonal and pseudo-hexagonal grid motifs in supramolecular cobalt(II) and nickel(II) cupferronato complexes incorporating neutral N-donors with intermolecular NH_2 connectors and solvent molecules
Acta Crystallogr. *2001*, **B 57**, 303-310.

305. Claudio A. Tellez- S, Eduardo Hollauer, M.I. Pais da Silva, M.A. Mondragon, I. Haiduc, M. Curtui
Density functional theory study of the Fourier transform infrared and Raman spectra of dichloro-bis(2,4-pentanedionate)tin(IV)
Spectrochim. Acta, Part A *2001*, **57**, 1149-1161.

304. Ionel Haiduc, Mary F. Mahon, Kieran C. Molloy and Monica Venter
Synthesis and spectral characterisation of organotin(IV) 1,3,5-triazine-2,4,6-trithiolato complexes, including the crystal structures of 1,3,5-$(R_3SnS)_3C_3N_3$ (R = Me, Ph)
J. Organomet. Chem. *2001*, **627**, 6-12.

303. Ionel Haiduc
Thiophosphorus and related ligands in coordination, organometallic and supramolecular chemistry. A personal account
J. Organomet. Chem. *2001*, **623** (1/2) 29-42.

2000

302. M. Bolboaca, S. Cinta, M. Venter, A. Deak, I. Haiduc, O. Cozar, T. Iliescu, P. Rosch and W. Kiefer
Vibrational behavior of transition metalcupferronato complexes: Raman studies on cobalt(II) cupferronato derivatives
Spectrosc. Lett. *2000*, **33** (6) 857-865.

301. Linda H. Doerrer, Jennifer C. Green, Malcolm L.H. Green, Ionel Haiduc, Christian N. Jardine, Sofia I. Pascu, Luminita Silaghi-Dumitrescu and David J. Watkin
Group 6 transition metal carbonyl complexes with chalcogen-bridged diarsenic(III) ligands
J. Chem. Soc., Dalton Trans. *2000* (19) 3347-3355.

300. Ionel Haiduc
Cyclic inorganic oligomers and polymers
in vol. **"Cyclic Polymers"**, Second edition, Edited by J.A. Semlyen
Kluwer Academic Publishers, Dordrecht, 2000, Chapter 14, pp. 601-698.

299. Luminita Silaghi-Dumitrescu, Ioan Silaghi-Dumitrescu, Radu Silaghi-Dumitrescu, Ionel Haiduc, Alexander J. Blake and D. Bryan Sowerby
Bromination of $(AsPh_2)_2O$; the structure of tribromo-diphenylarsenic(V)
Rev. Soc. Quim. Mexico, *2000*, **44** (2) 134-138.

298. Danut Bilc, Anca Silvestru, Cristian Silvestru, Ionel Haiduc and John E. Drake
New palladium(II) tetraorganodichalcogenoimido diphosphinates. Cystal and molecular structure of $Pd[(SPMe_2)_2N]_2$ and *cis*-$Pd[(OPPh_2)(SPMe_2)_n]_2$
Rev. Soc. Quim. Mexico, *2000*, **44** (2) 116-121.

297. Lai Yoong Goh, Weng Kee Leong, Pak-Hing Leung, Zhiqiang Weng and Ionel Haiduc
Chemistry of cyclopentadienyl tricarbonylchromium dimer. Cleavage of bis(thiophosphinyl)disulfanes and bis(thiophosphoryl)disulfanes. Synthesis of $CpCr(CO)_2(S_2PPh_2)$ and $CpCr(S_2PPh_2)_2$. X-Ray crystal structure of $CpCr(S_2PPh_2)_2$
J. Organomet. Chem. *2000*, **607** (1/2) 64-71.

296. Herbert W. Roesky and Ionel Haiduc
Molecular solids: self-assembled host-guest organometallic aggregates
Adv. Mol. Struct. Res. *2000*, **6**, 75-95.

295. Anca Silvestru, Danut Bîlc, Roland Rösler, John E. Drake and Ionel Haiduc
First nickel(II) complexes containing tetrahedral NiO_2S_2 cores. The molecular structures of $Ni[(OPPh_2)(SPR_2)N]_2$ (R = Ph, Me)
Inorg. Chim. Acta *2000*, **305** (1) 106-110.

294a. Rodica Micu-Semeniuc, Ionel Haiduc, Radu Semeniuc and Onuc Cozar
Spectroscopic studies of som metallic bis-dithiophosphonates, $M(DTP)_2$, and of some adducts
Studia Univ. Babes-Bolyai, Chemia *2000*, **45** (1/2) 185-197.

294. R. A. Varga, C. Silvestru and I. Haiduc
Synthesis and spectroscopic characterization of new organolead(IV) complexes containing organophosphorus ligands
Syn. React. Inorg. Met.-org. Chem. *2000*, **30** (3)485-498.

293. I. Haiduc, J. Zukerman-Schpector, E. Castellano and R. Cea-Olivares
A spirobiyclic complex of Schmidpeter's ligand, bis(tetraphenylimidodiphosphinato) beryllium, $Be(OPh_2PNPPh_2O)_2$, an inorganic analog of beryllium bis(β-diketonates)
Heteroatom. Chem. *2000*, **11** (3) 244-248.

292. I. Pavel, S. Cîntă, M. Venter, A. Deák, I. Haiduc, P. Rösch, O. Cozar, T. Iliescu and W. Kiefer:
Vibrational behavior of transition metal cupferonato complexes. Raman and SERS studies on nickel(II) cupferronato complexes
Vib. Spectrosc. *2000*, **23** (1) 71-76.

291. E. V. Garcia-Baez, Maria J. Rozales-Hoz, Heinrich Nöth, Ionel Haiduc and Cristian Silvestru:
Rupture of a P=S bond in a disulfurimidophosphinate ligand. The X-ray crystal structures of [(μ_2-H) Ru_3(μ_3-S){μ_2-*S,S,P'*-($SPPh_2$)(PPh_2)N}($CO)_8$] and [(μ_2-H)Ru_3{μ_2-*S,S,P'*-($SPPh_2$)(PPh_2)N}($CO)_9$].
Inorg. Chem. Commun. *2000*, **3** (4) 173-177.

290. Ildikó Székely, Cristian Silvestru, John E. Drake, Gabor Balázs, Sorin I. Fãrcas and Ionel Haiduc
Preparation and single-crystal characterization of manganese(II) complexes of dichalcogenoimido-diphosphinato ligands. Monomeric vs. dimeric Mn[($OPPh_2$)($XPPh_2$)N]$_2$ (X = S, O)
Inorg. Chim. Acta *2000*, **299** (2) 247-252.

289. Andrea Deák, Monica Venter, Alajos Kálmán, László Párkányi, Lajós Radics and Ionel Haiduc
Synthesis and structural characterization of tin(IV) N-nitroso-N-phenylhydroxylaminato complexes: crystal structures of $Sn(O_2N_2Ph)_4$, $Ph_2Sn(O_2N_2Ph)_2$ and [$Me_2Sn(O_2N_2Ph)_2$]$_2$
Eur. J. Inorg. Chem. *2000* (1), 127-132.

1999

288a. Radu Florin Semeniuc, Rodica Micu Semeniuc, Ionel Haiduc and Onuc Cozar
Spectroscopic characterization of some chromium O-alkyldithiocarbonates
Studia Univ. Babes-Bolyai, Chemia, 1999, **44** (1/2) 203-212 (Pub. 2000)

288. Simona Cinta, Monica Venter and Ionel Haiduc
FT-Raman investigation of the biological active cupferron and its thallium(I) complex
Spectrosc. Biol. Mol.: New Dir., Eur. Conf., **8th** (**1999**) 559-560.

287. Ionel Haiduc, Axel Fischer and Frank T. Edelmann
A quasi-cyclic structure of tetraphenylimidodiphosphinato(triphenylphosphine)-gold(I), $Ph_3P{\cdot}Au(SPh_2PNPPh_2S)$, involving Au···S secondary bonds
Rev. Roum. Chim. 1999, **44** (9) 805-809

286. José S. Casas, Eduardo E. Castellano, Javier Ellena, Ionel Haiduc, Agustin Sánchez and José Sordo The crystal and molecular structure of mercury(II) bis(isopropyl)dithiophosphate, Hg[$S_2P(OPr^i)_2$]$_2$, revisited: new comments about its supramolecular self-organization
J. Chem. Crystallogr. *1999*, **29** (7) 831-836.

285. Ioan Silaghi-Dumitrescu, Attila Kún[illegible]d Ionel Haiduc
Stable isomers of sila- and germadodecahedrane. A semiempirical (AM1) investigation of the structure of 4/6 and 4/5/6 ring containing E_{20} (E = Si, Ge) systems
Fullerene Sci. Technol. *1999*, **7** (5) 841-854.

284. S. Cinta, M. Venter, T. Iliescu, O.Cozar, I. Haiduc and W. Kiefer
SERS application in elucidation of the nature of homologue Cu(I) triazenido complexes
Vibr. Spectrosc. *1999,* **19** (2) 223-226.

283. Andrea Deák, Ionel Haiduc, László Párkányi, Monica Venter and Alajos Kálmán
Main group metal directed self-assembly in a tetrameric trimethyltin(IV) *N*-nitroso-*N*-phenylhydroxylaminato complex containing an unprecedented 20-membered inorganic (carbon-free) metallamacrocycle
Eur. J. Inorg. Chem., *1999*, 1593-1596.

282. Josef Novosad, Marek Necas, Jaromir Marek, Panagiotis Veltsistas, Christos Papadimitriou, Ionel Haiduc, Makoto Watanabe and J. Derek Woollins
Displacement of triphenylphosphine from $Cu(PPh_3)_2NO_3$ and $Co(PPh_3)_2Cl_2$ by a diselenoimido-diphosphinato ligand. X-ray crystal structure of $(PPh_3)Cu[Ph_2P(Se)NP(Se)Ph_2]$ and $Co[Ph_2P(Se)NP(Se)Ph_2]_2$ containing the novel $CuSe_2P_2N$ and $CoSe_2P_2N$ inorganic metallocycles.
Inorg. Chim. Acta, 1999, **290** (2) 256-260.

281. I. Haiduc, L. David, O. Cozar, R. Micu-Semeniuc, G. Mezei and M. Armenean
Spectroscopic and magnetic studies of some copper(II) and chromium(III) complexes with dithiophosphonates as ligands
J. Mol. Struct., *1999,* **482/483,** 153-157.

280. Herbert W. Roesky and Ionel Haiduc
Fluorine as a structure-directing element in organometallic fluorides: discrete molecules, supramolecular self-assembly and host-guest complexation
J. Chem. Soc., Dalton Trans., **1999** (14) 2249-2264 (Dalton Perspectives)

279. Mariana Rusu, Adrian R. Tomsa, Dan Rusu and Ionel Haiduc
New organotin and organosilicon derivatives of P/As/Sb/Bi polyoxotungstates
Synth. React. Inorg. Met.-Org. Chem., *1999*, **29** (6) 951-965.

278. Lászlo Párkányi, Alajos Kálmán, Andrea Deák, Monica Venter and Ionel Haiduc
A new inorganic (carbon-free) chelate ring: SnO_2N_2. Eight-coordinated tin(IV) in $Sn(O_2N_2Ph)_4$ and a self-assembled 20-membered macrocycle in $[Me_3Sn(O_2N_2Ph)]_4$.
Inorg. Chem. Commun., *1999*, **2** (6) 265-268.

277. Gábor Balázs, John E. Drake, Cristian Silvestru and Ionel Haiduc
New versatile phosphorus-containing ligands - asymmetric $(XPR_2)(YPR'_2)NH$ (X, Y = O, S; R, R' = Ph, OEt) and their potassium salts: the crystal and molecular structures of $(SPPh_2)[OP(OEt)_2]NH$, $K[(SPPh_2)\{OP(OEt)_2\}]NH.H_2O$ and $(OPPh_2)[OP(OEt)_2]NH.1/2HCl.1/4H_2O$
Inorg. Chim. Acta, *1999*, **287** (1) 61-71.

276. Ioan Silaghi-Dumitrescu and Ionel Haiduc
Possible C_{20} isomers containing 4/6 rings. An AM1 investigation of the stability of three 4/6 cages and of their hydrogenated analogues
Fullerene Science and Technol., *1999,* **7** (1) 17-24.

275. Luminita Silaghi-Dumitrescu, Ion Silaghi-Dumitrescu, Ionel Haiduc, Ruben-Alfredo Toscano, Veronica Garcia-Montalvo and Raymundo Cea-Olivares
Is the trigonal prismatic distortion the answer for the geometry of In^{III} four membered dithiochelate compounds? The crystal and molecular structure of $In(S_2AsR_2)_3$ (R = Me, Ph)
Z. Anorg. Allg. Chem., *1999***, 625** (2), 347-351.

1998

274. Claudio A. Tellez, Sergio De La Riva, Eduardo Hollauer, Ionel Haiduc and Cristian Silvestru
Vibrational spectra of dimethyldithiophosphinate anion, $(CH_3)_2PS_2^-$
Spectrosc. Lett. 1998, 31 (7) 1469-1483.

273. Roland Rösler, Mihaela Stanciu, Jincai Yang, John E. Drake, Cristian Silvestru and Ionel Haiduc
New versatile organophosphorus ligands. Crystal and molecular structures of isomeric P,P-dimethyl-P',P'-diphenyl-P-thioimidodiphosphinic and P,P-dimethyl-P',P'-diphenyl-P'-thioimidodiphosphinic acids
Phosphorus, Sulfur and Silicon 1998, 132, 231-250.

272. Ioan Silaghi-Dumitrescu, Francisco Lara-Ochoa and Ionel Haiduc
"Edge" or "vertex" invesrion at phosphorus in the *cis-trans* isomerization of diazadiphosphetidines? Model MNDO and *ab initio* molecular orbital calculations
Main Group Chem. 1998, 2 (4) 309-314.

271. Sofia Pascu, Luminita Silaghi-Dumitrescu, Alexander J. Blake, Ionel Haiduc and D. Bryan Sowerby
Coordination and self-assembly in the crystal structure of $K(AsMe_2S_2).2H_2O$
Polyhedron 1998, 17 (23/24) 4115-4119.

270. A. Deák, L. Párkányi, A. Kálmán, M. Venter and I. Haiduc
Dimethylbis(N-nitroso-N-phenylhydroxylaminato-O,O')cobalt(II)
Acta Crystallogr. 1998 (8) CIF Acces Paper IUC 9800036 [electronic publication, available at http://www.iucr.org/journals/acta/tocs/actac/actac.htm or by e-mail at getcif@iuc.org]

269. Ionel Haiduc and Luminita Silaghi-Dumitrescu
Investigations in organoarsenic chemistry
in vol. **Arsenic and Old Mustard: Chemical Problems in the Destruction of Old Arsenical and Mustard Munitions**, Edited by J.F. Bunnett and M. Mikolajczyk, NATO ASI Series 1. Disarmament Technologies, Vol. 19, Kluwer Academic Publishers, Dordrecht, Boston, London, 1998, pag. 149-150.

268. S. Cinta, M. Venter, C. Fickert, I. Haiduc, P. Scholz and W. Kiefer
FT-Raman studies on new triphenylphosphin-copper(I) triazenido complexes
J. Mol. Struct. 1998, 446 (3), 209-214.

267. Frank T. Edelmann, Ionel Haiduc, Hans-Georg Schmidt, Mathias Noltemeyer and Cristian Silvestru
Supramolecular self-assembly in triphenyllead(IV) dimethyldithiophosphinate, $_x^1[Ph_3PbS_2PMe_2]$, a chain polymer built through intermolecular Pb···S secondary bonds
Polyhedron, 1998, 17 (11/12) 2043-2047.

266. Monica Venter, Andrea Deák and Ionel Haiduc
Synthesis and characterisation of 4,4'-di(aryltriazenido)diphenylmethanes as new bis-triazenido proligands. Copper(II) complexes
Syn. React. Inorg. Metal-org. Chem. 1998, 28 (6) 985-996.

265. Roland Rösler, John E. Drake, Cristian Silvestru, Jincai Yang and Ionel Haiduc
The first crystal structure of mixed chalcogen derivatives
$SnR_2[(OPPh_2)(SPPh_2)N]_2$, R = Me or Ph
J. Chem. Soc., Dalton Trans., 1999 (3) 391-

264. Sofia Pascu, Luminita Silaghi-Dumitrescu, Alexander J. Blake, Wan-Sheung Li, Ionel Haiduc and D. Bryan Sowerby
trans-Dichlorotris(cyclo-hexyl)arsenic(V)
Acta Crystallogr. 1998, C54(2) 219-221.

263. John E. Drake, Anca Silvestru, Jincai Yang and Ionel Haiduc
Triphenyltellurium(IV) dichalcogenoimidodiphosphinates containing novel six-membered $TeXYP_2N$ chelate rings. X-Ray structures of $Ph_3Te[(SPPh_2)(OPPh_2)N]$ and $Ph_3Te[(OPPh_2)_2N]$
Inorg. Chim. Acta, 1998, 271(1/2) 75-82.

262. Cristian Silvestru, Roland Rösler, John E. Drake, Jincai Yang, Georgina Espinosa-Perez and Ionel Haiduc
Bis(thiophosphinoyl)amines and their neutral cobalt(II) complexes, containing stable tetrahedral CoS_4 cores. Crystal structures of $NH(SPMe_2)(SPPh_2)$ and $[Co\{[(SPMe_2)(SPPh_2)N\}_2]$.
J. Chem. Soc. Dalton Trans. 1998 (1) 73-78.

261. Francisco Cervantes-Lee, Hemant K. Sharma, Ionel Haiduc and Keith Pannell
A unique self-assembled tricyclic stannasiloxane containing a planar Sn_3SiO_5 fused 6.4.4 tricyclic ring system.
J. Chem. Soc. Dalton Trans. 1998(1) 1-2.

STUDIA UNIVERSITATIS BABEŞ-BOLYAI, CHEMIA, XLVII, 1-2, 2002

Dedicated to Professor Ionel Haiduc
on the occasion of his 65th birthday

A CHALLENGE FOR CHEMISTRY: VERY LARGE INORGANIC MOLECULES PENETRATE THE MESOSCOPIC REALM

ADRIAN PATRUT, ADRIAN NICOARA and DRAGOS MARGINEANU

"Babes-Bolyai" University, Faculty of Chemistry and Chemical Engineering,
11 Arany Janos, 3400 Cluj-Napoca, Romania

ABSTRACT. The paper aims to denominate and present the largest synthesized and structurally characterized molecules.

To begin with, the terms chemical compound and molecule are analyzed and differentiated. Two types of very large/giant molecules are defined: a) collective large molecules, generated through an inflationary multiplication (in one, two or three dimensions) of one or several species of smaller discrete molecules and b) discrete/individual large molecules, constructed by actual synthesis through the assembly of appropriate building blocks.

The candidates for the title of the largest molecule are sought among the discrete giant molecules.

Reviewed are very large molecules synthesized over the past 30 years, starting with the classical molecular polyoxometalate clusters $[As_4W_{40}]$ and $[P_8W_{48}]$ and continuing with the new supramolecular polyoxometalate clusters, such as $[Mo_{57}M_6]$, $[Mo_{132}]$, $[Mo_{72}Fe_{30}]$, $[Mo_{102}]$, $[Mo_{154}]$, $[Mo_{176}]$, $[Mo_{248}]$ and $[Ln_{16}As_{12}W_{148}]$. The $[Mo_{368}]$ cluster, currently the largest synthesized and structurally characterized molecule, concludes the presentation.

The possibility of synthesizing even larger molecules is also envisaged.

1. INTRODUCTION

According to a frequent simple definition, chemistry is the discipline that studies the composition, structure, properties and transformations/reactions of chemical substances. The definition underlines that the object of study, i.e. the prime matter of chemistry, is represented by chemical substances that can be conventionally divided into chemical elements and chemical compounds.

One of the criteria of evaluation of the development and progress of chemistry is also the continual diversification of its objects of study. The discovery and later the "creation" in laboratory of new elements, with an ever higher atomic number and atomic mass, has always been immediately popularized. The discoverers of new chemical elements enjoy general recognition in the scientific community and certain elements are even named after them. But the number of chemical elements, which is currently of 113 (a previous number

of 115 elements (in 1999) was reduced to 113 (in 2001), because the existence of elements 116 and 118 now seems to be suspect after which subsequent experiments failed to reproduce the original data of the authors which had announced their discovery) [1], seems to approach a limit that is rather physical than experimental in nature.

On the other hand, the problem of chemical compounds is much more confusing. Due to the fact that the possibility of combination of the elements seems to be limitless, obtaining new chemical compounds is pursued in a frenzy and represents the favorite occupation, almost a "hobby-horse", of chemists today. Chemists tend to turn into "laboratory robots" running in a rat race to discover, list and characterize an ever increasing number of chemical compounds, basically molecules often with no clearly defined purpose. Due to the joint effort of chemists all over the world, the number of registered organic and inorganic substances/compounds is of 20,120,922, to which 21,479,781 biosequence substances can also be added, thus increasing the total number of registered chemical substances/compounds to 41,600,703, according to the statistics offered by **Chemical Abstracts Service** (as of August 13, 2002) [2]. Thus, the words of Berthelot that "*chemistry creates its own object"* are more topical than ever. Developing this idea we can also characterize our discipline by the following statement: "*Chemistry is a natural science which creates and diversifies its object of study by the activity of its practitioners who construct in laboratory ever new molecules"*.

Within the efforts of chemists to obtain more or less surprising and expected new chemical compounds/molecules, the activity of those who construct ever larger molecules, with high symmetry and aesthetic qualities, has a pride of place and it represents the starting point of this paper. In essence, the topic of the paper is the presentation of the largest molecules synthesized by chemists and the evolution of the record in the field, a subject that has never really been satisfactorily treated in literature up to now.

Before discussing these aspects, we will try to throw light upon the terms of chemical compound and molecule that seem more complex and complicated than they might appear at first sight.

2. CHEMICAL COMPOUNDS AND MOLECULES

Almost automatically we identify chemical compounds with molecules, in the sense that chemical compounds would be constructed of molecules, if not actual at least conventional ones. We calculate for every chemical compound a molecular mass taken to be the mass of an (actual or conventional) molecule of the respective compound.

In fact, chemical compounds represent complex systems of atoms and/or ions, which are electrically neutral and have a well-defined composition and structure. This somewhat ambiguous and vague definition is due to the high diversity of chemical compounds.

According to the defining structural unit, chemical compounds can be divided into molecular and ionic compounds.

The actual chemical compounds are the molecular ones and they are by far the most numerous. The molecular compounds are in fact molecular species with clearly defined constituents and structure.

The molecule, as the structural unit of molecular compounds, is a system of atoms linked by covalent bonds (to which can also be added noncovalent bonds).

On the other hand, ionic compounds are systems of ions with opposite charges, kept together by electrostatic forces. The ions with opposite charges generate an ionic crystal, in which they are arranged tridimensionally in a crystalline lattice. In the case of ionic compounds the notion of molecule is practically meaningless. That is why ionic compounds should rather be considered ionic aggregates or ionic substances than actual chemical compounds.

But the classification of chemical compounds into ionic and molecular is not always sufficient and satisfactory. Thus, certain ionic compounds which form ionic crystalline lattices also contain a molecular unit and cannot be reduced to pure ionic compounds. For example, the lattice of sodium carbonate, i.e. Na_2CO_3 is composed of Na^+ and CO_3^{2-} ions, but the CO_3^{2-} anion is in fact a molecular anion (anionic molecule) with covalent bonds between carbon and oxygen atoms. In their turn coordination compounds, which are characterized by a great number of coordinative and covalent bonds are not, with the exception of the electroneutral ones, pure molecular compounds. So, the first characterized heteropolyoxometallic acid, i.e. $H_3[PW_{12}O_{40}] \cdot 6H_2O$ with the structure determined by Keggin, has as a main constituent a molecular unit, namely the $[PW_{12}O_{40}]^{3-}$ molecular anion (anionic molecule). But between the molecular anion and the acidic H^+ there are only electrostatic interactions (i.e. ionic bonds) and the crystal water is linked to the compound only through noncovalent bonds (i.e. hydrogen bonds).

Consequently, the concept of chemical compound remains somewhat conventional and confusing. On the other hand, the concept of molecule seems to be relatively straightforward and unambiguous; it is independent of the electrical charge and, as a result, there are neutral molecules, cationic molecules (molecular cations) and anionic molecules (molecular anions). Only in the particular case of certain neutral molecules can the chemical compound and the corresponding molecule be mixed up.

However, for the moment we shall forbear to ask the following delicate question: In the case of densely packed metal-atom arrangements, where does the molecule (the molecular state) end and when does the solid-state bulk metal begin?

We also mention the case where a certain molecule, even with complex structure and high symmetry, does not belong/correspond to a chemical compound proper. Thus, the famous C_{60} neutral molecule, the so-called *buckyball* or fullerene, is not an actual chemical compound but rather it is an allotrope state of carbon distinct from diamond and graphite.

One may well ask oneself what is the sense and especially the accuracy of the notion of molecular mass, which is usually calculated for every chemical compound.

The attempt to clarify the exact status of molecules and why they cannot be identified with the corresponding chemical compounds is an important but not sufficient step in the search for the largest synthesized molecules.

The next step involves the identification and nominalization of the researched molecules by a previous selection of various kinds of species.

Our intention is to eliminate from the beginning the giant molecules resulting from an excessive multiplication of one or more smaller molecules or fragments, such as for instance common polymers. In this type of molecules, the degree of multiplication is sometimes so high, that it is undetermined or even cannot be determined and is formally taken to be infinite. It is obvious that such types of molecules, resulting from a simple photocopying multiplication (in one, two or three dimensions), do not belong to the species looked for by us.

Our attention has been focused on giant molecules generated by actual synthesis and built up through successive assemblies, which can be considered discrete or individual molecules.

But the differentiation and especially the pinpointing of the distinctions between the two types of molecules is far from being simple and easy, all the more so since both are made up of smaller (actual or formal) molecules and/or fragments. The differences obtain especially concerning their production and usually their symmetry. The development of supramolecular chemistry, with its by now famous supramolecules, further complicates the attempts at general classification of giant molecules and molecular buildings.

With the above mentioned reservations, we shall name and define the two types of very large and giant molecules (which are obtained/prepared in laboratory), as follows:

a) *collective large molecules*, generated through an inflationary multiplication of one or several smaller species of discrete molecules or molecular fragments, in one, two or three dimensions, with formation of chains (1D), layers (2D) or networks (3D).
The multiplication process occurs through reactions of addition and/or condensation and presupposes necessarily covalent bonds between units. The existence of noncovalent intermolecular interactions beside the covalent ones, as well as of linkers/spacers is also allowed and sometimes possible. Usually, collective large molecules have low symmetry or at least low local symmetry and are qualitatively a molecular assembly of smaller molecules/molecular units/fragments expanded in one, two or three dimensions. The most widely known collective molecules are the classical/common polymers and copolymers.

b) *discrete/individual large molecules*, constructed by actual synthesis through the assembly of appropriate building blocks which are molecular units/moieties/fragments.

The bonds between the molecular units are necessary (and) covalent. The existence of noncovalent intermolecular interactions, in addition to the covalent ones, as well as of certain linkers/spacers, heretoatoms and other small molecules, is allowed and relatively frequent. Discrete large molecules usually have high or very high symmetry and are qualitatively different from the building blocks/molecular units out of which they have been assembled.

When the bonds between molecular units are exclusively covalent, it is the case of classical discrete molecules, which belong to molecular chemistry. But the largest and more spectacular discrete molecules belong to supramolecular chemistry and represent supramolecular discrete molecules. Supramolecules are characterized by a cooperative action among the composing entities which act as building blocks in the assembly process (self-assembly and even self-organization) and also the mandatory presence of noncovalent bonds (hydrogen bonds, ionic/electrostatic interactions, π bonding interactions, secondary bonds (soft-soft interactions), week interactions (i.e. van der Waals forces) etc.) [3, 4].

Thus, the differences between the two types of large molecules remain ones concerning their production, to which qualitative elements are also added. In the case of collective molecules, the original molecular species act(s) as a unit or pattern/matrix for multiplication. On the other hand, in the case of discrete/individual molecules, the original molecular species acts as building blocks in the assembly and organization (sometimes self-assembly and self-organization) processes. If in the first case the result is more or less a molecule which is a conglomerate of molecules, in the second case the product is a distinctly individual molecule with high symmetry.

Nevertheless, certain additional remarks are necessary. In some cases, certain discrete large molecules, including supramolecules, can further condense, generating chains, layers or networks. The final product is a giant collective molecule made up of large discrete molecules.

In both cases under discussion, only the molecular units integrated in the assembly exclusively or inclusively by covalent bonds belong to the giant molecule. When the assembly also contains components integrated exclusively through noncovalent bonds, the whole assembly is no longer identical with the giant molecule and can be defined as a supramolecular array [3, 4].

To round off the topic, we must also mention that over the last decades a high number of so-called (ligand-stabilized) metal clusters have been reported. They consist of a “core” of a certain number of metal atoms surrounded by a “shell” of organic ligands which stabilize the metal core and inhibit nucleation to metal bulk. The metal-atom core, composed of a central atom and concentric shells of densely packed atoms, contains occasionally a huge number (up to hundreds and even over one thousand) of metal atoms. But usually, structural analysis is not possible due to the lack of crystalline samples. On the other hand, these metal clusters should rather be considered intermediates between molecules and the bulk metal than actual molecules. For all these reasons, we shall neglect the metal clusters in our search for the largest molecule.

3. VERY LARGE SYNTHESIZED AND STRUCTURALLY CHARACTERIZED MOLECULES

After the qualitative identification of the researched candidates for the title of the largest molecule, i.e. discrete giant molecules constructed by the assembly of building blocks, it is necessary to select them following a quantitative criterion.

In this sense, the following criteria/parametres can be used:

- the (total) number of metal centres (=a);
- the (total) number of heavy atoms (=b);
- the number of non-hydrogen atoms (=c);
- the relative molecular mass (=M);
- the linear dimensions, e.g. the diametre (=d).

A number of observations are in order. The first two criteria/parametres are inoperative in the case of organic molecules. The number of heavy atoms and metal centres is not necessarily equal, not even in the case of clusters, for example when they contain heavy non-metal atoms. The last criterion is also relative, because huge molecules usually have one or more internal cavities.

The literature shows that the largest discrete molecules belong to inorganic chemistry, while organic chemistry is remarkable especially for large collective molecules. That is why we shall use the first parametre, i.e. the number of metal centres, as the main criterion to differentiate the largest molecules; mention will however be made of the values of the other parametres.

Over the last decades, the largest synthesized and structurally characterized molecules were the polyoxometalates (POMs). POMs are metal oxide-based clusters and represent the polyoxoanions of the early transition metals/elements, especially Mo, W and V, constructed of linked MO_n units (usually MO_6 octahedra). The M metal centres, which may belong to one or more atomic species, are named addenda [5].

In the case of POMs, we shall consider that the number of metal centres is equal to the number of actual addenda (to which may be added other metal atoms that occupy the place of some absent/missing addenda). On the other hand, by heavy atoms we mean metal centres (including those replacing absent/missing addenda), to which are added, as the case may be, other heavy atoms acting as linkers/spacers (between building blocks) and heteroatoms. Thus, heavy atoms are atoms (exclusively or inclusively) coordinated by ligands.

For every POM cluster/molecule a complete formula, which notes all the atoms, and an abridged/short formula, which notes only the heavy atoms, can be written.

3.1. CLASSICAL MOLECULAR POLYOXOMETALATES

After decades of heated controversy concerning the accurate formulation of POMs, Keggin first determined in 1933 the structure which was to bear his name, by investigating the $[PW_{12}0_{40}]^{3-}$ molecular anion [6]. In the following years, the structure of numerous classical POMs, which belong to molecular chemistry, was determined.

We shall present only two of them, which at the very moment of their characterization were at the top of the list of the largest molecules with determined structure.

$[As_4W_{40}]$ and derivatives

The first molecule with a minimum of 40 metal centres, the $[As^{III}_4W_{40}O_{140}]^{28-}$ POM cluster, abridged as $[As^{III}_4W_{40}]$, was reported in 1974 [7]. The $[As_4W_{40}]$ cluster was shown to bind two additional transition metal cations. The first structure determination was only performed in 1980 by Robert, Leyre and Hervé [8] on the complex with Co(II) having the formula $[|NH_4|As^{III}_4W_{40}O_{140}Co^{II}_2(H_2O)_2]^{23-}$ or $[As^{III}_4W_{40}Co^{II}_2]$ (a=42, b=46, c=189, M=10065.18).

The structure determination revealed that the parent cyclic $[As_4W_{40}]$ unsaturated cluster is built up from four α-B-$[As^{III}W_9O_{33}]^{9-} \equiv [AsW_9]$ trilacunary Keggin fragments/units, linked together by four bridging cis-$[WO_2]^{2+}$ groups (Fig. 1).

The $[As_4W_{40}]$ cluster, with D_{4h} symmetry, is a cryptand and has a central cryptate site (S_1) and four lacunary sites (S_2). The S_1 site can be occupied by alkali, alkali-like, alkaline earth and lanthanide ions, with the formation of stable cryptates. Two of the four S_2 sites can be occupied by di- or trivalent metal ions, which have a single terminal H_2O ligand. Only Ag^I can occupy all four S_2 sites.

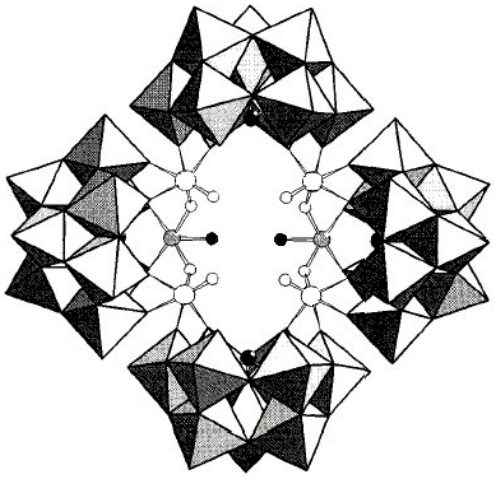

Fig. 1. Structure of the $[|NH_4|As^{III}_4W_{40}O_{140}Co^{II}_2(H_2O)_2]^{23-} \equiv [As^{III}_4W_{40}Co^{II}_2]$ POM cluster. The four $[AsW_9]$ units are shown in polyhedral representation, while the four cis-$[WO_2]^{2+}$ groups (W large white spheres; O small white spheres) and the two $[Co^{II}(H_2O)]^{2+}$ groups (Co small gray spheres; H_2O small black spheres) are figured in ball-and-stick representation. The encapsulated NH_4^+ ion has been omitted.

$[P_8W_{48}]$

In 1985, Contant and Tézé [9] synthesized and determined the structure of an even larger POM, namely $[P^{V}_{8}W_{48}O_{184}]^{40-}$ or $[P_8W_{48}]$ (a=48, b=56, c=240, M=12016.05).

The very massive $[P_8W_{48}]$ ring, having a high symmetry (D_{4h}), is built up from four $[H_2P_2W_{12}O_{48}]^{12-} \equiv [P_2W_{12}]$ units. The $[P_2W_{12}]$ unit is the hexalacunary fragment of the $[P_2W_{18}O_{62}]^{6-}$ Dawson anion, resulting from the removal of an enormous block of six lengthwise adjacent W atoms, i.e. six WO_6 octahedra, sharing edges and corners (Fig. 2).

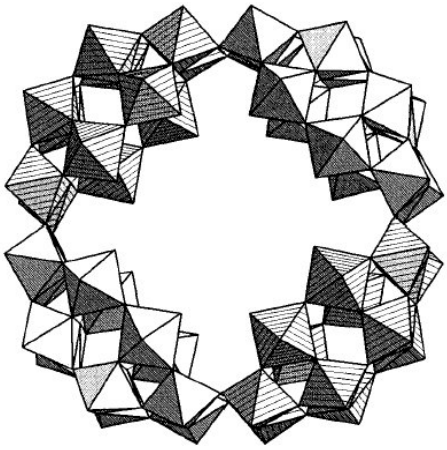

Fig. 2. Structure of the $[P^{V}_{8}W_{48}O_{184}]^{40-} \equiv [P_8W_{48}]$ POM cluster in polyhedral representation, as a cyclic assembly of four lacunary $[P_2W_{12}]$ groups. The internal $[PO_4]$ tetrahedra of the latter have been omitted and only the $[WO_6]$ octahedra are figured.

3.2. THE NEW GENERATION OF VERY LARGE SUPRAMOLECULAR POLYOXOMETALATES

Starting in the 1990s, the development of supramolecular chemistry and especially the activity of Achim Müller and his research team from Bielefeld University (Germany) opened a new chapter in the synthesis of exceptionally large inorganic molecules.

Currently, chemists construct more complex and large molecules in a step-wise manner through a time-consuming and hard-work sequential synthesis, isolation and purification of each intermediate, following the logic of retrosynthesis. But recent developments in supramolecular chemistry brought a very different approach for the synthesis of giant molecules, which is characterized more by “intelligence” than by hard-work and is not time-consuming.

The so-called bottom-up method uses a type of unit construction under a multicomponent one-pot synthesis. The novel synthesis strategy allows on the basis of a number of simple combinatory linkable building blocks/ units at the disposition, the obtaining, by successive and rapid processes of

self-assembly, self-organization and molecular growth, of a huge variety of very large molecules. This is the starting point of a new type of chemistry, which is directed by geometrical and topological rules.

The basic chemical principles for the new strategy provide a number of features that offer excellent prerequisites for the synthesis of giant molecular species.

Müller [10-13] mentions the following conditions/parametres that favour the emergence of molecular complexity and the obtaining of very large molecules:

1. *Abundance of transferable building blocks.* This concept does not only refer to the geometrical/structural decomposition into smaller entities/units/motifs/building blocks, but reflects also their well-defined reactivities determining the unit-specific local matching rules according to which these building blocks can be linked.
2. *Versatile redox chemistry.* Different degrees of reduction of a number of metal centres to obtain mixed-valence species offer the possibility to tune the electron density of the cluster.
3. *Integration of hetero elements and exchange of ligands.* This allows altering reactivity, functionality and the physical properties, such as the magnetism of the final resulting cluster.
4. *Tunable charge/size ratio.* The charge of the growing molecular fragment can be modified by the exchange of ligands, inclusion of hetero elements, exchange of some metal centres or an optimal reduction of the existing metal centres using an adequate reducing agent. An increased absolute (negative) charge, while keeping the charge density constant of the intermediates in solution, guarantees a good solubility that is necessary for the ongoing molecular growth and prevents possible degradations by hydrolysis.
5. *Template functionality.* The formation of very large molecules is in special cases facilitated by supramolecular-type interaction between the growing fragments and other species present in the reaction solution, for instance those which can act as templates.

These conditions can only be optimally fulfilled in POM systems, especially molybdenum oxide-based POMs, which possess the relevant variety of molecular and electronic structures/configurations.

The suitable systems for such research work are solutions of tetrahedral oxoanions of the early transition metals/elements of the MO_4^{n-}-type ($M=W^{VI}$, V^{V} and especially Mo^{VI}). Using the same reaction type, i.e. the acidification of aqueous solutions of these oxoanions, a large variety of discrete giant POM molecules, with amazing structures and properties, can be obtained (essentially through a process which involves successive condensations).

Additional external chemical interventions, e.g. those mentioned above, such as the presence of reducing agents (especially those with the possibility of multi-electron transfer), appropriate templates and hetero elements, lead to an even greater molecular and structural diversity.

It is to mention that the condensation process may continue, leading to chains, layers or networks which have as multiplication units even these discrete nano-sized POM molecules and represent macroscopic solid-state systems (supramolecular arrays).

Consequently, for the first time the possibility to construct in a planned and deliberate way giant molecules, i.e. POM clusters, under one-pot synthesis has become available. The step-wise building process fundamentally entails the existence of adequate linkable building blocks and possibly of different types of linkers/spacers as well as a control parametre, such as the reduction degree (but also the pH value), which influences the kind of successive building blocks formed.

Accordingly, the following question should be addressed: Into what types of structural building blocks can a giant molecule be conventionally reduced, with the possibility of generating a structural and functional hierarchy starting just from these blocks?

Müller [10-13] has done important work in the inventory of the virtual library of building blocks, out of which can be constructed all the molybdenum oxide-based POMs known up to now. These linkable building blocks/units/ fragments/motifs/groups, in the form of Platonic and Archimedean solids, allow the chemist to operate conceptually with a large variety of distinct molecular modules derived from these units.

In essence, all known molecules and structures can be ultimately reduced to $[Mo_1]$ units (containing one Mo atom surrounded by a number of O atoms in different geometries) or to $[Mo_2]$ units (resulted, at least formally, of two $[Mo_1]$ units linked in various ways by edges and/or corners). But the most interesting are the larger building blocks which act as directing molecular modules and may lead to very large molecular systems of higher structural variability and versatility than is possible with arrangements of metal atoms having spherical symmetry. These basic/essential building blocks are the following: $[(Mo)Mo_5]$, $[Mo_8]$, $[Mo_{11}]$ and $[Mo_{17}]$.

A scientist with deep philosophical and aesthetical concerns, Müller [13] gives a special importance to the pentagonal building block/unit/motif. He has noticed the quasi-magical fascination exerted by pentagons over time; these have had an extraordinary role in the cultural and science history of mankind.

The pentagonal $[(Mo)Mo_5]$ building block with C_5 (or C_S when distorted) symmetry, consists of a central MoO_7 pentagonal-bipyramidal unit sharing its equatorial edges with five additional MoO_6 octahedra (Fig.3). Pentagons can be utilized as potential building blocks, especially for constructing spherical clusters of icosahedral symmetry. The icosahedral symmetry (I_h) can be achieved even if the pentagons do not share edges, but are interconnected by appropriate linkers, for instance in the so-called *giant sphere*-type POMs.

The $[Mo_8] \equiv [(Mo_1)[(Mo)Mo_5](Mo_1)]$ building block, characteristically curved, is built up of the densely packed pentagonal $[(Mo)Mo_5]$ unit to which two additional MoO_6 octahedra (sharing only corners) are more weakly connected and can more easily be removed. The $[Mo_8]$ unit makes possible the synthesis of even larger POMs, for instance of the so-called *giant wheel*-type.

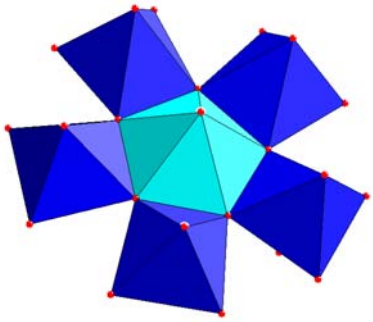

Fig. 3. Structure of the $[(Mo)Mo_5O_{21}]^{6-} \equiv [(Mo)Mo_5]$ building block in polyhedral representation. The central MoO_7 pentagonal bipyramid shares edges with five equatorial MoO_6 octahedra. Color code: MoO_7 unit blue-turquoise; MoO_6 units blue; O red.

The $[Mo_{11}] \equiv [(Mo)^0(Mo_5)^I(Mo_5)^{II}]$ building block has as its central part a pentagonal-bipyramidal MoO_7 unit of $(Mo)^0$-type with a directing function. Five MoO_6 octahedra of $(Mo_5)^I$-type are condensed to the equatorial plane of the central MoO_7 unit sharing edges, while the next five MoO_6 octahedra of $(Mo_5)^{II}$-type share corners with the former octahedra (the superscript 0, I, II indices mention the zero, first or second generation of the building unit) (Fig. 4). $[Mo_{11}]$ is the basic building block for POM molecules which can be formulated as $[Mo_{11}]_n$, i.e. *giant spheres* and *giant wheels*.

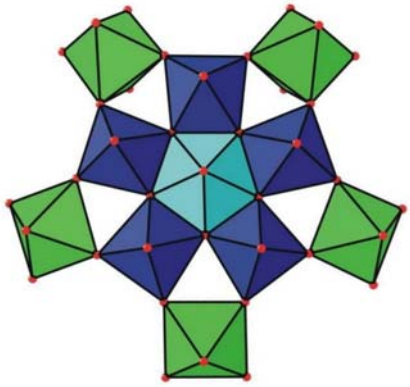

Fig. 4. Structure of the $[Mo_{11}] \equiv [(Mo)^0(Mo_5)^I(Mo_5)^{II}]$ building block in polyhedral representation. The central $MoO_7 \equiv (Mo)^0$ pentagonal bipyramid (zero generation) is connected to five equatorial $MoO_6 \equiv (Mo_5)^I$ octahedra (first generation) by sharing edges to which another five $MoO_6 \equiv (Mo_5)^{II}$ octahedra (second generation) are added by sharing only corners. Color code: $(Mo)^0$ unit blue-turquoise; $(Mo_5)^I$ units blue; $(Mo_5)^{II}$ units green; O red.

Finally, the large $[Mo_{17}] \equiv [(Mo_8)(Mo_1)(Mo_8)] \equiv [(Mo_8)_2(Mo_1)]$ building block can be reduced to two $[Mo_8]$ units fused via eight O atoms and symmetrically linked by an MoO_6 octahedron. The $[Mo_{36}]$ and $[Mo_{57}M_6]$ clusters are made up of two, respectively three such units.

Further, we shall present the largest POM clusters and the fascinating evolution of the record-holding largest synthesized molecule with structure determination.

$[Mo_{57}M_6]$ and derivatives

The three-fragment POM clusters of the $[Mo_{57}M_6]$-type (M=V, Fe) were the first synthesized molecules with over 60 metal centres.

In 1993, Zhang et al. [14], respectively Müller et al. [15] independently reported the synthesis of a large cluster of the $[Mo_{57}M_6]$-type. The molecular formula $[Mo_{57}V_6(NO)_6O_{183}(H_2O)_{18}]^{6-}$ given by the Chinese team was obviously false with respect to its composition, structure and the oxidation numbers of the metal centres. The molecule was structurally analyzed by Müller and coworkers in 1994 [16], who also established the correct formula, namely $[H_3Mo_{57}V_6(NO)_6\text{-}O_{180}(OH)_3(H_2O)_{18}]^{21-}$ or $[[V^{IV}(H_2O)O]_6[Mo^{V}(H_2O)_2(OH)Mo^{V}]_3\text{-}[Mo^{VI}{}_{15}(Mo^{VI}NO)_2O_{58}(H_2O)_2]_3]^{21-}$, abridged as $[Mo_{57}V_6]$ or $[Mo^{VI}{}_{51}Mo^{V}{}_6V^{IV}{}_6]$ (a=b=63; c=276; M=9212.54; d=2.2nm).

The $[Mo_{57}V_6]$ molecule, with 63 metal centres and 276 non-hydrogen atoms, has a high symmetry (D_{3h}) and contains three large $[Mo^{VI}{}_{17}]$ building blocks linked by six V^{IV} centres and three $[Mo^{V}{}_2]$ units (Fig.6a). More precisely, the doughnut-shaped cluster (which corresponds to an ellipsoid with the dimensions 2.2 x 2.2 x 1.0 nm) consists of three highly negatively charged $[Mo^{VI}{}_{15}(Mo^{VI}NO)_2O_{58}(H_2O)_2]^{20-}$ units, connected by six $[V^{IV}(H_2O)O]^{2+}$ groups and three dinuclear $[Mo^{V}(H_2O)_2(OH)Mo^{V}]^{9+}$ units.

In 1995, Müller and his team [17] also synthesized and characterized the analogous cluster with M=Fe, having the formula $[Mo_{57}Fe_6(NO)_6O_{174}(OH)_3(H_2O)_{24}]^{15-} \equiv [[Fe^{III}(H_2O)_2]_6[Mo^{V}(H_2O)_2(OH)Mo^{V}]_3\text{-}[Mo^{VI}{}_{15}(Mo^{VI}NO)_2O_{58}(H_2O)_2]_3]^{21-}$, abridged as $[Mo_{57}Fe_6]$ or $[Mo^{VI}{}_{51}Mo^{V}{}_6Fe^{III}{}_6]$ (a=b=63; c=276; M=9251.09; d=2.2nm). The structure is similar to the previous cluster, with the difference that six Fe^{III} centres occupy the place of the six V^{IV} centres, more precisely the molecule has six $[Fe^{III}(H_2O)_2]^{3+}$ instead of six $[V^{IV}(H_2O)O]^{2+}$ units (Fig. 5).

The relatively large cavity inside the $[Mo_{57}M_6]$ molecular anions is formally accessible through two openings in the cluster shell. The cavity (with a diametre perpendicular to the S_3 axis of $\approx$ 0.9 nm and parallel to it of $\approx$ 0.5 nm) is delimited by a central $[O_{33}]$ polyhedron. The two openings are delimited by two alternating Mo-O-M-O 12-membered rings.

An interesting structural feature is the presence of six rather large cavities on the outher sphere between the $[Mo_{17}]$ units. These cavities are accessible to the coordination of further electrophyllic metal-oxygen fragments, i.e. $[MoO]^{4+}$ units. As a consequence, in aqueous solutions under strong reducing conditions and in excess of molybdate(VI) may undergo a step-by-step molecular growth process, which enables all $[Mo_{57+x}M_6]$ (x=0-6) species to

be formed. Each $[MoO]^{4+}$ unit binds to three O atoms (two terminal) of the $[Mo_{57}M_6]$ core, resulting in a tetrahedral coordination of the incorporated additional Mo atoms. The degree of occupation of the cavities (the x value) can be correlated with the reduction degree of the $[Mo_{57}M_6]$ cluster. Reduction increases the nucleophilicity of the core-cluster and initiates a growth process in which up to as many six electrophilic units can be incorporated.

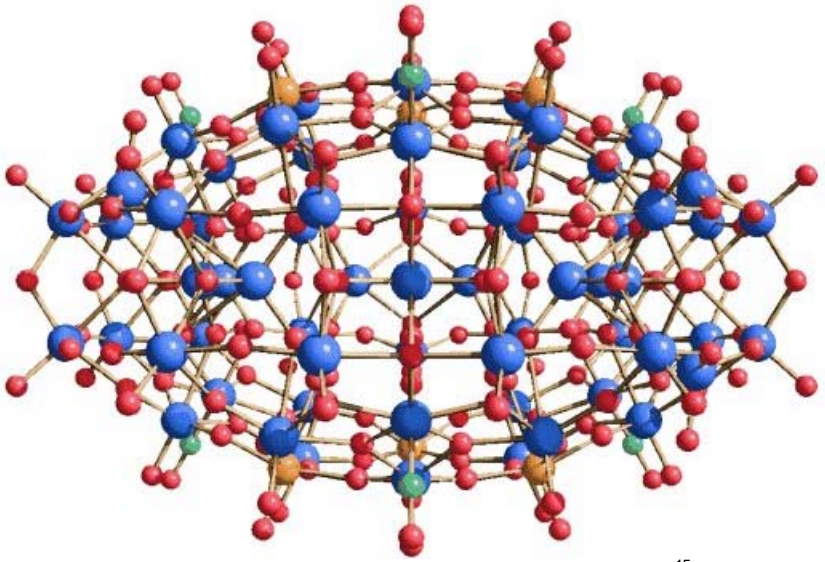

Fig. 5. Ball-and-stick representation of the $[Mo_{57}Fe_6(NO)_6O_{174}(OH)_3(H_2O)_{24}]^{15-} \equiv [Mo_{57}Fe_6]$ POM cluster along one of the $2(C_2)$ axes. Color code: Mo light gray; Fe orange; O red; N green.

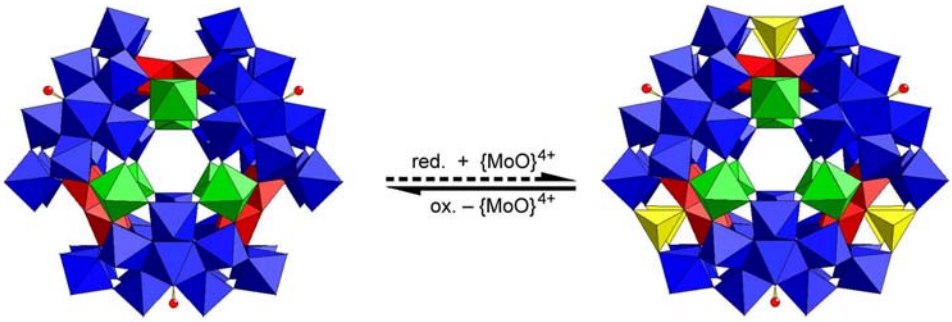

Fig. 6. Quasi-reversible molecular growth within the $[Mo_{57}V_6]$ (a) / $[Mo_{63}V_6]$ (b) POM cluster system. Six $[MoO]^{4+}$ units can be taken up to form the $[Mo_{63}V_6]$ cluster under reducing conditions and can be expelled when the latter is oxidized. Color code: $[Mo_{17}]$ units blue; $[Mo^{V}_2]$ linker units red; $[V^{IV}]$ linker units green; additional $[Mo^{VI}O]^{4+}$ units yellow.

Thus in 1998, Müller et al. [18] synthesized under reducing conditions the saturated cluster with six additional Mo^{VI} centres, i.e. $[H_3Mo_{57}V_6(NO)_6O_{189}(H_2O)_{12}(MoO)_6]^{21-}$, abridged as $[Mo_{63}V_6]$ or $[Mo^{VI}{}_{51}Mo^{V}{}_{12}V^{IV}{}_6]$ (a=b=69; c=288; M=9869.07; d≈2.2nm) (Fig. 6b).

In 2000, working with vanadate(V) instead of molybdate(VI), Yang et al. [19] synthesized the analogue cluster with six additional V^{V} metal centres, i.e. $[H_3Mo_{57}V^{IV}{}_6(NO)_6O_{189}(H_2O)_{12}(V^{V}O)_6]^{15-}$, abridged as $[Mo_{57}V_{12}]$ or $[Mo^{VI}{}_{45}Mo^{V}{}_{12}V^{IV}{}_6V^{V}{}_6]$.

Giant spheres: $[Mo_{132}]$, $[Mo_{72}Fe_{30}]$ and $[Mo_{102}]$

In spite of the over 100 metal centres, the spherical $[Mo_{132}]$, $[Mo_{72}Fe_{30}]$ and $[Mo_{102}]$ clusters, so-called *giant spheres*, were never at the top of the list of the largest molecules. And because scientific discoveries do not always respect a step-by-step rigorous succession, their synthesis suffered a delay of several years, so that even larger molecules had the chance to be earlier synthesized.

Nevertheless, the spherical clusters of the type $(pentagon)_{12}(linker)_{30}$, with the highest possible symmetry, i.e. icosahedral (I_h), have a special importance in the picture of giant POMs and their presentation is almost mandatory.

In 1999, Müller and his team [20] presented a very large spherical mixed-valence POM cluster, i.e. $[Mo^{VI}{}_{72}Mo^{V}{}_{60}O_{372}(CH_3COO)_{30}(H_2O)_{72}]^{42-}$, abridged as $[Mo_{132}]$, $[Mo^{VI}{}_{72}Mo^{V}{}_{60}]$ or $[Mo_{11}]_{12}$ (a=b=132; c=696; M=21684.43; d≈2.9nm). The new "dodecameric" (such a term made up of a numeral + the suffix *mer* is specific and adequate for collective molecules, e.g. polymers, and should be use only figuratively in the case of large discrete molecules) cluster was also named *giant ball* (*giant sphere*).

The central Mo^{VI} atoms of the 12 $[(Mo^{VI})Mo^{VI}{}_5]$ pentagons define the 12 corners, while the 30 $[Mo^{V}{}_2]$ linkers, i.e. the $[Mo^{V}{}_2O_4]^{2+}$ units, define the 30 edges of an icosahedron. This corresponds to the formulation $[[(Mo^{VI})Mo^{VI}{}_5O_{21}(H_2O)_6]_{12}[Mo^{V}{}_2O_4(CH_3COO)]_{30}]^{42-}$ or $[[(Mo^{VI})Mo^{VI}{}_5]_{12}\ [Mo^{V}{}_2]_{30}] \equiv (pentagon)_{12}(linker)_{30}$. Based on a topological concept, the molecule can also be formulated as $[[(Mo^{VI})^{O}(Mo^{VI}{}_5)^{I}(Mo^{V}{}_5)^{II}]_{12}$ or $[Mo_{11}]_{12}$. This formulation takes formally into account that the Mo atoms of each rather stable $[Mo^{V}{}_2]$ dumbbell belong to two adjacent $[Mo_{11}]$ groups.

The cluster can be considered as built up of 12 $[Mo_{11}]$ units with central $[MoO_7]$ pentagonal-bipyramidal groups, such that the fivefold symmetry axes are retained in the resulting spherical structure, which shows an overall icosahedral symmetry (I_h) (Fig. 7a, 8a).

The 30 classical $[Mo^{V}{}_2]$ dumbbell units span an Archimedean solid of icosahedral symmetry which corresponds to that of the well-known C_{60} fullerene molecule, in the present case a polyhedron with 12 regular pentagons and 20 trigonal hexagons, i.e. the truncated icosahedron (Fig. 7).

Thus, both systems with 60 atoms, i.e. the C_{60} fullerene molecule (d≈0.75 nm; Fig. 9c) and the much larger [Mo^{V}_{60}] fragment (d≈2.5 nm; Fig. 9a) of the [Mo_{132}] molecule, correspond to the Archimedean truncated icosahedron which has the same symmetry as the Platonic icosahedron itself. Therefore, Müller [20] also named the [Mo_{132}] molecule *superfullerene*.

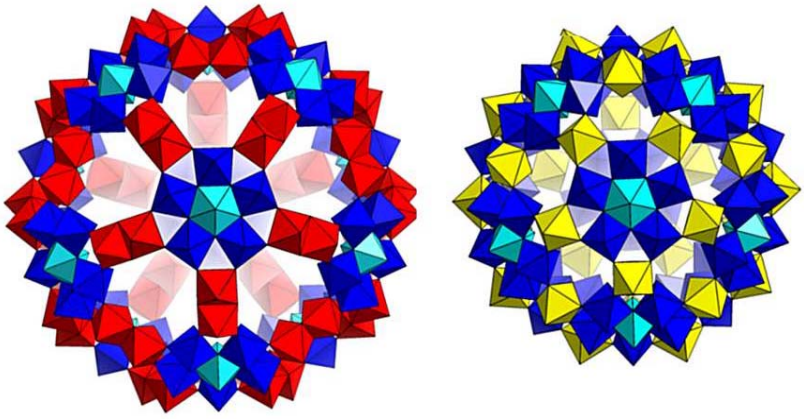

a **b**

Fig. 7. Structural comparison between the [Mo_{132}] (a) and [$Mo_{72}Fe_{30}$] (b) clusters in polyhedral representation. Both clusters consists of 12 pentagonal [(Mo^{VI})Mo^{VI}_{5}] building blocks (blue, with the central MoO_7 pentagonal bipyramid in blue-turquoise), but the 30 linker units are different, i.e. [Mo^{V}_{2}] (a) (red) and [Fe^{III}_{1}] (b) (yellow).

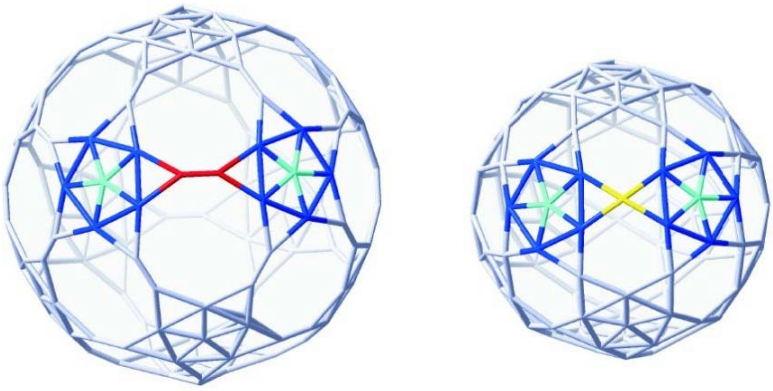

a **b**

Fig. 8. Structural comparison between the [Mo_{132}] (a) and [$Mo_{72}Fe_{30}$] (b) clusters in wire-frame representation. Two of the 12 pentagonal [(Mo^{VI})Mo^{VI}_{5})] building blocks (blue, with the central MoO_7 pentagonal bipyramid in blue-turquoise) and one of the 30 linker units, i.e. [Mo^{V}_{2}] (a) (red) and [Fe^{III}_{1}] (b) (yellow), are emphasized.

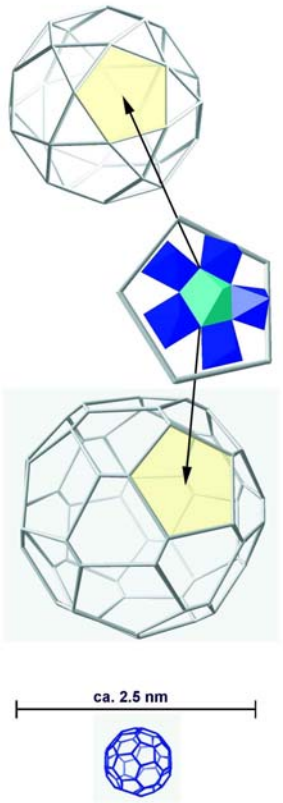

If starting 1985, the almost legendary C_{60} fullerene or *buckyball* was acclaimed as "*the most beautiful molecule"* (this is also the title of a book [21]), there is no question that today the $[Mo_{132}]$ *giant ball* can be considered "*the most aesthetic molecule"* [22].

Müller [20] has also proposed to call the $[Mo_{132}] \equiv [Mo_{11}]_{12}$ molecule a *keplerate*, corresponding to Kepler's early cosmological model, as described in his magnum opus *Mysterium Cosmographicum*. Kepler believed that the orbits of the planets could be explained if the ratios between successive orbits were designed to be equivalent to the spheres successively circumscribed around and inscribed within the five Platonic solids (i.e. the tetrahedron, cube, octahedron, dodecahedron, icosahedron). By analogy, the $[Mo_{132}]$ cluster correspondingly shows concentric spherical shells of the 132 terminal O and 132 Mo atoms, while the centres of the 12 $[(Mo^{VI})Mo^{VI}_5]$ pentagons, i.e. the 12 Mo atoms of the central $[MoO_7]$ bipyramids, span an icosahedron [11, 13, 20, 22].

Fig. 9. Structural comparison between the $[Mo^{V}_2]_{30}$ fragment of the $[Mo_{132}]$ cluster (a), the $[Fe^{III}_1]_{30}$ fragment of the $[Mo_{72}Fe_{30}]$ cluster (b) and the C_{60} fullerene (c) in wire-frame representation. The three molecules correspond each to an Archimedean solid, i.e. the truncated icosahedron with 12 regular pentagonal and 20 trigonal hexagonal faces (a and c), respectively the icosidodecahedron with 12 regular pentagons and 20 triangular faces (b). A pentagonal $[(Mo)Mo_5]$ unit occurring in the two clusters is emphasized.

The external diametre of the $[Mo_{132}]$ *giant ball* is ≈ 2.9 nm, while the diametre of the large internal cavity is ≈ 2.0 nm.

It is to be noted that the $[Mo_{132}]$ *giant ball* contains only localised reduced metal centres, i.e. Mo^{V} atoms. In the absence of other cromophores, the corresponding compounds have a characteristic brown colour.

In 1999, Müller and coworkers [23] synthesized another molecule of the same class, namely the $[H_4Mo^{VI}_{72}Fe^{III}_{30}O_{252}(CH_3COO)_{12}(H_2O)_{98}]$ cluster, abridged as $[Mo_{72}Fe_{30}]$, $[Mo^{VI}_{72}Fe^{III}_{30}]$ or $[Mo_6Fe_{5/2}]_{12}$ (a=b=102; c=500; M=15089.27; d≈2.5nm). The new molecule, also called *iron ball (iron sphere)*, is no longer an anion but a neutral species and it is a POM any more but only a metal oxide-based cluster, more precisely a molybdenum oxide-based cluster (Fig. 7b, 8b, 10).

Out of topological reasons, the $[Mo_{72}Fe_{30}]$ neutral cluster can also be formulated as $[[(Mo^{VI})^{O}(Mo^{VI}{}_{5})^{I}(Fe^{III}{}_{5/2})^{II}]_{12}$ or $[Mo^{VI}{}_{6}Fe^{III}{}_{5/2}]_{12}$, by analogy with the formulation $[Mo_{11}]_{12}$. Another topological formulation, corresponding to $(pentagon)_{12}(linker)_{30}$ is $[[(Mo^{VI})Mo^{VI}{}_{5}]_{12}[[Fe^{III}{}_{1}]_{30}]$, more precisely $[[(Mo^{VI})Mo^{VI}{}_{5}O_{62/3}(OH)_{1/3}(H_2O)_n]_{12}\ [Fe^{III}(H_2O)_2]_{30}]$.

By analogy with the $[Mo_{132}]$ cluster, the central Mo^{VI} atoms of the 12 $[(Mo^{VI})Mo^{VI}{}_{5}]$ building units define the 12 corners and the 30 $[Fe^{III}{}_{1}]$ linker units, i.e. the $[Fe^{III}(H_2O)_2]^{3+}$ groups, define the 30 edges of an icosahedron (Fig. 10a). The 30 $[Fe^{III}{}_{1}]$ linkers also span an Archimedean solid, in this case an icosidodecahedron with 12 pentagonal and 20 triangular faces (Fig.10b). Thus, the $[Mo_{72}Fe_{30}]$ cluster can also be considered a *superfullerene*.

But the special interest of this cluster is due to its magnetochemistry, because $[Mo_{72}Fe_{30}]$ has 30 high-spin Fe^{III} centres (with s=5/2) with a total of 150 unpaired electrons (S=150/2). Thus, $[Mo_{72}Fe_{30}]$ is the discrete molecule with the highest number of paramagnetic centres known up to the present.

The external diametre of the $[Mo_{72}Fe_{30}]$ cluster is ≈ 2.5 nm and of its internal cavity is ≈1.6 nm.

Finally, in 2000, Müller et al. [24] reported another *giant sphere*-type molecule, obtained through sizing the $[Mo_{132}]$ *giant ball*. It is the case of the mixed-valence neutral $[Mo^{VI/V}{}_{72}Mo^{V}{}_{30}O_{282}(CH_3COO)_{12}(H_2O)_{78}]$ cluster, abridged as $[Mo_{102}]$ or $[Mo^{VI/V}{}_{72}Mo^{V}{}_{30}]$ (with six delocalized Mo^{V} centres), having rather an unusual electronic configuration (a=b=102; c=510; M=16411.55; d≈2.5 nm). The new cluster was also named (only as compared to the $[Mo_{132}]$ *giant ball*) *little ball (little sphere)* (Fig. 11). Unlike the $[Mo_{132}]$ *giant ball,* the $[Mo_{102}]$ *little ball* contains also six delocalized Mo^{V} centres to be found somewhere in the Mo_{72} set.

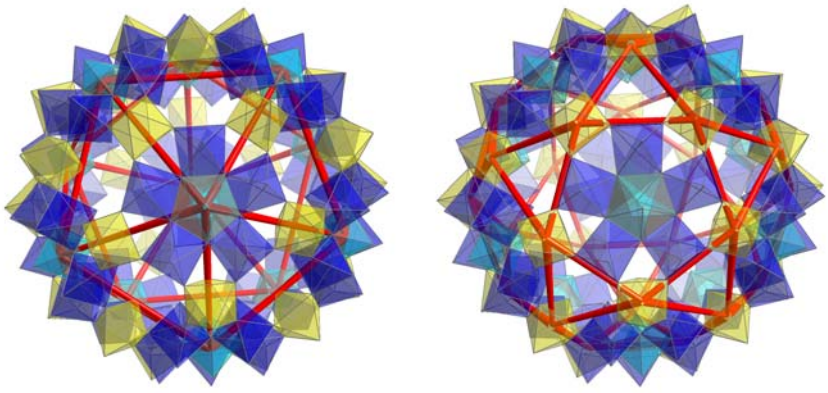

a **b**

Fig. 10. Structure of the neutral $[H_4Mo^{VI}{}_{72}Fe^{III}{}_{30}O_{252}(CH_3COO)_{12}(H_2O)_{98}] \equiv [Mo_{72}Fe_{30}]$ keplerate cluster in transparent polyhedral representation with the two inscribed polyhedra. The icosahedron (a) is defined by the central Mo^{VI} atoms of the 12 $[(Mo^{VI})Mo^{VI}{}_{5}]$ groups and the icosidodecahedron (b) by the 30 $[Fe^{III}{}_{1}]$ centres. Color code as in Fig. 7.

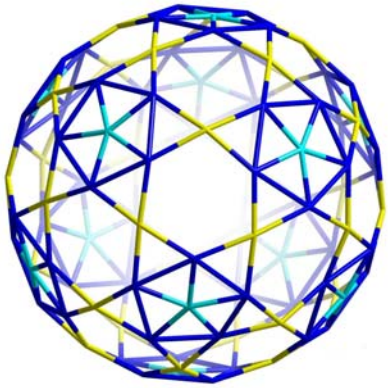

Fig. 11. Structure of the neutral $[Mo^{VI/V}_{72}Mo^{V}_{30}O_{282}(CH_3COO)]_{12}(H_2O)_{78}] \equiv [Mo_{102}]$ cluster in wire-frame representation. The 12 pentagonal $[(Mo^{VI})Mo^{VI}_5]$ building blocks (blue, with the central MoO_7 pentagonal bipyramid in blue-turquoise) are linked by 30 $[Mo^{V}_1]$ units (yellow).

Like the other *giant spheres*, the $[Mo_{102}]$ cluster can also be formulated as $(pentagon)_{12}(linker)_{30} \equiv [[(Mo^{VI})Mo^{VI/V}_5O_{21}(CH_3COO)\text{-}(H_2O)_4]_{12}[Mo^{V}(H_2O)]_{30}] \equiv [[(Mo^{VI})Mo^{VI/V}_5]_{12}[Mo^{V}_1]_{30}]$, respectively $[[(Mo^{VI})^{O}(Mo^{VI/V}_5)^{I}(Mo^{V}_{5/2})^{II}]_{12}$ or $[Mo^{VI/V}_6Mo^{V}_{5/2}]_{12}$.

All three *giant spheres*, namely $[Mo_{132}]$, $[Mo_{72}Fe_{30}]$ and $[Mo_{102}]$, obey the mathematical relation N=12a+20b+30c+60d (where: N= number of metal centres; a, b, c=0 or 1; d=arbitrary integerer) and can be considered *keplerates* [25].

Giant wheels: $[Mo_{154}]$ and $[Mo_{176}]$

Many generations of chemists have tried without success to isolate pure crystalline compounds from the well-known molybdenum blue solutions, obtained by adding an appropriate reducing agent to an acidified aqueous molybdate(VI) (i.e. MoO_4^{2-})-containing solution. Müller and his team have demonstrated that the molybdenum blue solutions mainly contain extremely soluble so-called *giant wheel*-type clusters, i.e. $[Mo_{154}]$ and $[Mo_{176}]$ in proportions that especially depend on the pH value.

The circular $[Mo_{154}]$ and $[Mo_{176}]$ clusters of the *giant wheel*-type are closely related to the spherical clusters of the *giant sphere*-type. Both types contain identical building blocks, namely $[Mo_{11}]$, $[Mo_8]$ and $[(Mo)Mo_5]$.

But in opposition to the $[Mo_{132}]$ *giant ball*, the *giant wheel* and *giant wheel*-derived molecules contain delocalized reduced Mo^{V} metal centres and, as a consequence, the corresponding compounds have an intense blue colour.

The $[Mo_{11}] \equiv [(Mo)^{O}(Mo_5)^{I}(Mo_5)^{II}]$ building blocks of the $[Mo_{132}] \equiv [Mo_{11}]_{12}$ *giant sphere* have a fivefold local symmetry (C_5). But due to the presence of certain reducing agents during synthesis (at pH≈4), all the five peripheral Mo centres of each of the $(Mo_5)^{II}$ units are reduced to Mo^{V}. In exchange, the $[Mo_{11}]$ building blocks of the $[Mo_{154}] \equiv [Mo_{11}]_{14}$ and $[Mo_{176}] \equiv [Mo_{11}]_{16}$ *giant wheels* have a distorted fivefold symmetry (C_s). The *giant wheels*

under discussion are prepared in the presence of weaker reducing agents, so that the five peripheral Mo centres are only in part reduced, which determines a non-equivalence between them, generating a perturbation of the local symmetry.

The close relationship of the two $[Mo_{11}]$-type clusters is also provided by the possibility of interconversion by redox processes, such as:

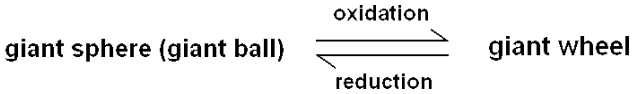

(for instance oxidation of $[Mo_{132}]$ to $[Mo_{176}]$, with H_2O_2 in the presence of transition metal cations, such as Mn^{2+}, Co^{2+}, Ni^{2+} and Zn^{2+}) [26].

Chronologically, the "tetradecameric" $[Mo_{11}]_{14} \equiv [Mo_{154}]$-type POM cluster reported by Müller et al. in 1995 [27] having the definitive formula $[Mo^{VI/V}{}_{154}(NO)_{14}O_{448}H_{14}(H_2O)_{70}]^{28-}$ was the first structurally characterized molecule with over 100 metal centres (a=b=154; c=700; M=23637.93; d≈3.7nm).

Containing 154 metal centres (126 Mo^{VI} and 28 Mo^{V}), 700 non-hydrogen atoms and having a relative molecular mass of 23638, the new molecule (Fig. 12) was named *the (Bielefeld) giant wheel*, instantly rousing the interest and enthusiasm of the scientific community. This lead to the following metaphorical statement in **New Scientist**: "*Big wheels rolls back the molecular frontier"* [28].

Later, Müller also obtained certain other $[Mo_{154}]$-type molecules, with slight ligand modifications, for instance $[Mo^{VI/V}{}_{154}O_{462}H_{14}(H_2O)_{70}]^{14-}$ [11-13].

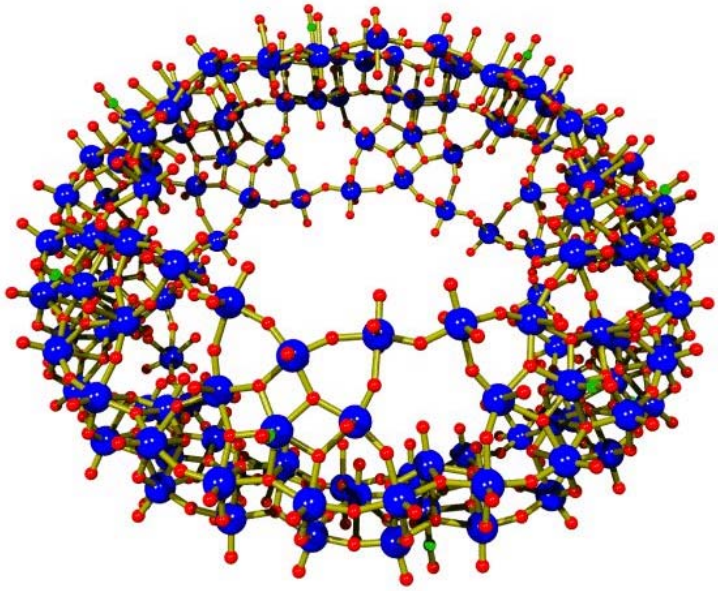

Fig. 12. The structure of the $[Mo_{154}(NO)_{14}O_{448}H_{14}(H_2O)_{70}]^{28-} \equiv [Mo_{154}]$ POM cluster in ball-and-stick representation. Color code: Mo blue; O red; N green.

In a first topological description, the $[Mo_{154}]$-type cluster contains 14 $[Mo_{11}] \equiv 14\ [(Mo)^{O}(Mo_5)^{I}(Mo_5)^{II}] \equiv 14\ [[Mo_2][Mo_8][Mo_1]]$ building blocks. Another description is based on the $[Mo_8]$ unit as a fragment of the $[Mo_{11}]$ building block. Each of the basic $[Mo_8]$ units contains the central pentagonal-bipyramidal MoO_7 polyhedron which is symmetrically connected to five MoO_6 octahedra by sharing edges, resulting in the $[(Mo)Mo_5]$ pentagon. Four of these MoO_6 octahedra are linked to two further MoO_6 octahedra via corners to form the $[Mo_8]$ building block. Starting from the $[Mo_8]$ units the complete $[Mo_{11}]_{14}$-type ring is built up following well-defined rules (Fig. 13a) [12].

The $[Mo_{154}]$-type cluster has a diametre of ≈3.7 nm, a thickness of ≈1.5 nm and a large internal cavity with a diametre of ≈2.0 nm.

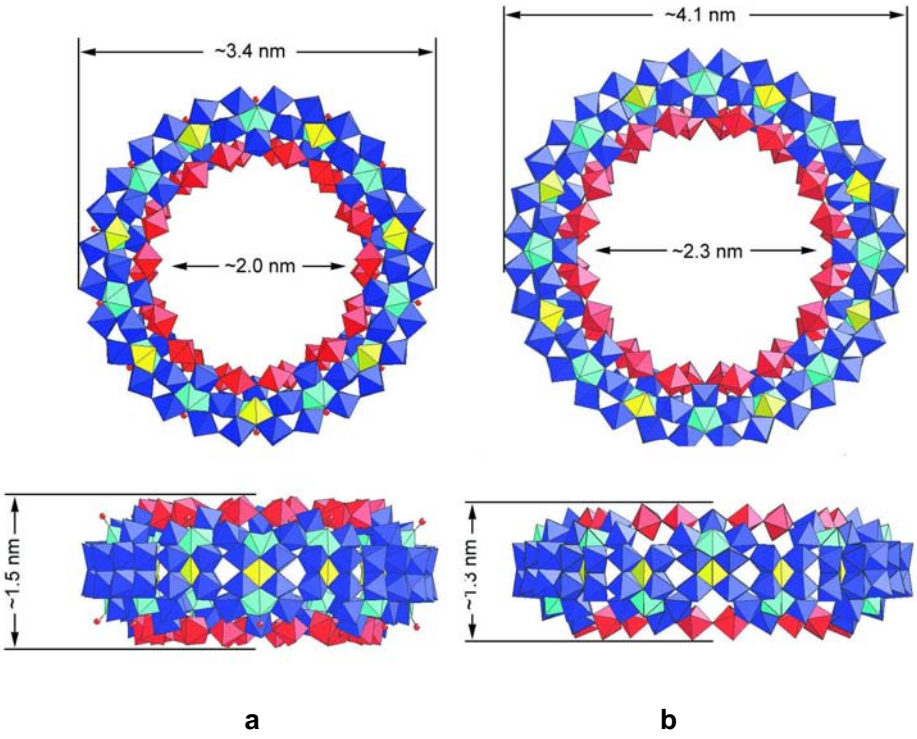

Fig. 13. Polyhedral representation of the $[Mo_{154}] \equiv [Mo_{11}]_{14}$ (a) and $[Mo_{176}] \equiv [Mo_{11}]_{16}$ (b) POM clusters along the C_7 (a) and C_8 (b) axes (top) and perpendicular to them (bottom). The figure shows three different building blocks: the 14(a)/16(b) $[Mo_8]$ units (blue, with the central MoO_7 pentagonal bipyramid in blue-turquoise) which are linked by 14(a)/16(b) $[Mo_2]$ units (red) as well as 14(a)/16(b) $[Mo_1]$ units localized at the equatorial plane (yellow).

The next record-holder was the "hexadecameric" $[Mo_{11}]_{16} \equiv [Mo_{176}]$-type *giant wheel*, reported by Müller et al. in 1998 [29], with the definitive formula $[Mo^{VI}_{176}O_{528}H_{16}(H_2O)_{80}]^{16-}$ (a=b=176; c=784; M=26790.67, d≈4.1 nm). The

formula is somewhat surprisingly because it does not contain reduced metal centres. Slightly later, the Müller team [30] synthesized by exchanging ligands a mixed-valence $[Mo_{176}]$-type cluster, i.e. $[Mo^{VI/V}{}_{176}O_{528}(H_2O)_{63}(CH_3OH)_{14}H_n]^{(17-n)-}$ (with 144 Mo^{VI} and 32 Mo^{V} centres).

After further period of a few months, Jiang et al. [31] independently reported a mixed-valence neutral cluster, having the formula $[Mo^{VI/V}{}_{176}O_{496}(OH)_{36}(H_2O)_{80}]$.

The structure of the $[Mo_{176}] \equiv [Mo_{11}]_{16}$-type cluster is similar to that of the $[Mo_{154}] \equiv [Mo_{11}]_{14}$ cluster, with a mention of the two additional $[Mo_{11}]$ building blocks (Fig. 13b).

The dimensions of the $[Mo_{176}]$ cluster are also somewhat larger: diametre ≈ 4.1 nm, thickness ≈ 1.3 nm and the internal cavity has a diametre of ≈ 2.3 nm.

$[Mo_{248}]$

In 1998, Müller and his team synthesized a new record-sized molecule, which they presented in early 1999 directly in **Nature** [32]. The huge POM cluster has the formula $[Mo^{VI/V}{}_{248}O_{720}H_{16}(H_2O)_{128}]^{16-} \equiv [[Mo^{VI}{}_2O_5(H_2O)_2]_{16}[Mo^{VI/V}{}_8O_{28}H(H_2O)_3Mo^{VI/V}]_{16}[Mo^{VI}{}_{12}Mo^{V}{}_{24}O_{96}(H_2O)_{24}]_2]^{16-}$, abridged as $[Mo_{248}]$ or $[[Mo_{176}][Mo_{36}]_2] \equiv [[Mo_{11}]_{16}[Mo_{36}]_2] \equiv [[(Mo_2)\ (Mo_8)(Mo_1)]_{12}[Mo_{36}]_2]$ (a=b=248; c=1096; M=37635.05, d≈4.1 nm).

Under special conditions, the $[Mo_{176}]$ *giant wheel* even starts growing with the consequence that two (unstable) $[Mo^{VI}{}_{12}Mo^{V}{}_{24}O_{96}(H_2O)_{24}] \equiv [Mo_{36}]$ neutral fragments cover the cavity of the $[Mo_{176}]$ cluster like hubcaps, thus generating the $[Mo_{248}]$ cluster. The two $[Mo_{36}]$ hubcaps are each connected to eight terminal O atoms of the eight $[Mo_2]$ units on both the upper and the lower parts of the ring (Fig. 14). Consequently, the $[Mo_{248}]$ cluster is not a *giant wheel* proper, but rather a *giant wheel*-derived molecular system.

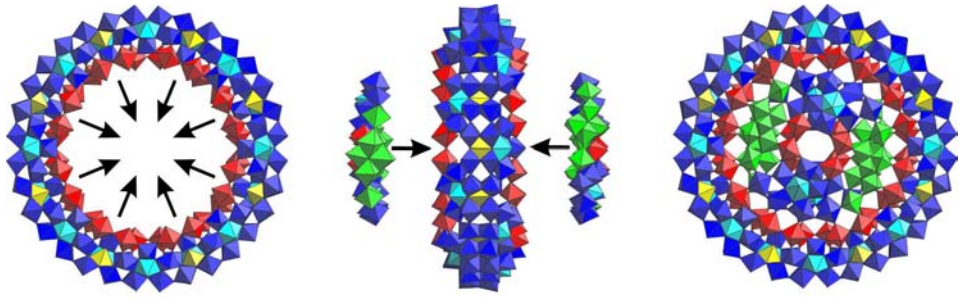

Fig. 14. Schematic view of the relation between the $[Mo_{176}]$ and $[Mo_{248}]$ POM clusters in polyhedral representation. Shown are the $[Mo_{176}]$ cluster viewed from the top (with arrows indicating the pathway of the growth process) (a) and from the side with the two additional $[Mo_{36}]$ fragments acting as hubcaps (b), thus generating the $[Mo_{248}]$ cluster (c). Color code: $[Mo_8]$ units blue (with the central MoO_7 pentagonal bipyramid in blue-turquoise); $[Mo_8]^{**}$ units green; $[Mo_2]$ units red; $[Mo_1]$ units yellow.

$[Ln_{16}As_{12}W_{148}]$

In 1997, Wassermann, Dickmann and Pope [33] reported the synthesis of an amazing new molecule having the formula $[Ce^{III}_{16}As^{III}_{12}W_{148}O_{324}(H_2O)_{36}]^{76-}$, abridged as $[Ce^{III}_{16}As^{III}_{12}W_{148}]$ (a=148; b=176; c=536; M=36181.75; d≈4.0 nm).

Because the place of Ce may also be occupied by other lanthanides (Ln=La, Ce, Nd, Sm) it is rather the case of a series of clusters with the $[Ln^{III}_{16}As^{III}_{12}W_{148}]$ short general formula.

The $[Ln_{16}As_{12}W_{148}]$-type molecule is the only known exception within the new generation of supramolecular POM clusters. All other giant POM molecules are molybdenum oxide-based clusters, while the $[Ln_{16}As_{12}W_{148}]$-type molecule is a tungsten oxide-based cluster. Unlike polyoxomolybdates, the synthesis of polyoxotungstates does not have an abundant library of multifunctional building blocks with a large structural and linking versatility, owing especially to the tendency of W to form (too) strong metal-metal bonds.

That is why, the giant polyoxotungstates are constructed through linking of large fragments originating from Keggin or derived from Keggin structures. But the synthesis of a POM with no less than 148 W atoms/centres (the previous record was of 48 W atoms) was considered a general surprise. Its existence confirms that lacunary polyoxotungstate fragments can be linked by transition metal, lanthanide and actinide ions to form water-soluble polyoxotungstate clusters.

The $[Ln_{16}As_{12}W_{148}]$-type cluster (with only unreduced W^{VI} centres) contains an assembly of 12 α-$[As^{III}W_9O_{33}]^{9-} \equiv [AsW_9]$ trilacunary Keggin units, linked by trivalent Ln cations and additional W atoms into a folded structure of D_{3d} symmetry. The structure is further embellished by five $[W_5O_{18}]^{6-}$ lacunary units. The 16 Ln atoms carry a total of 36 H_2O ligands [33, 34] (Fig. 15).

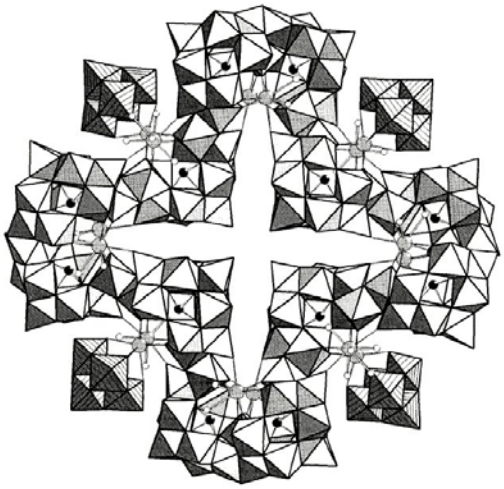

Fig. 15. Structure of the $[Ln^{III}_{16}As^{III}_{12}W_{148}O_{324}(H_2O)_{36}]^{76-} \equiv [Ln_{16}As_{12}W_{148}]$ POM cluster, as a folded cyclic assembly of 12 $[AsW_9]$ groups linked by additional W centres (all shown in polyhedral representation) and four $[LnW_5]$ groups. (Ce(La) large gray spheres; As small black spheres; H_2O small white spheres).

In time, the $[Ce_{16}As_{12}W_{148}]$ molecule was reported between the $[Mo_{154}]$ and $[Mo_{176}]$ *giant wheels*. From the point of view of the first criterion selected by us, i.e. the number of metal centres (a=148), the $[Ce_{16}As_{12}W_{148}]$ cluster was never the record-holder. On the other hand, at the time, it headed the list according to other mentioned criteria, having a number of 176 heavy atoms, a relative molecular mass of 36182 and a diametre of ≈ 4.0 nm.

$[Mo_{368}]$

In November 2001, Müller and his team synthesized and characterized an exceptionally large molecule which was presented to the scientific community a few months later in a paper with the exciting title: *Inorganic Chemistry Goes Protein Size* [35]. The new molecule, with the size of hemoglobine, is a supramolecular POM cluster having the formula $[H_xMo^{VI/V}_{368}O_{1032}(H_2O)_{240}(SO_4)_{48}]^{48-}$ (x≈16), abridged as $[Mo_{368}]$ (a=b=368; c=1880; M=60768.54; d≈6.0 nm). The amazing molecule was also named *nano-hedgehog* or *blue lemon*.

The $[Mo_{368}]$ cluster has been prepared by reducing (with $Na_2S_2O_4$) a molybdate(VI) solution which was acidified with H_2SO_4.

Defining the formal building blocks/units, the $[Mo_{368}]$ cluster can also be formulated as $[H_x[Mo(Mo_5)]^*_8[Mo(Mo_5)]^{**}_{32}[Mo_2]^*_{16}[Mo_2]^{**}_8[Mo_2]^{***}_8\text{-}[Mo_1]_{64}]^{48-}$ (where: x≈16; $[Mo(Mo_5)]^* \equiv [Mo_6O_{21}(H_2O)_6]$; $[Mo(Mo_5)]^{**} \equiv [Mo_6O_{21}(H_2O)_3(SO_4)]$; $[Mo_2]^* \equiv [Mo_2O_3(H_2O)_2]$; $[Mo_2]^{**} \equiv [Mo_2O_{(t)2}O_{(br)3}(SO_4)]$; $[Mo_2]^{***} \equiv [Mo_2O_{(t)4}O_{(br)}(SO_4)]$; $[Mo_1] \equiv [MoO(H_2O)]$; $O_{(t)}$ = terminal oxygen; $O_{(br)}$ = bridging oxygen).

The molecule, which has approximately D_4 symmetry, contains a central $[Mo_{288}O_{784}(H_2O)_{192}(SO_4)_{32}]$ ball-shaped fragment and two $[Mo_{40}O_{124}(H_2O)_{24}(SO_4)_8]$ capping units; thus it can also be formulated as $[[Mo_{288}][Mo_{40}]_2]$ (Fig. 16-18).

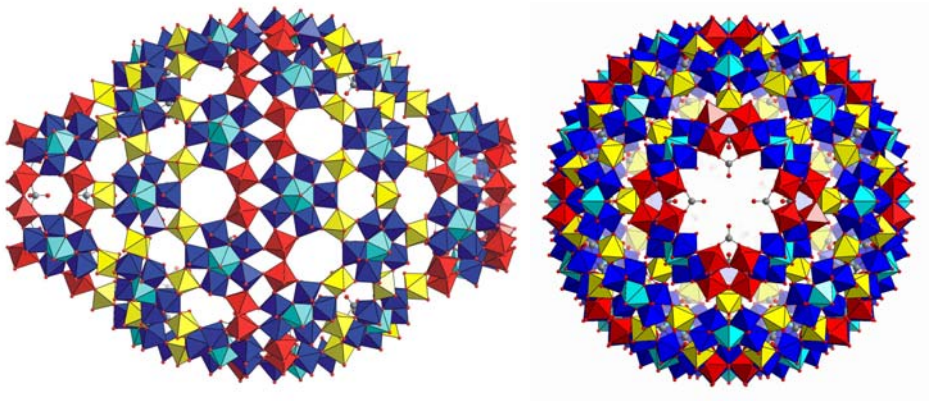

a **b**

Fig. 16. Structure of the $[H_xMo_{368}O_{1032}(H_2O)_{240}(SO_4)_{48}]^{48-} \equiv [Mo_{368}]$ POM cluster in polyhedral representation perpendicular to the C_4 axis (a) and along the C_4 axis (b).
Color code: $[Mo_1]$ units yellow, $[Mo_2]$ units red, $[(Mo)Mo_5]$ units blue (with the central MoO_7 pentagonal bipyramid in blue-turquoise).

The $[Mo_{368}]$ cluster can be considered as a giant container, with a huge cavity (diametre ≈ 2.5x4.0 nm at its most extended points), offering space for about 400 H_2O molecules which are encapsulated.

The two types of $[Mo(Mo_5)]$ units differ in the number and coordination type of the SO_4^{2-} ligands. The three types of $[Mo_2]$ units differ concerning the number of bidentate SO_4^{2-} ligands and of terminal and bridging O atoms. The $[Mo_1]$ units, with only Mo^V centres, are classic and contribute to the highly reduction state of the cluster anion. The other formal Mo^V centres are distributed over several parts of the cluster area, which determines a widespread delocalization of the Mo 4d electrons.

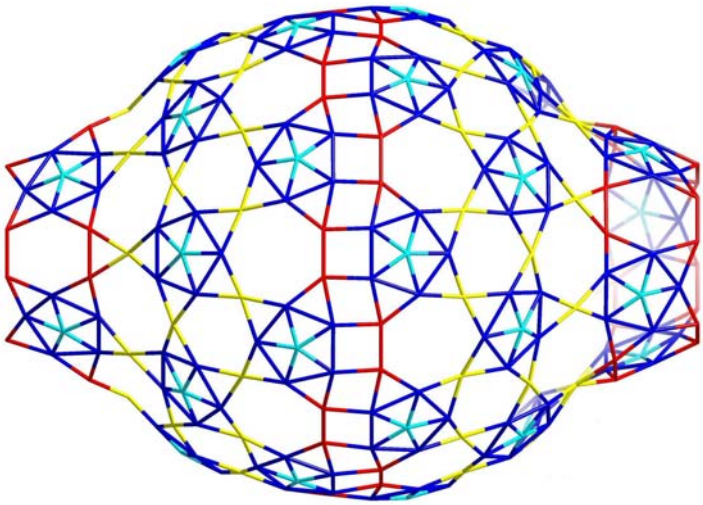

Fig. 17. Structure of the $[H_xMo_{368}O_{1032}(H_2O)_{240}(SO_4)_{48}]^{48-} \equiv [Mo_{368}]$ POM cluster in wire-frame representation perpendicular to the C_4 axis. Color code as in Fig. 16.

The highly reduction state (ca. 256 Mo^{VI} and 112 Mo^V centres) reflects that strong reducing conditions favour molecular growth.

The structure of the $[Mo_{368}]$ POM cluster contains $[Mo(Mo_5)]$ and $[Mo_1]$ units of the $[Mo_{102}]$ *ball*, as well as $[Mo(Mo_5)]$ and $[Mo_2]$ units of the $[Mo_{176}]$ *giant wheel*. Thus, the $[Mo_{368}]$ cluster can be considered a hybrid between the *giant sphere* and *giant wheel*-type clusters.

Having 368 metal centres, no less than 1880 non-hydrogen atoms, a relative molecular mass of 60769 and a diametre of ≈ 6.0 nm, the new $[Mo_{368}]$ POM cluster is the current absolute record-holder in what concerns the largest synthesized molecule with structure determination.

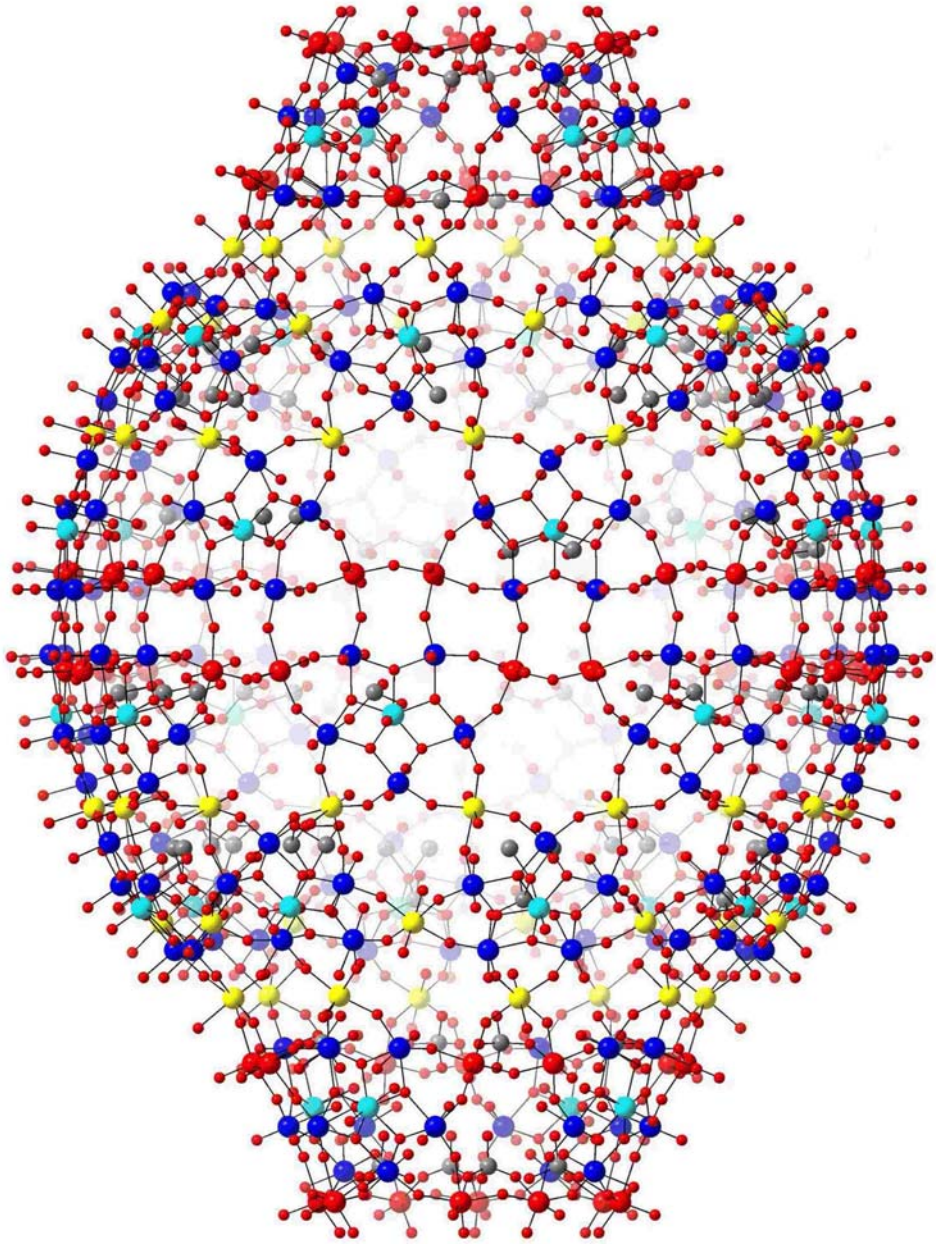

Fig. 18. Structure of the $[H_xMo_{368}O_{1032}(H_2O)_{240}(SO_4)_{48}]^{48-} \equiv [Mo_{368}]$ POM cluster in ball-and-stick representation perpendicular to the C_4 axis. Color code: Mo of the $[Mo_1]$ units yellow; Mo of the $[Mo_2]$ units red; central Mo of the $[(Mo)Mo_5]$ units blue-turquoise; peripheral Mo of the $[(Mo)Mo_5]$ units blue; S grey; O red.

4. CONCLUSIONS

Our survey of the field of the largest synthesized and structurally characterized molecules is almost complete.

The giant molecules, essentially supramolecular POM/metal oxide-type clusters, have reached sizes up to 6 nm, opening new directions and perspectives in a so-called nanoworld.

As a consequence, we have left the domain of classical molecular chemistry and we approach the final limit of supramolecular chemistry, which is localized in a mesocosmic realm, to be found between the micro- and the macroscopic realms. Thus, the new giant POM molecules can be considered true nano-objects of the mesocosmic world.

However, certain questions still need to be addressed: Is the size of such clusters limited or can we construct even larger assemblies? Is the [Mo_{368}] cluster, the current record-holder, the ultimate molecule?

Müller believes that shortly today's record will be surpassed by his research team of Bielefeld or perhaps by another team. He considers that following the novel strategy he has developed molecular growth can continue even farther, up to molecules with over 500 metal centres [36].

The new strategy entails the existence of an adequate library of multi-linkable building blocks which can adapt their shape and size following the boundary conditions, the use of optimal reducing agents and appropriate ligands; this should allow the main fragment to become ever more nucleophile (by increasing the negative charge through reducing metal centres and/or the introduction of negatively charged ligands) thus directing the formation of electrophiles with which it is capped, thereby continuing to grow.

Is Müller's opinion only the expression of the enthusiasm of a very gifted researcher who, carried away like a "sorcerer's apprentice", has obtained results unheard of by chemists 10-20 years ago? Or will the challenge continue and one more time it will be proved that reality is not only beyond what we currently believe, but also beyond what we could imagine?

Acknowledgement: The authors would like to thank Prof. Dr. Dr. h. c. mult. Achim Müller and Dr. Hartmut Bögge for the unstinted support and for providing the figures included in this paper. The authors also would like to thank Prof. Eugene Gergely for the generous help in preparing this paper.

REFERENCES

1. http://www.webelements.com
2. http://www.cas.org/cgi-bin/regreport.pl
3. Lehn, J.M., *Supramolecular Chemistry: Concepts and Perspectives*, VCH, Weinheim, 1995.

4. Haiduc, I, Edelmann, F.T., *Suproamolecular Organometallic Chemistry*, Wiley-VCH, Weinheim, 1999.
5. Pope, M. T., *Heteropoly and Isopoly Oxometalates*, Springer, Berlin, 1983.
6. Keggin, J.F., *Nature*, 1933, **131**, 908.
7. Leyrie, M., Martin-Fr□re, J., Hervé, G., *C. R. Acad. Sci., Ser. C,* 1974, **279**, 895.
8. Robert, F., Leyrie, M., Hervé, G., Tézé, A., Jeannin, Y., *Inorg. Chem.*, 1980, **19**, 1746.
9. Contant, R., Tézé, A., *Inorg. Chem.*, 1985, **24**, 4610.
10. Müller, A., Kögerler, P., *Coord. Chem. Rev.*, 1999, **182,** 3.
11. Müller, A., Kögerler, P., Kuhlmann, C., *Chem. Commun.*, 1999, 1347.
12. Müller, A., Kögerler, P., Bögge, H., *Struct. Bond.*, 2000, **96**, 203.
13. Müller, A., Kögerler, P., Dress, A.W.M., *Coord. Chem. Rev.*, 2001, **222**, 193.
14. Zhang, S., Liao, D., Shao, M., Tang, Y., *J. Chem. Soc. Chem. Commun.,* 1986, 835.
15. Müller, A., Krickemeyer, E., Dillinger, S., Bögge, H., Plass, W., Rohlfing, R., *Naturwissenschaften*, 1993, **80**, 560.
16. Müller, A., Krickemeyer, E., Dillinger, S., Bögge, H., Plass, W., Proust, A., Djoczik, L., Menke, C., Meyer, J., Rohlfing, R., *Z. Anorg. Allg. Chem.*, 1994, **620**, 599.
17. Müller, A., Plass, W., Krickemeyer, E., Dillinger, S., Bögge, H., Armatage, A., Proust, A., Beugholt, C., Bergmann, U., *Angew. Chem. Int. Ed.*, 1994, **33,** 849.
18. Müller, A., Meyer, J., Krickemeyer, E., Beugholt, C., Bögge, H., Peters, F., Schmidtmann, M., Kögerler, P., Koop, M.J., *Chem. Eur. J.*, 1998, **4**, 1000.
19. Yang, W., Lin, X., Lu, C., Zhuang, H., Huang, J., *Inorg. Chem.*, 2000. **39**, 2706.
20. Müller, A., Krickemeyer, E., Bögge, H., Schmidtmann, M., Peters, F., *Angew. Chem. Int. Ed.*, 1998, **37,** 3360.
21. Aldersey-Williams, H., *The Most Beautiful Molecule: The Discovery of the Buckyball*, Wiley, New York, 1995.
22. Müller, A., Patrut, A., *Rev. Chim. (Bucharest)*, 2001, **52** , 289.
23. Müller, A., Sarkar, S., Shah, S.Q.N., Bögge, H., Schmidtmann, M., Sarkar, S., Kögerler, P., Hauptfleisch, B., Trautwein, A.X., Schünemann, V., *Angew. Chem. Int. Ed.*, 1999, **38,** 3238.
24. Müller, A., Shah, S.Q.N., Bögge, H., Schmidtmann, M., Kögerler, P., Hauptfleisch, B., Leiding, S., Wittler, K., *Angew. Chem. Int. Ed.*, 2000, **30,** 1614.
25. Delgado, O., Dress, A., Müller, A., in M.T. Pope and A. Müller (eds.), *Polyoxomatalate Chemistry: From Topology via Self-Assembly to Applications*, Kluwer, Dordrecht, 2001, p. 69.
26. Müller, A., Beckmann, E., unpublished results.
27. Müller, A., Krickemeyer, E., Meyer, J., Bögge, H., Peters, F., Plass, W., Diemann, E., Dillinger, S., Nonnenbruch, F., Randerath, M., Menke, C., *Angew. Chem. Int. Ed.,* 1995, **34,** 2122.
28. Bradley, D., *New Scientist*, November 1995, **148**, 18.

29. Müller, A., Krickemeyer, E., Bögge, Schmidtmann, M., Beugholt, C., Kögerler, P., Lu, C., *Angew. Chem. Int. Ed.*, 1998, **37,** 1220.
30. Müller, A., Koop, M., Bögge, H., Schmidtmann, M., Beugholt, C., *Chem. Commun.*, 1998, 1501.
31. Jiang, C.C., Wey, Y.G., Liu, Q., Zhang, S.W., Shao, M.C., Tang, Y.Q., *Chem. Commun.*, 1998, 1937.
32. Müller, A., Shah, S.Q.N., Bögge, H., Schmidtmann, M., *Nature*, January 1999, **397**, 48.
33. Wassermann, K., Dickmann, M.H., Pope, M.T., *Angew. Chem. Int. Ed.*, 1997, **36,** 1445.
34. Müller, A., Peters, F., Pope, M.T., Gatteschi, D., *Chem. Rev.*, 1998**, 98***,* 239.
35. Müller, A., Beckmann, E., Bögge, H., Schmidtmann, M., Dress, A., *Angew. Chem.*, 2002, **114**, 1210.
36. Müller, A., Private communication, 2002.

STUDIA UNIVERSITATIS BABEŞ-BOLYAI, CHEMIA, XLVII, 1-2, 2002

Dedicated to Professor Ionel Haiduc
on the occasion of his 65th birthday

SOLVENT EFFECTS IN ^{1}H NMR SPECTRUM OF 3-FORMYL-10-METHYL-PHENOTHIAZINE

LUIZA GĂ INĂ [a], CASTELIA CRISTEA[a], IOAN A. SILBERG[a*], TAMAS LOVASZ[a], CĂ LIN DELEANU[b], SILVIA UDREA[b]

[a] *"Babes-Bolyai" University, Faculty of Chemistry and Chemical Engineering, Arany Janos 11, RO-3400 Cluj-Napoca, Romania*
[b] *Institute for Organic Chemistry, Spl. Independentei 202-B, P.O. BOX 15-258, RO-71141, Bucharest, Romania*

ABSTRACT. High resolution NMR spectra were recorded in order to assign the spin-spin couplings pattern of aromatic protons in the 3-formyl-10-methyl-phenothiazine structure. The effect of non polar [D]-chloroform, polar [D_6]-DMSO and magnetically anisotropic [D_6]-benzene solvents upon the chemical shifts of the 3-formyl-10-methyl-phenothiazine protons are discussed.

INTRODUCTION

The structure of 3-formyl-10-methyl-phenothiazine [1,2] was completely assigned using the 400 MHz ^{1}H NMR spectrum, the ^{13}C NMR spectrum together with the DEPT experiment spectrum and the two-dimensional homonuclear (H-H-COSY) and heteronuclear (HMQC and HMBC) experiments spectra.

The registered 2D H-H-COSY spectrum and the registered 2D HMQC spectrum of 3-formyl-10-methyl-phenothiazine are presented in the figure 1 together with the assignments of the protons and the carbon atoms.

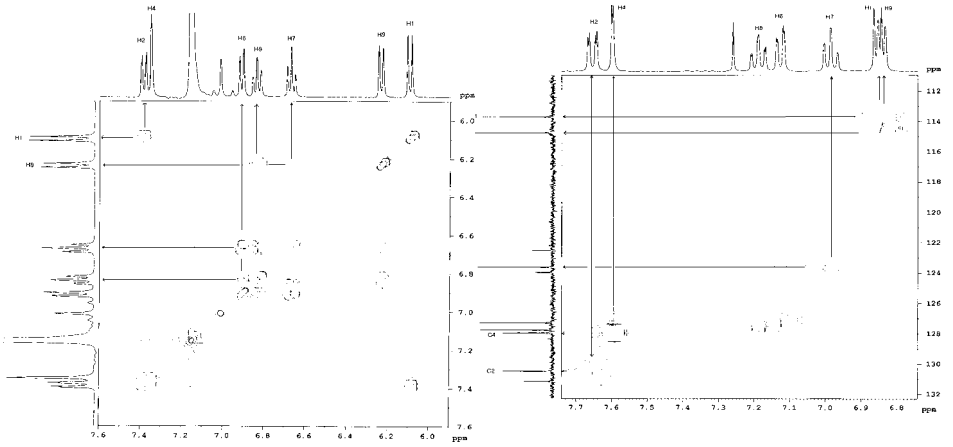

Fig. 1. 400 MHz spectra of 3-formyl-10-methyl-phenothiazine
a) 2D H-H-COSY spectrum in [D_6]-benzene solvent. b) 2D HMQC spectrum in [D]-chloroform.

The examination of the cross peaks presented in figure 1a., shows the couplings between vicinal protons and also the long distance *meta* protons couplings (*orto* coupling constants ^3J values are approximately 8 Hz and *meta* coupling constants ^4J are approximately 1.4 Hz). The correlation between the already assigned protons and the carbon atoms, shown by the cross peaks in the HMQC spectrum presented in figure 1b. made possible the assignment of all the tertiary carbon atoms. The 2D HMBC spectrum was used in quaternary carbon atoms assignments.

RESULTS AND DISCUSSIONS

The 400 MHz ^1H NMR spectrum of 3-formyl-10-methyl-phenothiazine was recorded in: non polar [D]-chloroform, polar [D_6]-DMSO and magnetically anisotropic [D_6]-benzene solvents. The interaction between these solvents and 3-formyl-10-methyl-phenothiazine determined the shifts of the aromatic protons signals as shown in figure 2.

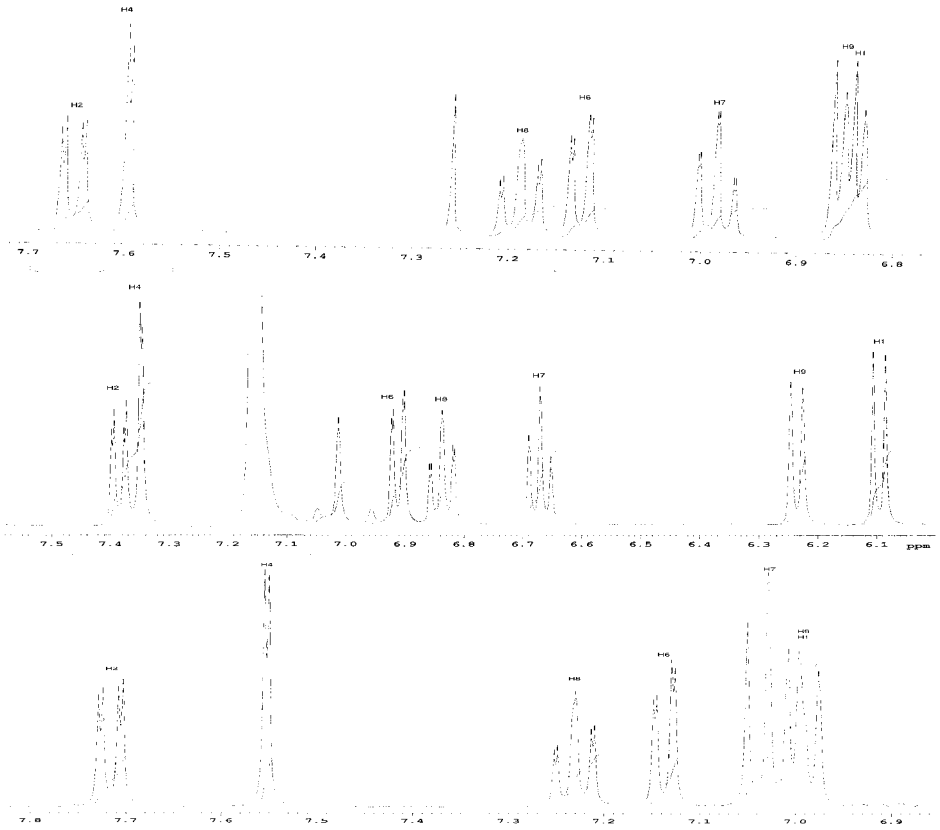

Figure 2. 400 MHz ^1H NMR spectra of 3-formyl-10-methyl-phenothiazine in: 1). [D]-$CHCl_3$; 2). [D_6]-C_6H_6; 3). [D_6]-DMSO

The greater chemical shift values for all the aromatic protons of the studied structure were recorded in the polar DMSO solvent, a fact that might be explained by donor-acceptor relation between the phenothiazine electrono-donor nucleus and the electrono-acceptor DMSO molecules. The less affected chemical shifts were those of protons labeled H_2 and H_4 strongly influenced by the electron withdrawing formyl group situated in their neighborhood.

The magnetic anisotropy of the formyl neighboring group determined the shielding of the H_4 signals as compared to the H_2 signals position, possibly due to a preferential conformation of the structure with respect to the attached formyl group in conjugation with the aromatic nucleus. In figure 3 we describe the spatial anisotropy of the carbonyl double bond, which determined the increased shielding zone near the H_4 proton. As seen in the figure, only a cisoid arrangement of the C=O–C=O system can explain the relative shielding of H_4 and the deshielding of H_2. As the heterocyclic S-atom is expected to experience a slight electron deficit (due to the combined action of the N atom and of the formyl group) this conformation leads to a minimization of the dipolar moment in the α form, as compared to the β form.

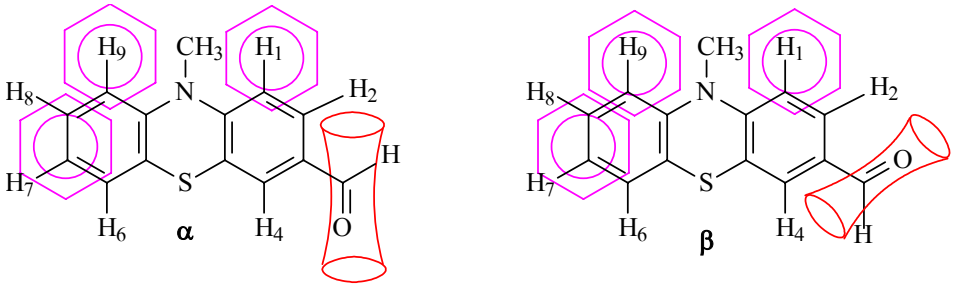

Figure 3. Shielding contributions due to the magnetic anisotropy of carbonyl double bond and benzene solvent molecules.

The interaction between the phenothiazine dissolved molecules and benzene solvent determined the shielding of all phenothiazine protons signals, due to a face to face orientation of the aromatic rings; thus, the phenothiazine protons were situated in the zone of increased shielding due to the induced *ring current* of the benzene nucleus. In figure 3 we described the possible spatial distribution of the benzene molecules, which determined the differenticlly increased shielding zones around the phenothiazine aromatic protons.

CONCLUSIONS

As it can be seen in table 1, which summarizes the recorded chemical shifts for the protons of the 3-formyl-10-methyl-phenothiazine structure in [D]-chloroform, [D_6]-DMSO and [D_6]-benzene solvents, the polar DMSO solvent induced the greater chemical shifts, and in the mean time, an ASIS

effect of benzene solvent determined the smaller induced values. Both the preferred conformation of the formyl group, and the spatial interactions with benzene rings thus determined could give better insights for interpreting drug-receptor relationships in the phenothiazine class.

Table 1.

Chemical shifts for 3-formyl-10-methyl-phenothiazine protons in [D]-chloroform, [D_6]-DMSO and [D_6]-benzene solvents

δ(ppm)	CHO	H_2	H_4	H_8	H_6	H_7	H_1	H_9	NCH_3
$CDCl_3$	9.80	7.65	7.59	7.18	7.12	6.98	6.85	6.84	3.42
DMSO-d_6	9.72	7.71	7.55	7.23	7.13	7.04	7.00	6.98	3.33
C_6D_6	9.55	7.38	7.34	6.91	6.83	6.67	6.23	6.09	2.49

A preferential conformation of the 3-formyl-10-methyl-phenothiazine structure with respect to the attached formyl group in conjugation with the aromatic nucleus was described.

EXPERIMENTAL

400 MHz Bruker NMR

REFERENCES

1. C. Bodea, V. Fă rcă șan, I. Oprean, *Rev. Roum. Chim*., 1965, **10**, (11), 1100-1109
2. V. Fă rcă șan, I. Oprean, C. Bodea, *Rev. Roum. Chim*., 1968, **13**, 647-652

STUDIA UNIVERSITATIS BABEŞ-BOLYAI, CHEMIA, XLVII, 1-2, 2002

Dedicated to Professor Ionel Haiduc
on the occasion of his 65th birthday

THE SYNTHESIS OF NEW PHENOTHIAZINE COMPOUNDS BY THE THIATION OF DIPHENYLAMINO DERIVATIVES

IOAN-DAN PORUMB, CASTELIA CRISTEA, IOAN A. SILBERG

"Babes-Bolyai" University, Faculty of Chemistry and Chemical Engineering, Organic Chemistry Department.

ABSTRACT. The thiation of 1, 3, 5 –*tris*-phenylamino-benzene was studied under various reaction conditions, such as conventional heating and microwaves activation. New 2, 4-diphenylamino-phenothiazine and 6-phenylamino-1,4-benzothiazino[3,2-b]-phenothiazine were thus obtained. Structural assignments were performed using high resolution NMR – spectroscopy.

INTRODUCTION

The first phenothiazine synthesis, reported by Bernthsen more than one century ago [1], was performed by melting the diphenylamine with sulphur at high temperature as shown in scheme 1. Since, many improvements of this method were proposed, due to practical reasons. The use of catalysts such as iodine or $AlCl_3$ [2, 3], inert gas atmosphere [4] and a proper solvent [5, 7] were very effective improvements leading to higher yields and purity of the product.

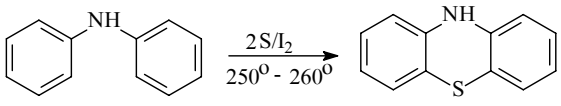

Scheme 1

The thiation of 1,3–diphenylaminobenzene [8] with sulphur in the presence of iodine lead to 1,4–benzothiazino[3,2-b]–phenothiazine [9] as shown in scheme 2:

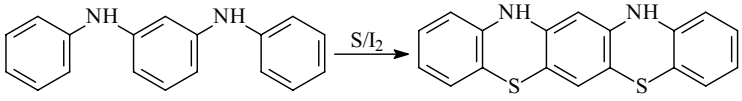

Scheme 2

We studied the thiation of 1,3,5-*tris*-phenylamino-benzene, a reaction which may lead to various phenothiazine derivatives as shown in scheme 3, by a mono, double or triple thiation of the central benzene nucleus of this substrate.

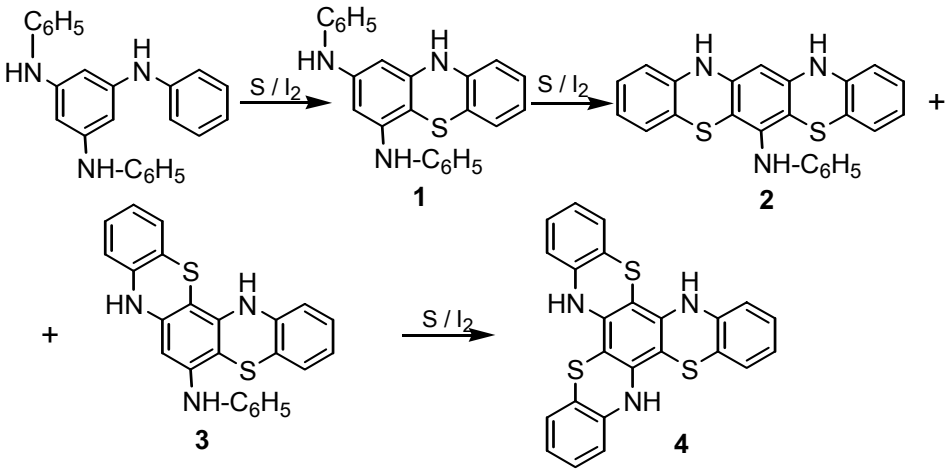

Scheme 3

RESULTS AND DISCUSSIONS

1,3,5-*tris*-phenylaminobenzene, prepared by the condensation of fluoroglucine with aniline using a previously described method [8], was subjected to the thiation reaction under the following conditions:

a) A mixture of 1,3,5-*tris*-phenylaminobenzene and sulphur in 1:6 molar ratio and 1% iodine was heated at 250 – 260°C for 30 minutes.
b) A mixture of 1,3,5-*tris*-phenylaminobenzene and sulphur in 1:6 molar ratio and 1% iodine were heated in 1,2,4-trichloro benzene solvent for 15 minutes.
c) The mixture of 1,3,5-*tris*-phenylaminobenzene, sulphur and 1% iodine were subjected to microwave activation (in a modified domestic microwave owen) under “dry medium” conditions. The reaction was performed with and without dry support. The tested supports were aluminum oxide and acid bentonite (in this later experiment no iodine catalyst was requested).

The main reaction product in all these conditions was 2,4–diphenylamino phenothiazine **1**, as shown in scheme 3.

Structural assignments for compound **1** were performed using the 400MHz ^{1}H-NMR and ^{13}C-NMR spectra together with the 2D correlation spectra: COSY 45

and HETCOR (HMQC and HMBC). Figure 1 shows the 2D homocorrelation COSY 45 spectrum used for the assignement of the spin-spin couplings between aromatic protons of compound **1**.

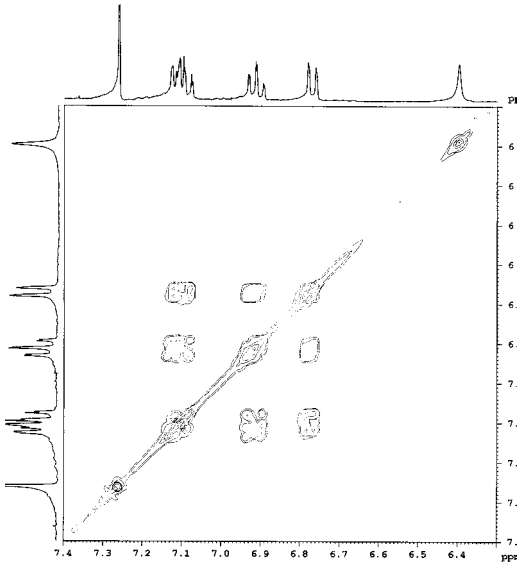

Fig. 1. 400MHz COSY 45 spectrum of compound **1** in $CHCl_3$-d_1

The thiation of 1,3,5-*tris*-phenylaminobenzene with a large excess of sulphur in 1,2,4-trichlorobenzene solvent, under prolonged reaction time, lead to a low yield of 6–phenylamino-1,4–benzothiazino[3,2-b]–phenothiazine **2** (scheme 3).

Structural assignments of this compound were performed using high resolution ^{1}H-NMR spectrum. The linear annelation by this double thiation, similar to the thiation which generated the 1,4–benzothiazino[3,2-b]-phenothiazine, suppressed the possibility of the third thiation of the central benzene nucleus.

Theoretical calculations of the rotational energy for the conformers of 2,4– diphenylamino-phenothiazine involved in the thiation reaction, showed a 10 kcal/mol rotational barrier for the rotation of the substituent at C^4 (conformer involved in the angular annelation) and only 2 kcal/mol rotational barrier for the rotation of substituent at C^2 (conformer involved in the linear annelation), may be due to the sterical hindrance of the sulphur atom of the phenothiazine heterocycle upon the neighboring substituent situated at C^4.

CONCLUSIONS

The thiation of 1,3,5-*tris*-phenylaminobenzene with sulphur in the presence of iodine as catalyst generated 2,4-diphenylamino-phenothiazine **1**, under classical thermal activation. Microwaves activation of this reaction in dry medium presents the same selectivity and it may be considered as a convenient alternative synthetic method for phenothiazine derivatives synthesis.

The thiation of the 2,4-diphenylamino–phenothiazine generated the 6–phenylamino-1,4–benzothiazino[3,2-b]-phenothiazine **2** in low yields under thermal conditions and a presumable steric control of the reaction.

EXPERIMENTAL

Modified domestic microwave owen
400 MHz Brucker NMR spectrometer.

2,4-Diphenilamino-phenothiazine 1

a) 1 mmol 1,3,5-*tris*-phenylaminobenzene, 6 mmols sulphur and one crystal of iodine were melted together in an open vessel; the temperature was maintained at 250 – 260^{o}C for 10 minutes and H_2S evolved. After cooling, the reaction mixture was extracted with acetone. After the solvent evaporation the raw product was recrystallised from xylene.

0,12 g (34 %) **1** with a green color and melting point 195-198^{o}C was obtained. ^{1}H-NMR: 6.4 ppm (s, 2H), 6,7 ppm (d, 4H), 6,9 ppm (t, 4H), 7,1ppm (m, 8H).

b) 1 mmol 1,3,5-*tris*-phenylaminobenzene, 6 mmols sulphur, one crystal of iodine and 4 ml 1,2,4 trichloro-benzene solvent were heated in a round bottom flask equipped with a reflux condenser. At 170^{o}C appeared with effervescence. After cooling the raw product was filtered and recrystallised from xylene. 0,18 g (52 %) **1** were obtained (m.p.=198^{o}C).

c) microwave activated syntheses

-0.17 g 1,3,5-*tris*-phenylaminobenzene, 0.1 g sulphur and 0.01 g iodine were solved in diethyl ether, then 1 g Al_2O_3 was added and the solvent was evaporated under stirring at reduced pressure. The mixture was introduced in a quartz open vessel and exposed to microwaves action for 30 seconds (at 500 W) or 20 seconds (at 750 W). After cooling, the product was extracted with acetone and after solvent evaporation it was recrystallised from xylene. Yields, 0,06g (35%) of **1**, m.p.=195^{o}C.

-0.17g 1,3,5-*tris*-phenylaminobenzene and 0.1 g sulphur were solved in diethyl ether, then 1 g acidic bentonite was added and the solvent evaporated under stirring. The product was obtained after 2 minutes irradiation at 500 W, 23 seconds at 750 W or 2 s at 900 W. (The reaction progress was monitored by thin layer chromatography). The product was extracted with acetone; the solvent was evaporated to dryness and then recrystallised from xylene. 0,05g (yield 26%) **1** were obtained (m. p.= 195^{o} C).

6–phenylamino-1,4–benzithiazino[3,2–b]–phenothiazine 2

0.19 g 2,4-diphenylamino-phenothiazine, 0.2g sulphur and 0.01 g iodine were heated in 4 ml 1,2,4–trichlorobenzene. At 175^{o}C the H_2S was evolved and this temperature was mantained for 30 minutes. After cooling, the dark colored precipitate was filtered and recrystallised from aniline. 0,02g (10% yield) product was obtained as a dark colored powder, which decomposes at temperature higher than 260^{o} C.

REFERENCES

1. A. Bernthsen; *Ber. Dtsch. Chem. Ges.***1883**, 16, 2896
2. F.Ackermann; Ger. Pat., 222, 879, Friedlander, **1911**, 10, 144, cf. S. P. Massie, Chem. Rev. **1954**, 54, 800
3. E. Knoevenagel; *J. Prakt. Chem.*, **1914**, 89, 2
4. Lyle M. Geiger; C. N. Beck; U. S. Pat. 2, 433, 658, 30 Dec. 1947, cf. *C. A*., **1948**, 42, 1974
5. S. P. Massie; P. K. Kadaba; *J. Org. Chem.*,**1956**, 21, 347
6. P. K. Kadaba; S. P. Massie; *J. Org. Chem.,* **1959**, 24, 623
7. H. Wunderlicht; H. Wunderlicht; *Ger., **20***, 104, cf. *C. A*., **1962**, 56, 4777
8. N. P. Büu-Hoi, *J. Chem. Soc.,* **1962**, 4, 4346
9. I. Silberg, C. Cristea, *Heterocyclic Communications* **1996**, 2, 118

ACKNOWLEDGEMENTS

Prof. Dr. I. Silaghi-Dumitrescu, “Babes-Bolyai” University, Faculty of Chemistry and Chemical Engineering, is greatly acknowledged for performing the theoretical calculations of rotamers of 2,4-diphenylamino-phenothiazine.

Dr. C. Deleanu, Spectroteam for Romania, is greatly acknowledged for recording the high resolution NMR spectra.

STUDIA UNIVERSITATIS BABEŞ-BOLYAI, CHEMIA, XLVII, 1-2, 2002

Dedicated to Professor Ionel Haiduc
on the occasion of his 65th birthday

AN IMPROVED SYNTHESIS OF 1,7-DIOXA-4,10-DIAZACYCLODODECANE

CERASELLA AFLOROAEI and MIRCEA VLASSA

"Babeş-Bolyai" University, Faculty of Chemistry and Chemical Engineering,
11 Arany Janos, 3400 Cluj-Napoca, Romania

ABSTRACT. An improved method for preparation of 1,7-dioxa-4,10diaza-cyclododecane is described.

INTRODUCTION

There is a continuing interest in the preparation of diazacoronards which have important uses as macrocyclic molecular receptors as well as being valuable intermediates for the synthesis of cryptands and related compounds[1].The title compound was obtained by classical procedures by reaction of the sodium salt of N,N'-ditosyl-2,2'-diaminodiethyl ether with diethyl glycol ditosylate by Richmon-Atkins method [2,3], α,ω-dicarboxylate esters or with dicarboxylyl dichlorides[4-6]. A similar method uses *o*-carbamoylbenzenesulfonyl group, derived from saccharin, as the nitrogen atom protecting group [7]. N,N'-Ditosyl-2,2'-diaminodiethylether and corresponding dibromide ether were used as starting materials in phase transfer catalysis procedure[8-10].

Taking into consideration the accessibility of starting material, the yields and the work-up of the crude reaction product the more attractive way to obtain compound **1** is Richmon-Atkins method.

RESULTS AND DISCUSSION

Ambel and Dall[3] applied Richmond-Atkins procedure according to the following reaction scheme:

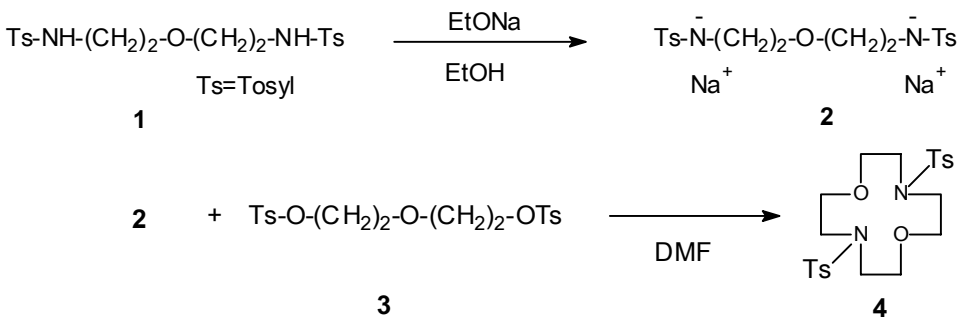

By adding to the disodium salt of N,N'-ditosyl-2,2'diaminodiethyl ether in DMF, the DMF solution of diethyl glycol ditosylate at 100 ^{0}C for 12 h, they obtained compound **4** with 87 %. Preparing this compound by this procedure we noticed that working at 120^{0}C the reaction time can be reduced at 2.5 h and the yield was almost quantitative.

Compound **4** was detosylated by gentle heating in 35% solution of anhydrous hydrogen bromide in glacial acetic solution in presence of phenol:

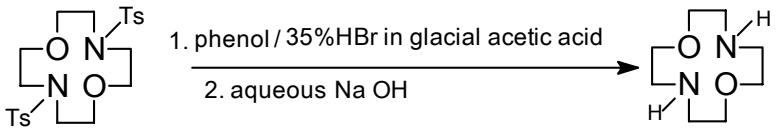

4 **5**

In conclusion with succeeded to improve the previous method of Ambell and Dall[2] obtaining compound **1** in a shorter reaction time, improved yield and a very simple work-up of the reaction product (see experimental).

EXPERIMENTAL

N,N'-Ditosyl-1,7dioxa-4,10-diazacyclododecane. The compound **1** [2] (0.025 mmol) was suspended in dry ethanol (20 mL) and warmed. To this hot suspension a solution of sodium (1.15 g, 0.05 mol) in dry ethanol (30 mL) was added. The mixture was then refluxed for about 20 min and the solvent evaporated under reduced pressure. The dry residue of the sodium salt **2** was then dissolved in DMF (180 mL) and heated at 120^0. A solution of diethyl glycol ditosylate **3** (0.025 mol) in DMF (50 mL) was added over a period of 2 h, keeping the temperature at 120^{0}C. Subsequently the reaction mixture was maintained at the same temperature for 30 min more. Then, after cooling, water was added (250 mL) and the precipitate collected and refluxed in ethanol (50 mL). The ethanolic mixture was filtered hot and the precipitate washed with cold ethanol when compound **4** was obtained almost quantitatively. M.p.= 202-203 (lit. m.p.[2]= 203-204).

^{1}H-NMR ($CDCl_3$), δ : 2.44 (s, 6H, CH_3), 3.25(t, J= 4.5, 8H, CH_2-NH), 3.77 (t, J= 4.8, 8H, CH_2-O), 7.34 (d, J=8.7, 4H), 7.72 (d, J= 8.1 4H). ^{13}C-NMR ($CDCl_3$), δ : 21.46, 50.83, 70. 06, 127.35, 129.72, 135.24, 143. 45.

1,7,-Dioxa-4,10-diazacyclododecane. A mixture of 0.005 mole of the compound **4** and 2 g of phenol in 20 g of 35 % solution of anhydrous hydrogen bromide in glacial acetic acid was stirred at 50 ^{0}C for 24 h. The solution was poured into 700 ml of anhydrous ether and the hydrobromide was extracted with a LiOH aqueous solution. The basic solution was acidulated

and extracted with chloroform (5x50 mL). The combined extracts were dried over anhydrous magnesium sulfate, solvent evaporated *in vacuo* and residue extracted with boiling hexane. After evaporation of the solvent the pure reaction product was obtained. Yield 80%. M.p. = 82-84 (lit. m.p.[2] = 82-84).

^{1}H-NMR ($CDCl_3$), δ : 2.42 (s, 2H, NH), 2.77 (8H, CH_2N), 3. 70 (8H, CH_2O)

REFERENCES

1. J. O. Sutheralnd, *Chem. Soc. Rev.,* **1986**, *15*, 63.
2. E. Richman, T. J. Atkins, *J. Am. Chem.Soc.,* **1974**, *96*, 2268.
3. E. Amble, J. Dale, *Acta Chem. Scand. B.33*, **1979**, 698.
4. J. M. Cowie, H. H. Wu, *Macromolecules*, **1988,** *21*, 2116.
5. D. J. Cram, S. P. Ho, C. B. Knobler, E. Maverick, K. N. Trueblood, *J. Am. Chem. Soc.,* **1986**, *108,* 1989.
6. B. J. Dietrich, J. M. Lehn. J. P. Sauvage, J. Blanzat, *Tetrahedron* , **1973**, *29*, 1629.
7. M. Wang, B. F. Hu, *Youji Xuaxue*, **1989,** *9,* 374; *Chem. Abstr.,*
8. N. G. Lukyanenko, S. S. Basok, L. K. Filonova, *J. Chem. Soc., Pekin Trans. I*, **1988,** 4141.
9. N. G. Lukyanenko, S. S. Basok, L. K. Filonova, *Zh. Org. Khim.*, **1988,** 1731.
10. A. V. Bogatskii, N. G. Lukyanenko, S. S. Basok. L. K. Ostrovskaya, *Synthesis,* **1984**, 138.

STUDIA UNIVERSITATIS BABEŞ-BOLYAI, CHEMIA, XLVII, 1-2, 2002

Dedicated to Professor Ionel Haiduc
on the occasion of his 65th birthday

APPLICATION OF PHASE TRANSFER CATALYSIS IN ACRIDINE SERIES VIII[1]. SYNTHESIS OF 9-(1,2,3-TRIAZOL-1-YL)ACRIDINES

CERASELLA AFLOROAEI, MIRCEA VLASSA

"Babeş-Bolyai" University, Faculty of Chemistry and Chemical Engineering, 11 Arany Janos, 3400 Cluj-Napoca, Romania

ABSTRACT. The syntheses of 9-(1,2,3-triazol-1-yl)acridine derivatives have been achieved by phase transfer catalyzed cyclisation reaction of 9-azidoacridine with either 1,3-dicarbonyl compounds or activated acetonitriles.

INTRODUCTION

Acridine derivatives have attracted the attention of medicinal chemists because of their broad-ranging biological properties[2]. In recent years the DNA binding propensities and topoisomerase II-inhibitory activities of acridines have been exploited in the development of clinically-active antitumor agents[3]. A derivative of a related pyridoacridine, 7-aminopyrido[2,3-c]acridine, has been shown to inhibit human gastric carcinoma MKN 45 cells: the planar aromatic tetracycle is more active than the 5,6-dihydroanalogue[4]. A series of polycyclic aromatic compounds based on 3H-pyrido[2,3,4-kl]acridine have been isolated from natural (marine) sources[5] and also shown to inhibit topoisomerase II.

Julino and Stevens[6] have exploited the Graebe Ullmann degradation[7] to construct 7H-pyrido[4,3,2-kl] acridine ring system using appropriate 9-(1,2,3-triazolyl)acridines as starting materials.

In the course of our project directed towards the development of new anticancer derivatives[8] we now report the synthesis of 9-(1,2,3-triazol-1-yl)acridines from 9-azidoacridine and reactive methylenic compounds using phase transfer catalysis. This route, comparatively with classic procedure[6], has the advantage of using nonanhydrous solvents, a more simple work-out of the reaction products and better yields.

RESULTS AND DISCUSSSION

It is well known that organic azides undergo base-catalyzed condensation reactions with activated methylenic compounds[9]. In order to prepare 9-triazolylacridine derivatives we used commercially available 1,3-dicarbonyl compounds as reaction partners of 9-azido-acridine[10]. When a dichloromethane solution of the azidoacridine **1**, was allowed to react with an excess of pentane-2,4-dione, in presence of tetrabutylammonium bromide (TBAB) as catalyst and of aqueous sodium hydroxide solution at room temperature, the corresponding 9-(1,2,3-triazol-1-yl)acridine **4** were obtained with 80% yield, comparatively with 65% by classical procedure (see Scheme 1).[6]

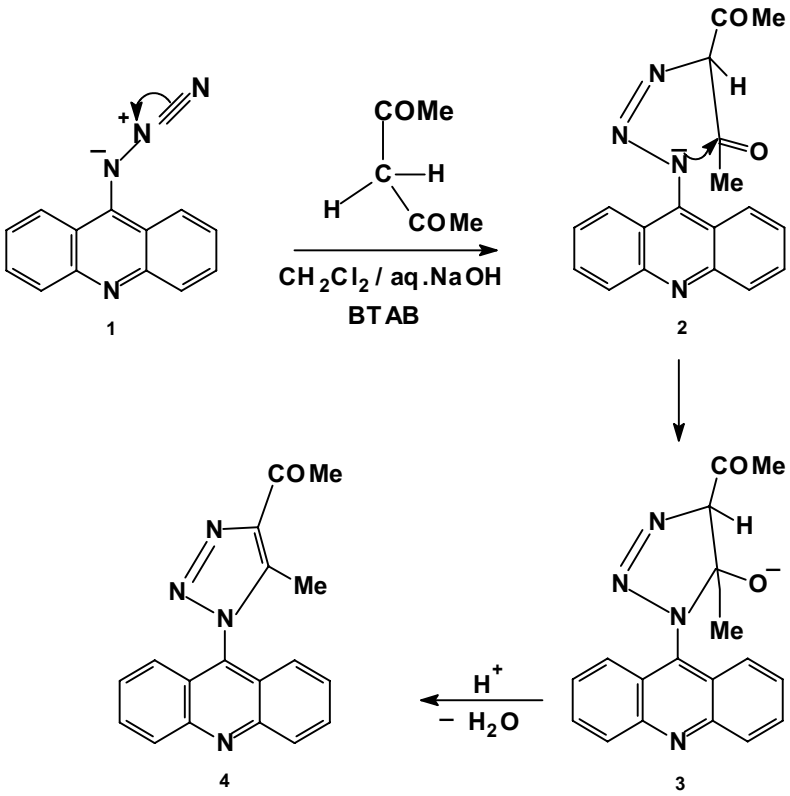

Scheme 1.

In contrast with previous procedure[6] the reaction didn't occur with keto-esters, likely due to the hydrolysis of the ester group.

In order to obtain the amino-substituted triazolylacridines from 9-azidoacridine **1**, activated acetonitriles were employed as the reactive methylenic parts, using the same technique as above (see Scheme 2).

The results of our experiments are shown in Table 1. The reaction is most likely directed by a bonding overlap of the LUMO of 9-azidoacridine and the HOMO of the α-methylene carbon of the carbanions.

Table 1

Compounds **7** prepared by PTC.

Nr. crt.	R	m.p. (lit.m.p.) (^{0}C)	η (lit. η) (%)
1.	- CN	249 –251 (248-250)	60 (47)
2.	- Ph	206-208 (207-209)	90 (76)
3.	-C_6H_4Cl-o	165-167 (167-169)	85 (73)
4.	-$CONC_5H_{10}$	231--233 (230-232)	50(26)

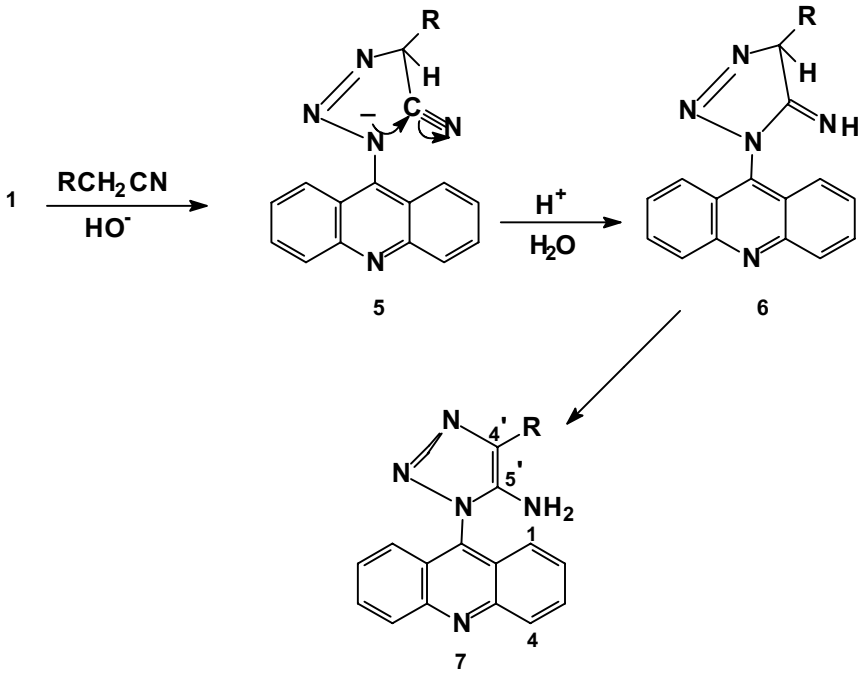

Scheme 2.

CONCLUSIONS

We obtained 9-(1,2,3-triazol-1-yl)- and 9-(amino-1,2,3-triazol-1-yl)-acridines by a more convenient procedure using phase transfer catalysis comparatively with the classical way[6]. Because of hydrolysis reaction of the ester group, the β-keto-esters could not be used as reaction partners in PTC method.

EXPERIMENTAL.

Melting points are uncorrected. The NMR spectra were recorded on Varian Gemini 300 spectrometer, in $CDCl_3$ or in DMSO.

9-(4-Acetyl-5-methyl-1,2,3-triazol-1-yl)acridine. 9-Azidoacridine (165 mg, 0.75 mmol), pentane-2,4-dione (150 mg, 0.75 mmol), and tetrabutylammonium bromide (1.00 molar equivalents) were dissolved in dichloromethane (15 mL). A 40% aqueous solution of sodium hydroxide(15 mL) were added to this mixture and stirred overnight in the dark.The organic layer was then separated, washed with water (3x10 mL), dried on anhydrous $MgSO_4$, filtered and organic solvent removed in vacuo. The precipitate thus obtained was recrystallised from ethylacetate-hexane furnished the triazole **4** as colorless crystals, yield 80%, m.p.=200-202 ^{0} C (lit. 203-205 ^{0}C). ^{1}H-NMR ($CDCl_3$) δ : 2.30 (3H, s, Me),

2.85(3H, s,Me), 7.20 (2H, d, J=8.5), 7.63 (2H, ddd, J=8.5, 6.4 and 1.0),. 7.80 (2H, ddd, J=8.7, 6.4 and 1.2) 8.70 (2H, d, J=8.7). ^{13}C-NMR ($CDCl_3$) δ : 9. 50, 29.00, 122.00, 123.00, 129.00, 130.00, 130.80, 135.00, 143.00, 143.20, 150.00, 194.30

9-(5-Amino-4-cyano-1,2,3-triazol-1-yl)acridine. 9-Azidoacridine (220 mg, 1.00 mmol), malononitrile (73mg, 1.1 mmol), and tetrabutylammonium bromide (1.00 molar equivalents) were dissolved in dichloromethane (25 mL). A 40% aqueous solution of sodium hydroxide(25 mL) were added to this mixture and stirred overnight in the dark.The suspension was filtered and the residue was washed with water and ethanol. the resulting yellow powder was purified by column chromatography on silica gel. Using hexane-diethyl ether (1:2) as eluent, small amounts of impurities were separated. The fraction from diethyl ether furnised the triazole as a lemon yellow powder. Yield 60%. m.p = 249-251(lit. m.p.= 248-250. ^{1}H-NMR, (DMSO-d_6), δ : 7.32 (2H, br, s, NH_2), 7.50 (2H, d, J=8.55), 7.70 (2H, ddd, J=8.6, 6.6, 1.0), 8.00 (2H, ddd, J=8.70, 6.6, 1.2), 8.35 (2H, d, J=8.6). ^{13}C-NMR (DMSO-d_6),δ : 101,00, 113.80, 122.73, 122.70, 129.00, 129,70, 131.00, 134.35, 149.30, 151.00.

9-(5-Amino-4-phenyl-1,2,3-triazol-1-yl)acridine. 9-Azidoacridine (220 mg, 1.00 mmol), phenylacetonitrile (1.17g, 10 mmol), and tetrabutylammonium bromide (1.00 molar equivalents) were dissolved in dichloromethane (15 mL). A 40% aqueous solution of sodium hydroxide were added to this mixture and stirred overnight in the dark. The precipitate was collected and washed with water and hot methanol to give the triazolylacridine as a bright yellow powder. Yield 90%, m.p.=206-208 ^{0}C(lit.m.p.= 207-209 ^{0}C).^{1}H-NMR, (DMSO-d_6), δ: 6.10 (2H, br s, NH_2), 7.35(1H, tt, J=7.4, 1.20), 7.43-7.52(4H,m), 7.70 (2H, ddd, J=8.7,6.6, 1.1), 7.90-8.00 (4H,m), 7.70 (2H, ddd, J=8.6,1.2, 1.0), 7.90-8.01 (4H, m), 8.35 (2H, ddd, J=8..5, 1.2, 1.0). ^{13}C-NMR, (DMSO-d_6) δ : 123.00, 123.10, 125.00, 126.00, 126.50, 128.40, 129.00, 129.80, 131.10, 132.10, 135.120, 142.40, 149.50.

9-[5-Amino-4-(4-chlorophenyl)1,2,3-triazol-1-yl]acridine. The compound was prepared as above using o-chlorophenylacetonitrile (10.0 mmol) and was obtained as a yellow crystalline powder. Yield =85%, m.p.= 165-167 ^{0} C (lit. m.p.= 167-179 ^{0}C). ^{1}H-NMR, (DMSO-d_6), δ: 5.90 (2H, br s, NH_2), 7.50-7.68 (5H, m), 7.70-7.80 (3H,m), 7.90 (2H, ddd, J=8.6, 6.7, 1.3), 8.40 (2H,d, J=8.6). ^{13}C-NMR, (DMSO-d_6), δ: 123.oo, 123.45, 124.80, 127.50, 128.45, 129.50, 130.00, 150.50, 131.20, 132.40, 133.40, 136.20, 143.60, 149,40.

9-[5-Amino-4-(piperidin-1-ylcarbamoyl)1,2,3-triazol-1-yl]acridine. 9-Azido- acridine (220mg, 1.00 mmol), 2-cyanoacetylpiperidine (167g, 1.10 mmol), and tetrabutylammonium bromide (1.00 molar equivalents) were dissolved in dichloromethane(15 mL). A 40% aqueous solution of sodium hydroxide were added to this mixture and stirred overnight in the dark. The precipitate was collected and washed with water and hot methanol to give the triazolylacridine

as a yellow powder. Yield 50%, m.p.=231-233 ^{0} C(lit.m.p.= 230-232 ^{0}C).^{1}H-NMR, (DMSO-d_6), δ: 1.70 (6H, br), 4.10 (4H, br), 6.50 (2H, d, J=9.0), 7.55 (2H, d, J=8.8), 7.70 (2H, ddd, J= 8.5, 6.6, 1.3), 8.00 (2H, ddd, J= 8.8, 6.6, 1.5), 8.40 (2H, d, J=8.8). ^{13}C-NMR, (DMSO-d_6), δ: 25.50, 25.90, 122.60, 128.00, 129.50, 130.80.

REFERENCES

1 M. Vlassa, C. Afloroaei, N. Dulămiță, P. Brouant, J. Barbe, *Heterocyclic Commun.*, **1999**, 5, 51.

2. A. Albert, The Acridines, 2nd edn., Edward Arnold (Publishers), Ltd., London, 1966.
3. G.J. Finaly, J.-F. Riou, B.C. Baguely, *Eur. J.Cancer., Part A.* **1996**, 32, 708.
4. P. Groundwater, M.A. Munawar, *J.Chem.Soc., Perkin Trans*.1, **1997**, 3381.
5. L.A. McDonald, G. S. Eldredge, L. R. Burrows, C. M. Ireland, *J. Med. Chem.*, **1994**, 37, 3819.
6. M. Julino, M.F.G. Stevens, *J. Chem. Soc., Perkin Trans.,***1998,** 1, 1677.
7. C. Graebe, F. Ullmann, *Liebigs Ann. Chem..,* **1986,** 291, 16.
8. C. Afloroaei, N. Dulămiță, M. Vlassa, J. Barbe, P. Brouant, *J. Heterocyclic. Chem.,* **2000**, 37, 1289.
9. O. Dimroth, *Chem. Ber.*, **1902**, 35, 4041; J. R. E. Hoover, A. R. Day, *J. Am. Chem. Soc.*, **1956**, 78, 5832; R. L. Tolman, C. W. Smith, R. K. Robins, *J. Am. Chem. Soc.*, **1972**, 94, 2530, E. Lieber, T. S. Chao, C. N. R. Rao, *J.* Org. Chem., **1957**, 22, 654; H. Wamhoff, W. Wambach, *Chem.-Ztg.*, **1989**, 113, 11; C. E. Olsen, C. Pederesn, *Tetrahedron Lett.*, **1968**, 3805.
10. M. Vlassa, I. Goia, M. Kezdi, Romanian Patent **1978**, 67301; *Chem.Abstr.* **1980,** 93, 204473 m.

STUDIA UNIVERSITATIS BABEŞ-BOLYAI, CHEMIA, XLVII, 1-2, 2002

Dedicated to Professor Ionel Haiduc
on the occasion of his 65th birthday

STUDY OF ACETYLATION ON TERPINEN-4-OL. SYNTHESIS OF THE 4-TERPINENYL-ACETATE

ERIKA KOZMA and IOAN CRISTEA*

* *Department of Organic Chemistry, "Babeş-Bolyai" University, 11 Arany Janos, 3400 Cluj-Napoca, Romania, Fax: 40-264-190818, E-mail: cristea@chem.ubbcluj.ro*

ABSTRACT. The reaction of terpinen-4-ol with acetic anhydride in acid or basic medium was reinvestigated. Details on the structure of the ester was established by spectroscopic methods (^{1}H-NMR and mass spectroscopy).

INTRODUCTION

Terpinen-4-ol and its acetate are natural monoterpenic compounds, used as odorants in cosmetic industry. There are many methods for separation and purification of the terpinenyl acetate[1-8], but only one method[9] concernes the synthesis of this compound and requires the treatment of terpinen-4-ol with acetic anhydride and sodium acetate in xylene by refluxing the reaction mixture for 24 hours.

Since 4-terpinenyl acetate is very important in cosmetic industry, we reinvestigated the acetylation of terpinen-4-ol.

RESULTS AND DISCUSSION

We made a study concerning the transesterification reaction of terpinen-4-ol using t-butylacetate, ethylenglycol diacetate, boron triacetate as transacetylation agents. The obtained yields in ester were very low, under 30%. Because of these unsatisfactory results, we investigated the direct acetylation reaction of terpinen-4-ol with acetic anhydride in acid and basic catalysis.

Basic catalysis

The acetylation reaction in basic catalysis was performed through alcoxide intermediate. Terpinen-4-ol was treated with NaH in anh. benzene to lead the sodate intermediate. We choosed this way for obtaining the ester, because the alcoxide intermediate is better nucleofile than the alcohol in reaction with acetic anhydride.

In this reaction, the ester **2** was obtained in 61% isolated yield with 68% conversion by using equimolar amounts of starting materials (see experimental part). The low conversion and yield is explained by lower nucleophilicity of alcoxide due to the sterical hindrance of isopropyl group.

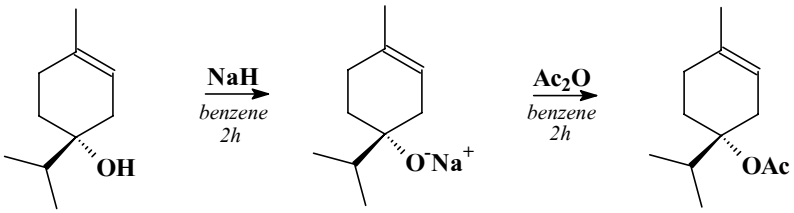

Scheme 1.

The acetylation in basic catalysis was also performed with acetic anhydride in pyridine in 65% yield (50% conversion) or acetic anhydride and sodium acetate in 52% yield (45% conversion).

Acid catalysis

The acetylation reaction with acetic anhydride in acid catalysis was performed at room temperature using equimolar amounts of starting materials, in presence of different acid catalysts: $HClO_4$, H_2SO_4, p-TsOH, H_3PO_4. The reaction was monitorized by GC-MS analysis, using a 20m siliconic capillary column. The reaction conditions and the distribution of reaction products are presented in Table 1. As shown in table 1, it was obtained smaller quantities of ester (30% yield in $HClO_4$ and 31% yield in H_2SO_4) in the presence of strong acids ($HClO_4$, H_2SO_4). In this reaction α- and γ-terpinens were obtained as major products (yields around 30% for **3** and 20% for **4**), by dehydration of terpinen-4-ol in acid catalysis (see Scheme 2). Good results were obtained using H_3PO_4 as catalyst.

The acetylation reaction in presence of H_3PO_4 was studied at different concentrations of acid and monitorized by GC-MS analysis (see table 2).

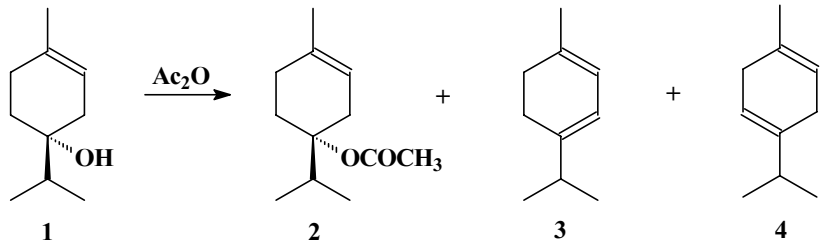

Scheme 2.

The best results were obtained at 0.1M concentration of H_3PO_4, when the concentration in ester was 72% in final reaction mixture (by gas chromatography analysis, see fig. 1).

Table 1.

Acetylation of **1** with Ac_2O in acid catalysis [a]

Acid catalyst	Alcohol unreacted (%)[b]	Products (%)[b]		
		2	**3**	**4**
$HClO_4$	1.5	30.5	30.0	20.0
H_2SO_4	4.2	31.5	32.0	18.0
p-Ts-OH	16.5	51.2	15.4	10.6
H_3PO_4	24.1	66.1	6.1	3.4

[a] All experiments were performed using equimolar amounts of starting materials at room temp. for 24 hours. Acid catalyst [c]=0.05M

[b] Analyzed by gas chromatography

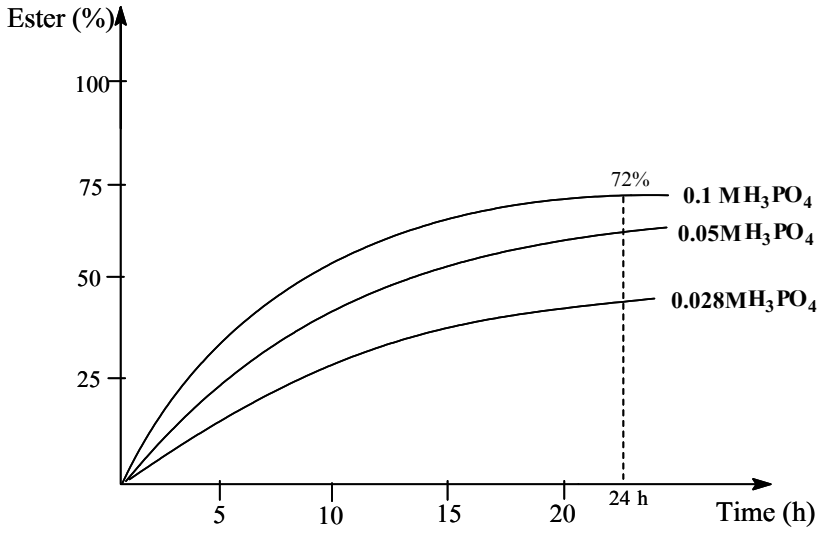

Figure 1. Variation of ester concentration at different concentrations of H_3PO_4

Terpinen-4-ol reacts in benzene at room temperature with acetic anhydride in the presence of 0.1M H_3PO_4 as catalyst to lead to acetate **2** in 90% yield and 82% conversion, analysed by gas-chromatography (see table 2).

The structure of ester **2** was confirmed by ^{1}H-NMR (see Fig. 2) and mass spectroscopy.^{1}H-NMR spectrum of compound **2** displays the caracteristic peaks for isopropyl group (position 4), methyl group (position 1) and methyl from ester group. Both methyls of isopropyl group are shown as doublet at δ=0.92 ppm (6H, J=7 Hz) and the proton from CH appears as heptet at δ=2.75 ppm (1H, J=7 Hz). The methyl group from position 1 shows as a singlet at δ=1.68 ppm and the methyl from the acetoxy group as a singlet at δ=1.98 ppm. The vinylic proton from position 2 is shown at δ=5.25 ppm as unresolved

multiplet. The chemical shifts for the equatorial and axial protons (positions 3, 5, 6) of the cyclohexane ring will be resolved by homo- and heteronuclear NMR studies.

Table 2.

Acetylation of **1** with Ac_2O in various concentrations of H_3PO_4 [a]

Time (h)	H_3PO_4 0.028M		H_3PO_4 0.05M		H_3PO_4 0.1M	
	Alcohol[b]	Ester	Alcohol	Ester	Alcohol	Ester
2	88.5	6.9	82.0	10.5	78.1	11.2
4	81.0	12.5	71.0	18.0	67.0	22.5
6	75.5	17.2	62.0	27.5	57.5	31.0
8	71.0	22.0	55.2	35.0	50.0	39.1
10	67.0	25.5	49.1	41.3	42.7	46.1
14	61.2	31.0	38.5	51.0	31.2	57.4
18	57.1	34.8	30.5	59.0	22.5	66.1
24	54.0	39.1	24.0	66.1	18.0	72.1

[a] All experiments were performed using equimolar amounts of starting materials at room temp. for 24 hours

[b] Analyzed by gas chromatography

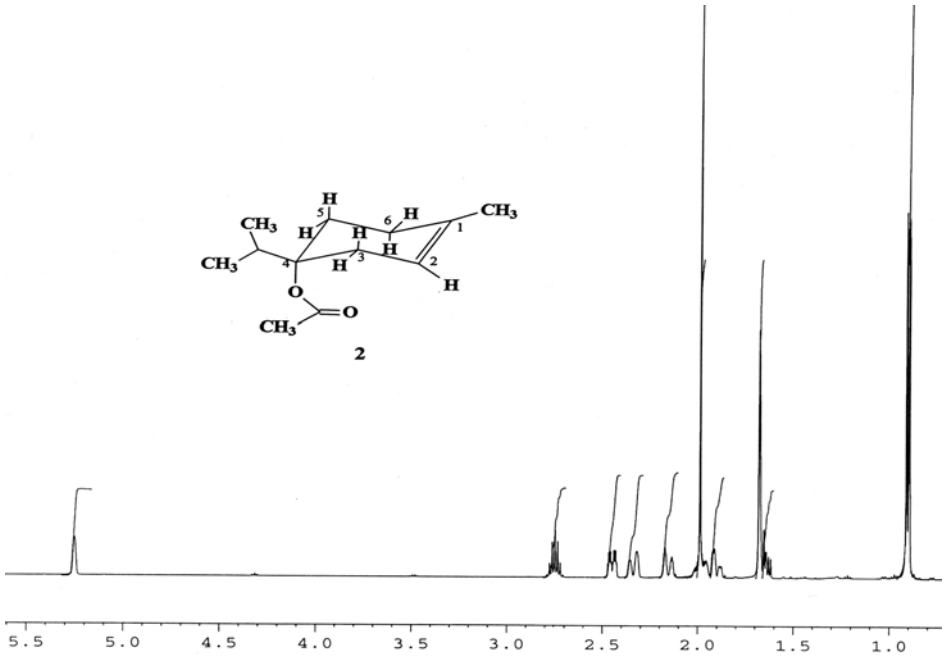

2

Figure 2. ^{1}H-NMR spectrum of 4-terpinenyl-acetate

Gas chromatography-mass spectroscopy analyses confirmed the structure of terpinenyl-4-acetate. The main peak (100%) shown as m/e=93 and its formation requires the lost of acetic acid (m/e=136, 40%) and also an isopropyl group. Another important peak appears at m/e=121 (60%) due to an acetic acid and methyl group lost.

EXPERIMENTAL

Gas chromatography-mass spectroscopy (GC-MS) coupling analyses were performed on a Hewlett-Packard 5890 (GCL)-5972 (MSD) using a HP-5MS 20m x 0.25 x 0.25 μm capillary. ^{1}H-NMR spectra were recorded using $DMSOd_6$ as solvent with a 300 MHz Varian spectrometer. The reactions were also monitored by TLC using Merck plates and pethroleum ether:ethyl ether 5:1 as eluent. Terpinen-4-ol was purchased from Aldrich.

Acetylation in basic catalysis

2.4 g NaH (50%, 0.05 mole) and 100 ml benzene was refluxed for 0.5 hour and than 7.7 g terpinen-4-ol (0.05 mole) was dropwise added. The reaction mixture was refluxed for 1 hour and than acetylated by adding 5.1 ml acetic anhydride (0.05 mole) and heating under reflux for an additional 2 hours. After the reaction time was expired, the final product was washed with water, aqueous sodium carbonate solution and again with water, and than the separated organic layer was dried over Na_2SO_4 anh.. After removal of benzene under reduced pressure, it was obtained a residual oil (8 g which represents 68% ester and 32% unreacted terpinen-4-ol, by GC-analyses). A part of this residual oil (2g) was chromatographed on silicagel (80 g) using pethroleum ether : ethyl ether 5:1 as eluent and gave 1.5 g ester (61.2% yield).

Acetylation in acid catalysis

A mixture of 3.2 g (0.02 mole) terpinen-4-ol, 10 ml benzene, 3 ml of acetic anhydride and 3 ml solution (10% H_3PO_4 in acetic anhydride) was stirred at room temperature for 24 hours. The reaction mixture was then washed with water, aqueous sodium carbonate solution and again with water. The aqueous phase discarded and the benzene solution dried over anhydrous sodium carbonate. After removal of the benzene under reduced pressure, the residual oil (4g) was chromatographed on silicagel (80 g). Elution with pethroleum ether: ethyl ether (5:1) gave two main fractions, A (3.2 g, 80% isolated yield) and B (0.8 g, 20%, unreacted terpinen-4-ol).

Compound A (terpinenylacetate), pale yellow oil; b.p.=71-73^0(1.3mm), n_D^{25}=1.4623. ^{1}H-NMR, δ(ppm): CH_3 (6H, d, 0.9); CH_2 (H_{5ax}, dd, 1.6; H_{5ec}, m, 1.9); CH_3 (3H, s, 1.6); CH_3CO (3H, s, 2.0); CH_2 (H_{6ax}, dd, 1.9; H_{6ec}, dd, 2.45); CH_2 (H_{3ax}, dd, 2.25; H_{3ec}, dd, 2.35); CH(1H, hept., 2.75); CH(1H, s, 5.25). GC-MS, m/e(%): 136(40%), 121(60%), 93(100%), 43(25%).

REFERENCES

1. F.V. Goi, *Izv.Vysshikl Uchebn. Zaravedenii, Pishchevaya Tekhnol.,* 1962, **2**, 46
2. L.A. Ignatova, G.A.Tolstikov, *Zh.Prikl.Khim.,* 1964, **37(6)**, 1389
3. F. Porsch, H. Farnow, H. Winkler, *Dragoco Rept.,* 1965, **12(3)**, 47
4. F.M. Couchman, E.V. Rudloff, *Can.J.Chem.*, 1965, **43(5)**, 1017
5. F.H.L. Van Os, *Pharm.Weekblad*, 1965, **100(12)**, 377
6. E. Kugler, E. Kovacs, *Helv.Chim.Acta*, 1963, **46**, 1480
7. T. Heide, *Fresenius Z.Anal.Chem.*, 1968, **236(1)**, 215
8. T. Heinrich, G. Schuster, *Deut.Apoth.-Ztg.*, 1968, **108(42)**, 1608
9. T. Suga, E. Von Rudloff, *Can.J.Chem.*, 1969, **47(19)**, 3682

STUDIA UNIVERSITATIS BABEȘ-BOLYAI, CHEMIA, XLVII, 1-2, 2002

Dedicated to Professor Ionel Haiduc
on the occasion of his 65th birthday

KINETICS AND MECHANISM OF P-XYLENE OXIDATION BY Ce(IV) IN AQUEOUS ACIDIC MEDIUM

CLAUDIA GEMMA MUREȘANU[1], GABRIELA-CRISTINA BUCȘA[2], IOAN BÂLDEA[3]

Faculty of Chemistry and Chemical Engineering, "Babeș-Bolyai" University of Cluj, 11 Arany Janos Str., 3400-Cluj-Napoca, Romania.
E-mail: [1]muresanu@chem.ubbcluj.ro; [2]gbucsa@chem.ubbcluj.ro; [3]ibaldea@chem.ubbcluj.ro

ABSTRACT. The oxidation of p-xylene by Ce(IV) in aqueous acidic media has been followed spectrophotometrically in a reaction mixture containing $HClO_4$ and $NaClO_4$. The effects of p-xylene and hydrogen ion concentration on the reaction rate have been studied. The kinetic study revealed a two-stage process. The experimental rate law exhibits a first-order dependence on Ce(IV) concentration and a complex dependence on p-xylene and hydrogen ion concentrations. Apparent activation parameters were also calculated. A reaction mechanism involving the formation of an adduct between p-xylene and Ce(IV) in the first step was suggested. The adduct is the subject of an inner electron transfer, in the next step, in order to yield the products.

Keywords: cerium, p-xylene, kinetics

Cerium is a strong oxidizing agent due to its relatively high oxidation potential in acidic media[1]. Although it is a widely used as oxidizing agent in analytical and inorganic chemistry, less attention has been given to its use to oxidize in organic compounds[2]. Nevertheless, the oxidation of different types of organic compounds is mentioned in literature and the kinetics of such reactions has been studied.[3-19] The rate laws and mechanisms for the oxidation of toluene and some substituted toluenes in aqueous sulphuric acid media are reported [20, 21, 22], and in the case of p-xylene oxidation with Ce(IV), the activation energy has been determined [21]. In order to get more details concerning the kinetic and the mechanism of p-xylene oxidation, we have investigated this reaction in perchloric acid medium, where no complex formation between Ce(IV) and ClO_4^- is to be expected.

EXPERIMENTAL

The chemicals used in this study were of reagent grade purity and came from commercial sources (Reactivul Bucuresti, Merck and Fluka). There were used without further purification.

Kinetic measurements were performed by means of a V-530 Able Jasco spectrophotometer, provided with a temperature jacket surrounding the cell holder. The jacket was connected to a Lauda M20 recirculatory water bath. Reaction mixtures were prepared directly in the quartz cell of the spectrophotometer with the path length of 5 cm. The reaction was started by adding a measured amount of cerium stock solution over the reaction mixture ($HClO_4$, $NaClO_4$, p-xylene and twice-distilled water). The reaction was followed by monitoring the decrease of absorbance at 315 nm, where the UV/VIS spectrum of Ce(IV) exhibits a maximum.

RESULTS AND DISCUSSIONS

The stoechiometry of the reaction has been determined by a spectrophotometrical titration.

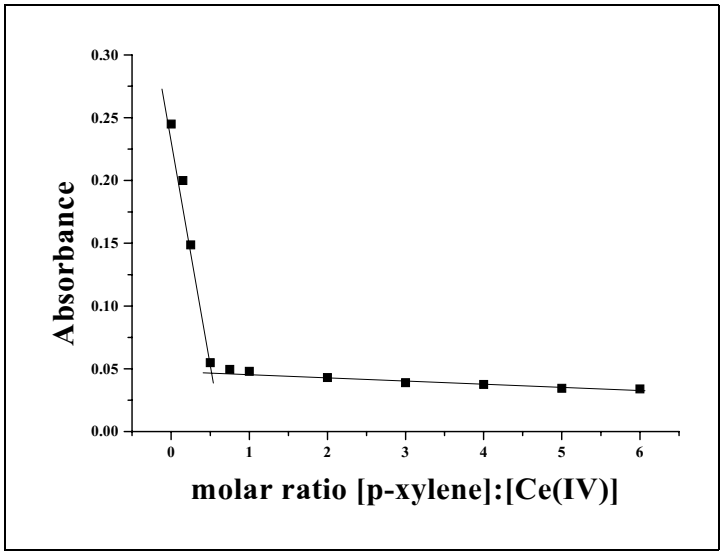

Figure 1. Determination of reaction stoechiometry

Various mixtures having increasing ratios of [p-xylene]:[Ce(IV)] were allows to react to completion at a constant acidity. The absorbance of the unreacted Ce(IV) were determined. The plot of absorbance difference between blank probe and those with p-xylene shows a turning point at the ratio 0.5, as can be seen in figure 1. It predicts the stoechiometry of 2 Ce(IV) for a molecule of p-xylene, indicating the oxidation to p-methylbenzylic alcohol.

Absorbance readings were processed according to the integrated form of a first-order rate law:

$$\ln(A - A_\infty) = k_{obs2}t \quad (1)$$

where: A_∞ ,A are the measured values of absorbance at the end and at different time moments of the reaction.

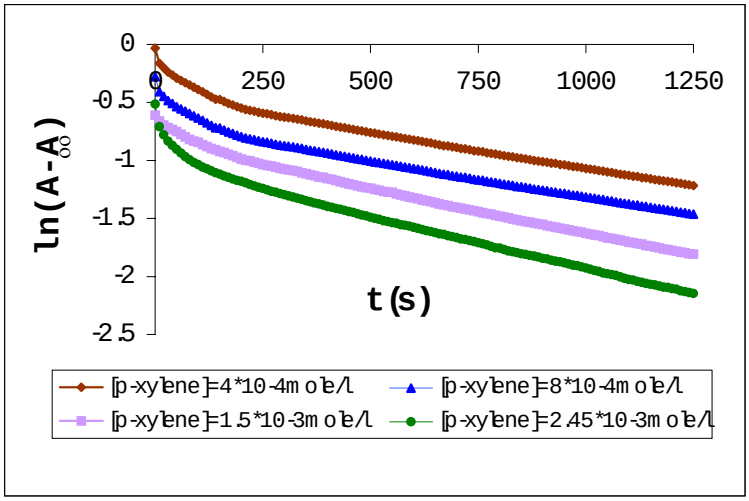

Figure 2. First order dependence for the oxidation reaction between p-xylene and Ce(IV); [Ce(IV)] = $8*10^{-5}$ mol/l; [H^+] = 1 mol/l; j = 2 mol/l; t = 40^0C

First – order semilogarithmic plots obtained, in the presence of an excess of p-xylene, at constant hydrogen ion concentration and constant ionic strength, are presented in figure 1. The initial part of the plots exhibits a curvature, followed by a linear dependence, characteristic to a first – order process, up to 90% of reaction. The bi-phasic character of the plot may be associated with the presence of two first-order successive stages.

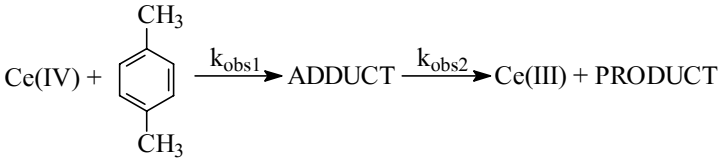

(2)

The first stage, perceptible at the beginning of transformation, could be attributed to the formation of an adduct between Ce(IV) and p-xylene. The second stage, perceptible at higher degrees of transformation, may be associated with oxidation by inner electron transfer yielding the products of the reaction.

As can be seen from the linear dependence lg (r) = f lg([Ce(IV)]) (Fig. 3), the reaction order with respect to Ce(IV) is one, either for the first or the second stage of the reaction.

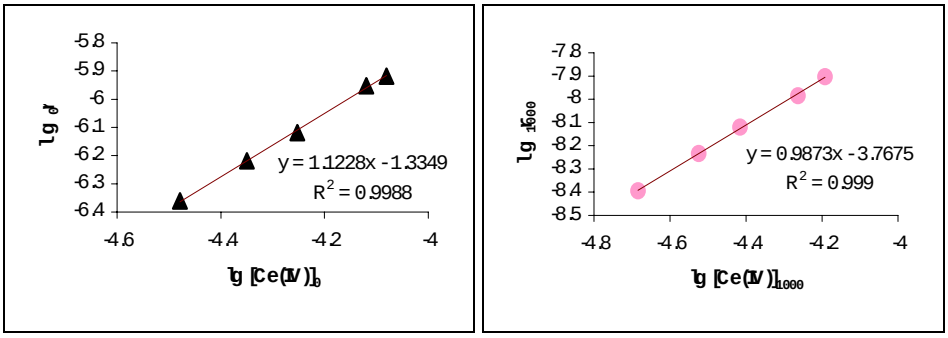

a) in the first stage b) in the second stage

Figure 3. Determination of reaction order with respect to cerium in the two stages of the reaction described above

The A = f (t) curves were the subject of derivation, at the initial moment and at t = 1000s, while the reaction rates and the corresponding concentrations of cerium were calculated by taking ε = 4039 M^{-1} cm^{-1}.

Once it was established, that both stages are first-order, we preferred to determine the rate constants by a non – linear fitting of the A = f (t) curves, with the biexponential:

$$A - A_\infty = C_1 \cdot \exp(-k_{obs1} \cdot t) + C_2 \cdot \exp(-k_{obs2} \cdot t) \qquad (3)$$

which describes the decay of the absorbance of the limiting component in a first order follow up reaction. A and A_∞ have the same meaning as in relation (1), C_1 and C_2 are constants including the molar absorbance coefficients of the absorbing species and k_{obs1} and k_{obs2} are apparent rate constants of the two reaction steps.

The effect of p-xylene concentration, always in large excess, upon the apparent rate constant at constant hydrogen ion concentration and ionic strength is presented in Table 1.

Table 1

Effect of p-xylene concentration on the apparent rate constants.
$[Ce(IV)]=8\cdot10^{-5}M$; $[H^+]=1M$; j =1M; $t=40^0C$

$10^4 \cdot [p\text{-xylene}]_0$ (mol/l)	4	6	8	10	15	24.5
$10^3 \cdot k_{obs1}$ (s^{-1})	4.50	5.24	6.21	6.60	7.79	10.05
$10^4 \cdot k_{obs2}$ (s^{-1})	3.69	4.92	5.50	6.29	7.37	8.00

In order to find the reaction order with respect to the p – xylene concentration, the logarithms of the apparent rate constants were plotted against the logarithms of p – xylene excess.

We obtained an order about 1 with respect to p – xylene for the first stage and an order near to 0.5 for the second stage of the reaction.

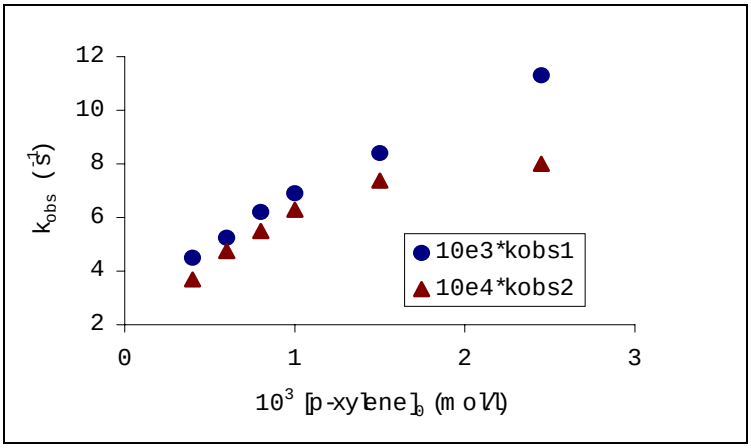

Figure 4. The effect of p-xylene for the first and the second stage of the reaction

The best fit, we could find for the data from table 1 is given by:

$$k_{obs1} = (0.38 \pm 0.02) + (262 \pm 16)[p - xylene]_0 \quad (4)$$

$$k_{obs2} = \frac{(1.5 \pm 0.08)[p - xylene]_0}{1 + (1439 \pm 129)[p - xylene]_0} \quad (5)$$

It is easy to recognize the Michaelis – Menten pattern for the electron transfer process.

The influence exerted by hydrogen ion concentration on the rate constant was investigated within the limits presented in the Table 2.

Table 2

Effect of hydrogen ion concentration on the apparent rate constant, 45^0C

$[H^+]$ (mol/l)	0.5	0.6	0.7	0.8	0.9
$10^2 \cdot k_{obs1}$ (s^{-1})	1.59	1.40	1.19	1.03	0.95
$10^4 \cdot k_{obs2}$ (s^{-1})	3.14	4.30	5.15	5.70	6.44

As it can be seen the concentration of hydrogen ion has an opposite effect on the two steps of the reaction. It diminishes the rate constants of the first step according to:

$$k_{obs1} = \frac{(0.13 \pm 0.05)}{1 + (13.7 \pm 6.6)[H^+]} \qquad t = 45^0C \qquad (6)$$

and causes a linear increase of the rate constant on the hydrogen ion concentration of the form:

$$k_{obs2} = (6.4 \cdot 10^{-4} \pm 7 \cdot 10^{-5})[H^+] \qquad t = 45^0C \qquad (7)$$

Activation parameters were determined for the second stage of the reaction from the Arrhenius and from the Eyring plot (Figure 5).

In order to determine the activation parameters, we employed:

$$k_2^* = k_{obs2}/([p - xylene]_0^{0.5} \cdot [H^+]) \qquad (8)$$

and obtained E_a = 62.37 kJ/mol, ΔH^* = 59.77 kJ/mol and ΔS^* = -89.87 J/mol·K.

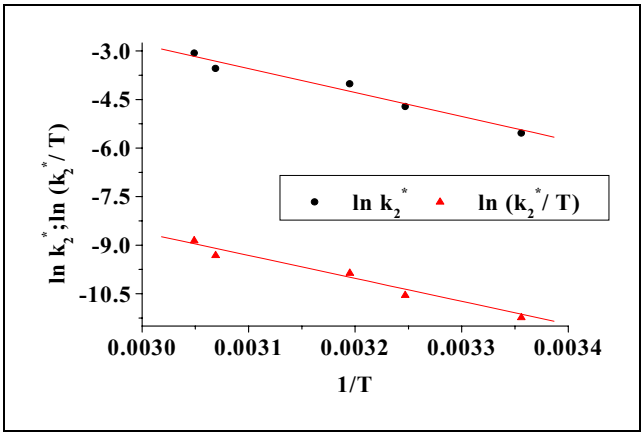

Figure 5. Determination of activation parameters.

The relatively small values of activation energy and activation enthalpy and the negative and relative large activation entropy may be explained by the oxidation of the adduct by inner electron transfer.

A reaction mechanism, can be suggested, based on the stoechiometry, rate law and literature data. It involves the formation of an adduct between p-xylene and the hydrocomplex of Ce(IV), followed by the oxidation of adduct by inner electron transfer. This step is the rate-determining step. The subsequent steps are very rapid leading finally to the major oxidation product, which is: p-methylbenzylic alcohol.

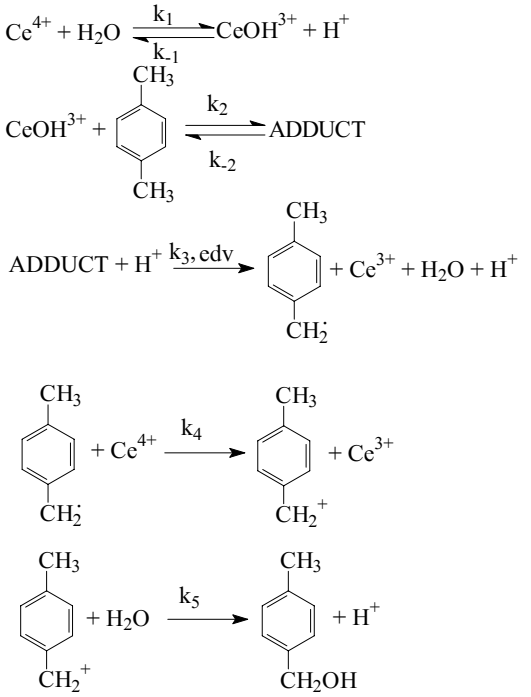

(12)

The two pre-equilibria can be combined as one, eliminating a hydrogen ion:

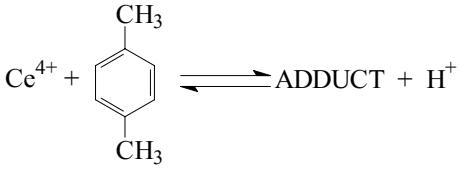

(13)

Based on the proposed mechanism the rate of alcohol formation is of the form:

$$r = k_3 K_h' K_2 \frac{[Ce(IV)] \cdot [H^+] \cdot [p-xylene]_0}{K_h'[H^+] + 1 + K_2[p-xylene]_0} \quad (14)$$

where: $K_h' = K_1 / [H_2O]$ and K_2 is the equilibrium constant for the second reaction.

REFERENCES

1. Hanna S. B., Kessler R. R., Mehrbach A., Ruzicka S., *J. Chem. Education*, **1976**, *53(8)*, 524
2. Trahanovsky W. S., Young L. B., *J. Chem. Soc.*, **1965**, 5777
3. Das A. K., Das M., *J. Chem. Soc. Dalton Trans.*, **1994**, 589
4. Willard H. H., Young P., *J. Am. Chem. Soc.*, **1930**, *52*, 132
5. Pondit A. K., Das A. K., Banerjea D., *Transition Met. Chem.*, **1991**, *16*, 324
6. Hintz H. L., Jhonson D. C., *J. Org. Chem.*, **1967**, *32*, 556
7. Duke F. R., Bremer R. F., *J. Am. Chem. Soc.*, **1951**, *73,* 5179
8. Waters W. A., Jones J. R., Litter J. S., *J. Chem. Soc.*, **1961**, 240
9. Muhammad S. S., Rao K. V., *Bull. Chem. Soc. Jpn.*, **1963**, *36*, 943
10. Ardon M., *J. Chem. Soc.*, **1957**, 1811
11. Hargreaves G., Sutcliffe L. H., *Trans. Faraday Soc.*, **1955**, *51*, 1105
12. Sankhla P. S., Mehrotra R. N., *J. Inorg. Nucl. Chem.*, **1972**, *34*, 3781
13. Rangaswamy M., Santappa M., *Acta Chim. Acad. Sci. Hung.*, **1968**, *56*, 413
14. Grover V. K., Gupta Y. K., *J. Inorg. Nucl. Chem.*, **1969**, *31*, 1403
15. Wells C. F., Husain M., *Trans. Faraday Soc.*, **1970**, *66*, 679
16. Balasubramanian T. R., Venkatasubramanian N., *Indian J. Chem.*, **1970**, *8*, 305
17. Dayal R., Bakore G. V., *Indian J. Chem.,* **1972**, *10*, 1165
18. Rao G. N., *Indian J. Chem.,* **1970**, *8*, 328
19. Krishna B., Tewari K. C., *J. Chem. Soc.*, **1961**, 3077
20. Baciocchi E., Rol C., Sebastiani G. V., *J. Chem. Research (Synopsis)*, **1983**, *9*, 232
21. Ramaswamy M. S., Venkatachalapathy M. S., Udupa H. V. K., *Bull. Chem. Soc. Jpn.*, **1962**, *35*, 214
22. Radhakrishna P. S., Pati S. C., *Chem. Ind.*, **1967**, *17*, 702

STUDIA UNIVERSITATIS BABEŞ-BOLYAI, CHEMIA, XLVII, 1-2, 2002

Dedicated to Professor Ionel Haiduc
on the occasion of his 65th birthday

DETERMINATION OF SOME AMINOACIDS FROM PHARMACEUTICAL PRODUCTS BY USING A KINETIC METHOD BASED ON A CLOCK LANDOLT-TYPE SYSTEM OF REDOX REACTIONS

SIMONA BUNGĂU*, IOAN BALDEA and LUCIAN COPOLOVICI****

* *Faculty of Medicine and Pharmacy University of Oradea, 29 Nicolae Jiga Str., Oradea, Roumania. E-mail: bungau@uoradea.ro*
** *Faculty of Chemistry and Chemical Engineering, Babeş–Bolyai University, 11 Arany Janos Str., Cluj– Napoca, Roumania*

ABSTRACT. A kinetic method is described for micro-determination of cysteine, methionine and L- tryptophan, based on a Landolt-type clock system. The reaction has been followed potentiometricaly. The method is sensitive, simple and allows the determination of the aminoacid concentration in pharmaceutical products with very good accuracy. The proposed method was compared to other standard method or to the certified content given by manufacturers.

Numerous pharmaceutical products contain various aminoacids that are essential for protein synthesis in living cells. There are 22 essential aminoacids combining to give around 22^{500} protein molecules [1]. Therefore they are essential for the growth of organic tissues [2]. It is worth mentioning that all of them are of L configuration. The D configuration has been found in some plants and micro-organisms [3]. Part of them are not synthesized by human body and it is necessary to be contained in food or taken as adjuvants with some medication.

The specific methods of aminoacids determination are rarely used. When mixture of aminoacids are analysed, as a rule, they are combined with the chromatographic methods [4,5,6] either paper, thin layer, ionic exchanger, gas or liquid chromatography [7,8], in order to separate them.

The purpose of this work is to determine cysteine, methionine and L-tryptophan from pharmaceuticals by a kinetic clock reaction method, using a Landolt redox reaction system [9]. Cysteine (L-2-amino-3-thio-propionic acid) and methionine (2-amino-4-(methylthio)-butiric acid) are from the group of thioaminoacids, while L-tryptophan or L-α-amino-β-indol-3-il-propionic acid, a precursor of serotanin and melatonin is from the group of heterocyclic aminoacids [10]. The method consists of three redox reactions: first bromate-bromide generating bromine in a relative slow process, the second involving the analyte consuming bromine in a fast process and the third consisting of the oxidation of substrate (analyte) by bromate in very slow process. The method is quite cheap, relative rapid and makes use of simple and available techniques.

Experimental

Chemicals. Stock solutions of $KBrO_3$ $3 \cdot 10^{-2}$ M , KBr 1.0 M and $HClO_4$ 0.5 M were prepared in four-distilled water by weighting or being standardised by titrimetric methods. The amino acid solution was freshly prepared before each set of runs. All the substances were of analytical grade purity and used without further purification. Aminoacids were either analytical grade or for pharmaceutical purposes. In order to obtain calibration lines, each reaction mixture had a total volume of 25 ml. The order of adding reagent solutions into the reaction vessel was KBr, $HClO_4$, the aminoacid solution and four-distilled water up to 22.5 ml. After circulating water from a thermostat for at least 10 minutes, 2.5 ml $KBrO_3$ previously kept in a temperature bath were rapidly injected into the stirred mixture. This moment has been considered the zero time for the run.

Experimental Device. Measurements were carried out by using a Digitronix DXP-2040 (Seiko) potentiometer [11], a data acquisition device and a computer. The measuring electrode was a platinum plate. A saturated calomel electrode was the reference. The scheme for experimental set-up is given in Fig. 1.

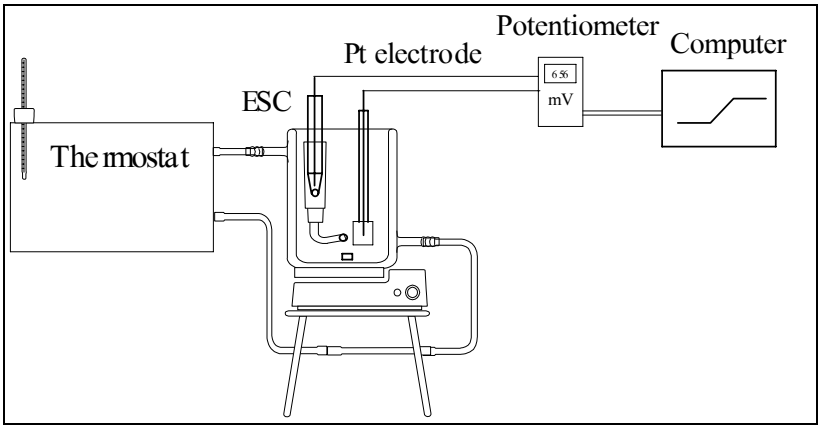

Fig.1. Schematic presentation of the experimental device.

Results and discussion

The successive and parallel processes consuming bromate (and bromine) for the simplest system under consideration, BrO_3^--Br^--cysteine are:

$$BrO_3^- + 5Br^- + 6H^+ \rightarrow 3Br_2 + 3H_2O \quad \text{relative slow} \quad (1)$$

$$Br_2 + 2Cys \rightarrow 2Br^- + 2H^+ + (Cys)_2 \quad \text{fast} \quad (2)$$

$$BrO_3^- + 6Cys \rightarrow Br^- + 3(Cys)_2 + 3H_2O \quad \text{slow} \quad (3)$$

Here, Cys stands for cysteine ($HSCH_2CH(NH_2)COOH$ and $(Cys)_2$ stands for cystine, a disulphide ($HOOCCH(NH_2)CH_2)_2S_2$), the oxidation product of cysteine. The kinetics of the reaction (1) is known [12]. The oxidation of cysteine by bromine (2) is a rapid process. The oxidation of cysteine by bromate, under experimental conditions employed, is a slow process. A test reaction in the absence of bromide proved that. An unnoticed modification of electrode potential has been measured for a long time elapse. When bromide is present from the beginning, the process takes place more rapid. Therefore, the oxidation of cysteine proceeds mainly by means of bromine. The considered amino acids are traps for bromine. It means that bromine concentration reaches a low steady-state value, as long as cysteine exists in the mixture. When cysteine has been completely consumed, bromine accumulates in the mixture, and a modification of the potential of the redox electrode takes place. By choosing appropriate concentrations for BrO_3^-, Br^- and H^+, the reaction rate is maintained quite constant for small degree of bromate consumption. Bromide is restored by reaction (2), bromate amount reacted is small because of the stoichiometry. Hydrogen ion concentration should be maintained constant, either by using buffered solutions or a large excess. Therefore, within equal time intervals the same amount of bromine is generated, and consequently, the same amount of cysteine is oxidized. Hence

$$\text{rate} = \frac{-\,\mathrm{d}[\mathrm{Cys}]}{\mathrm{dt}} = \frac{-\,\Delta[\mathrm{Cys}]}{\Delta t} = \frac{[\mathrm{Cys}]_t}{\tau} \qquad (4)$$

Under such circumstances, rate being constant, the concentration of cysteine in the mixture is proportional to the time elapse τ until the bromine concentration increases steeply.

Methionine behaves similarly, the oxidation yields a sulfoxide. The stoichiometry has been determined by a spectrophotometrical titration, bromine being generated from bromate in the presence of methionine under conditions employed in analytical measurements. The molar ratio was 1:1. Tryptophan reacts with bromine by a bromination process at the aromatic ring, consuming it rapidly. The molar ratio bromine:tryptophan was 2:1 indicating a double bromination.

The evolution of platinum electrode potential with time exhibits a shape of a titration curve, shown in Fig. 2. It has an inflexion point. The complete comsumption of the analyte corresponds to the moment of steep increase of the potential. The bromine evolution, as a result of reaction (1) only, is similar to the above described behaviour, but takes only a few seconds. The complete consumption time is in fact the diffference between the two inflexinon points, for the probe and the blank one. Nevertheless, we consider the end point of the reaction as being that of the inflexion, the blank probe needs no more than 2 - 3 seconds under the conditions employed. Since the same conditions are maintained for calibration line and measurements on real samples, no error is made by such an approach.

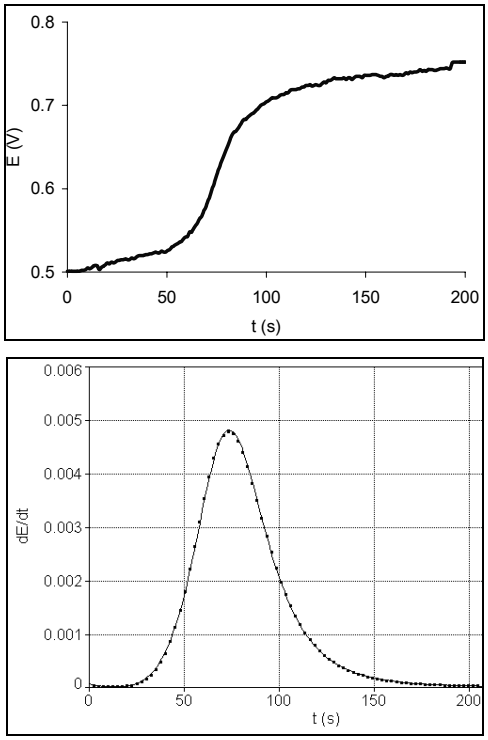

Fig. 2. Redox potential dependence on time and its derivative dE/dt = f(t) at [methionine] = $8 \cdot 10^{-5}$ M

The time for the inflexion can be determined more precisely from the derivative curve (also shown in Fig 2). This time period is proportional to the analyte concentration.

A plot of this time values, as a function of the aminoacid concentration is linear. Such a straight-line dependence represents the calibration line.

Searching for appropriate conditions.

a).The effect of the acidity. Several reaction time were determined using various concentration of mineral acid. The hyperbolic aspect of the curve confirms the second-order dependence of the rate with respect of hydrogen ion for the bromate-bromide reaction [9]. A value of mineral acid of 0.1 seems to be suitable for the analysis. It ensures a constant acidity within the initial period. Only minor hydrogen ion consumption occurs, although the reaction (1) stoichiometry requires 6 hydrogen ions.

b). The effect of potassium bromide. Eight bromide concentration values between 0.03 and 0.4 M were used to determine reaction time. A slope of 1.00 ± 0.07 from the graph lg $(1/\tau)$ - lg $[Br^-]$ confirming the first-order

dependence of the rate of bromate – bromide reaction [9]. A value of 0.2 M was chosen for the experiments to obtain calibration lines, ensuring its constant concentration.

c). Dependence on the conversion degree of bromate. By using different initial concentration of bromate and considering the degree of reaction defined by equation (5)

$$X = \frac{[BrO_3]_0 - [BrO_3]_{consumat}}{[BrO_3]_0} = \frac{\Delta[BrO_3]_0}{[BrO_3]_0} = \frac{[a\,min\,oacid]_0}{[BrO_3]_0} \qquad (5)$$

a linear dependence, as shown in Fig. 3, has been obtained, proving in fact the first- order dependence on bromate for the reaction (1) [9]

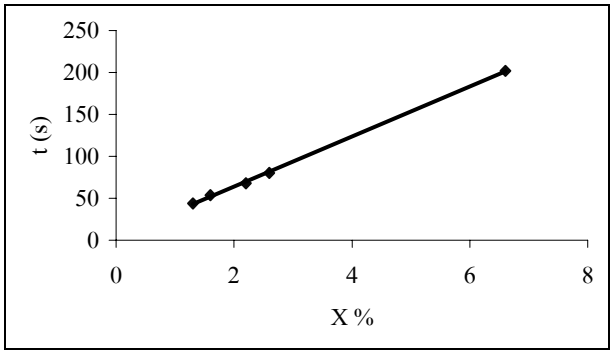

Fig.3. Dependence of reaction time on conversion using various initial concentration of bromate, [KBr] =0.2 M, [$HClO_4$] = 0.1 M, [tryptophan] = 4 x 10^{-5} M

A degree of reaction of 2.6 % has been chosen. It is in the range of initial rate determination ensuring a relatively constant concentration of bromate, and time values not too short to decrease the sensibility.

Calibration lines.

Under the same experimental conditions and using various known concentrations of the analytes, calibration lines were drowning. Figure 6 presents the data concerning tryptophan. The equation describing the line is:

$$t = (2{,}9 \pm 3{,}3) + (1{,}90 \pm 0{,}03) \cdot 10^6\,[\text{tryptophan}]_0 \qquad (6)$$

The correlation coefficient is r = 0.9995 and a standard deviation of 4.1 has been determined. The relative standard deviation (RSD) for a measurement is 2.2% for 5 individual measurements. Detection limit is 1.9x 10^{-6} M in accordance with IUPAC recommendation [14] It is obvious that the intercept is nearly zero as expected. The large slope indicates a good analytical sensitivity.

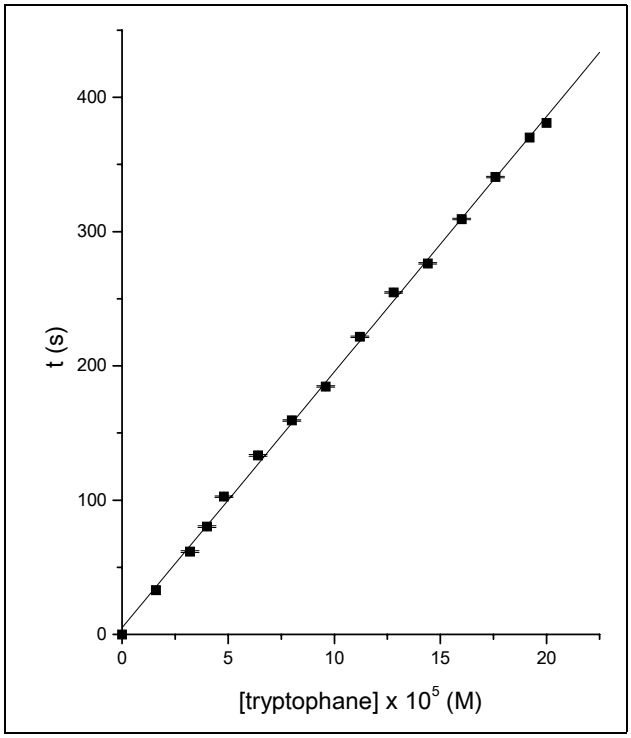

Fig. 4. Calibration line for tryptophan under the experimental conditions [KBr] = 0,2 M, $[KBrO_3] = 3 \cdot 10^{-3}$ M, $[H^+]$ = 0,1 M, and T = 293 K

The calibration line for methionine has been obtained by using the same redox system. The experimental conditions are [KBr] = 0.2 M, $[H^+]$ = 0.1 M, $[KBrO_3] = 3x10^{-3}$ M and T=293. A good straight line, with a very good correlation coefficient of 0.9991, has been obtained. It is described by:

$$t = (-6,0 \pm 4,2) + (1,56 \pm 0,06) \cdot 10^6 \left[\text{methionine}\right]_0 \quad (7)$$

The standard deviation for the line is 3.6 and a relative standard deviation of one point is 2.5 % using 5 individual measurements. The detection limit of $4.0x\ 10^{-6}$ M has been calculated. In this case also, the sensibility of the method is quite good.

The calibration line in the case of cysteine has been determined similarly, under the following conditions [KBr] = 0.2 M, $[H^+]$ = 0.1 M, $[KBrO_3]=3.0x10^{-3}$M and T = 293 K using 10 different concentrations of cysteine as trapping agent, each experiment having 3 - 7 replicate runs. The line is described by the equation

$$t = (-1,5 \pm 3,1) + (1,34 \pm 0,04) \cdot 10^6 \left[\text{Cys}\right]_0 \quad (8)$$

The standard deviation for the line is 2.7 and a relative standard deviation of one point is 2.8 % using 7 individual measurements. The detection limit is 1.7×10^{-6} M. It is worth mentioning here, that cysteine can be determined with another system of Landolt type reactions, using hydrogen peroxide - iodide reaction and cysteine being a trap for iodine [14]. Methionine and tryptophan do not react under such conditions, and cysteine concentration can be obtained from a mixture containing these aminoacids.

Figure 5 presents a calibration graph for methionine and its mixture with a constant concentration of cysteine. The effect of cysteine is additive because the calibration lines are parallel (the slopes almost the same).

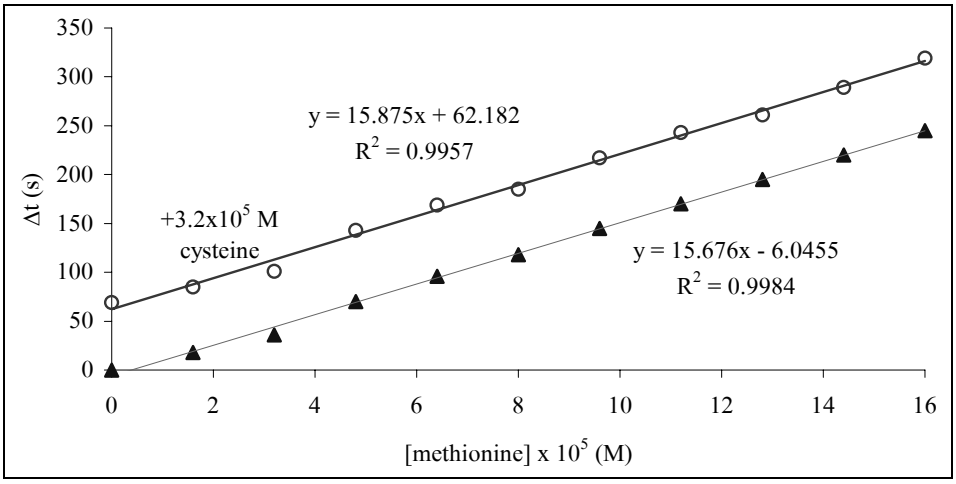

Fig. 5. Calibration line without and in presence of a constant concentration of cysteine 3.2 10^{-5} M.

The differences in the slopes of the three calibration lines are directly related to the reactivity of each aminoacid towards bromine, taking into account their structure and the reaction products. Nevertheless, the bromine consumption is quite rapid for all three analytes as compared to bromate oxidation. Consequently, the steady-state concentrations of bromine are slightly different for these reactions.

Several aminoacids, with possible interference were tested. As seen in Table 1, hystidine, tyrosine, guanine and phenylalanine do not interfere with the measurements, even in concentrations up to 1.0×10^{-3} M.

Table 1

Essential aminoacids that do not interfere in the determination of $4 \cdot 10^{-5}$ M methionine

Additive	Concentration ratio additive/ methionine)	Recovery %
Hystidine	100	102
Tyrozine	120	99
Guanine	150	99
Phenyl alanine	100	98

Validation on real samples

Methionine has been determined from the pharmaceuticals Mecopar forte, Metaspar and Infesol. The measurements were carried out by using the proposed clock method and the corresponding calibration lines as well as by using a spectrophotometrical method [15,16], The results were compared with certified content given by the manufacturers. For example, for the drug Mecopar forte the results are presented in Table 2.

Table 2

The content of methionine per tablet of Mecopar Forte

Methionine mg/ tablet	RSD %	Mean value mg
101	1	100
99		
100		
99		
101		

The amount of methionine contained in the product Metaspar, has been also obtained. The results are collected in Table 3. Five tablets were weighed, ground to powder, dissolved, filtered out and made up the solution to a volumetric flask. Various aliquots were measured and the content determined by means of the calibration line. The results were expressed as mg per tablet. The replicate runs gave reproductible results.

Table 3

Methionine Content of the pharmaceutical product Metaspar

Methionine found [mg]	RSD %	Mean content mg
65.6	0.2	65.64
65.7		
65.6		
65.8		
65.5		

Both series of measurements, the proposed one and the spectrophotometrical one, as an internal norm for its determination [15,16]. gave similar values with the manufacturers' certified contents [17] (see also Table 4)

Another determination of methionine was made from the complex product Infesol 40, manufactured by *Berlin-Chemie Menarini Group*.A. It is a solution containing many aminoacids [17]. A sample of 0.125 ml of solution was introduced in the reaction mixture and the consumption time determined. No separation or filtration was necessary. No one of the aminoacids contained in the solution interferes. The comparative results are given in Table 4. Recovery (R %) is between 99 and 100.6 %

Table 4

Methionine content in Mecopar forte, Metaspar and Infesol. 40

Pharmaceutical form		Landolt method		Spectrophoto-metric method		Manufacturers' certified content	R %
		mg*	RSD	mg*	RSD	mg*	
Metaspar	Capsule	64	0.8	65.6	0.2	64.5	99
Mecopar Forte	Tablet	100.5	0.5	100	1	100	100.5
Infesol 40	Perfusable solution	1760	0.2	-	-	1750	100.6

*) the content refers to mg/capsule, mg/tablet, and mg/100 ml solution respectively.

As seen in the table 4, the results are similar to those obtained by spectrophotometrical method and the certified content given by producers for all investigated pharmaceuticals. The data show the reliability of the proposed kinetic method for the determination of methionine.

REFERENCES

1. G. Hill, J. Holman, *Chemistry in context*, *Fourth edition*, Nelson, 1995, p. 578
2. A. Glannouslos, C. Papadopoulos, *Analyst*, 1996, 121, 413
3. * * *, *Tables scientifiques*, Ed. J. R. Geigy S.A., Département Pharmaceutique, Sixième édition, 1963, p.479
4. P. MacLaurin, P. J Worsfold, P. Norman, M. Crane, *Analyst*, 1993, 18, 617
5. R. J. Poppi, C. Pasqulni, *Chemom. Intell. Lab. Syst.*, 1993, 19, 243
6. J. Saurina, S. Hernandez – Cassou, *Anal. Chim. Acta*, 1992, 259, 219
7. M. Bianco, J. Coello, H. Iturrlaga, S. Maspoch, M. Redon, J. Riba, *Anal. Chim. Acta*, 1992, 259, 219
8. I. Lukkari, W. Lindberg, *Anal. Chim. Acta*, 1990, 241, 23
9. H. A. Espson *Chemical Kinetics and Reaction Mechanisms*, McGraw-Hill, New-York, 1981, p. 5; J. J. Clarke, *J. Chem. Educ.,*1970, 47, 75.
10. C. D. Nenițescu, *Chimie organică, vol. II*, Ed. Didactică și Pedagogică, București, 1980, p.354

11. L. C o p o l o v i c i, I. B â l d e a, A. B â l c, *Determination of Aromatic Amines by Kinetic Methods, 7th International Symposium on Kinetic in Analytical Chemistry*, Bucharest, 26-29 Sept., 2001
12. A. E. B u r g e s, J. L. La t h a m, *Analyst*, 1966, 91, 343
13. A n a l y t i c a l M e t h o d C o m m l t t e e, *Analyst*, 1987, 112, 199
14. S. B u n g ă u, I. B â l d e a, *Kinetic Methods for Determination of Ascorbic Acid and Cysteine, The 10th Conference on Physical Chemistry*, Iași, 26-29 Sept., 2000
15. * * *, Norma internă, MICh-NII 3972-68, Mecopar Forte Comprimate
16. * * *, Norma internă, MICh-NII 5195-73, Metaspar capsule
17. * * *, *Agenda medicală 2000*, Editura Medicală, București, 2000, p. 1070, 1249, 1269

STUDIA UNIVERSITATIS BABEŞ-BOLYAI, CHEMIA, XLVII, 1-2, 2002

Dedicated to Professor Ionel Haiduc
on the occasion of his 65th birthday

MODELING AND SIMULATION OF 3-AMINOPROPIONITRILE SYNTHESIS USING DEDICATED SOFTWARE PACKAGES

CĂLIN CORMOŞ*, ŞERBAN AGACHI**

** S.C. "Terapia" S.A., Fabricii 124, 3400, Cluj-Napoca, Romania, tel: +40 (64) 415222, ext. 115, e-mail: calin.cormos@personal.ro*

*** "Babes-Bolyai" University, Faculty of Chemistry and Chemical Engineering, Arany Janos 11, 3400, Cluj-Napoca, Romania, e-mail: sagachi@chem.ubbcluj.ro*

ABSTRACT. Calcium pantothenate is one of the most used pro-vitamins in the therapy for human beings and for veterinary use. In the synthesis of D,L calcium panthotenate, pantolactone and β-alanine are used as starting materials. β-Alanine is obtained from alkaline hydrolysis of 3-aminopropionitrile. The synthesis of 3-aminopropionitrile involves the addition of ammonia at acrylonitrile at high temperature and pressure.

In this paper the continuous synthesis of 3-aminopropionitrile is described. The synthesis takes place at temperature (100 – 120°C) and pressure (15 – 20 atm). Secondary products can be formed; to avoid this fact a high molar ratio between reactants (ammonia / acrylonitrile = 10 / 1) is used. The synthesis process was modeled and simulated using HYSYS Plant, PRO/II and ChemCAD software packages to demonstrate the reliability of the packages and their performances. From simulation results very valuable information can be obtained regarding real plant operation.

1. INTRODUCTION

Calcium pantothenate is one of the most used pro-vitamins in the therapy for the human beings and for the veterinary use. Pantothenic acid is a vitamin from the complex of vitamins B; it plays an important role in the metabolism [1] (its biological active form is Coenzyme A). The chemical formula of calcium pantothenate is presented below:

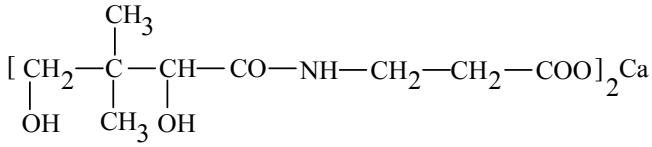

The synthesis of D,L calcium pantothenate is a complex process. The synthesis involves three major steps [2]: the first step is the manufacture of pantolactone (α-hydroxy-β,β-dimethyl-γ-butyrolactone), the second step consists of the manufacture of sodium β-alaninate and in the final step of the synthesis these intermediates are coupled resulting the target product.

One of the intermediates, sodium β-alaninate, is obtained from alkaline hydrolysis of 3-aminopropionitrile. 3-Aminopropionitrile can be obtained from addition reaction of acrylonitrile and ammonia at high temperature (100 – 120°C) and pressure (15 – 20 atm) using high molar ratio between reactants (acrylonitrile / ammonia = 1 / 10) [3, 4, 5].

In this paper, the continuous synthesis of 3-aminopropionitrile is described. The chemical reactions are presented below:

(i) Main reaction:

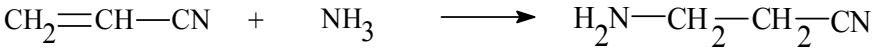

Acrylonitrile — Ammonia — 3-Aminopropionitrile (beta-Aminopropionitrile)

(ii) Secondary reactions:

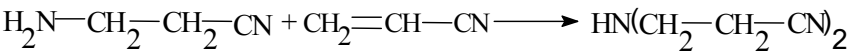

3-Aminopropionitrile (beta-Aminopropionitrile) — Acrylonitrile — 3,3'-Iminodipropionitrile (bis-(beta-cyanoethyl)-amine)

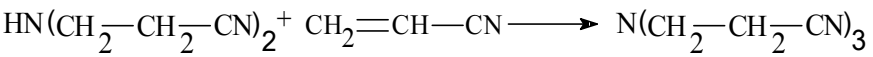

3,3'-Iminodipropionitrile (bis-(beta-cyanoethyl)-amine) — Acrylonitrile — 3,3',3"-Nitrilotripropionitrile (tris-(beta-cyanoethyl)-amine)

The continuous synthesis of 3-aminopropionitrile involves the following steps. The raw materials, acrylonitrile and a solution of ammonia are introduced in the process using two dispensing pumps (output pressure 15 atm). Ammonia solution stream is heated at about 105 - 110°C and mixed with acrylonitrile stream. The mixture of the reactants is introduced in a Plug Flow Reactor (PFR) where the chemical reactions take place. Because of the secondary reactions, a high molar ammonia excess is used (acrylonitrile / ammonia = 1 / 10). The synthesis process is exothermic. The reaction heats are the following: the first reaction ΔH_{r1} = -45.76 kJ/mole, the second reaction ΔH_{r2} = -60.815 kJ/mole and the third reaction ΔH_{r3} = -79.871 kJ/mole. Temperature of the outlet stream is about 100 – 120°C. Because of high ammonia excess the product stream must be processed in order to recycle ammonia. The reactor outlet stream is depressurised at 2 atm and the gaseous phase resulted is separated from liquid phase using a flash unit. The liquid phase, containing 3-aminopropionitrile, is fed to a desorbtion column when the rest of ammonia from the product stream is removed. The gaseous phases, containing ammonia, resulted from flash unit and from desorption column are mixed and cooled. The resulted stream is fed to a flash unit where a phase separation takes place. The liquid phase (containing a small quantity of 3-aminopropionitrile) is recycled to desorption

column. The gaseous phase, containing ammonia, is sent to an absorption column where gaseous ammonia is absorbed in water. Ammonia solution resulted from absorption column is recycled in the process. 3-Aminopropionitrile stream resulted at the bottom of desorption column is sent to alkaline hydrolysis in order to obtain sodium β-alaninate.

2. MODELING AND SIMULATION OF THE SYNTHESIS

The continuous synthesis of 3-aminopropionitrile can be modeled and simulated using a CAD software package for chemical processes. In this case HYSYS Plant, PRO/II and ChemCAD were used. These software packages use flowsheet modeling environment techniques. One of the purposes of the work was to establish how reliable the simulation software packages are and if the results are comparable.

The parameters of the model are presented below:

- Dispensing pumps (for ammonium solution and acrylonitrile streams)
  - Output pressure: 15 atm
- Heat exchanger for ammonia solution
  - Output temperature: 105 - 110^{o}C
- Synthesis reactor (Plug Flow Reactor)
  - Length of tube: 140 m
  - Diameter of tube: 0.04 m
  - Number of tube: 1
  - Reaction temperature: 100 – 120^{o}C
  - Pressure: 15 atm
  - Molar ratio between reactants: acrylonitrile / ammonia = 1 / 10
  - Heat of reactions: Reaction 1: ΔH_{r1} = -45.76 kJ/mole
    Reaction 2: ΔH_{r2} = -60.815 kJ/mole
    Reaction 3: ΔH_{r3} = -79.871 kJ/mole
  - Kinetic data: Reaction 1: Rate = $k_1 C_{NH3} C_{Acryilonitrile}$
    Reaction 2: Rate = $k_2 C_{3\text{-}Aminopropionitrile} C_{Acryilonitrile}$
    Reaction 3: Rate = $k_3 C_{3,3'\text{-}Iminodipropionitrile} C_{Acryilonitrile}$
  - Contact time: 2 – 5 min
- Lamination (depressurise) valve
  - Output pressure: 2 atm
- Flash units
  - Use inlet temperature and pressure
- Desorbtion column
  - Number of trays: 6
  - Top pressure: 1.6 atm
  - Bottom pressure: 2 atm
  - Recovery of 3-aminopropionitrile (bottom): 99 %
- Heat exchanger for gaseous phase
  - Output temperature: 25^{o}C
- Absorption column
  - Number of trays: 6
  - Top pressure: 2 atm

Bottom pressure: 2.5 atm
Side cooler: tray 3
Heat duty for side cooler: -200 MJ/h
Recovery of ammonia (bottom): 99.9 %

For 3-aminopropionitrile synthesis the flowsheet is presented below (using ChemCAD and HYSYS Plant software packages).

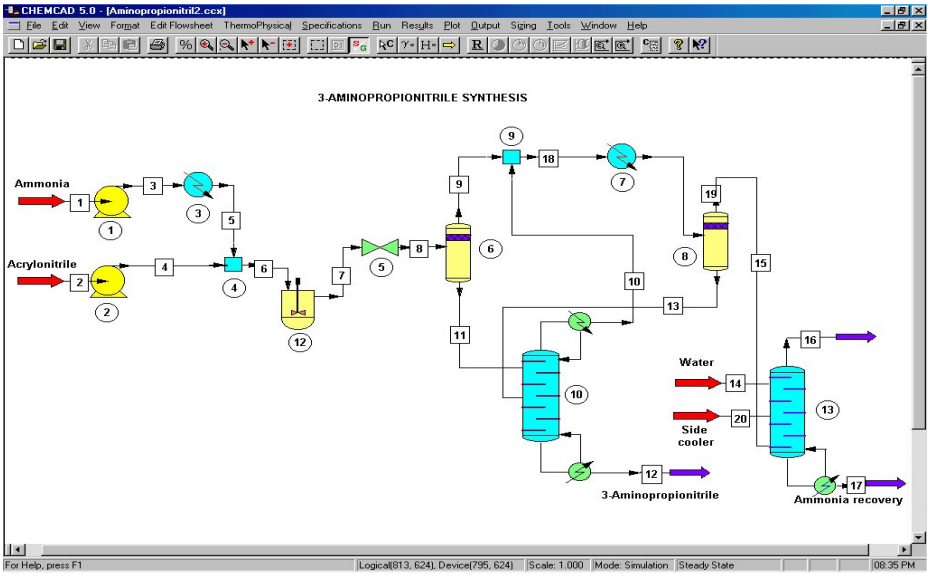

Figure 1. Simulation of 3-aminopropionitrile synthesis using ChemCAD

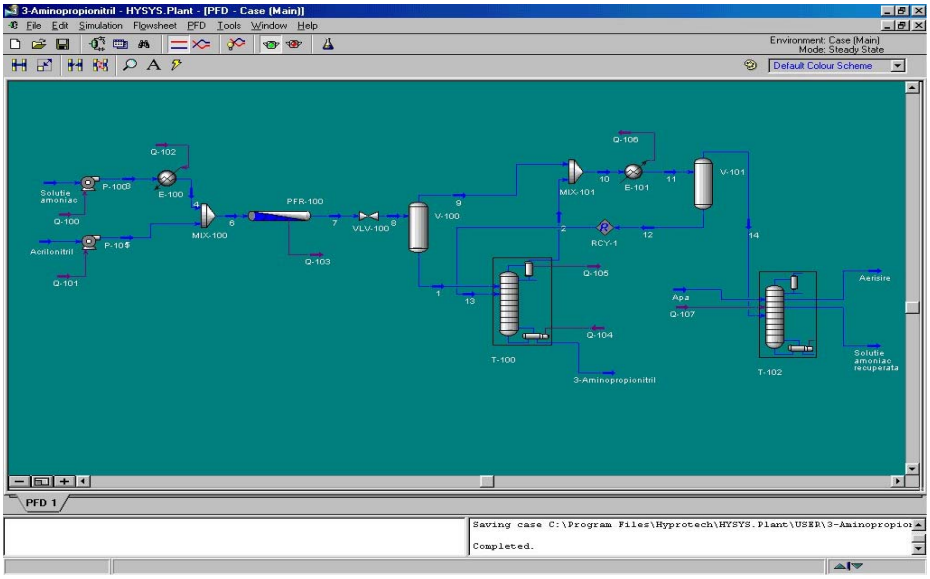

Figure 2. Simulation of 3-aminopropionitrile synthesis using HYSYS Plant

3. RESULTS AND DISCUSSIONS

The synthesis process of 3-aminopropionitrile was simulated using parameters described above. The process was simulated using PRO/II, ChemCAD and HYSYS Plant. The results obtained from simulation using these three simulation software packages are very similar.

For the synthesis reactor, the variation of the composition (molar fractions) for the reaction mass insight the Plug Flow Reactor (PFR) are presented below. Because of the high ammonia ratio the main reaction yield is about 75 – 80 %, the second reaction yield is about 20 - 25 % and the third reaction doesn't practically take place (yield small than 1 %).

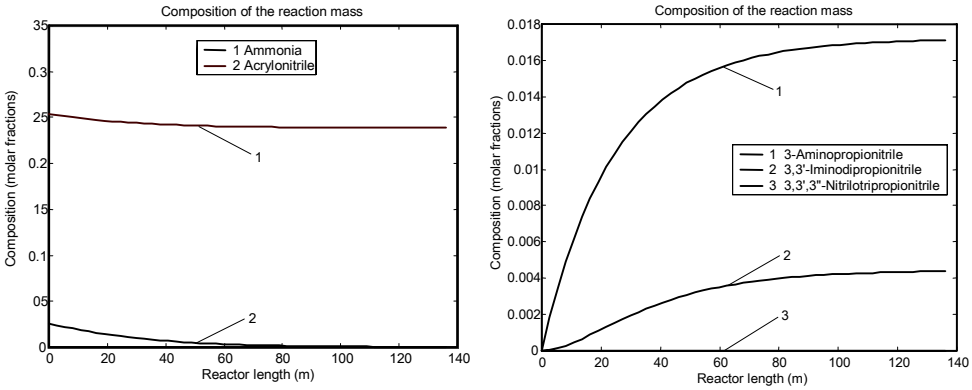

Figure 3. Composition (molar fractions) for reaction mass insight of PFR

For desorption and absorption columns below are represented temperature, liquid and vapour rates for each tray. These simulation results are similar using different software packages (PRO/II, ChemCAD and HYSYS Plant).

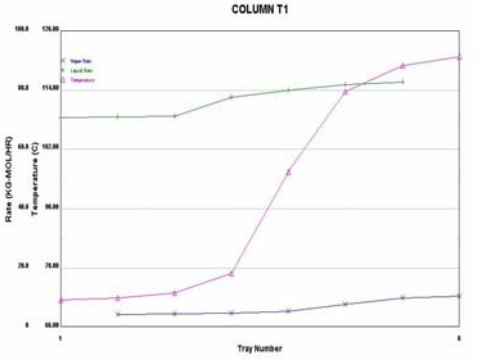

Figure 4. Desorption column

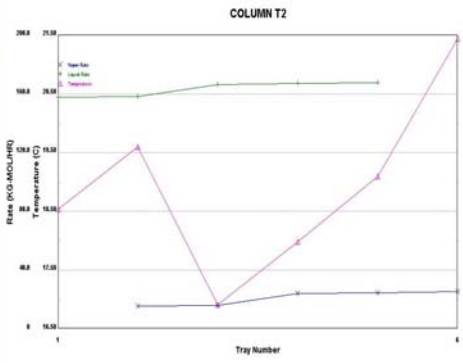

Figure 5. Absorption column

Calculated heat duties for different units of the plant are similar using PRO/II, ChemCAD and HYSYS Plant. For example, heat exchanger for heating ammonia solution has a duty about 600 MJ/h. For desorption column the reboiler duty is about 450 MJ/h. For absorption column heat duty for cooling ammonia solution is about –360 MJ/h and heat duty for side cooler is –200 MJ/h.

The model of the 3-aminopropionitrile synthesis can be used for sensitivity analysis. For example, the production of the plant (dependent variable) can be analyzed for different molar ratio between reactants (independent variable). A sensitivity study, realized using ChemCAD, is presented below (variation of the three products flows vs. ammonia solution flow).

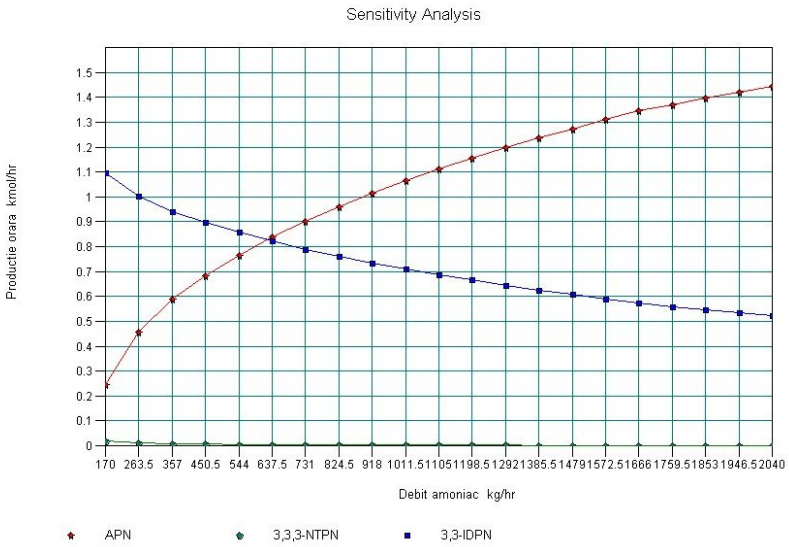

Figure 6. Variation of products flows vs. ammonia solution flow

4. CONCLUSIONS

In this paper the continuous synthesis of 3-aminopropionitrile has been described. The synthesis process was modeled and simulated using HYSYS Plant, PRO/II and ChemCAD software packages. The results obtained from simulation using these three simulation software packages are similar.

The model proved to be a reliable tool for analyzing this chemical process. Using the model of the synthesis process and the simulation results (for different conditions) very valuable information can be obtained for the real plant operation. Sensitivity studies can be made in order to analyze the influence of different factors (independent variables) on the process outputs (dependent variables).

REFERENCES

1. G. Neamtu, *Substante naturale biologic active*, Editura Ceres, vol. 1, 1996, 329 – 346.
2. C. Cormos, S. Agachi, *Modeling and simulation the process of synthesis of D,L calcium pantothenate*, International Conference on Quality Control, Automation and Robotics Q&A-R 2000, vol. 2, Cluj-Napoca, 19th – 20th May 2000, 7 – 12.
3. L. Kolofon, A. Pikulsky, A. Radu, *Raport de cercetare. Procedeu continuu la prepararea β-alaninei*, I.C.C.F. Cluj-Napoca, 1975, 3 – 18.
4. I. Hudrea, M. Pintican, *Proces tehnologic pilot pentru sinteza beta-alaninatului de sodiu în flux continuu*, I.C.P.A.O. Mediaș, 1997, 28 – 35.
5. K. Yamakami, O. Akazawa, Y. Shibata, N. Fujimoto (Daiichi Seiaku Co. Tokyo), U.S. Patent 3914280 (1975).

STUDIA UNIVERSITATIS BABEŞ-BOLYAI, CHEMIA, XLVII, 1-2, 2002

Dedicated to Professor Ionel Haiduc on the occasion of his 65th birthday

STUDY OF LIPOPHILICITY OF SOME 4,4'-DIAMINOBENZANILIDE BASED DIRECT DYES IN THE CELLULOSE DYEING

SIMONA FUNAR-TIMOFEI*, GEORGETA SIMU, EUGENIA SĂRĂNDAN

** Institute of Chemistry, Romanian Academy, Bul. Mihai Viteazul 24, 1900 Timisoara, Romania*

ABSTRACT. This paper presents an experimental evaluation of chromatographic mobilities i.e. R_f values of a series of 16 direct dyes containing 4,4'-diaminobenzanilide as a middle component. The R_f values were obtained by reverse-phase thin-layer chromatography and were quantitatively analysed by MLR (Multiple Linear Regression) analysis. Good correlation with the scores of the R_f values obtained by principal component analysis and predictability were noticed. Hydrophobicity of the direct dyes influences significantly their lipophilic behaviour.

Keywords: direct dyes, RP-TLC (reverse-phase thin-layer chromatography), lipophilicity, PCA (Principal Component Analysis), MLRA (Multiple Linear Regression Analysis)

INTRODUCTION

Lipophilicity is an important characteristic of dyestuffs, which can affect their affinity for the textile substrates [1-2]. Other interactions also influenced by lipophilicity include dye-dye aggregation [3-5] and dye-surfactant complexation [6,7]. Furthermore, toxicity can correlate with lipophilicity [8].

It has been stated that lipophilicity can be expressed by a volume or cavity term accounting for hydrophobic and dispersion forces and polarity terms, which express electrostatic interactions [9]. The polarity terms are more difficult to be expressed.

An experimental procedure used for assessing lipophilicity is the reverse-phase thin-layer chromatography (RP-TLC) [10]. Chromatographic mobility in such systems has been extensively used as a measure of the lipophilic character, though not apparently by dyestuffs or textile workers [11].

In the present work, chromatographic mobilities of a series of disazoic and trisazoic direct dyes with 4,4'-diaminobenzanilide as middle component were qualitatively analyzed by PCRA (Principal Component Regression Analysis). The experimental R_f values were obtained by RP-TLC analysis and are presented in Table 1.

EXPERIMENTAL

Materials and RP-TLC measurements

The investigated dyestuffs were asymmetric disazoic and trisazoic direct dyes, of general formula (I).

* *Corresponding author, e-mail: timofei@acad-tim.utt.ro*

(I)

where for dye: 1-10, 12, 15, 16 C_1 represents the first coupling component (salicylic acid) and C_2 - the second coupling component, as follows: the monoazoic compound 2-amino-phenol-4-sulphoneamide→resorcine (dye 1), γ acid (dye 2), resorcine (dye 3), the monoazoic compound sulphanilic acid→2,4-diaminotoluene (dye 4), p-aminobenzoyl I acid (dye 5), benzoyl I acid (dye 6), the monoazoic compound 5-nitro-anthranilic acid→H acid (dye 7) and the monoazoic compound 5-nitro-anthranilic acid→I acid (dye 8), 2-amino-phenol-5-sulphone-amide→ resorcine (dye 9), salicylic acid (dye 10), 4 nitro-aniline→H acid (dye 12), I acid (dye 15), benzoyl γ acid (dye 16). For dye 11 the coupling components are: γ acid (C_1), respectively H acid (C_2); for dye 13 the coupling component C_1 is the monoazoic compound aniline →acid H and C_2 is m-phenylenediamine; for dye 14 the coupling component C_1 is the Schäffer acid and C_2 is the monoazoic compound 5-nitro-anthranilic acid→I acid. These dyes were synthesized and purified at the Institute of Chemistry of Timișoara [12].

The measurement of the chromatographic R_f values was performed by RP-TLC analysis. The chromatographic plates used were of Merck, DC Fertigplatten Kieselgel 60 type. They were pre-developed during 24 hours in a hexane:paraffin oil of 95:5 (v:v) mixture. The eluting solvent, which is imposed to be a binary system, was isopropanol:NH_3 25 %, at 80-60 % ratios, which varied with an increment of 5% of organic phase.

To ascertain the reproducibility of the experimental chromatographic mobilities, the dyes were each spotted ten times onto the RP-TLC plates. Average R_f values were obtained by successive experiments.

METHODS

Definition of parameters

As independent variable the scores obtained by Principal Component Analysis (PCA) from chromatographic R_f values performed by RP-TLC analysis were used. They are presented in Table 1.

Molecular dye structures were built by the ChemOffice package [13], energy minimized using the MM2 force field. The minimum energy structures found in this way for each compound were then used for energy minimization by the semiempirical continuum-solvation model COSMO-AM1 [14] and employed for further analyses. Molecular surface area (A_{COSMO}) and volume (V_{COSMO}) refered to solution-phase (COSMO-AM1) structures were calculated using MST van der Waals radii [15].

Several quantum-chemical parameters were considered, like: the maximum (QMAX) and minimum (QMIN) atom charge in the dye molecules, the atomic formal charge on the most positive hydrogen atom (which reflects the electrostatic part of the acidity term and expresses the hydrogen-bond acceptor basicity, Q+).

The difference between the maximum and minimum atomic charge in a molecule (MAXMIN) was used as a submolecular polarity parameter. The HOMO and LUMO molecular orbital energies (E_{HOMO} and E_{LUMO}) were used in order to study possible interactions of the dye molecule with the textile fibre. Also, from the same quantum-mechanical calculations, dipole moments (μ) were considered in order to express possible dipole effects in dye-fibre interactions.

Table 1.

R_f scores (t[1]) and structural descriptors of the direct azo dyes

Dye	t[1]	A_{COSMO} [Å^2]	E_{HOMO} [eV]	E_{LUMO} [eV]	μ [D]	MAXMIN	ClogP	MR
1	1.45	581.77	-9.14	-1.42	9.91	4.13	6.25	19.16
2	1.94	513.9	-8.49	-1.58	22.99	4.13	4.26	17.16
3	1.72	435.51	-8.85	-1.48	12.23	0.99	6.48	14.23
4	1.62	590.16	-8.35	-1.3	4.77	4.17	5.00	19.68
5	1.33	612.45	-8.51	-1.63	17.19	3.92	5.08	20.54
6	1.09	600.49	-8.53	-1.52	13.65	4.17	5.08	20.54
7	-3.09	650.36	-8.46	-1.83	17.33	4.12	4.73	22.02
8	0.32	677.25	-8.35	-2.14	15.95	4.14	1.95	23.04
9	-1.32	577.75	-8.97	-1.52	14.57	4.15	6.25	19.16
10	2.84	454.59	-8.94	-1.52	22.99	0.99	7.57	14.73
11	-5.62	605.67	-8.19	-1.76	22.29	4.20	-3.84	20.43
12	-2.42	659.32	-8.52	-2.03	13.9	4.13	2.18	22.39
13	-0.69	626.10	-8.33	-1.96	20.56	4.12	1.77	21.65
14	-3.63	696.46	-8.53	-1.82	14.78	4.14	2.61	24.08
15	-0.29	513.47	-8.53	-1.54	7.54	4.15	4.26	17.16
16	1.42	602.05	-8.93	-1.6	14.42	4.12	5.99	20.17

Connolly Solvent Accessible Surface Area (SAS), Connolly Molecular Surface Area (MS) and Connolly Solvent-Excluded Volume (SEV) [16] and the hydrophobicity (ClogP) parameter (the logarithm of octanol/water partition coefficient) were performed by the ChemOffice package.

The molecular weight (MW) and molar refraction (MR) were used as a measure of the bulkiness of the azo dyes.

Principal Component Analysis (PCA)

The purpose of PCA is to find the simplest mathematical model able to describe satisfactorily a given set of data. In the latent variable analysis, the main objective is to find the possible relations between one or more dependent variables and a potential number of explanatory variables [17]. During this analysis the data matrix for a given set of objects are examined. The variables are described as linear combinations of the new variables, called principal components (PC), which are orthogonal vectors.

The latent variables directions in the M-dimensional space are specified by the "p" vectors and the location of the scores along this axis are given by the "t" vectors. The "t" vectors are describing the direction of the principal component axis, while the components of "p" represent the cosines of the angles between the principal component and the co-ordinates axis. The levelheaded coefficients are also called the loadings of the variables over the principal component [18].

The PCA analysis was performed by the MASCA package [19].

Multiple Linear Regression (MLR) Analysis

Multiple Linear Regression Analysis relates one experimental variable y_k to one or several structural variables x_i by the equation [20]:

$$y_k = b_o + \sum_i b_i \cdot x_{ik} + e_k \quad (1)$$

where b represents partial regression coefficients and e the deviations and residuals. The leave-one-out (similar to the leave-n-out [21]) and leave-half-out [22] cross validation procedure was applied in order to verify the reliability of our results. In this procedure one, respectively half of all molecules are held out from the set, the correlation equation is computed for the rest of molecules and the result is used to calculate the estimated affinity of the left out molecule. These estimated affinities are compared with the respective experimental values and 'predictive r^2' (r^2_{CV}) was obtained. MLR calculations were performed by the SYSTAT package [23].

RESULTS AND DISCUSSION

The experimental R_f chromatographic values have been analyzed by the PCA method. The correlation matrix of the R_f values is presented in Table 2. Significant intercorrelations between these values are observed. Therefore the scores of the first principal component were used as independent variable in further regressional calculations. The dependence of the obtained score values for the first two principal components (t[2] versus t[1]) is presented in figure 1.

Table 2.

Correlation matrix of the chromatographic R_f values

	Rf(75/25)	Rf(70/30)	Rf(65/35)	Rf(60/40)	Rf(80/20)	Rf(85/15)
Rf(75/25)	1.00	0.94	0.89	0.77	0.97	0.86
Rf(70/30)		1.00	0.97	0.87	0.89	0.75
Rf(65/35)			1.00	0.91	0.86	0.77
Rf(60/40)				1.00	0.70	0.58
Rf(80/20)					1.00	0.94
Rf(85/15)						1.00

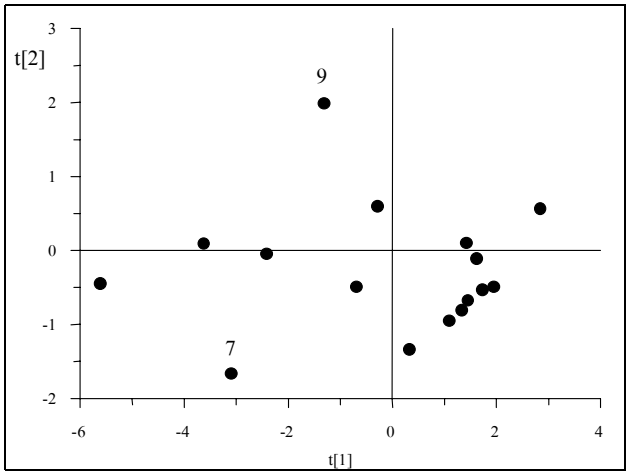

Figure 1. Dependence of the first principal component scores of the R_f matrix

Even if two direct dyes seemed to act differently in comparison to the others: dye 7 having as coupling component monoazoic compound 5-nitro-anthranilic acid→H acid and dye 9 having as coupling component 2-amino-phenol-5-sulphoneamide→resorcine, they were not found to be outliers in the R_f space.

In figures 2 the variation of the first two principal components loadings (p[2] vs. p[1]) in the R_f space is presented.

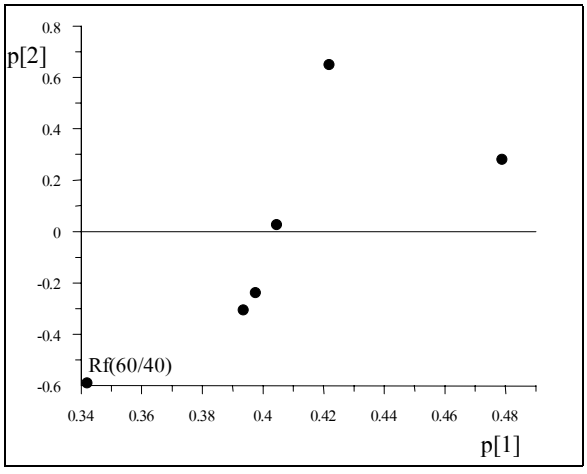

Figure 2. Dependence of the first two principal components loadings

Even if the chromatographic R_f values are interrelated, a different behavior in the case of the chromatographic mobility of the eluting solvent isopropanol:NH_3 25%= 60:40 (R_f (60/40)) could be observed from figure 2.

Principal Component Analysis was then applied to the descriptor matrix. The correlation matrix between the original descriptors and the first three principal components is presented in Table 3. Volume and bulkiness parameters produce an important contribution to the first PC. Polarity parameters contribute to the second principal component. The first PC describes, mainly, a measure of the steric parameters of the dye molecules, the second PC is a measure of hydrophobic and electronic effects.

Table 3.

Correlation matrix between the original descriptors and the first three principal components

	PC1	**PC2**	**PC3**
A_{COSMO}	0.98	-0.11	-0.13
V_{COSMO}	0.98	-0.03	-0.15
SAS	0.97	-0.09	-0.11
MS	0.98	-0.11	-0.12
SEV	0.99	-0.02	-0.09
MW	0.98	0.04	-0.14
OVAL	0.88	-0.38	-0.22
E_{HOMO}	0.57	0.54	0.38
E_{LUMO}	-0.68	-0.50	0.34
μ	0.02	0.78	-0.22
QMAX	0.80	-0.25	0.44
QMIN	-0.79	0.26	-0.44
Q+	0.38	0.23	0.65
ClogP	-0.60	-0.59	-0.15
MR	0.99	-0.06	-0.10
Eigenvalues	10.09	1.88	1.28
Eigenvalues cumulative, %	67.24	79.75	88.30

The dependence of the principal component scores of the descriptor matrix is presented in figure 3. Two direct dyes, having as coupling component resorcine (for dye 3), respectively salicylic acid (for dye 10) have a different behaviour in the descriptor space in comparison to the other 14 dyes. This can be explained by the presence of only one phenylic group in each of the coupling components.

Starting from the set of descriptors described above, MLR approach has been applied to model the scores of the chromatographic R_f values. Starting from the entire data set of 16 structural descriptors, intercorrelations between these descriptors have been inspected for the set of 16 compounds. Variable selection by a stepwise regression procedure based on the Fischer test was performed. All the statistical tests were tested at a significance level of 5 % or less.

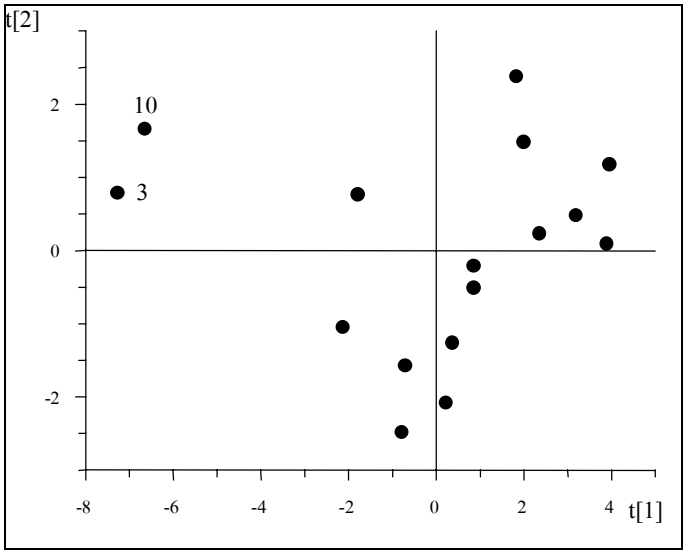

Figure 3. Dependence of the first principal scores of the descriptor matrix

Following MLR equation (correlation coefficient r, standard error s, F-test, and crossvalidated correlation coefficients $r^2_{CV_{LHO}}$ and $r^2_{CV_{LOO}}$ resulting from the leave-half-out and leave-one-out procedures, respectively) was obtained:

$$t[1] = -2.92(\pm 0.748) + 0.66(\pm 0.15) C\log P$$
$$r^2 = 0.572 \quad s = 1.625 \quad F = 18.69 \quad r^2_{CV_{LHO}} = 0.372 \quad r^2_{CV_{LOO}} = 0.488 \qquad (2)$$

Equation (2) indicates that dye hydrophobicity influences significantly the lipophilic dye behaviour.

CONCLUSIONS

This paper presents an experimental and theoretical evaluation of chromatographic mobilities i.e. R_f values of a series of 16 direct dyes containing 4,4'-diaminobenzanilide as a middle component. Molecular dye structures were energy minimized using the MM2 force field and by the semiempirical continuum-solvation model COSMO-AM1. Several molecular descriptors were derived from the energetically minimized molecules. Principal Component Analysis was then applied to the descriptor matrix. Volume and bulkiness parameters produced an important contribution to the first PC. Polarity parameters contributed to the second principal component. Two direct dyes, having only one phenylic group in each of the coupling component (resorcine, respectively salicylic acid) have a different behaviour in the descriptor space in comparison to the other 14 dyes. The R_f values were obtained by reverse-phase thin-layer chromatography

and then were quantitatively analysed by MLR (Multiple Linear Regression) analysis. Good correlation with the scores of the R_f values obtained by principal component analysis and predictability were noticed. Hydrophobicity of the direct dyes influences significantly their lipophilic behaviour.

ACKNOWLEDGEMENTS

Parts of the results presented in this paper were supported from the GAR contract of the Romanian Academy no. 29/2001.

REFERENCES

1. W. Biedermann, Migrating cationic dyes for acrylic fibers. *Rev. Prog. Col.,* **1979**, *10*, 1-10.
2. K. Greider, Determination of Acid-dye Standard Affinities for Nylon Fibres from Sorption Isotherms. *J. Soc. Dyers Colour.,* **1976**, *92,* 8-13.
3. D.G. Duff, D.J. Kirkwood, D.M. Stevenson, Behaviour of Dyes in Aqueous Solutions. I. The Influence of Chemical Structure on Dye Aggregation – a Polarographic Study. *J. Soc. Dyers Colour.,* **1977**, *93*, 303-306.
4. H. Zollinger, Dye and substrate. Role of hydrophobic bonding in dyeing process. *J. Soc. Dyers Colour.,* **1965**, *81*, 345-350.
5. T. Imae, C. Mori, A.. Ikeda, Adsorption and micellization of a surface-active dye in aqueous methanol solutions. *J. Chem. Soc., Faraday Trans. 2,* **1982**, *78*, 1359-1368.
6. W. Biedermann, A.. Datyner, The interaction of nonionic dye with sodium dodecyl sulfate and its correlation with lipophilic parameters, *J. Colloid and Interface Sci.,* **1981**, *82*, 276-285.
7. D.M. Stevenson, D.G. Duff, D.J. Kirkwood, The Behaviour of Dyes in Aqueous Solutions. Part II – Anionic Dye – Nonionic Surfactant Interactions. *J. Soc. Dyers Colour.,* **1981**, *97*, 13-17.
8. H. Van de Waterbeemd, B. Testa, In: *"Advances in Drug Research"*, (B. Testa, *Ed*.), Academic, London, 1987, Vol.16, p. 85-225.
9. D.G. Duff, R.W. Horobin, G.B. Proctor, Estimating the Hydrophobic Character of Dyestuff: A Comparison of Partition, Reverse-Phase Thin-Layer Chromatography and Calculations. *Dyes Pigm.,* **1985**, *6*, 61-73.
10. P. Mukerjee, A.K. Ghosh, Isoextraction method and the study of the self-association of methylene blue in aqueous solutions. *J. Am. Chem. Soc.,* **1970**, *92*, 6403-6407.
11. E. Tomlinson, Chromatographic hydrophobic parameters in correlation analysis of structure-activity relations. *J. Chromatogr.,* **1975**, *113*, 1-45.
12. G. Simu, L. Kurunczi, S. Timofei, E. Dulău, M. Grad, C. Bologa, Application of the multimodal adsorption by cotton of some benzidine-free direct dyes. *Annals of West University of Timișoara, ser. chem.*, **1999**, *8*, 31-36.

13. **ChemOffice 6.0**, CambridgeSoft.Com, Cambridge, MA, U.S.A.

14. A. Klamt, G. Schüürmann, COSMO: a new approach to dielectric screening in solvents with explicit expressions for the screening energy and its gradient. *J. Chem. Soc. Perkin. Trans.* 1993, *2*, 799-815.

15. G. Schüürmann, Assessment of semiempirical quantum chemical continuum-solvation models to estimate pKa of organic compounds. In: *Quantitative Structure-Activity Relationships in Environmental Sciences*. F. Chen, G. Schüürmann, Eds.; SETAC Press, (FL) USA, Volume VII, 1997, p. 225-242.

16. M. L. Connolly, The Molecular Surface Package. *J. Mol. Graphics* **1993,** *11,* 139-141.

17. R. Franke, *Theoretical Drug Design Methods*, Akademie-Verlag, Berlin, 1984

18. D. J. Livingstone, *Methods in Enzimology*, Vol. 203, Academic Press, Inc., 1991, p. 613-638.

19. P. P. Mager, H. Rothe, H. Mager, H. Werner, Advances in Multivariate QSAR on IBM-PC/XT/AT under MS-DOS. In: *QSAR in Design of Bioactive Compounds,* J.R. Prous Science Publishers, 1992, pp.131-182.

20. S. Wold, W.J. Dunn III, Multivariate Quantitative Structure-Activity Relationship (QSAR): Conditions for Their Applicability. *J. Chem. Inf. Comput. Sci.* **1983**, *23*, 6-13.

21. R. Franke, *Theoretical Drug Design Methods*, Akademie-Verlag, Berlin, 1984, pp. 227

22. D. Ciubotariu, E. Deretey, T. I. Oprea, T. Sulea, Z. Simon, L. Kurunczi, A. Chiriac, Multiconformational Minimal Steric Difference. Structure-Acetylcholinesterase Hydrolysis Rates Relations for Acetic Acid Esters. *Quant. Struct.-Act. Relat.*, **1993**, *12*, 367-372.

23. **SYSTAT** package, from Systat Inc., Evenston, IL, SUA

Dedicated to Professor Ionel Haiduc
on the occasion of his 65th birthday

CHLORHIDRIC ACID REMOVAL FROM REACTION EFFLUENT IN MAKING ACETOCHLOR

GHERGHE ALINA*, GHEORGHE OCTAVIA*, COSTICĂ STRĂTULĂ, MIHAELA PETRE****

** Students at the Oil Technology and Petrochemistry Faculty, University "Petrol şi Gaze" from Ploieşti, Ploieşti-2000, Bulevardul Bucureşti nr. 39, Romania*
***Advisers (Prof. Dr. eng. and Asist. eng.), Oil Technology and Petrochemistry Faculty, University "Petrol şi Gaze" from Ploieşti, Ploieşti-2000, Bulevardul Bucureşti nr. 39, Romania*

ABSTRACT. The paper present an experimental study of HCl extraction with water from the mixtures: HCl -ethanol-benzene-water, HCl-ethanol-xilene-water, HCl-ethanol-acetochlor-benzene-water. In this study repartition coeficcients of HCl between aqueous phase and organic phase were determinated. Also, base on experimental data it was established that the named systems obey the Nernst-Silov law.

1. General considerations

In the last few years, in herbicides production was appeared new products which depend on acetochlor, as active substance for compounding.

In order, to obtain this chemical compound ther are used ethanol, formaldehyde, 2-methyl 6-ethyl aniline, the succession of reactions, which takes place in the xylene or benzene medium are next [1, 2]:

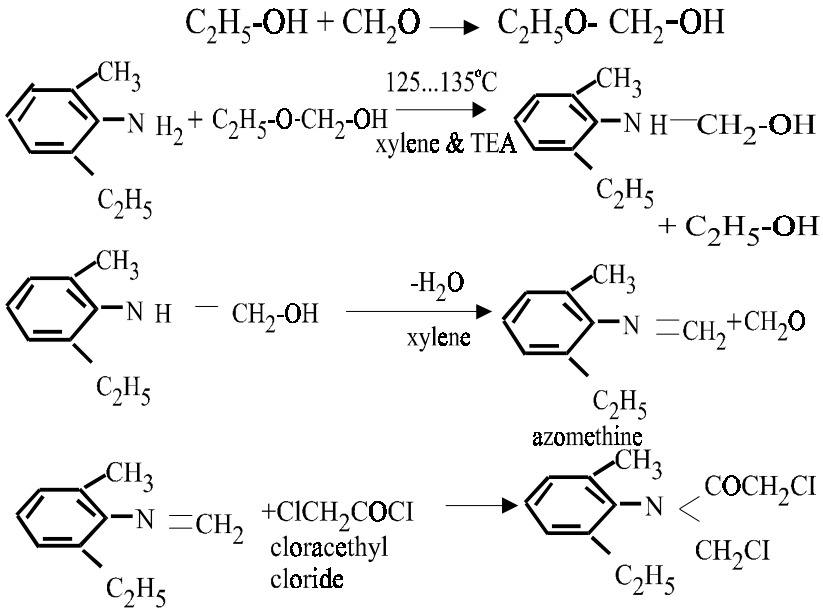

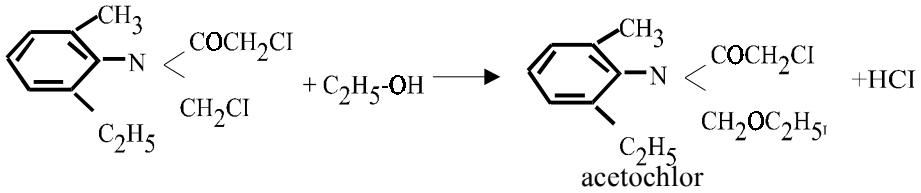

acetochlor

Finally, it was obtained an ethanol, benzene (or xylene), acetochlor and HCl mixture prezented in table1.

Table 1

The final composition of reaction mixture

Component	Concentation, % weight
Acetochlor	27.12
Ethanol	41.56
Benzene (xylene)	26.7
HCl	4.62
Total	100

In nowadays, in order to HCl removal from this mixture ther are uses two processes, based on two patents [1, 2]: first, a process based on the HCl neutralizating with NH_3, the NH_4Cl formed is removed from the system by filtration [1] and second process is based on HCl extracting with water [2].

The filtration presents some troubles because the danger of frecvently clog of filtrant medium. For eliminated this inconvenient, a Romanian chemical company adopts an ICECHIM prosess for a acetochlor synthesis and for HCl removal it is proposed extraction with water.

In the literature [3] there are the liquid-liquid equilibrium data in the system HCl -water-benzene (xylene or toluene), presented graphicaly in figure 1.

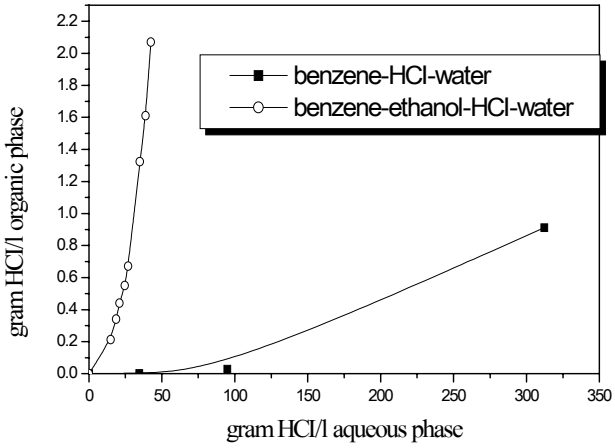

Figure 1. Comparative equilibrium liquid-liquid curves for systems: benzene-HCl -water and benzene-ethanol-HCl -water

The final mixture contains also benzene, acetochlor and ethanol, which significantlly changes the HCl repartition coefficient, especially because, simultaneous with HCl extraction from the organical phase the ethanol is extracted also.

Because the technological design of the HCl extraction with water requires to knowledges liquid-liquid equilibrium data, respectively the HCl repartition coefficients between the aqueous phase and the organic phase in this paper was proposed the experimental determination of these coefficients for this mixture.

2. Experimental determinations

The experimental determinations of HCl repartition coefficients was effectueted with a equilibrium cells at 20^0C, for a synthetic mixture with composition presented in table 1, in two ways: first, it were determinated the repartition coefficients between the aqueous phase and the organic phase which contains only benzene (or xylene) and ethanol, in order to observe the influence of the ethanol presence on repartition coefficients and second, it were determinated the repartition coefficients between the aqueous phase and the organical phase which contains benzene, acetochlor and ethanol conform the synthesis reaction. The experimental results obtained in these two ways are presented graphical in figures 1, 2, 3, 4 and 5.

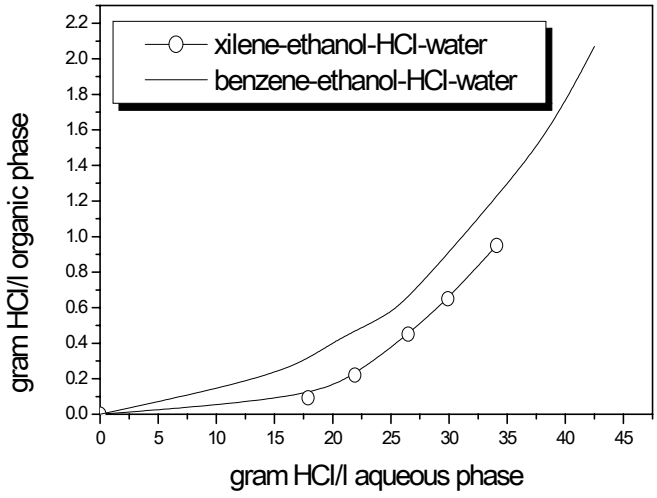

Figure 2. Comparative equilibrium liquid-liquid curves for systems: xylene-ethanol-HCl –water and benzene-ethanol-HCl –water

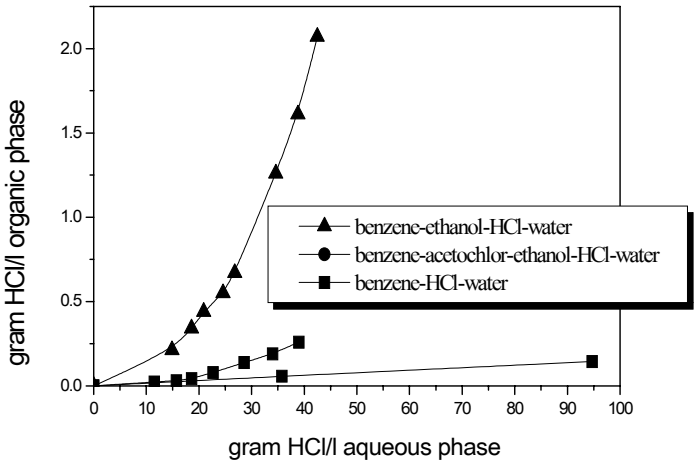

Figure 3. Comparative equilibrium liquid-liquid curves for systems: benzene-ethanol-HCl –water, benzene-acetochlor-ethanol-HCl -water and benzene-HCl -water

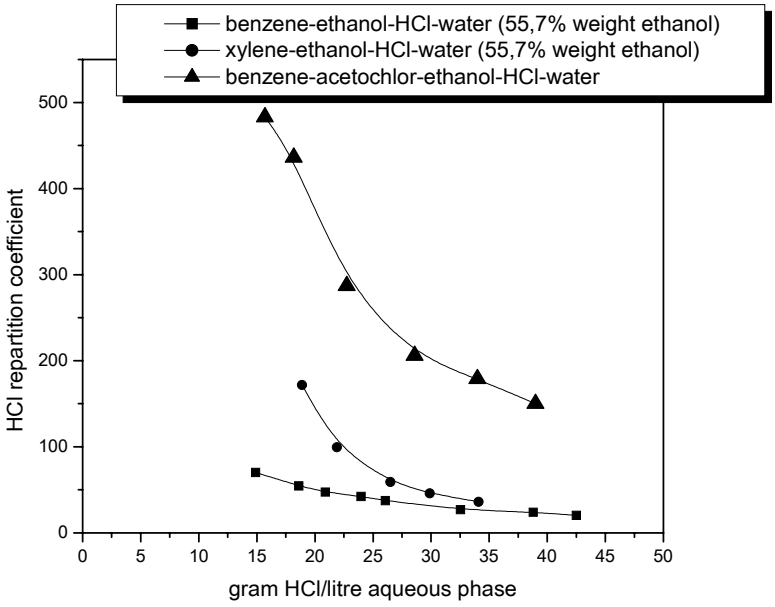

Figure 4. Comparative HCl repartition coefficient curves at 20˚C function by HCl concentration in aqueous phase for systems: benzene-ethanol-HCl –water, xylene-ethanol-HCl water and benzene-acetochlor-ethanol-HCl -water

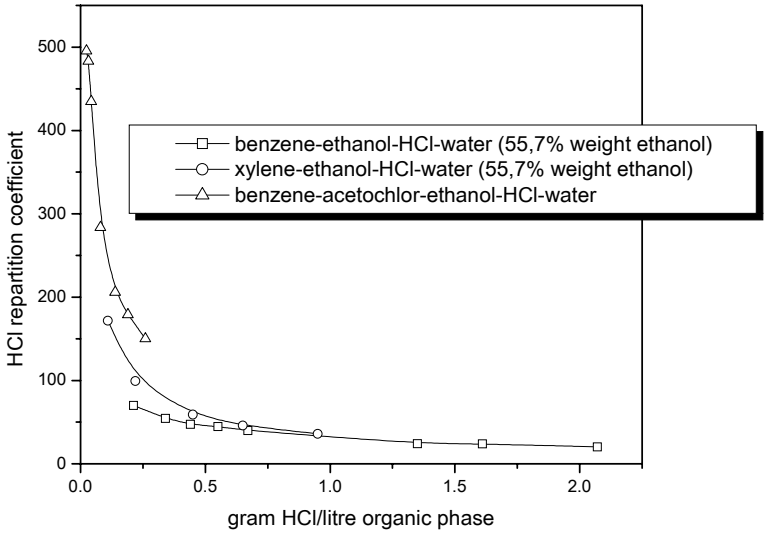

Figure 5. Comparative HCl repartition coefficient curves at 20˚C function by HCl concentration in organic phase for systems: benzene-ethanol-HCl –water, xylene-ethanol-HCl water and benzene-acetochlor-ethanol-HCl -water

For all the cases, including the literature case, the HCl repartition coefficients decrease with the increasing its concetration in the aqueous phase (view figure 4).

The presence of ethanol in the aqueous phase substantial change the HCl repartition coefficients in sense of their decreasing. For example, in case of the mixture in which the ethanol by in organic phase is in a proportion of 55,7% against benzene, respectively xylene, the repartition coefficients decrease from 70,3 to 20,5 in benzene case, respectively from 171,8 to 35,9 in xylene case (view figure 4, 5). This thing is the result of two cumulative effects, namely: first, the high solubility of the ethanol in water, simultaneous with the HCl extraction, take place the extraction of a high quantity of ethanol from organic phase in aqueous phase. The quantity of this phase raise and, in consequently, for a quantity of HCl extract, the concetration in the aqueous phase will be lower and the second, in the organic phase still remains unextract ethanol which favorises the water solubility in the organic phase and, consequently, the HCl solubility, raising in this way the HCl concentration in organic phase.

The HCl repartition coefficients in the benzene-ethanol-HCl -water mixture are lower than the xylene-ethanol-HCl -water mixture case (view figure 4 and 5), because the way in which the ethanol and the water between the hydrocarbon phase and the aqueous phase are distributed.The liquid-

liquid equilibrium data in the benzene-ethanol-HCl -water and xylene-ethanol-HCl -water systems, show that the solubilities of ethanol and water in organic phase are higher in the benzene case than in the xylene case (view figure 2).

3. The mathematical processing of experimental data

In the liquid-liquid extraction with imiscible solvents [4, 5], in the equilibrium data can be exprimate either through Nernst's liniar relation (equation 1), or through Nernst-Silov's nonliniar relation (equation 2), or through a certain curve:

$$K=C_1/C_2 \quad (1)$$

$$K = {}^{C_1}\!/_{C_2^n} \quad (2)$$

where:

K represent the HCl repartition coefficient ;

C_1-concentration of HCl in the aqueous phase;

C_2 -concentration of HCl in the organic phase;

n-specific constant of the system.

A simple looking through the liquid-liquid equilibrium data graphically represented in figures 1, 2 and 3 show that this data can be described either by the Nernst-Silov's rule or by a certain curve. In order to find this we appeal to the second equation which after logarithmation, becomes:

$$ln\ C_1 = lnK + n lnC_2 \quad (3)$$

So, in logaritmic coordinates the (3) equation represented the equation of a straight line with the slope equal to *n* and the intercept equal to *lnK*.

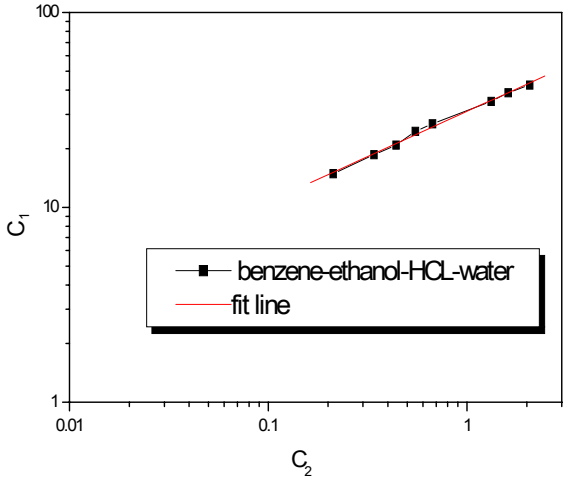

Figure 6. Graphical representation of Nernst-Silov rule for benzene-ethanol-HCl –water system

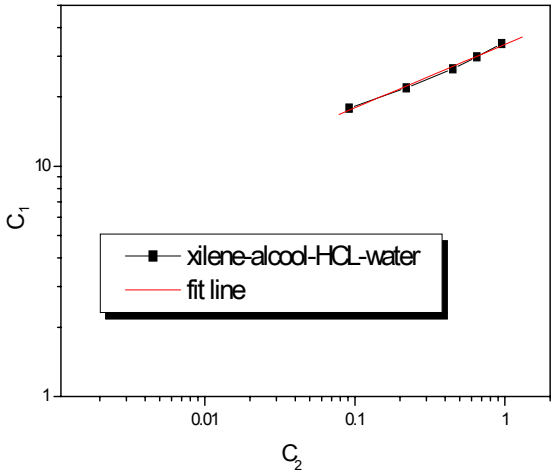

Figure 7. Graphical representation of Nernst-Silov rule for xylene-ethanol-HCl –water system

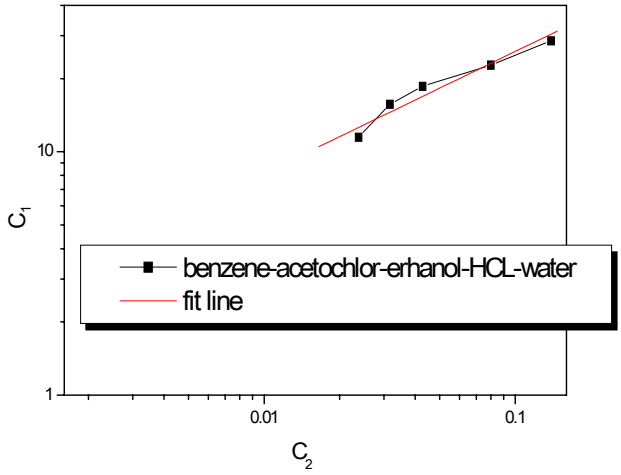

Figure 8. Graphical representation of Nernst-Silov rule for benzene-acetochlor-ethanol-HCl –water system

Grafical represention of these corelation in logarithmic graphics (view figure 6, 7, 8), show that: benzene-ethanol-HCl -water and xylene-ethanol-HCl-water systems obey very well the Nernst-Silov's rule (staight line), while the third system the points spread is a litlle higher.

Conclusions

An experimental study about HCl extraction with water from several systems, namely: benzene-ethanol-HCl-water, xylene-ethanol-HCl-water and benzene-ethanol-acetochlor-HCl-water at 20^0C, was done. In the future will be elaborate a HCl removal technology using washing with water of the reaction effluent based on this experimental study.

The experimental data show that the present of the ethanol in organical phase decreases the HCl solubility in this phase; in this way the value of repartition coefficients between the aqueous phase and the organic phase become lower.

Finally, the mathematical processing of experimental data shows that these above-mentioned systems obey to the Nernst-Silov's rule.

REFERENCES

1. Javdani, K., Nady, L. A., Sih, P.H., Rodriques, G., *Process for the production of azomethines and alphahaloacetanilides*, patent WO 097/1105, sept. 19, 1996
2. Rodrigues, G., *Process for conducting chemical reactions with formaldehyde*, U. S. patent 5.399.759, apr. 22,1992
3. Nenițescu, C. D., *Manualul inginerului chimist*, vol.2, Editura Tehnică, 1952
4. Ionescu, C., ș.a., *Poluare și protecția mediului în petrol și petrochimie*, Editura Briliant, București, 1998
5. Taran, C., Strătulă, C., *Procese difuzionale de separare*, vol. 2, I.P.G., Ploiești, 1979

STUDIA UNIVERSITATIS BABEŞ-BOLYAI, CHEMIA, XLVII, 1-2, 2002

Dedicated to Professor Ionel Haiduc
on the occasion of his 65th birthday

HYDROGEN GAS SEPARATION SYSTEM OPTIMISATION IN HYDROTREATING PLANTS

DANIEL MIHAESCU*, FLORIN OPREA**

** Student at the Oil Technology and Petrochemistry Faculty, University "Petrol şi Gaze" from Ploieşti, Ploieşti-2000, Bulevardul Bucureşti nr. 39, Romania*
***Adviser (Assoc. Prof. Dr. eng.), Oil Technology and Petrochemistry Faculty, University "Petrol şi Gaze" from Ploieşti, Ploieşti-2000, Bulevardul Bucureşti nr. 39, Romania*

ABSTRACT. Actual study reffers to the eficiency of main four separating systems from the most new high performance hydrotreaters.The principal performance criterions are: purity of hydrogen separated, eficient heat integration, lower overall costs due to savings heat exchanger surface, separator investment and operation costs.The data are processed with two important simulation programs: PRO II 3.3, CHEMCAD 5.0.The results of the study show that the design for reactor effluent separation into gas and liquid streams has major impacts on plant operability and economics for both new and revamped units.

1. GENERAL CONSIDERATIONS ABOUT HYDROGEN RICH GAS MAIN SEPARATION SYSTEMS FROM HYDROTREATING PLANTS

Hydrotreating of oil cuts represents a catalytic process to eliminate compounds like: sulphur, oxigen and nitrogen which are transformed in water, hydrogen sulphide and ammonia. The application of this process in oil industry was stimulated by the sources of hydrogen from the catalytic reforming process in the reffinery.

The hydrotreating process includes the next three steps (fig. 1): reaction, phases separation and stripper column step.In this process between reactor and stripper column an important role have phases separators which ensure the separation of hydrogen rich gas, gas that with the completion hydrogen becomes recycle in process.

The literature recommend four separation systems of the phases from effluent reactor.

- System 1 (fig. 2) includes a cold low pressure separator (CLPS) (pressure: 39 bar, temperature: 52^0C). The reactor effluent is cooled through 2 heat exchangers before entering in the separator. The first cooling step of effluent is ensured by heat exchanger E1, cooling agent is the liquid fraction from the separator F1 which is heated to 255^0 C, stripper column entering temperature. In heat exchanger E2 the effluent reactor is cooled using untreated diesel oil (feed of the reactor) like cooling agent, which is preheated before entering the fired heater. The gas phase which result from separator F1 is compressed with C1 compressor to the desulphurization system with MEA and becomes recycle in process.

- System 2 (fig. 3) includes 2 separators: a hot high pressure separator (HHPS) F1 (pressure:41 bar, temperature:191^{0}C) followed by a cold low pressure separator (CLPS) F2 (pressure:39 bar, temperature: 52^{0}C). The reactor effluent is cooled through 2 heat exchangers before entering in the first separator F1. The first cooling step of effluent is ensured by the heatexchanger E1, cooling agent is the total liquid fraction from separators F1, F2 which is heated to 255^{0}C, stripper column entering temperature. In heat exchanger E2 the effluent reactor is cooled using untreated diesel oil (feed of the reactor) like cooling agent, which is preheated before entering the fired heater. Between separators F1 and F2 the gas phase resulted from F1 is cooled in aircooler E3. The hydrogen rich gas separated from F2 is compressed with C1 compressor to the desulphurization system with MEA and becomes recycle in process.

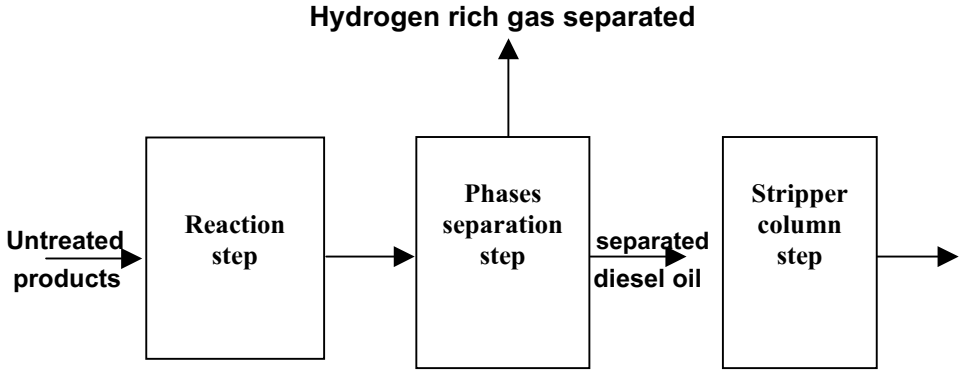

Fig. 1. Main steps of hydrotreating process

- System nr 3 (fig.4) includes 2 separators: a cold high pressure separator (CHPS) F1 (pressure: 39 bar, temperature: 52^0 C) followed by a cold low pressure separator F2 (CLPS) (pressure: 4.5 bar, temperature: 52^0 C). The reactor effluent is cooled through 2 heat exchangers before entering in the separator F1. The first cooling step of effluent is ensured by the heat exchanger E1, cooling agent is the total liquid fraction from separator F2 which is heated to 255^{0}C, stripper column entering temperature. In heat exchanger E2 the effluent reactor is cooled using untreated diesel oil (feed of the reactor) like cooling agent which is preheated before entering the fired heater. Hydrogen rich gas separated from F1 is compressed with C1 compressor to the desulphurization system with MEA and after that becomes recycle in process. The gas separated from separator F2 is used like fuel gas.
- System 4 (fig.5) includes 4 separators: a hot high pressure separator (HHPS) F1(pressure: 41 bar, temperature: 191^{0}C) followed by a cold low pressure separator (CLPS) F2 (pressure 39 bar, temperature: 52^{0}C), a

hot high pressure separator (HHPS) F3 (pressure: 6 bar, temperature: 191^0C), followed by a cold low pressure separator (CLPS) F4 (pressure: 4.5 bar, temperature: 52^0C). The reactor effluent is cooled through 2 heat exchangers before entering the first separator F1. The first cooling step of effluent is ensured by the heatexchanger E1, cooling agent is the total liquid fraction from separator F3 which is heated to 255^0C, stripper column entering temperature. In heat exchanger E2 the effluent reactor is cooled using untreated diesel oil (feed of the reactor) like cooling agent, which is preheated before entering the fired heater.Between separators F1 and F2 the gas phase resulted from F1 is cooled in aircooler E3 and between separators F3 and F4 the gas phase from F3 is cooled in the aircooler E4. Hydrogen rich gas separated from F2 is compressed with C1 compressor to the desulphurization system and becomes recycle in process. The gas phase from F4 separator is used like fuel gas. [1, 2, 3]

2. SIMULATION OF SEPARATION SYSTEMS TO GET THE OPTIMUM VARIANT

The aim of the present study is the technical and economic analysis of the four hydrogen separation systems to identify the optimum variant. In order to simulate the four separation systems were used two important simulation programs: PRO II 3.3 and CHEMCAD 5.0 and data from industrial process of diesel oil hydrotreating. The properties of untreated cycle oil and products resulted from the hydrotreating process are presented in tables nr: 1, 2 and 3. Other input data about the streams of the reactor are presented in the table nr 4.

Table nr. 1

ASTM D86 curve for untreated diesel oil

T, ^{0}C	180	215	240	264	285	321	360
% vol	0	10	30	50	70	90	97
d_4^{20}=0.835 g/cm^3							

Table nr. 2

ASTM D86 curve for hydrotreated diesel oil

T, ^{0}C	179	213	244	260	284	324	362
% vol	0	10	30	50	70	90	97
d_4^{20}=0.827 g/cm^3							

Table nr. 3

ASTM D86 curve for gasoline

T, C	47	118	157
% vol	0	50	97
d_4^{20}=0.827 g/cm^3			

Table nr. 4

Input and output reactor flow rates

Compounds	Diesel oil	Hydrogen rich gas from R.C	Input reactor flow rate	Output reactor flow rate
	kg/h	kg/h	kg/h	kg/h
H_2		6422	6422	5622
H_2S				2211
C1		10580	10580	10660
C2		5801	5801	6551
C3		3649	3649	4489
iC4-nC4		1626	1626	2130
iC5-nC5		3428	3428	2886
GASOLINE				8257
DIESEL OIL	138800		138800	127500
TOTAL	138800	31506	170306	170306
REACTOR PARAMETERS : PRESSURE: 66 bar TEMPERATURE: 326^0C				

The main data from the simulation used to identify the optimum variant of separation system are:

- Separators costs
- Heat exchangers duty
- The flowrate and purity of hydrogen rich gas separated
- Liquid flowrate before entering into stripper column
- Temperature of cycle oil (feed of the reactor) preheated, with influence to fired heat duty

All this data are presented in tables nr. 5 and nr. 6.
Analysing the data from table nr 5 comes out the next conclusions:

- From the viewpoint of separators costs, system nr 1 is the most advantageous and system nr 4 the most expensive, price diference between system nr 1 and nr. 4 is 170000 USD.
- Analysing the heat exchangers surfaces, system nr 4 is the most advantageous using the smallest total heat exchanger surface, being followed by the system nr 2 due to savings of heat exchanger total surfaces. System nr.4 has an efficient heat integration due to elimination of excessive cooling and lower overall costs due to savings in heat exchanger surfaces.

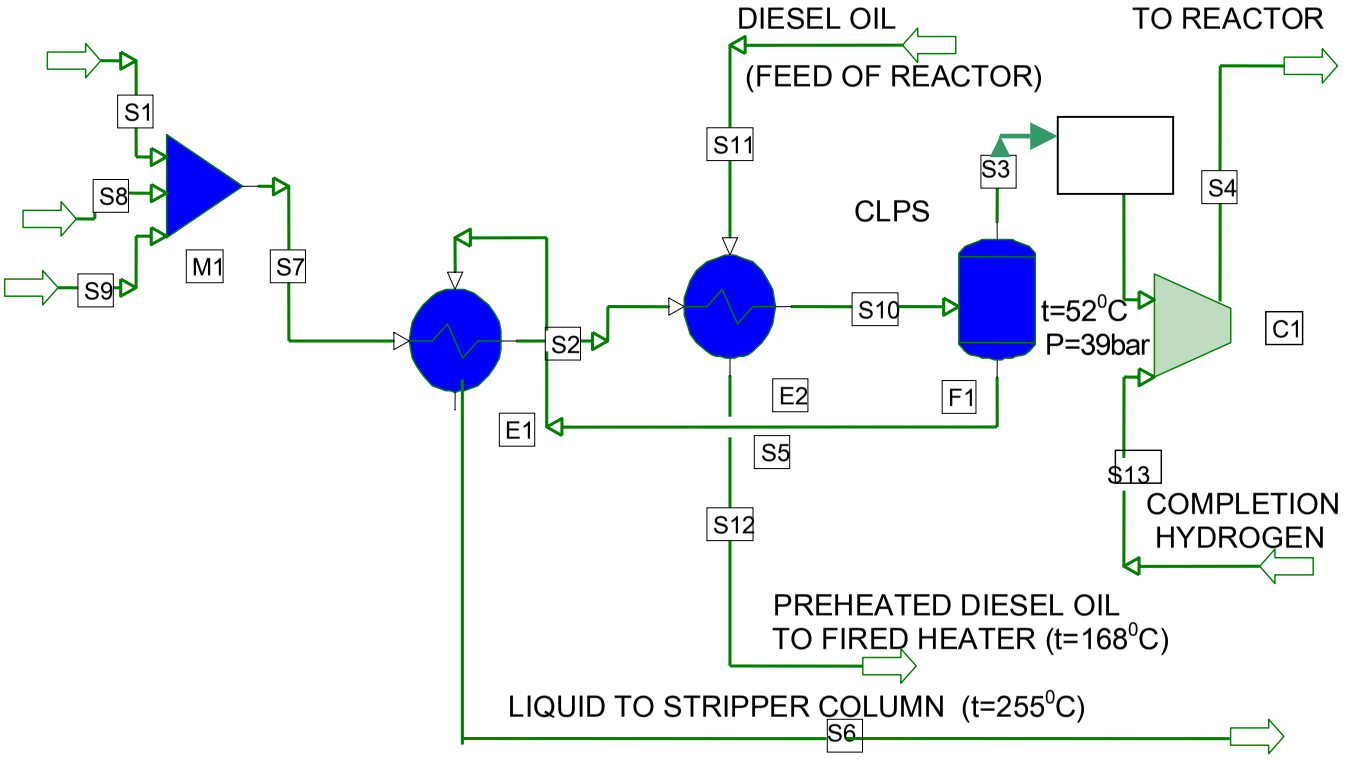

Fig. 2 SEPARATION SYSTEM NR. 1

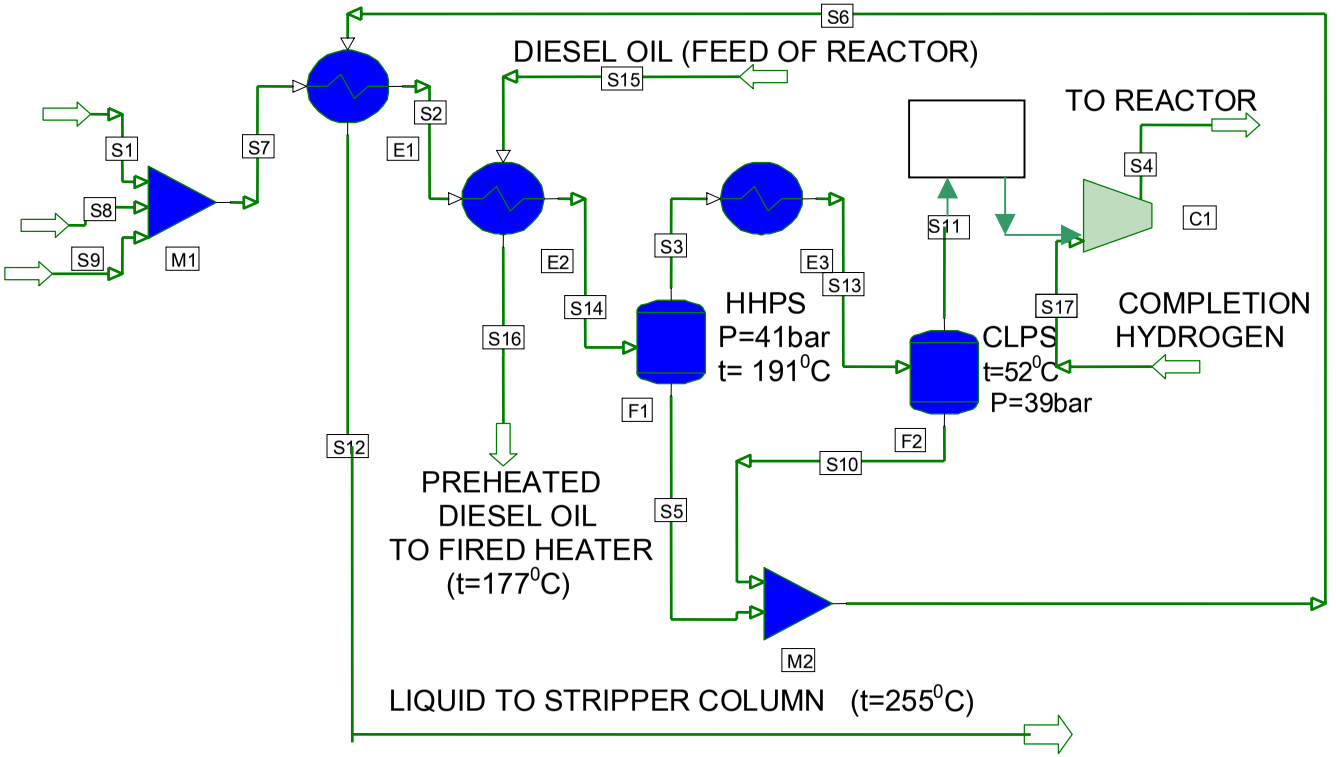

Fig. 3 SEPARATION SYSTEM NR. 2

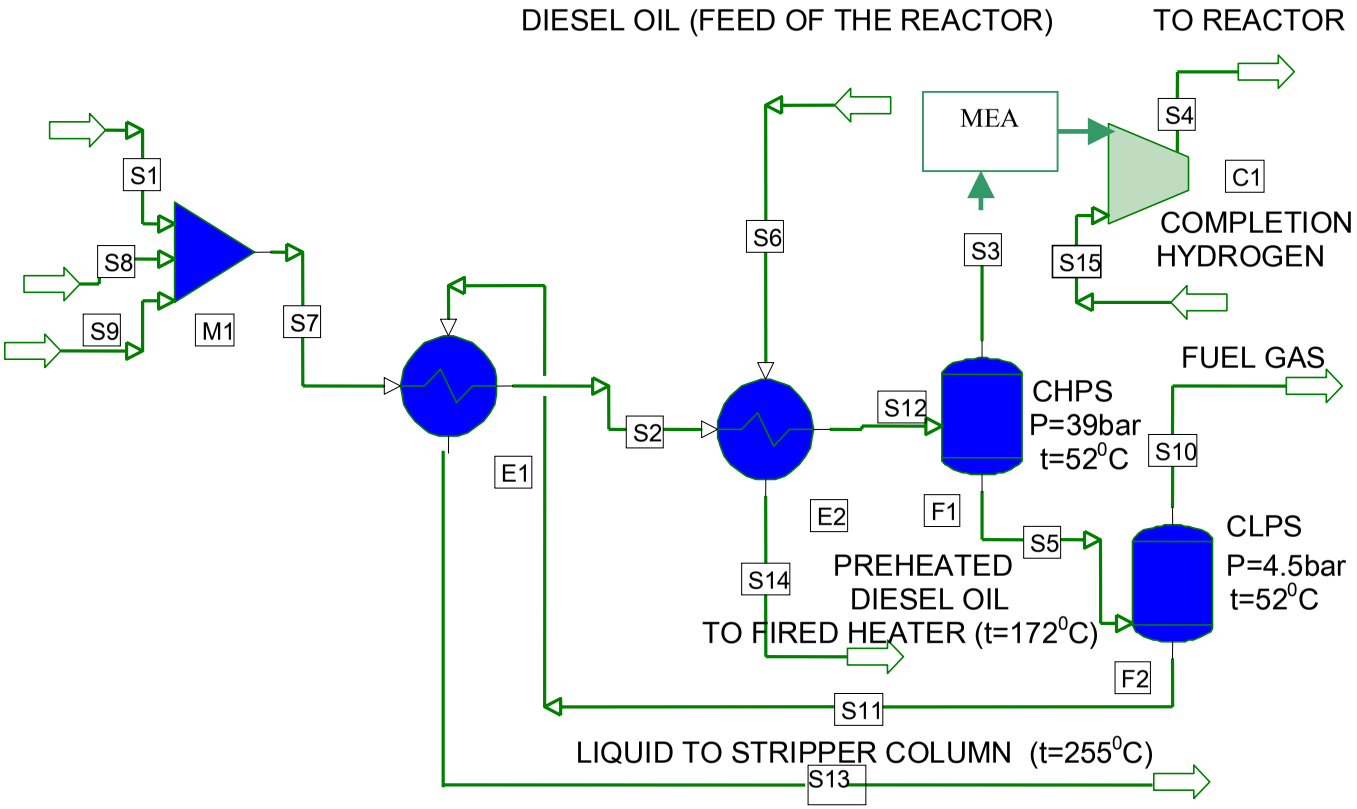

Fig.4 SEPARATION SYSTEM NR. 3

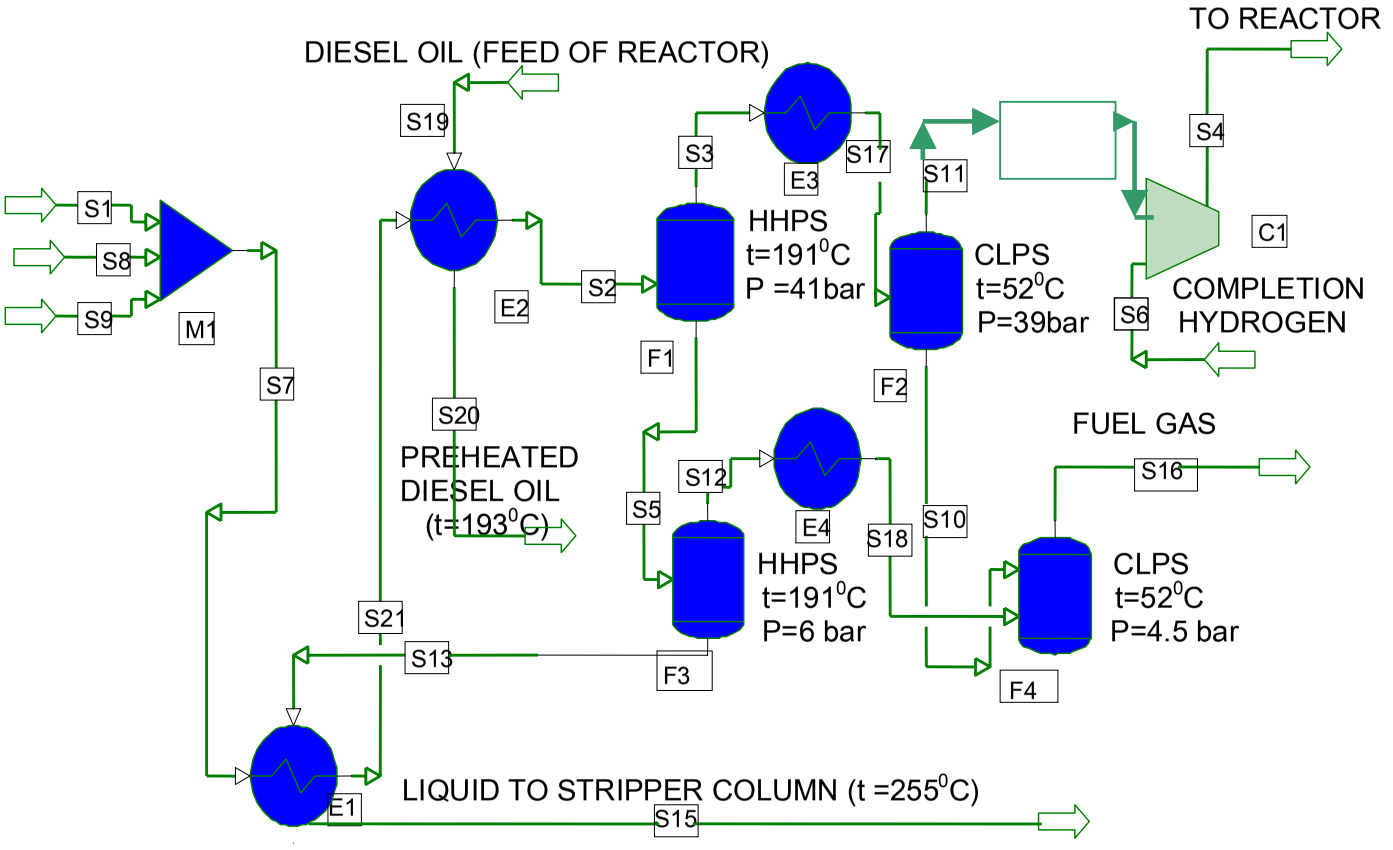

Fig.5. SEPARATION SYSTEM NR. 4

Table nr. 5

Separators costs, duty and total surfaces of heat exchangers (simulation output data)

Separation system	Separators costs, USD	Ratio separators costs to system 1	Heat exchanger		Total heat exchangers surfaces, m^2	Ratio heat exchangers total surfaces to system 4
			Duty, $W*10^{-5}$	Surfaces, m^2		
1	208826	1	E1:198	724	1663	1.67
			E2:182.23	939		
2	200256	1.26	E1:76	364	1004	1.01
	63026		E2:122	336		
	Total:263282		E3:73	304		
3	208826	1.4	E1:190.69	775	1784	1.79
	84364					
	Total:293190		E2: 206.73	1009		
4	200258	1.83	E1: 137.67	394	997	1
	63026		E2: 59.84	289		
	84096		E3: 72.66	304		
	34379		E4: 2.46	10		
	Total: 381759					

Table nr. 6

Flowrate and purity of hydrogen rich gas; flowrate of the liquid to stripper column and temperature of preheated diesel oil (simulation output data):

Separation system	Hydrogen rich gas separated flowrate (to desulphurization), kg/h	Purity of hydrogen rich gas separated, mol. fr.	Hydrogen rich gas flowrate without hydrogen sulphide, (ecycle), kg/h	Purity of hydrogen rich gas (recycle), mol. fr.	Flowrate of hydrogen rich gas(feed of the reactor, H_2 recycle+ completion) kg/h	Purity of hydrogen rich gas (feed of the reactor), mol. fr.	Liquid product flowrate to stripper column, kg/h	Liquid product flowrate ratio to system 4	Preheated diesel oil temperature, ^0C
1	28434	0.738	26223	0.745	27057	0.769	141872	1.14	168
2	32941	0.720	30730	0.736	31582	0.762	137365	1.1	177
3	28434	0.738	26223	0.745	27057	0.769	140397	1.12	172
4	32941	0.720	30370	0.736	31582	0.762	124874	1	193

From the data presented in table nr 6 comes out the next conclusions:

- System nr 4 is the most advantageous from the viewpoint of diesel oil preheated .The temperature of diesel oil resulted from system nr 4 is higher than in other 3 system cases .The fired heater duty is lowest.
- The flowrate of liquid which enter into stripper column is the lowest at system nr 4 because of the oportunity to flash off light fractions from the liquid phase whithout going into column .This offloads the column and the overhead compressor system significantly. [4]

- From the viewpoint of hydrogen gas purity the differences between all four systems are not important.

As results, it is obvious that system nr 4 although is more complicated like design and require a higher cost for the separators with 83%, (170000 USD) more than system 1 case, the savings due to heat exchangers total surfaces; offloading the columns and the overhead compressor and especially lower overall fired heater duty (because of preheated cycle oil temperature); it reduces the fired heater duty with 2 400 000 Kcal/hour, that represents 230 kg fuel less (for fired heater)/hour with value 230 000 USD/ year, recommend system nr. 4 as the optimum variant for both new and revamped hydrotreating plants. [5]

REFERENCES

1. Feyer-Ionescu, S., Hidrofinare–Hidrocracare, cap V, *Ingineria Prelucrării Hidrocarburilor*, vol II, Ed Tehnică, București, 1967
2. Nastasi, A., *Ingineria Prelucrării Hidrocarburilor*, vol 2, cap. Hidrofinarea, Ed. Tehnică, București, 1974
3. Suciu, G. C., *Ingineria Prelucrării Hidrocarburilor,* vol. 4, cap. Procedee de tratare cu hidrogen, Ed. Tehnică, București, 1993
4. Stratula, C., *Vaporizarea și condensarea, principii și metode de calcul*, cap. 6, Ed. Tehnică, București, 1988
5. Dobrinescu, D., *Procese de transfer termic și utilaje specifice*, cap. 3, Editura Didactică și Pedagogică, București, 1983

STUDIA UNIVERSITATIS BABEŞ-BOLYAI, CHEMIA, XLVII, 1-2, 2002

Dedicated to Professor Ionel Haiduc
on the occasion of his 65th birthday

POSITRON EMISSION TOMOGRAPHY (PET) – PRINCIPLES AND GENERAL CHARACTERISTICS

AUREL-VASILE MARTINIUC[*,], LUC CINOTTI[**], VICTOR BOCOŞ-BINŢINŢAN[*], LUMINIŢA UNGUREANU[***]**

[*] *Research Institute for Analytical Instrumentation, Cluj-Napoca, Romania*
[**] *Centre d'Exploration Médicale par Emission de Positons (CERMEP), Lyon, France*
[***] *"Babeş-Bolyai" University, Faculty of Mathematics, Cluj-Napoca, Romania*

ABSTRACT. Positron Emission Tomography (PET) is a powerful nuclear medicine technique. Nuclear medicine techniques allow the visualization of physiological phenomena *in vivo*, and most important in a non-invasive way, through an external detection. The steps required in PET are the following: synthesis of labeled molecules; administration of these labeled molecules to the subject; scanning process with PET camera; data acquisition and subsequent processing; and finally image assessment. The goal of this paper is to briefly review the essential aspects concerning the PET technique, focusing on its principles and characteristics.

1. Introduction

Positron Emission Tomography (PET) presents two useful specific characteristics concerning *in vivo* determination of physiologic, biochemical and pharmaco-kinetics parameters, applied to humans.

On one hand, PET performs a quantitative autoradiography of positron emitters' distribution by using the method of standardized tomography reconstruction, which means that the images of PET correspond to an evaluation of region radioactivity expressed in the quantity of radioactive element on mass unit or tissue volume.

On the other hand, among the positron emitters there are short-lived radioisotopes (like oxygen, carbon, nitrogen), which allow the marking of the majority of the metabolic substratum without introduction of any heteroatoms. Oxygen-15 (produced in a cyclotron) is a short-lived isotope and offers a real possibility to study the cerebral blood flow and the local oxygen consumption of brain, making PET investigation a true non-invasive method.

Speaking about the principle of operation, in Positron Emission Tomography the electron-positron pair suffers an annihilation process in order to form two γ photons of 511 keV energy each; these γ rays are simultaneously emitted in two quite opposite directions. The detection process is made electronically, since both photons are detected due to their interaction with mineral crystals (the detector chain) resulting in photoelectric effect; a photomultiplier chain detects the scintillation photons. The schematic diagram of a PET chamber is given in Figure 1, while the annihilation process is presented in Figure 2.

A PET chamber may be defined as a 3-D detection instrument for coincident 511 keV γ-rays. This chamber is a high-tech, very complex device, which includes: the instrument body (with the detectors and all the subsequent electronics); the bed for the patient (which may be x-y moved); and the computer used to drive the instrument, to store the acquired images, and finally to reconstruct these images.

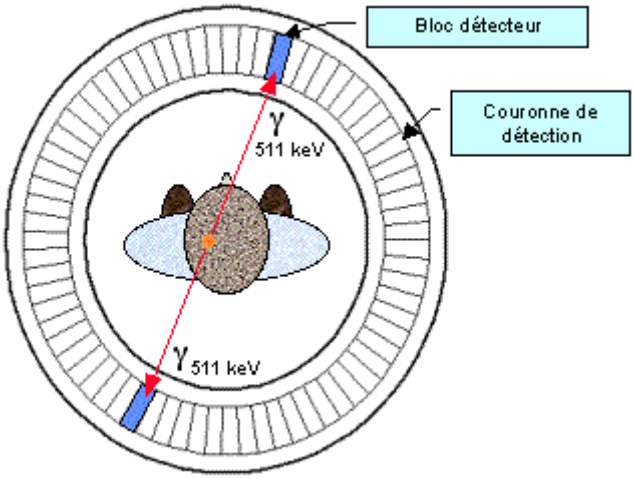

Fig. 1. Schematic of the PET chamber

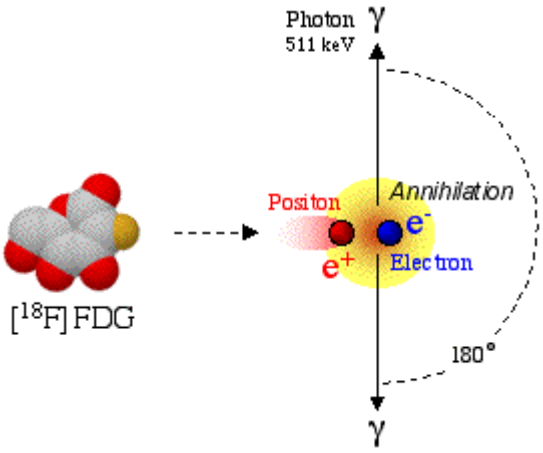

Fig. 2. Diagram of the annihilation process

It is important to remind that the calculation of the physiologic parameters using PET images is a difficult approach, which necessitates the elaboration and validation of the methods and models using numerical analysis appropriate to the studied systems and also to the technical performances of the detectors [1].

2. General characteristics of Positron Emission Tomography

2.1. Principles of PET

2.1.1. Principle of emission

After the synthesis process of the labeled molecules, the molecules of short-lived radioisotopes (positron emitters) are injected or inhaled into the human body and then follow either a metabolic process (glucose or protein syntheses, etc.), a physiological process (flow, distribution volume), or a pharmacological process (being fixed on a ligand, for instance). During the time, the isotopes incorporated in these molecules suffer a radioactive disintegration with positron emission. This is an isotrope emission proportional to the activity, and in fact with the local concentration of the tracer. The positron covers a certain distance within the subject in concordance with its maximum emission energy, until it meets and suffers an interaction with a free electron [2].

The electron-positron pair, having a 1.022 MeV/c^2 repose mass, suffers an annihilation in order to form two gamma (γ) photons of 511 keV energy each. These γ rays are simultaneously emitted in two quite opposite directions, according to the residual quantity of movement after the collision. In reality, the detectors dimension and the quantity of the collected events do not allow measuring this angular scatter, hence the directions are considered as opposed.

The magnitude of time interval of the process is on the order of 10^{-9} seconds (nanosecond range) for both disintegration and β^+ (positron) emission detection. Thus, as an example, if the interaction has taken place in the center of a 90-cm diameter tunnel, the time needed by the photon to reach the detector is equal with 1.5 ns.

2.1.2. Principle of detection

In PET the detection process is made electronically; both photons are detected due to their interaction with the mineral crystals, resulting in a photoelectric effect. Each of the interactions will produce a scintillation photon, which is detectable by a photomultiplier that in turn transforms the light impulse into an electric impulse.

An event is recorded in concordance with its spatial direction, at that moment when two detectors of the ring get independently a signal in coincidence (or in others words at the same time). It is very important to note that in reality the probability of detection at an instant time *'t'* is zero, so that is why one takes into account a Δt, time domain, called "coincidence window", which is electronically commanded and which records the coincidence events included in the Δt period.

This type of detection presents a number of limits, due to the fact that a same pair of detectors can accept a number of different types of coincidences:

1. True coincidences - the pair of detected photons via electronic signal corresponds effectively to the β annihilation process.
2. Coincidences measured after the diffusion process of the rays: one or two photons of 511 keV suffered a modification of initial direction, due to Compton scattering in the subject.

3. Random coincidences: when two radioactive disintegration events take place simultaneously in different points of scanned object, and consequently a pair of photons (one from the first, and the other from the second disintegration) will be recorded as a coincidence.

It is obvious that all these obstacles concerning image quality should be taken into account, meaning that the technique characteristics of tomography will try to reduce these types of coincidences. To limit scattered coincidences one should choose one of the following methods:

- Increasing the minimal (threshold) energy of selection: the higher the better, because the photon loose energy in diffusion process.
- Window of coincidence should be as narrow as possible, because due to diffusion the time difference between the impact of two photons detected will be increased.
- Introduction of the collimators will reduce the diffusion from a tomograph plane to another.

On the other hand, there are two variants to limit the random coincidences:

a) By reducing the window of coincidence (Δt), because the probability to measure random coincidences increases with time; thus a reduced coincidence window will lead to an increase of the image's quality but in the same time to a lower number of recorded events.

b) By using posterior calculus, based on two type of measurements. In the first case, the counting rate of simple events recorded by some detectors placed on the ring around the subject is used; this rate is proportional with the activity seen by each detector, so that the probability of simultaneous counting by a detector is proportional with the product of both activities: $N_{random} \sim Activity^2 \, \Delta t$. In the second case, a second counting window is open immediately after the first one was stopped (or after a well known delay time), and because the photons have not enough time to arrive to detectors, all the recorded events are random coincidences and should be subtracted from the total data.

2.1.3. Time-of-flight principle. Comparison between TOF systems vs. conventional PET

The basic principle of adding time-of-flight (TOF) information to conventional coincidence counting in PET is to measure the time difference between the two annihilation photons arriving on coincident detectors:

$$\Delta t = 2 x / c,$$

where x is the difference of range and c the light velocity. It allows the spatial localization of the emission event in the vicinity of the positron source, instead of spreading it over the coincidence line. The method supposes that the very fast time-coincidence technique is used, and for this purpose the choice of the crystal and associated electronic circuit used is crucial. As an example, if x= 15 cm

and t= 1 ns, thus an accuracy of 50 ps for Δt would correspond to a 7.5 mm spatial resolution and is equivalent to that obtained with scintillators 15 mm in size, without any reconstruction procedure. In a few words, by using TOF information a coincidence event will be not only localized by lengthways of the coincidence line, but also it will be localized more accurately by the difference of path lengths of annihilation photons between the each coincident detectors. Thus, it is necessary to build up a faster window of coincidence.

The essential advantages of TOF information when used in PET are:

1) As a consequence of the very short scintillation time delivered by fast crystals, a TOF system is able to handle very high counting rates without a pile-up effect and consequently enables for fast dynamics studies.
2) The short range of γ-ray TOF (on the order of 2 ns for a 30-cm object) enables a good elimination of random events.
3) Approximate localization of the source positron results in an improvement of the S/N ratio, which provides a good sensitivity gain [3,4].

Random coincidence rate with TOF:

It is obvious that high random rates introduce dramatic image contrast degradation and even if they are correctly evaluated and subtracted the additional noise could increase the quantitative uncertainty. One of the advantages of random rejection is that one can use more active transmission sources and therefore reduce the acquisition time necessary for an accurate attenuation correction in quantitative studies.

Sensitivity:

TOF can substantially improve the S/N ratio of the tomographic images obtained and qualitatively illustrates this S/N improvement as compared to that obtained with a PET conventional back-projection procedure. The information is much more concentrated in the vicinity of the point source in the TOF technique than in the conventional method, where the information is back-projected only on a fraction of the object. In practice this is equivalent with a substantial decrease in the number of pixels concerned in the reconstruction procedure [4].

Spatial resolution:

Spatial resolution of TOF systems is limited by the size of the detectors for at least two reasons: their lower intrinsic stopping efficiency, and unavailability of small, very fast commercial photomultipliers.

For these reasons, small high spatial resolution detection elements cannot be used currently in TOF-based PET system and a compromise should be chosen between spatial resolution and resolving time. There are essentially two major advantages of the use of TOF over conventional PET, namely its ability to handle very high-count rates without saturation, and a good rejection of random coincidence rate [5].

On the other hand, the sensitivity gain can hardly balance the intrinsic lower efficiency of a fast scintillator compared to that of BGO (bismuth germanate oxide) used in conventional PET, and spatial resolution of TOF system is limited

by the relatively large detector size. As to the first point BaF_2 scintillator being non-hygroscopic, the compact arrangement of such crystals on ring detectors will improve the overall sensitivity, especially when expressing it in terms of counts per seconds / μCi / cm of axial length. Moreover, with BaF_2 the resolving time of a ring detector with a large number of crystals will be on the order of 300 ps (FWHM), thus corresponding to an equivalent sensitivity of 4 to 10 fold greater than conventional PET system (with a comparable geometry) as a function of the object dimensions.

2.1.4. The sensitivity of detection in PET

Sensitivity of detection is defined as the number of the detected events per second for a given radioactivity concentration enclosed in a volume unit. The sensitivity actually determines the counting statistics.

Crystal sensitivity:

The sensitivity of the crystal varies with:

- the nature of the scintillation crystal. Studies are conducted to more efficient detectors than NaI/Tl, such as bismuth germanate ($Bi_4Ge_3O_{12}$ or BGO), cesium fluoride (CsF) or barium fluoride (BaF_2). Factors such as light randament of scintillation (which establishes the number of photons sent to the photomultiplier PM - see Table 1) and stopping capacity of γ photons in connection with density of detection mineral (for BGO, after a pathway of 25 mm up to 90% of 511 keV photons are stopped) have to be considered.
- crystal size, essentially in two modes [6]:
  - section surface increases the sensitivity but decreases spatial resolution;
  - high energy of rays detected imposes the use of thick detectors (Table 1)
- threshold of energy selection: the lower is energy selection, the more photons of annihilation are restrained but there will be a higher number of scattered or random coincidences.

Table 1.

Detectors characteristics over sensitivity

Material	Scintillation time constant	Window of coincidences (ns)	Light yield (mm)	Crystal density (g/cm^3)
BGO	300 ns	12 – 20	8 – 12	7.13
BaF_2	0.8 ns (TOF)	4.1	5	4.89
CsF	3 ns (TOF)		8	4.64
Na/Tl	230 ns	12 – 20	100	3.67
GSO	60 ns		16	6.71
$YalO_4$	31 ns		24	5.35
$PbSO_4$	135 ns		67	6.20

Sensitivity of the photomultiplier tubes (PMT)

The PMT intervenes in sensitivity with both its selection (which allows him to collect the light according to its surface), and respectively the quantum yield of the cathode.

The chain detectors - PM has a determinant importance in counting statistics. If for example the number of photons produced by a γ (511 keV) interaction is up to 2000 then the measurement has an error of 5% [7].

2.1.5. The resolution of positron emission tomography

a) Intrinsic spatial resolution

For the newest PET devices for animal studies, a spatial resolution of 2-mm full width at half maximum (FWHM) is attained; for human studies a 5-mm resolution is achieved. High resolution is needed in order to measure tracers' flow in vascular spaces and the uptake and clearance of tracers in small structures. A high-resolution image will appear to be noisier, but the placement of reconstructed activity will more accurately reflect the true distribution. This accuracy is compromised for a low resolution image, no matter how many events are taken.

Intrinsic spatial resolution is fully determined by the machine geometric characteristics – crystal disposal around the ring and especially the size of elementary crystal section.

To achieve a high spatial resolution while retaining a good temporal resolution and detection efficiency, it is necessary to consider the following factors [5]:

- multiple rings of closely packed detectors of high density and atomic number for a good detection efficiency;
- small crystal for a good spatial resolution;
- a minimum of detector sampling motion (stationary or two position claim) for short imaging time ($\leq$ 2s);
- many parallel detectors channels for low dead-time and high rates;
- photopeak light selection on each crystal for rejection of tissue–scattered annihilation photons and multiple crystal interactions;
- good timing resolution (3-10 ns full coincidence window) for accidental background rejection;
- optimal shielding design for the rejection of prompt scatter and accidental backgrounds.

The factors that influence the resolution of PET are:

1- size of crystal – the smaller is the crystal, the better is resolution (this effect is inverse to that one concerning sensitivity);

2- initial energy of positron emission (isotope energy), which increases positron range before the interaction (Table 2).

Table 2.

Correlation between energy of positron emission (isotope energy) and positron range before the interaction

Isotope	Eβmax (MeV)	Δ(FWHM) $FWHM_0$=11mm	Free distance covered (mm) 75%
18-F	0.64	0.22	1.29
11-C	0.96	0.28	2.10
15-O	1.72	1.10	4.80
82-Rb	3.35	2.60	12.40
13-N	1.19	0.50	3.00
68-Ga	1.90	1.35	5.40

The annihilation events distribution at a point source has an approximately Gaussian form, having FWHM (in mm), approximately equal to ratio of maximum energy E_{max} (MeV) of positron and tissue density. In brain, image degradation due to positron range for the most usual isotopes (C-11; O-15; F-18) will be up to 1 cm (for F-18 2.3 mm, O-15 over 8 mm). Certain isotopes such as 38-K or 82-Rb provide positrons of high energy, which is an impediment, due to the decrease of the resolution. Additionally, even though γ rays of annihilation are generally emitted in opposite directions (at 180°), there would be a deviation from the direction and also the resolution quality will decrease (there is an uncertainty concerning collinearity of $\pm$0.25°). At 50-cm diameter rings may appear deviations that provide a decrease in resolution up to 1 mm, and for 100-cm diameter a resolution damage of 2 mm could occur. Even if the detector is made by discrete elements, all these form a continuous cylindrical detector (ring) and this fact leads to problems in accuracy of localization of scintillation events due to Compton scatters and others interactions. The range of this effect is up to 1 or 2 mm. It is important to underline here that an important phenomenon takes place when the annihilation photon arrives on detector surface under an angle: this will lead to a decrease of radial resolution for large distances from the image center.

3- object position over the tunnel center (Table 3).

Table 3.

Intrinsic resolution

0		10	20	Distance by center (cm)
BaF_2	5.4×5.7	5.4×6.2	6×8.6	Tangential and radial resolution (mm)
	8.9/7	10.2/10.4	12.5/21.4	Axial resolution (mm)
BGO	6.0	6.3	7.1	Radial resolution (mm)
	5.4	6.3	7.1	Axial resolution (mm)

The ring size in the slice plan (x,y) determines if the scanner should be used for cerebral exploration only, or for the whole body. Diameter of ring will modulate the resolution (peak), the homogeneity at FWHM as a function of distance to the center (a ring for whole body will provide a more homogenate

center), and the sensitivity. In accordance with the number of rings, z-axis is more or less explored which involves a movement or not of the patient within the tomograph for visualizing the whole organ (Table 4).

Table 4.

Ring size and slices to be explored

	Axial field	Elements
BaF_2	8.4 cm	7 cups of 9 mm , space of 12 mm
BGO	10.8 cm	31 cups 3.375 mm
	16.2 cm	47 cups of 3.125 mm (67 cups of 2.64 mm- to be developed)

Summarizing, the spatial resolution limits in PET could be briefly reviewed as a function of: positron range; deviation from 180° emissions; detectors size and detection efficiency; linear density of detectors in use; and multiple interactions within the crystal.

b) Temporal resolution:

Temporal resolution depends not only by the limits imposed by counting statistics, but also by the cycle of elementary sampling. With a rotational speed maximum of one round (circle) per second we can obtain one image each second.

In practice it is necessary to have a sequential mode for collecting data on a support and also to perform the reconstruction after choosing the optimal sequences.

For a bolus injection of 20 mCi of labeled water (with 15-O) for cardiac study, an image of right ventricle can be done by accumulating the coincidence events within the 2 seconds and in 4 seconds for left ventricle.

3. Conclusions

In this work the general characteristics and principles of PET were briefly discussed.

One should realize the increasing importance of this particular technique over the conventional nuclear medicine, from several points of view. First of all, PET may offer a non-invasive investigation method, being in fact the best method in brain disorders investigation [8]. Furthermore, PET technology uses short-lived radioactive isotopes and biocompatible-labeled molecules as markers, so that the tracer carrier is extremely fast and well assimilated by the body; therefore, PET is a very suitable technique for metabolic studies [7].

PET technique presents the auto-attenuation feature, which is not yet available for other conventional nuclear medicine techniques; also, the possibility of quantification has a crucial importance for the comprehension of the physiological mechanisms' studies.

Last, but not least, PET technique offers a pretty fast imaging response (the whole cycle of investigation takes from few minutes to few hours).

BIBLIOGRAPHY

1. Depresseux, J.C., *"Modèles et méthodes cinétiques en imagerie fonctionelle médicale"*, Ed. John Libbey, London – Paris, pp. 35-44 (1989)
2. Masanori, I; Ballinger, J.R.; Golan, A.; Vines, D.; Luong, A.; Tsai, S.; Kung, H.F., *"Noninvasive quantification of dopamine D2 receptors with iodine-123-IBF SPECT"*, Journal of Nuclear Medicine, Vol. 37, No. 3, pp. 513-519 (1996)
3 Anderson, J.L.R.; Schneider, H., *"Weighted summation of O-15-water PET data to increase signal to noise ratio for activation studies"*, Journal of Nuclear Medicine, Vol. 38, No. 2, pp. 334-340 (1997)
4. Greitz, T.; Ingvar, D.H.; Widen, L., *"New developments in PET instrumentation using the time-of-flight information"*, Raven Press, New York (1985)
5. Brownell, G.L.; Burnham, C.A.; Chesler, D.A., *"High resolution tomograph using analog coding"*, Raven Press, New York (1985)
6. Derenzo, S.E.; Budinger, T.F.; Huesman, R.H., *"Detectors for high resolution dynamic positron emission tomography"*, Raven Press, New York (1985)
7. Votaw, J.R.; Schulman, S.D., *"Performance evaluation of the pico-count flow-through detector for use in cerebral blood flow PET studies"*, Journal of Nuclear Medicine, Vol. 39, No. 3, pp. 509-515 (1998)
8. Ida, H.; Higano, S.; Tomura, N. et al., *"Evaluation of regional differences of tracer appearance time in cerebral tissue using [15-O]-water and dynamic Positron Emission Tomography"*, Journal of Cerebral Blood Flow, Vol. 8, No. 2, pp. 285-288 (1998)

STUDIA UNIVERSITATIS BABEŞ-BOLYAI, CHEMIA, XLVII, 1-2, 2002

Dedicated to Professor Ionel Haiduc
on the occasion of his 65th birthday

CLUJ POLYNOMIALS

MIRCEA V. DIUDEA

"Babes-Bolyai" University, Faculty of Chemistry and Chemical Engineering, 11 Arany Janos str., RO-3400, Cluj-Napoca, Romania

ABSTRACT. A novel class of distance property polynomials *P*(*G*,*x*) is proposed, as an extension of the well-known Hosoya polynomial. The polynomial coefficients are calculated by means of layer/shell matrices, built up according to the vertex distance partitions of a graph. Basic definitions and properties for the Cluj matrices and corresponding polynomials, as particular cases of the distance property polynomial, are given.

INTRODUCTION

A graph can be described by: a connection table, a sequence of numbers, a derived number (called sometimes a topological index), a matrix, or a polynomial. Quantum chemistry was the first field in Chemistry that used the polynomial description of a molecular graph. In the early Hűckel theory, the roots of the most studied *characteristic polynomial*:

$$Ch(G,x) = \det[x\mathbf{I} - \mathbf{A}(G)] \tag{1}$$

with **I** being the unit matrix of a pertinent order and **A** the adjacency matrix, are assimilated to the π-electron energy levels of the molecular orbitals in conjugated hydrocarbons. Other related topics are: Topological Resonance Energy TRE, Topological Effect on Molecular Orbitals, TEMO, the Aromatic Sextet Theory, AST, the Kekulé Structure Count, KSC, *etc.*[1-3]

The coefficients a_k of the characteristic polynomial of order *N* are calculable from the graph *G* on *N* vertices:

$$Ch(G,x) = \sum_{k=0}^{N} a_k(G) \cdot x^{N-k} \tag{2}$$

Relation (2), found independently by Sachs, Harary, Milić, Spialter, *etc.*,[2] makes use of the *Sachs graphs*, contained as subgraphs in *G*. More efficient are the numeric methods of linear algebra, such as the recursive algorithms of Le Verier, Frame, or Fadeev.[4,5]

An extension of relation (1) was made by Hosoya[6] and others[7-10] by changing the adjacency matrix with the distance matrix and next by any square topological matrix.

A different field using the polynomial description is that of finite sequences[2] of some graph invariants, such as the distance degree sequence or the sequence of the number of *k*-independent edge sets. The polynomial corresponding to the last sequence was introduced by Hosoya as the Z-counting polynomial.[11] The polynomial roots and coefficients are used for characterization of the topological nature of hydrocarbons.[2,3,11]

The present paper introduces novel distance-based sequence polynomials whose coefficients are calculable from two kinds of layer matrices.

BASIC DEFINITIONS

Define a *distance property polynomial* as:

$$P(G,x) = \sum_{k=0}^{d(G)} p(G,k) \cdot x^k \qquad (3)$$

with $p(G,0) = P = \sum_i p_i$. In relation (1), *p*(*G,k*) is twice the contribution to the global (molecular) property *P*=*P*(*G*) of the vertex pairs located at distance *k* from each other, in the graph *G*. The summation runs from zero to *d*(*G*), which is the *diameter* of *G* or the longest distance in the graph.[2,12]

When the local property p_i = 1 (*i.e.*, the vertex cardinality), *p*(*G,k*) denotes the number of pair vertices separated by distance *k* in *G*, and the classical Hosoya polynomial[13] (more exactly twice this polynomial) is recovered. In this case, $p(G,0) = N$, where *N* stands for the number of vertices in the hydrogen depleted molecular graph.

The polynomial coefficients *p*(*G,k*) are calculable as the column sums in the layer matrices **LM** and **SM**. They are non-square arrays collecting *shells of property*, located at distance *k* around each vertex.

Let us define the k^{th} layer/shell of vertices *v* with respect to the vertex *i* as:

$$G(i)_k = \left\{ v \middle| \; v \in V(G); \quad d_{iv} = k \right\} \qquad (4)$$

The collection of all its layers defines the partition of *G* with respect to *i*:

$$G(i) = \left\{ G(i)_k \; ; k \in [0,1,..,ecc_i] \right\} \qquad (5)$$

with ecc_i being the *eccentricity* of *i* (*i.e.*, the largest distance from *i* to the other vertices in *G*). Since **LM** was defined elsewhere,[14] (see also ref. 15) we give here only the *shell matrix* **SM**, the entries of which are defined as:

$$[\mathbf{SM}]_{i,k} = \sum_{v \left| d_{i,v} = k \right.} [\mathbf{M}]_{i,v} \qquad (6)$$

where **M** is any square topological matrix. Any other operation over the square matrix entries $[\mathbf{M}]_{i,v}$ can be used. The shell matrix is a collection of the above defined entries:

$$\mathbf{SM} = \left\{ [\mathbf{SM}]_{i,k}; i \in V(G); k \in [0,1,..,d(G)] \right\} \quad (7)$$

The zero column vector $[\mathbf{SM}]_{i,0}$ collects the diagonal entries in the parent square matrix. In the case that they are zero, by definition, $[\mathbf{SM}]_{i,0}$=1. The property p_i is usually introduced by means of the zero column. An example is given for the shell Cluj matrix of the graph 1 (see below).

The name of a property polynomial is built up by exchanging the letter *P* for a string including: L (or S) for the type of layer matrix, symbol of the *info matrix* **M**, and the local property p_i. For example, *SUCJ*(*G*,*x*) reads: the polynomial of the Shell, Unsymmetric Cluj matrix (see below). In the case of a graph theoretical property, p_i is implicitly 1, and therefore omitted.

Vertex contributions to the global polynomial can be written as:

$$P(i,x) = \sum_{k=0}^{d(G)} p(i,k) \cdot x^k \quad (8)$$

where *p*(*i,k*) is the contribution of vertex *i* to the partition *p*(*G,k*) of the global molecular property *P*. Note that *p*(*i,k*)'s are just the entries in **LM** or **SM**.

Usually, the contribution of vertices (*i.e.*, atoms) to the molecular property vary in a molecular graph, so that the polynomial for the whole molecule is obtained by summing all atomic contributions:

$$P(G,x) = \sum_i P(i,x) \quad (9)$$

In a vertex transitive graph, the vertex contribution is simply multiplied by *N*:

$$P(G,x) = N \cdot P(i,x) \quad (10)$$

A *distance-extended property* can be calculated by evaluating the *first derivative* of the polynomial, for *x* = 1:

$$P'(G,1) = \sum_{k=1}^{d(G)} k \cdot p(G,k) = D\_P(G) \quad (11)$$

Any square matrix can be used as an info matrix for the layer matrices, thus resulting in an unlimited number of property polynomials. The property *P* can be taken either as a crude property (*i.e.*, column zero in **LM**) or within some weighting scheme (*i.e.*, transformed by the sequence: **W**-operator **W**(**M**1,**M**2,**M**3), **W**(**M**) matrix, **LM**/**SM**).[2] In the present paper we limit discussion to some graph theoretical properties. Various property polynomials, using physico-chemical properties are exposed in a following paper.[16]

HOSOYA-LIKE POLYNOMIAL

In the case: p_i = 1, **LM** = **LC**, (*i.e.*, layer matrix of cardinalities) and the property polynomial, called the cardinality polynomial $C(G,x)$, is twice the Hosoya polynomial. The formulas given in the following represent well-known results.[13,17,18]

The index calculated as the polynomial first derivative[13,19] is (twice) the well-known Wiener index,[20] W. It is just a distance-extended property.

$$C'(G,1) = \sum_{k=1}^{d(G)} k \cdot p(G,k) = 2 \cdot W \tag{12}$$

The hyper-Wiener index WW, originated by Randić,[21] is calculated as:

$$WW(G) = W(G) + \Delta(G) \tag{13}$$

where $\Delta(G)$ is the non-Wiener part[22,23] of the hyper-Wiener number, calculable from the second derivative[17] of the Hosoya polynomial.

$$WW(G) = H'(G,1) + (1/2)H''(G,1) \tag{14}$$

In terms of $C(G,x)$, the relation is trivially deduced from (14):

$$WW(G) = (1/2) \cdot C'(G,1) + (1/4)C''(G,1) \tag{15}$$

For the graph G_1, the Cardinality polynomial is:

$$C(G,x) = LC(G,x) = 7 + 12x + 14x^2 + 12x^3 + 4x^4 \tag{16}$$

Real Roots = -0.723, -0.723, -0.134, -0.134.

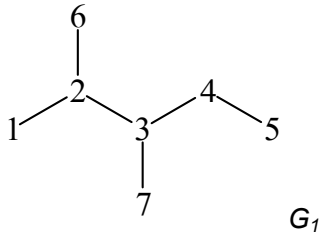

G_1

CLUJ POLYNOMIALS

Cluj polynomials, as particular cases of the distance property polynomial, make use of the shell matrix **SM** for re-arrange the basic Cluj matrices.

Define the *Cluj fragments*[2,23] $CJ_{i,j,p}$ as the set of vertices v lying closer to i than to j and at least one path $p(i,v)$ exists so that it intersects the path $p(i,j)$ at most in i.

$$CJ_{i,j,p} = \left\{ v \middle| v \in V(G); d(G)_{i,v} < d(G)_{j,v}; \text{and } \exists\ p(i,v) \cap p(i,j) = \{i\} \right\} \quad (17)$$

The above definition holds in any undirected graph. The intersecting condition means at least one path $p(i,v)$ is external to the "prohibited" path $p(i,j)$. In trees, due to the unicity of paths joining any two vertices, $CJ_{i,j,p}$ means the number of paths going to *j* through *i*. In this way, we characterize the path $p(i,j)$, designed as *p* hereafter, by a single endpoint, that suffices for the unsymmetric Cluj matrix **UCJ**.[23]

In cycle-containing graphs, more than one path could join the pair (*i,j*), thus resulting more than one fragment related to *i* (with respect to *j* and a given path *p*). By definition, the entries in the Cluj matrix are taken as the maximum cardinality among all such fragments/sets:

$$\mathbf{[UCJ]}_{i,j} = \max_{p} \left| CJ_{i,j,p} \right| \quad (18)$$

When the path *p* belongs to the set of *distances* (*i.e.*, geodesics) *D*(*G*), the corresponding Cluj matrix is designed as **UCJDi**. When $p \in \Delta(G)$ (*i.e.*, detours), the symbol will be **UCJDe**.

A variant of Cluj fragmentation,[2,24] called $CF_{i,j,p}$ considers all the paths $p(i,v)$ external to $p(i,j)$. It is possible by cutting the "prohibited" path $p(i,j)$, excepting its endpoints. Thus, relation (17) becomes:

$$CF_{i,j,p} = \left\{ v \middle| v \in V(G); d(G_p)_{i,v} < d(G_p)_{j,v};\ G_p = G - p(i,j) \right\} \quad (19)$$

Relation (18) also holds, in terms of *CF* fragments. The corresponding matrices, denoted by **UCFDi** and **UCFDe**, are in general unsymmetric, apart from some symmetric graphs. This is also true for the **CJ** matrices. They can be made symmetric by the Hadamard multiplication with their transposes:

$$\mathbf{M}_p = \mathbf{UM} \bullet (\mathbf{UM})^{\mathrm{T}} \quad (20)$$

$$\mathbf{M}_e = \mathbf{M}_p \bullet \mathbf{A} \quad (21)$$

The subscript *p* means that the matrix is defined on paths (*i.e.*, on all pair vertices) while *e* designates an edge defined matrix. Note that, in trees, the four variants of Cluj matrices are one and the same, so that the symbol **CJ** (unless otherwise specified) will hereafter be used. Only tree graphs are considered here. The shell matrix and its parent **UCJ** for the graph 1 are illustrated in Table 1. Relations for the column sums are given in the bottom of the table.

Table 1

	SUCJ(G_1)						**UCJ**(G_1)							
i \ *k*	0	1	2	3	4	$\sum_{k=1}^{d(G)}$	1	2	3	4	5	6	7	*RS*
1	1	1	2	2	1	6	0	1	1	1	1	1	1	6
2	1	15	6	3	0	24	6	0	3	3	3	6	3	24
3	1	15	13	0	0	28	4	4	0	5	5	4	6	28
4	1	8	4	4	0	16	2	2	2	0	6	2	2	16
5	1	1	1	2	2	6	1	1	1	1	0	1	1	6
6	1	1	2	2	1	6	1	1	1	1	1	0	1	6
7	1	1	2	3	0	6	1	1	1	1	1	1	0	6
CS	7	42	30	16	4	92[a]	*CS* 15	10	9	12	17	15	14	92
CS·k		42	60	48	16	166[b]								

(a) 2x*W*; (b) 2x*WW*

For the graph G_1, several Cluj polynomials are exemplified:

$$SUCJ(G,x) = 7 + 42x + 30x^2 + 16x^3 + 4x^4 \quad (22)$$

Real roots = -5.264 -0.389 -0.173 -0.173

$$SURCJ(G,x) = 7 + 8.656x + 5.645x^2 + 3.642x^3 + 0.916x^4 \quad (23)$$

Real roots = -0.783 -0.391 -0.031 -0.031

$$SCJ(G,x) = 7 + 92x + 50x^2 + 20x^3 + 4x^4 \quad (24)$$

Real roots = -12.593 -0.305 -0.122 -0.122

$$SIUCJ(G,x) = -3.975 - 1.804x + 2.464x^2 + 3.225x^3 + x^4 \quad (25)$$

Real roots = -0.515 -0.515 -0.486 1.061

$$SWUCJ(G,x) = 92 + 42x + 30x^2 + 16x^3 + 4x^4 \quad (26)$$

Real roots = -0.324 -0.324 0.096 0.096

In the above polynomials, the matrices are as follows: unsymmetric Cluj (22); unsymmetric reciprocal Cluj (23); symmetric Cluj (24); inverse unsymmetric Cluj (25) and walk (of rank 1) of unsymmetric Cluj (26). The free term in (22) to (24) equals the number of vertices in *G*, which is taken by definition for the zero diagonal matrices. The different free term in the last two examples indicates matrices having non-zero diagonals. The diagonal entries in the walk matrix of rank *e* (relation 26) equals the row sum in the matrix **M** raised to the power *e*, $[^e\mathbf{WM}]_{ii} = R(\mathbf{M}^e)_i$. Note that in (26) the free term is twice the Wiener number.

The walk matrix **W**(**M**) is constructed by following the $^{e}\mathbf{WM}$ algorithm,[14] extended for walk count in general graphs and any square matrix. The walk matrix together with the triple matrix walk operator[25] **W**(**M**1,**M**2,**M**3) is used for mixing the info matrices and weighting the topological descriptors (property polynomials included) by various physico-chemical attributes. Details are given in a following paper of this topic.[16] The calculations were performed by the TOPOCLUJ software package.

* * *

Reverting to the polynomials, the distance-extended property, calculated on the Cluj polynomial (*cf*. (11)), is, in trees, twice the hyper-Wiener index:

$$SUCJ'(G,1) = 2 \cdot WW \tag{27}$$

The sum of polynomial coefficients (for $k > 0$) gives twice the Wiener index:

$$SUCJ(G,1,)_{k>0} = 2 \cdot W \tag{28}$$

In case of *SUCJ*(*G*,*x*), the non-Wiener part of the hyper-Wiener index is:

$$2 \cdot \Delta(G) = SUCJ'(G,1) - SUCJ(G,1,)_{k>0} \tag{29}$$

In case of a symmetric Cluj matrix, the sum of polynomial coefficients gives twice the hyper-Wiener index:

$$SCJ(G,1)_{k>0} = 2 \cdot WW \tag{30}$$

The distance-extended property leads, in this case, to twice the Tratch index.[26]

The non-Wiener part of the hyper-Wiener index $\Delta(G)$ (see eq 13) is now obtained as the difference of the Cluj polynomial coefficients for the symmetric **CJ** and unsymmetric **UCJ** matrices.

$$2 \cdot \Delta(G) = SCJ(G,1) - SUCJ(G,1) \tag{31}$$

CONCLUSIONS

Extension of the well-known Hosoya polynomial, grounded on vertex distance partitions of a graph, resulted in a novel class of distance property polynomials *P*(*G*,*x*). The polynomial coefficients are obtained as the column sums in the layer/shell matrices. The polynomial roots and coefficients can be used for the topological (and chemical) characterization of chemical structures. Examples were given for the Cluj matrices and corresponding polynomials.

Acknowledgements. The paper is supported by the CNCSIS Romanian GRANT, 2002. The author thank to the referees for useful comments.

REFERENCES

1. M. V. Diudea and O. Ivanciuc, *Molecular Topology,* Comprex, Cluj, 1995 (in Romanian).
2. M.V. Diudea; I. Gutman; L. Jäntschi, *Molecular Topology*. Nova Science, Huntington, New York, 2001.
3. N. Trinajstić, *Chemical Graph Theory*, IInd Ed. CRC Press, 1992.
4. P. S. Dwyes, *Linear Computations*, Wiley, N. Y. 1951.
5. D. K. Fadeev and I. S. Sominskii, *Problems in Higher Algebra*, Freeman, San Francisco, 1965.
6. H. Hosoya, M. Murakami and M. Gotoh, Distance polynomial and characterization of a graph. *Natl. Sci. Rept. Ochanomizu Univ.,* **1973**, *24*, 27-34.
7. R. L. Graham and L. Lovasz, Distance matrix polynomials of trees. *Adv. Math*. **1978**, *29*, 60-88.
8. M. V. Diudea**,** O. Ivanciuc, S. Nikolić, and N. Trinajstić**,** Matrices of Reciprocal Distance. Polynomials and Derived Numbers. *Commun. Math. Comput. Chem.* (*MATCH*), **1997**, *35*, 41-64.
9. O. Ivanciuc, M. V. Diudea, and P. V. Khadikar, New Topological Matrices and Their Polynomials. *Indian J. Chem.* **1998**, *37A*, 574-585.
10. O. Ivanciuc, T. Ivanciuc, and M. V. Diudea, Polynomials and Spectra of Molecular Graphs. *Roum. Chem. Quart. Rev*. **1999,** *7***,** 41-67.
11. H. Hosoya, Topological index. A newly proposed quantity characterizing the topological nature of structural isomers of saturated hydrocarbons. *Bull. Chem. Soc. Japan*, **1971**, *44*, 2332-2339.
12. F. Harary, *Graph Theory*, Addison - Wesley, Reading, M.A., 1969.
13. H. Hosoya, On some counting polynomials in chemistry. *Discrete Appl. Math*., 1988, *19*, 239-257.
14. M. V. Diudea, Layer Matrices in Molecular Graphs. *J. Chem. Inf. Comput. Sci.,* **1994**, *34*, 1064-1071.
15. M. Randić, Graph valence shells as molecular descriptors. *J. Chem. Inf. Comput. Sci.* **2001**, *41*, 627-630.
16. O. Ursu and M. V. Diudea, Layer Matrices and Distance Property Polynomials. *Commun. Math. Comput. Chem.* (*MATCH*), submitted.
17. G. G. Cash, Relationship between the Hosoya polynomial and the hyper - Wiener index. *Appl. Math. Lett*. **2001**, *14*, in press.

18. I. Gutman, S. Klavžar, M. Petkovšek, and P. Žigert, On Hosoya polynomials of benzenoid graphs. *Commun. Math. Chem.* (*MATCH*), 2001, *43*, 49-66.

19. E. V. Konstantinova and M. V. Diudea, The Wiener polynomial derivatives and other topological indices in chemical research. *Croat. Chem. Acta,* **2000**,*73*, 383-403.

20. H. Wiener, Structural determination of paraffin boiling points. *J. Am. Chem. Soc.,* **1947***, 69*, 17-20.

21. M. Randić, Novel molecular descriptor for structure-property studies. *Chem. Phys. Lett*., **1993**, *211*, 478-483.

22. M. V. Diudea, Wiener and hyper-Wiener numbers in a single matrix. *J. Chem. Inf. Comput. Sci.* **1996**, *36*, 833-836.

23. M. V. Diudea, Cluj matrix invariants. *J. Chem. Inf. Comput. Sci.* **1997**, *37*, 300- 305.

24. L. Jäntschi, G. Katona, and M. V. Diudea, Modeling Molecular Properties by Cluj Indices. *Commun. Math. Comput. Chem.* (*MATCH*), **2000**, *41*, 151-188

25. M. V. Diudea and Randić, Matrix Operator, $W_{(M1,M2,M3)}$ and Schultz-Type Numbers. *J. Chem. Inf. Comput. Sci.* **1997**, *37*, 1095-1100.

26. S. S. Tratch, M. I. Stankevitch, and N. S. Zefirov, Combinatorial models and algorithms in Chemistry. The expanded Wiener number – a novel topological index. *J. Comput. Chem*., **1990**, *11*, 899-908.

STUDIA UNIVERSITATIS BABEŞ-BOLYAI, CHEMIA, XLVII, 1-2, 2002

Dedicated to Professor Ionel Haiduc on the occasion of his 65th birthday

KINETIC DETERMINATION OF B_1, B_2 and B_6 VITAMINS

SIMONA BUNGĂ U[*], LUCIAN COPOLOVICI[**], GAVRIL NIAC[***] and IOAN BALDEA[**]

[*]Faculty of Medicine and Pharmacy University of Oradea, 29 Nicolae Jiga Str., Oradea, Roumania. E-mail: bungau@uoradea.ro

[**]Faculty of Chemistry and Chemical Engineering, Babeș–Bolyai University, 11 Arany Janos Str., Cluj–Napoca, Roumania

[***] Faculty of Material Science, Technical University, 105 Muncii Av., Cluj–Napoca, Roumania

ABSTRACT. A kinetic method for separate determination of B_1, B_2 and B_6 vitamins has been proposed. It is based on the Landolt type system of redox reactions, is very sensitive, cheap and make use of simple technique. Calibration lines have been obtained under appropriate conditions. Good detection limits as well as good accuracy and precision were found. Some interference of various organic compounds and metal ions have been investigated. The method has been tested to several pharmaceutical products yielding results similar to the certified content given by producers.

INTRODUCTION

Lack of some nutrients causes serious diseases for human, even though small amounts of them are required to maintain good health [1]. The indispensable nutrients are vitamins and are supplemented by eating appropriate food. They can be categorised into two groups: water-soluble and fat-soluble vitamins. The B complex (B_1, B_2 and B_6) are in the first group.

Thiamine (vitamin B_1), which is found in many animal and plant tissue, has been widely used for prevention and treatment of beriberi and neurological diseases in medical doses. Riboflavine (vitamin B_2) is an essential vitamin and it has been used for the treatment of growth disorders, keratite, hypogalactie, steatoree. Pyridoxine (vitamin B_6) is also an essential vitamin for human, possessing many different physiological properties [2, 3]. It is used in prevent nutritional dermatitis.

Many analytical methods for qualitative and quantitative determination of B vitamins have been developed. For determination of thiamine, fluorometry [4-7], spectrophotometry [8,9], chromatography [10-12] and electrochemical analyses [13,14] have been used. Chemiluminiscence has been also explored

to determine thiamine [15,16]. Cherysh *et. al*. [15] first reported that a bright chemiluminiscent radiation appeared during oxidation of thiamine to thiochrome. Grekas and Calokerinos [16] developed a continuous flow-through chemiluminscent system for determination of thiamine based on the oxidation of thiamine to thiochrome by potassium hexancyanoferrate (III) in alkaline medium. However, the drawback of these methods are unsatisfactory detection limit and need of oxidation agent addition for initiating the chemiluminiscence [17].

Hence to establish an analytical method for the determination of pyridoxine in real samples would be useful for the evaluation of various medicine quality and quantitative control. A number of reports on this analysis are mainly liquid chromatography [18-20] and capillary electrophoresis [21-23]. There have been a large number of HPLC studies on determination of vitamins in food, beverages, drugs and biological tissues or fluids [24-26]. Recent studies for quantitative HPLC determination of water-soluble vitamins [27-29] involved extraction and quantification of vitamin B_1, B_2 and B_6 either separately or simultaneously.

In the present work, a simple and quite sensitive method for the separate determination of pyridoxine, thiamine and riboflavine is described. It is based on a Landolt type reaction.

The bromate-bromine mixture has been used since long ago as a way of generating bromine for analytical applications and a number of bromination reactions have been used in classical analysis [30]. Bromine is produced in a relative slow reaction according to the stoichiometry

$$BrO_3^- + 5Br^- + 6H^+ \rightarrow 3Br_3 + 3H_2O \quad (1)$$

and the rate law [31]:

$$\frac{d[Br_2]}{dt} = k \cdot [BrO_3^-] \cdot [Br^-] \cdot [H^+]^2 \quad (2)$$

The bromine generated *in situ* reacts with organic analytes as phenols, aromatic amines and other [32], either brominating or oxidising them rapidly. The vitamins under study react similarly. A steady state Br_2 concentration is maintained as long as the analyte is not entirely consumed and concentration increase take place at completely consumption.

EXPERIMENTAL

Apparatus

The instrumental set up is depicted in Figure 1. It consists from a reaction vessel with temperature control connected to a thermostat. The sensor was a platinum plate electrode, the potential being measured against a saturated calomel electrode by means of a potentiometer (Digitronix DXP 2040). The potentiometer was connected to a computer by means of a data acquisition device.

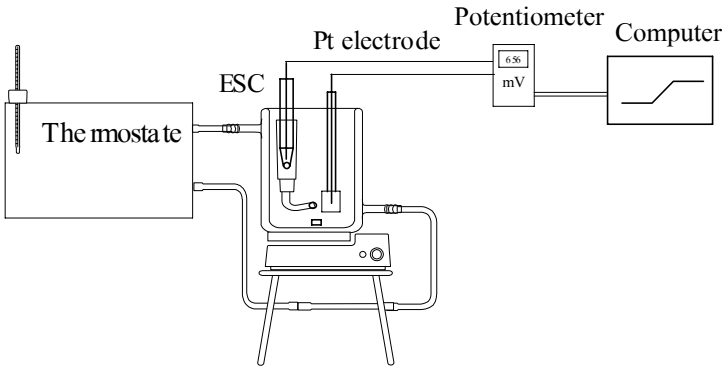

Fig. 1 Experimental device

Chemicals

All reagents used were of analytical-reagent grade. De-ionised and tetra-distilled water was used throughout. Stock solution of perchloric acid (0.5 M), potassium bromide (1 M) and potassium bromate ($3 \cdot 10^{-2}$ M) were prepared and standardized. Vitamin solutions (B_1, B_2, and B_6), in concentration of $2 \cdot 10^{-3}$ M were prepared before each set of experiments.

Procedures

In the case of the determination of thiamine for example, 3 ml of perchloric acid 0.5 M and 5 ml KBr 1 M were mixed with various aliquots of vitamin solution and accurately diluted to 22.5 ml with de-ionised and tetra-distilled water. Over this mixture, 2.5 ml $KBrO_3$ ($3 \cdot 10^{-2}$ M) solution was injected quickly. The zero moment of the reaction is considered that when bromate solution was injected into the mixture.

When medicine was presented as tablets, ten tablets were weighted and pulverised by gentle grinding. An accurate weight of the powder was dissolved and made up to a 100-ml volumetric flask.

When the medicine was injectable vitamins, ten ampoules were dissolved in de-ionised and tetra-distilled water and diluted conveniently.

RESULTS AND DISCUSSION

The reaction stoechiometry was measured by a kind of spectro-photometrical titration previously described [33]. For thiamine the ratio Br_2: thiamine was found to be 2. The stoechiometry is

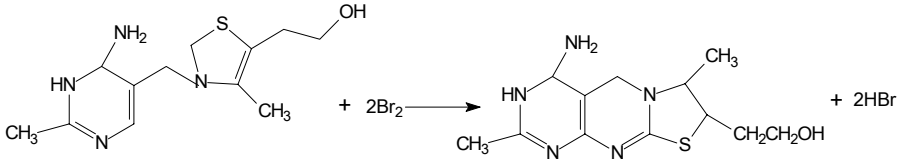

(3)

yielding thiochrome.

For pyridoxine the ratio Br_2 : pyridoxine was found to be 1. We are inclined to consider a bromination reaction rather than an oxidation:

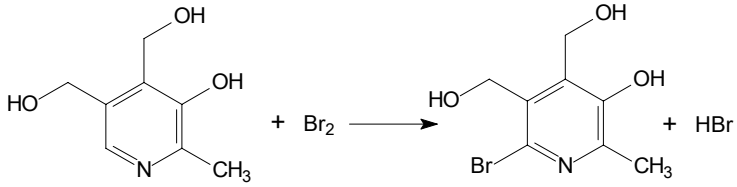

(4)

For riboflavine the ratio Br_2 : riboflavine was found to be 2. The bromination reaction at the aromatic ring is:

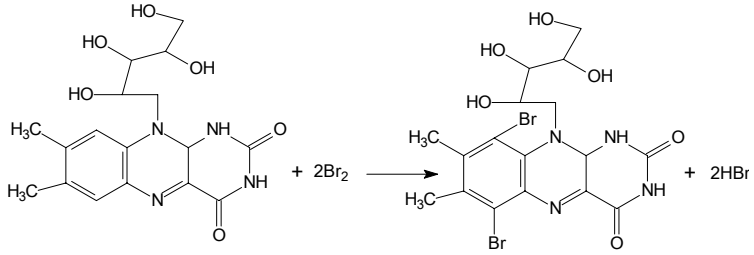

(5)

Under the conditions of a small concentration of bromine, bromination of benzene ring is more probable than the oxidation.

From the analytical point of view, only the reaction ratio is important, not the nature of products or mechanism.

Determination of appropriate conditions for analysis

Appropriate reaction conditions regarding concentration of reagents were searched for in order to ensure a high slope of calibration graphs. Therefore, kinetic runs were performed at various concentrations of potassium bromide, potassium bromate and perchloric acid. All the reagents should be present in excess relative to analyte. The concentration of trapping agent at the largest concentration for obtaining calibration lines should be two orders of magnitude smaller than potassium bromate. The later condition ensures that no more than 5% reaction extent is attained at the end-point. A small extent of the reaction presents the advantage that the side reactions, such as oxidation of vitamins with bromate, will not affect the experimental results.

Figure 2 shows the dependence of reaction time on the acid concentration. According to equation (2), the bromine generation shows a second order dependence on the H^+. Therefore, the acidity strongly affects the bromine generation reaction rate. Because the end point time should be not to short, to avoid errors, and not to long, to avoid side reactions an appropriate value of $6 \cdot 10^{-2}$ M $HClO_4$ has been chosen.

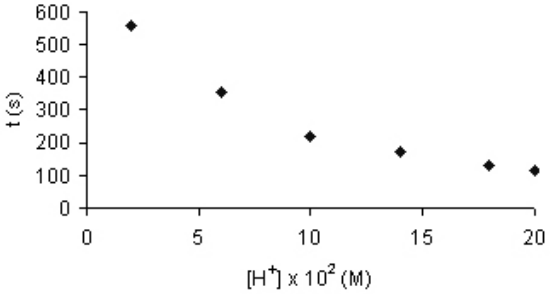

Fig. 2 Influence of $[H^+]$ on kinetic determination of [thiamine] = 4.10^{-5} M, [KBr] = 0,2 M, X = *2,6 %*

As seen in equation (2), the reaction rate of bromine generation follows a first-order dependence on the potassium bromate.and potassium bromine. The concentration of bromate was chosen at $3 \cdot 10^{-3}$ M. A great excess of bromide (0.2 M).has been used. The rate constant of bromine generation change with temperature according to the Arrhenius equation. A value of activation energy of 51 kJ/mol was found within the temperature range 15 and 40 ^{0}C [34]. Following the criteria of obtaining suitable times of analysis, the temperature of 20 ^{0}C seemed to be convenient.

Analytical parameters

Calibration graphs were obtained under the appropriated conditions described above for each vitamin B_1, B_2 and B_6 and are presented in Fig. 3. Each point is a mean of at least 5 individual measurements.

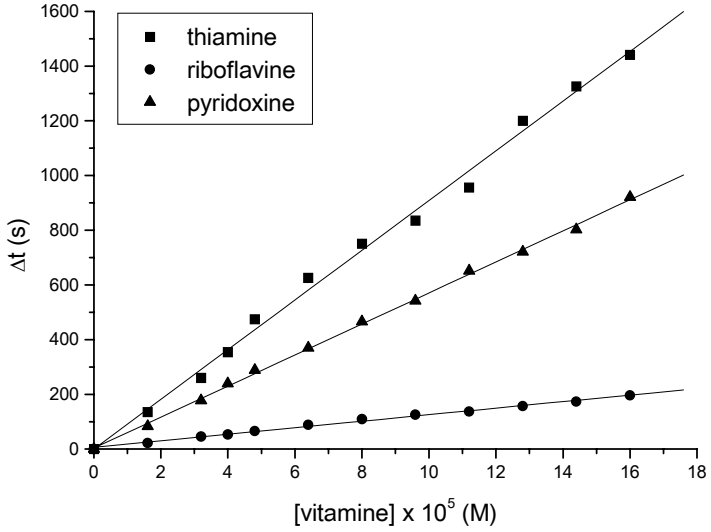

Fig. 3 Calibration lines

Linear regression parameters of calibration graphs are presented in table 1. The limit of detection was defined as $C_L = 3 \cdot S_B/m$ [35], where S_B and m are standard deviation of the blank signal and slope of calibration graph respectively.

Table 1

Linear regression parameters of calibration graphs for vitamins

Compound	Slope x 10^{-6} (s/M)	Intercept (s)	Correlation coefficient (N = 7)	Detection limit x 10^7 (M)
Vitamin B_1	9.02±0.51	0.3±2.3	0.9975	0.9
Vitamin B_2	1.09±0.06	6.0±4.3	0.9975	62.0
Vitamin B_6	5.67±0.12	3.3±5.9	0.9993	7.2

Although the conditions for bromine generation are the same, different slope and consequently different sensibility are obtained for the three B vitamins. The explanation for that is quite simple. The nature of the reaction with bromine is different (B_1- two steps oxidation and ring closure, B_2- two steps bromination and B_6- one step bromination). The rate constants for these reactions are different, but greater than the one for bromine generation. Thus, the level of steady state concentration of bromine is different, causing different rate of its consumption. Unfortunately, these differences in rate are not large enough to provide a way for discrimination between the vitamins under consideration of this clock method.

To evaluate the accuracy and precision of method, a series of independent standard samples was used. The results are given in table 2.

Table 2

Accuracy and precision of the proposed method

Vitamins taken x 10^5 (M)		Relative error (%)	RSD (%)
B_1:	4.0	2.5	1.9
	6.4	1.3	1.6
	14.4	0.5	0.9
B_2:	3.2	3.1	2.2
	4.8	2.0	1.7
	11.2	0.6	1.1
B_6:	8.0	0.8	1.3
	16.0	0.3	0.6

Selectivity

The effect of some organic compounds and heavy metals associated with drugs was studied. The results are summarised in table 3. The tolerance limit was defined as the concentration of added ion causing less than ± 3 %

relative error. Most cations and organic substance did not interfere even when present in 200-fold excess relative to vitamins. On the contrary, ascorbic acid, acetylsalicylic acid, cysteine, and paracetamol interfere in the determination of vitamins.

Table 3

Tolerance limit for diverse organic substance and ions on the determination of $8 \cdot 10^{-5}$ M thiamine

Interference	Tolerance limit ratio (mol/mol)
Citric acid, oxalic acid, tartric acid, glucose, starch, ethanol, methanol	400*
Zn(II), Cd(II), Ni(II), Mo(VI), V(V), EDTA	200*
Fe(III), Cu(II)	90
Vitamin B_{12}	100*
Cysteine, methionine, ascorbic acid, acetylsalicylic acid, paracetamol	1

*maximum limit tested

Applications

The proposed method was applied to the determination of thiamine, riboflavine and pyridoxine in pharmaceutical products. The results are shown in table 4.

Table 4

Results of the determination of B vitamins in pharmaceutical formulations

Formulation	Active substance	Found	Reported	Recovery (%)
Tablet (mg/tablet)	thiamine	10.2	10	102.0
	pyridoxine	248	250	99.0
Injectable (mg/ampoule)	thiamine	50.1	50	100.2
	riboflavine	9.9	10	98.0
	pyridoxine	50.3	50	100.2

As can be seen, an acceptable correlation is found between certified content given by producers and the results obtained by the proposed method.

REFERENCES

1. C. M. C h o, J. H. K o, W. J. C h e o n g, *Talanta,* **2000**, 50, 799-806
2. J. E .F. R e y n o l d s, *The Extra Pharmacopoeia*, 31st Edition, The Royal Pharmaceutical Society, Council of the Royal Pharmaceutical Society of Great Britain, London, **1996**, 1724, 1384
3. Authority of the United States, *Pharmacoperial Convention, Inc., The US Pharmacopoeia/ The National Formulary, the United States Pharmaccopeial Convention, Inc.,* 12601 Twinbrook Parkway, Rockville, MD, **1994**, 1348

4. D. J. Hennesy, L. R. Cerecedo, *J. Am. Chem. Soc*., **1939**, 61, 179.
5. B. Karlberg, S. Thelander, *Anal. Chim. Acta,* **1980**, 114, 129.
6. United States Pharmacopoeial Convention, *US Pharmaco-poeia*, XXI Ed, Mack, Easton, PA, **1985**.
7. T. Perez – Rulz, C. Martinez – Lozano, V. Tomas, I. Ibarra, *Talanta,* **1999**, 39, 907.
8. F. Danet, J. M. Calatayud, *Talanta* **1994**, 41, 2147.
9. Morelli, *Anal. Lett.,* **1994**, 27, 2751.
10. U. Jegle, *J. Chromatogr.,* **1993**, 652, 495.
11. N. Diaz, A. G. Paniagua, F. G. Sanchez, *J. Chromatogr*,. **1993**, 39, 655.
12. L. Gamiz-Gracia, M. M. Luque de Castro*, J. Liq. Chromatogr., Relat. Technol.,* **1997**, 20, 2123.
13. Huang, B. H. Yu, P. B. Li, M. Jiang, Y. S. Bi, S. F. Wu, *Anal. Chim. Acta,* **1995**, 312, 329.
14. Y. F. Zhang, Z. R. Meng, G. R. Zhao, *Fenxi Huaxue,* **1997**, 25, 248.
15. G. P. Chernysh, R .P. Poponina, V. I. Buntushkin, *J. Anal. Chem. USSR,* **1976**, 31, 1475.
16. N. Grekas, A. C. Calokerinos, *Talanta*, **1990**, 37, 1043.
17. Zhang, G. Zhou, Z. Zhang, M. Alzawa, *Anal. Chim. Acta*, **1999**, 394 165
18. S. Kurioka, I. Noriak, S. Junko, J. Nakamura, *Biomed. Chromatogr.,* **1993**, 7, 162.
19. Blanco, L. A. Sanchez, M. P. Gutlerrez, *J. Liq. Chromatogr*., **1994**, 17, 1525.
20. M. J. Esteve, R. Farre, A. Frigola, J. M. Garcia – Cantabella, *J. Chromatogr. A,* **1998**, 795, 383.
21. S. Boonkerd, M. R. Detaeveniner, Y. Michotte, *J. Chromatogr. A,* **1994**, 670, 209.
22. L. Fotsing, M. Fillet, I. Bechet, Ph. Hubert, J. Crommen, *J. Pharm. Biomed. Anal.,* **1997**, 15, 1113.
23. Y. F. Yik, H. K. Lee, S. F. Y. Li, *J. Chromatogr.,* **1991**, 585, 139.
24. M. J. Shearer, in: C. K. Lim (Ed.), *HPLC of Small Molecules-a Practical Approach*, IRL Press, Oxford, **1986**.
25. N. Papadoyannis, *HPLC in Clinical Chemistry*, Marcel Dekker, New York, **1990**.
26. P. J. Van Niekerk, in: R. Macrae (Ed.), *HPLC in Food Analysis*, Academy press, London, **1987**
27. J. S. Powers, J. Zimmer, K. Meurer, E. Manske, J. C. Collins, H. L. Greene, *J. Parent. Enternal Nutr.*, **1993**, 17, 315.
28. T. S. Agostini, H. T. Godoy, *J. High Resol. Chromtogr.*, **1997**, 20, 245.
29. Blanco, L. A. Sanchez, M. D. Gutierrez, *J. Liq. Chrom*., **1994**, 17, 1525.
30. H. A. Laitinen, *Chemical Analysis*, McGraw-Hill, New-York, **1960**, 431
31. J. H. Esperson, *Chemical Kinetics and Reaction Mechanisms*, McGraw-Hill, New-York, **1981**, 5
32. Perez-Bendito, M. Silva, *Kinetic Methods in Analytical Chemistry*, Ellis Horwoord, Chichester, **1988**, 146
33. S. Bungau, I. Baldea, L. Copolovici, *Studia Univ. "Babes-Bolyai" Seria Chemia*, *this issue*
34. Lopez-Cueto, M. Ostra, C. Ubide, *Anal. Chim. Acta*., **2001**, 47, 1
35. Analytical Method Committee, *Analyst*, **1987**, 112, 199

STUDIA UNIVERSITATIS BABEŞ-BOLYAI, CHEMIA, XLVII, 1-2, 2002

Dedicated to Professor Ionel Haiduc
on the occasion of his 65th birthday

CHARACTERIZATION OF THE CHEMICAL WARFARE AGENT SIMULANT METHYL SALICYLATE BY ION MOBILITY SPECTROMETRY / MASS SPECTROMETRY (IMS/MS) AT AMBIENT TEMPERATURE

VICTOR BOCOS-BINȚINȚAN[1,2], C.L. PAUL THOMAS[2], ALAN H. BRITTAIN[3]

[1] - *Research Institute for Analytical Instrumentation Cluj-Napoca, Romania*
[2] - *Department of Instrumentation and Analytical Science (DIAS), University of Manchester Institute of Science and Technology (UMIST), United Kingdom*
[3] - *Graseby Dynamics Limited, Watford, Hertfordshire, United Kingdom*

ABSTRACT. Ion Mobility Spectrometry (IMS) is one of the most powerful and versatile analytical techniques currently available for the trace detection of chemicals, in the gas phase and at atmospheric pressure. IMS plays an important role in many practical applications, from industrial and environmental monitoring to narcotics and explosive detection. Also, IMS hand-held instrumentation is the backbone of chemical warfare agents (CWA) detection system in the USA and NATO countries. This paper describes the behavior of the CWA simulant methyl salicylate, using IMS and IMS/MS at room temperature in the negative operation mode. Ionic mobility spectra and atmospheric pressure ionization chemistry of methyl salicylate are presented.

1. Short description of Ion Mobility Spectrometry

Ion Mobility Spectrometry (IMS) is a modern analytical technique used to detect ultra-traces (at sub-ppb to ppm levels) of both organic and inorganic compounds in the air and so far quite less known worldwide. This technology emerged in 1970 *[1,2]* and then rapidly developed, especially in the last decade. After a period of slight stagnation in the 1980s a true resurrection of IMS happened, due to the real-time response, to its amazing detection limits and also to several practical considerations concerning the instrumentation (such as great simplicity compared with the complex instruments used in mass spectrometry, reliability, ruggedness and miniaturization) *[3,4,5]*. It must be emphasized here another important advantage: IMS fits perfectly to field and process applications.

IMS is based upon the separation of ions - generated by the ionization of the neutral chemical species in gaseous phase at atmospheric pressure - due to their different mobilities in a relatively weak (<300 V/cm) electric field. Separation of ions occurs because of their mobility differences in a neutral drift (buffer) gas - usually nitrogen or air. In IMS the ions produced are effectively

subjected to atmospheric pressure time-of-flight measurements. Using an ionization source in air, a very complex and fast ion-molecule reaction chemistry leads to the formation of many ion clusters, called reactant ions. Water plays an important role in that atmospheric pressure ion-molecule chemistry, so it is obviously necessary to control its concentration. To obtain an optimum performance, it is best to operate the ion mobility spectrometer with dry air (several ppm water vapor) as drift gas; in that case, the degree of clustering is limited and, most important, kept constant.

Positive reactant ions:	*Negative reactant ions:*
$(H_2O)_xH^+$; $(H_2O)_yNO^+$; $(H_2O)_zNH_4^+$	$(H_2O)_xO_2^-$; $(H_2O)_yO^-$; $(H_2O)_zO_4^-$
predominant species: $(H_2O)_xH^+$	predominant species: $(H_2O)_xO_2^-$

In other words, Ion Mobility Spectrometry is first of all an identification technique of trace vapors by measuring their ionic mobilities in the gaseous phase. IMS provides many possibilities for analysis in a whole variety of fields, and in particular in the chemical warfare agents (CWAs) detection; explosives and narcotics detection, as well as occupational hygiene and environmental spheres, are also the application niches preferred for IMS.

A typical ion mobility spectrometer is illustrated in Figure 1.

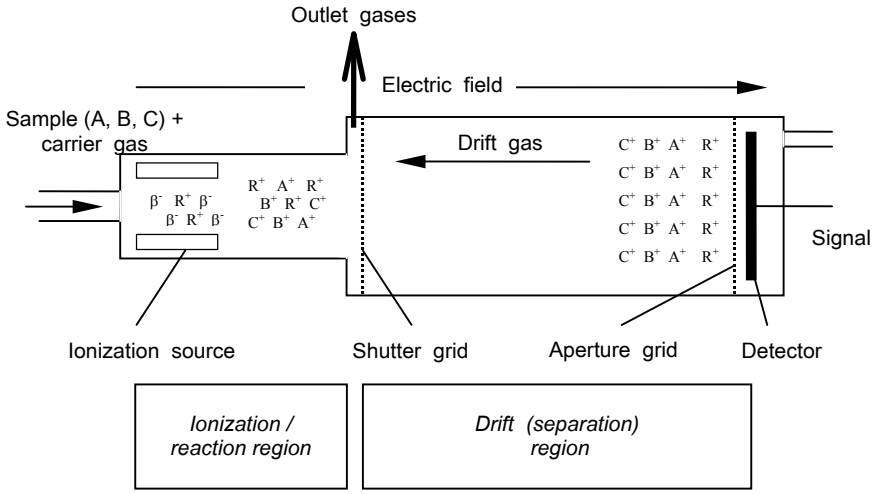

Fig. 1. Schematic of ion mobility spectrometer cell

By applying an electric field, ions of one polarity are extracted from the ionization region before their recombination can occur; these ions are periodically allowed to enter drift region, using a so-called “shutter grid”, periodically triggered open and close by a specialized electronic circuit *[3]*.

Ions migrate towards the detector (a Faraday plate) as a function of their mobility *K*, which is related to mass, size, temperature, pressure and the nature of the neutral species present in the drift region (hence, the drift gas); the Mason-Schamp equation, given below, describes these dependences. Monitoring the ion current in time generates a single ion mobility spectrum; several spectra are averaged to improve the signal to noise ratio, resulting in an ion mobility spectrum (called also plasmagram or IMS signature). After averaging a pre-programmed number of spectra (from 4 to 256, for instance), a processing routine is activated and/or peak measuring programs are used to determine the magnitude of the peaks associated with target analyte. The entire process (data acquisition, averaging and quantitation) can be accomplished in a time interval of 0.5-3 seconds, which means definitely a true real-time response.

The main theoretical issues concerning Ion Mobility Spectrometry are as follows:

- *drift rate equation:* $v_d = K \cdot E = I_d / t_d$ (1)

This proportionality constant ***K*** is exactly *ionic mobility*, v_d is the drift rate, *E* represents the electric field intensity, I_d is the drift length, and t_d is the drift (flight) time of an ion *[1,4]*. The equation (1) describes the behavior of an ion migrating with a constant rate through a neutral drift gas, at atmospheric pressure, under the influence of a relatively weak (with an intensity up to several hundred V/cm) electric field.

- *reduced mobility equation:* $K_0 = (273/T)(P/760)K$ (2)

, where K_0 is the reduced mobility (in $cm^2 \cdot V^{-1} \cdot s^{-1}$), *T* is the absolute temperature of the drift gas, and *P* is the atmospheric pressure *[3,4]*. The role of this particular relationship is to normalize the measured ionic mobilities for temperature and pressure variations.

- *Mason-Schamp equation:* Because the collisions between particles are controlled by forces occurring between them, the mobility should clearly depend on the force between ion and neutral molecule; this dependence appears as an integral of diffusional collision, or the average collision cross section, Ω_D:

$$K = \frac{3}{16} \cdot \frac{q}{N} \cdot \left(\frac{1}{m} + \frac{1}{M} \right)^{1/2} \cdot \left(\frac{2\pi}{kT} \right)^{1/2} \cdot \frac{1}{\Omega_D} \quad (3)$$

Mason-Schamp equation

, where *q* is the electric charge of the ion, *N* is drift gas density, *m* is the mass of the ion, *M* is the mass of drift gas molecule, *k* is the constant of Boltzmann, and *T* is the temperature *[4,5]*.

The samples may be introduced into the ionization/reaction region by using many techniques, but the most common are the semi-permeable membrane inlets (used at ambient temperature, and consequently in the portable hand-held IMS spectrometers) and direct introduction using a heated inlet (used in IMS desktop-sized explosive and narcotics detectors).

The introduction of sample molecules with high proton (or electron) affinity relative to the reactant ions results in the formation of so-called “product ions”, which are ions containing one (or more) sample molecules. Product ions are therefore formed in the reaction region, mainly by collisional charge transfer reactions between the reactant ions and analyte neutral molecules from the sample; they could be also generated by attachment reaction of a reactant ion to the neutral species *M* of analyte *[3,4,5]*:

$$(H_2O)_xH^+ + M \longrightarrow (H_2O)_xMH^+ \quad \text{- for positive ions}$$
$$(H_2O)_xO_2^- + M \longrightarrow (H_2O)_xMO_2^- \quad \text{- for negative ions.}$$

Usually, these product ions (very similar to CI-MS secondary ions) are larger and more massive than the original reactant ions. Therefore, they have longer drift times and consequently lower reduced mobilities.

Very important is the IMS response, which could be briefly defined as the intensity change of the product ions with the modification of analyte concentration. Figure 2 illustrates such a response for an IMS spectrometer equipped with a radioactive ^{63}Ni ionization source.

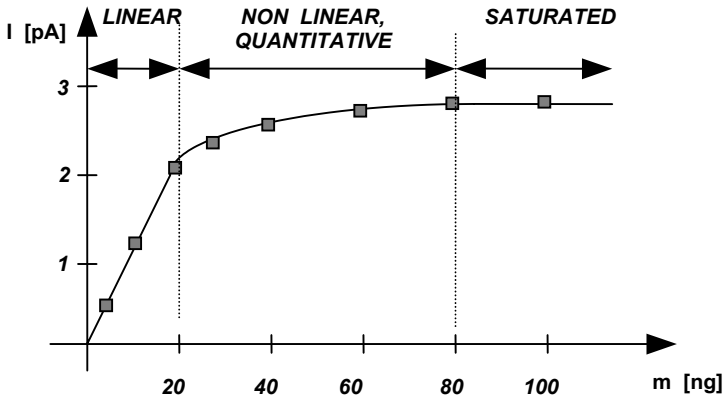

Fig. 2. Typical quantitative IMS response

In the radioactive ionization source the distribution of available charge is done in a competitive way. The consequence is that the appearance of an ion should lead, because of the charge conservation, to a decrease in intensity of another ion (or ions). In a first approximation, the charge seems to be distributed proportionally with the concentration of each component in the sample and according to its proton (or electron) affinity.

In most instances, the charge goes to the neutral with the highest proton/electron affinity and it maybe that only a low concentration will take all this charge. Such happens with CW agents and so, the charge will not distribute to any compound in the vapor sample. In the absence of a high proton affinity

(PA) neutral, lower PA materials can be ionized; thus, if the chemical compounds which compose a given sample have similar proton (or electron) affinities, then the charge will distribute virtually to any compound present in the vapor sample, and this is exactly the cause of the IMS extraordinary versatility. However, because most of commercial drift tubes used currently have a low resolution, they can't be used to separate complex mixtures of ions *[4]*. In conclusion, the specificity of IMS might be said to rely on the various target materials having high PA, such as chemical warfare agents (or electron affinities, in the negative operation mode); when common airborne materials (such as ethanol, aldehydes etc., monitored on NASA International Space Station)) are targeted, one must employ GC-IMS to separate the analytes to achieve specificity.

An ion mobility spectrometer can be successfully used to detect a great range of chemicals, both organic and inorganic. This device was for a long time considered as an ideal detector for organic vapors monitoring, but it can also be used to detect many inorganic gases. As a matter of fact, the applications of Ion Mobility Spectrometry can be grouped into several categories:

- ➲ industrial monitoring and hygiene - organic and inorganic pollutants detection *[6,7,9]*
- ➲ process monitoring *[8,9]*
- ➲ detection of medical related materials (such halogenated anesthetics) and in forensic medicine
- ➲ laboratory applications - ionic mobilities measurements and studies concerning ion structure
- ➲ military applications - detection of chemical warfare agents (both nerve and blister gases)
- ➲ explosives and illicit drugs detection
- ➲ use of IMS spectrometer as a chromatographic detector *[3]*.

Ion Mobility Spectrometry has several important advantages:

- ☺ analytical flexibility, because it can be applied to analyze both organic and inorganic vapors, and also ca be monitored both positive and negative ions.
- ☺ very fast response (the drift times are in the millisecond range); so, a complete analysis cycle can be less than a second - a true real-time response
- ☺ very good sensitivity, in the parts-per-billion and even parts-per-trillion range
- ☺ good selectivity; it can be improved by using dopants and/or different ionization sources
- ☺ the analysis is done at atmospheric pressure, and not in vacuum like in mass spectrometry
- ☺ the instrumentation is very robust (no delicate components, no liquid reagents, few moving parts) and can be easily miniaturized.

IMS has also a number of major drawbacks:

- ☹ the theoretical concepts concerning ion mobility spectrometry are not yet perfectly defined
- ☹ there are no comprehensive models for the response characteristics
- ☹ the dynamic range is quite limited, which in turn restricts the quantitation.

The crucial demand by military forces who might be exposed to Chemical Warfare Agents (CWAs) is the ability to detect the presence of these colorless, odorless compounds; this detection must be early enough so that the forces have an opportunity to protect themselves before they are exposed to incapacitating doses of these extremely dangerous materials. Similar situations exist for applications in and around chemical weapons storage and destruction sites. In both situations the primary goal and use of the detector systems is to warn workers or military personnel of imminent danger associated with their possible exposure to toxic chemicals.

Methyl salicylate is an important chemical in IMS technology, since it is being used:

- ❒ As a CWA simulant for blister agents (mustard gas), in the negative operation mode of IMS spectrometer *[9,10]*; methyl salicylate and dipropylene glycol monomethyl ether (DPM) are the materials used to verify in the field that a military hand-held IMS device of CAM type (Graseby Dynamics, Ltd., UK) is operational.
- ❒ As a IMS calibrant standard in the negative mode, when its reduced mobility K_0 is taken exactly as 1.474 $cm^2 \cdot V^{-1} \cdot s^{-1}$ and this way the IMS cell constant may be calculated *[6,9]*.
- ❒ As a dopant used in IMS for the detection of hydrogen fluoride (HF), especially in industrial applications or in the analysis of submarine's recycled air *[8,11]*.

The goal of this paper is the attempt to elucidate the main aspects concerning the ion mobility spectrometric response of methyl salicylate. All experiments were performed at DIAS (Department of Instrumentation and Analytical Science) - UMIST (University of Manchester Institute of Science and Technology).

2. Experimental

Standard atmospheres with known concentrations of methyl salicylate were generated using a thermostated gas rig based on permeation tubes. Methyl salicylate (2-$(HO)C_6H_4COOCH_3$, purity 99+%, MW 152.15, purchased from Aldrich Chemical Ltd., U.K.), was introduced (1 cm^3) in a glass chromatographic vial, and the vial was sealed using a silicone rubber cap. This improvised permeation source was then conditioned at 50°C for 48 hours; by repeatedly measuring the mass of the vial, the permeation source was gravimetrically calibrated and it was found to deliver a concentration of 10 mg m^{-3} of methyl salicylate into a flow of 40 $cm^3 \cdot min^{-1}$ air.

Both IMS drift gas and carrier gas were compressed air, supplied from air cylinders (BOC Gases, UK) and further purified (dried) using molecular sieve filters.

Ion mobility spectrometer - instrument characterization:

- IMS cell: modified CAM (Chemical Agent Monitor), manufactured by Graseby Dynamics Ltd. (Watford, Herts., UK)
- data acquisition card: ASP (Advanced Signal Processing), from Graseby Dynamics Ltd. (Watford, Herts., UK)
- data acquisition software: WASP (Waveform Analysis Signal Processing) - Version 1.35 [1991/1992], also from Graseby Dynamics Ltd. (Watford, Herts., UK)
- hardware control PC: Intel 386 processor, 40 MHz, 4 MB RAM.

IMS cell configuration:

- stacked rings drift tube
- drift length: 4.25 cm
- drift voltage: 850 V
- membrane inlet (dimethylsilicone rubber membrane)
- radioactive ionization source (10 mCi ^{63}Ni)
- operating temperature: room temperature (25°C).

Spectral generation for IMS:

- Averages = 250
- Samples = 1024 per waveform
- Frequency = 50 kHz
- Gating pulse width = 180 μs.

The filters for drift and carrier gases were cartridges containing as filtering material molecular sieve 15A.

Methyl salicylate ($C_6H_4OHCOOCH_3$, with M= 152.15, CAS # 119-36-8, density 1.186, purity 99+%) was purchased from ALDRICH and used as received, without any further purification.

Spectra were recorded in the negative mode of operation.

The diagram of instrumentation for experiments is given in Figure 3.

Experimental parameters were as follows:

- Negative mode of operation
- T = 298 K
- P = 722 torr
- Drift flow: 120 cm^3min^{-1}, clean air
- Source (carrier) flow = 200 $cm^3 \cdot min^{-1}$, clean air
- Sample inlet flow = 40 $cm^3 \cdot min^{-1}$, clean air passed through the thermostated holder containing the permeation source

- Emission rate of the permeation source with methyl salicylate: R= 400 ng· min^{-1}
- Methyl salicylate concentration: C = R/Q = 400/40 = 10 mg· m^{-3}

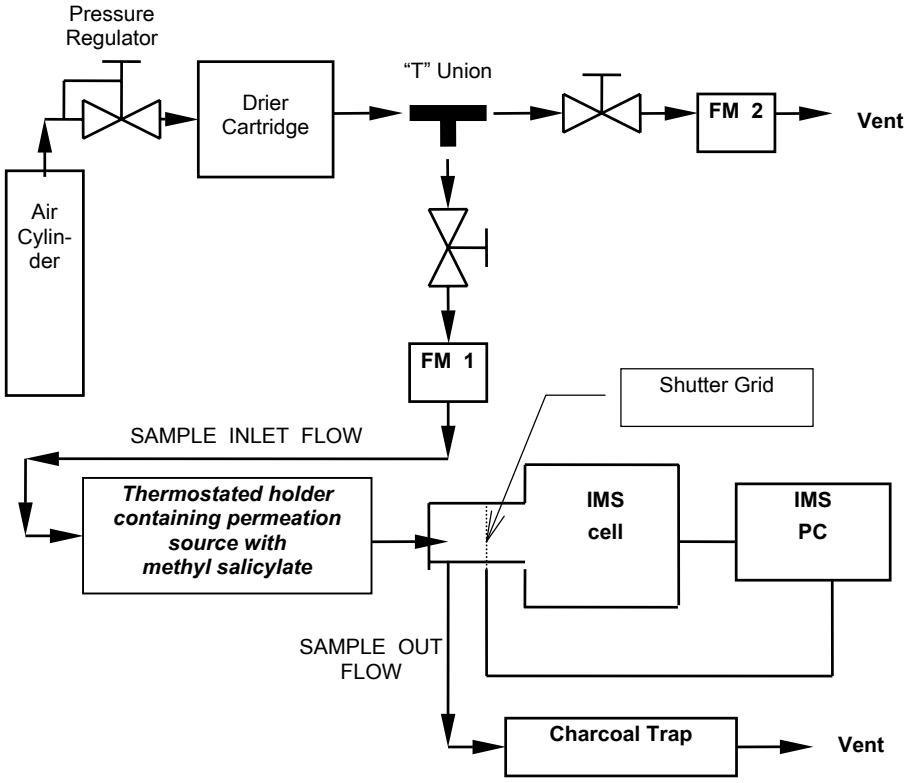

Fig 3. Schematic diagram of instruments for IMS experiments

, where FM = Flow Meter.

3. Results and discussion

Ion mobility spectra were obtained for both clean air (these spectra contain only the negative reactant ion peak RIP) and methyl salicylate at 10 mg· m^{-3}. The IMS spectra are presented in Figures 4 and 5, respectively.

The features seen at the beginning and the end of the ion mobility spectra are the shutter grid pulses.

One can observe that IMS spectra of methyl salicylate were very simple, with only one product ion peak (PIP) at drift time t_d= 8.960 ms.

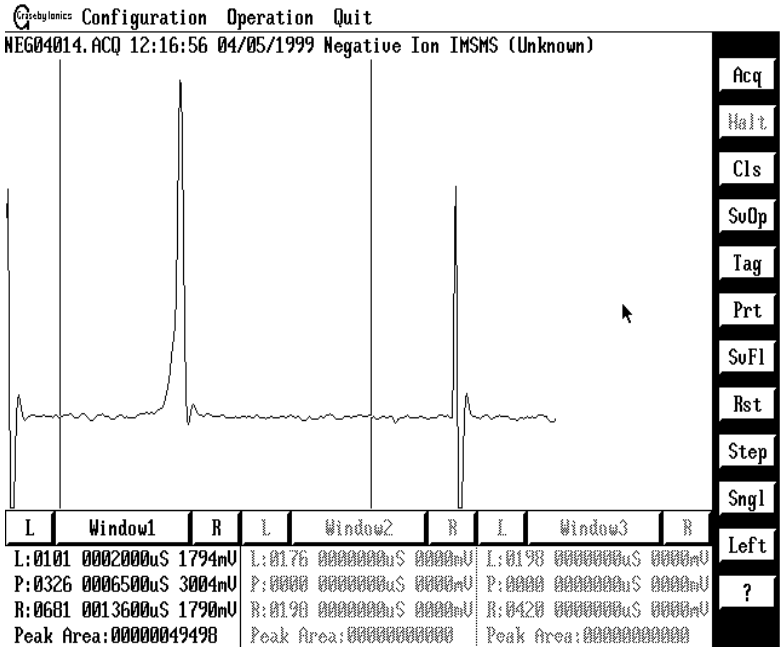

Fig. 4. IMS spectrum for clean air, negative mode

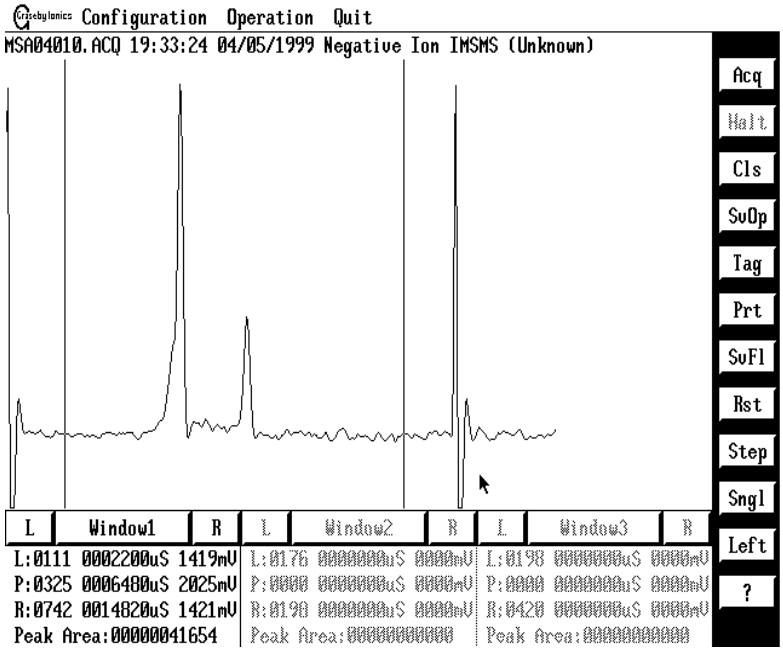

Fig. 5. IMS spectrum for methyl salicylate, 10 mg m^{-3}, negative mode

The atmospheric pressure ionization of methyl salicylate has been investigated successfully by using IMS/MS technique, where the IMS spectrometer was coupled to a quadrupole MS spectrometer (EXTREL C-150, Extranuclear Laboratories, Pittsburgh, USA). This way total atmospheric pressure chemical ionization (APCI) spectra (with the IMS shutter grid fully open), as well as "tuned" ion mobility spectra (when the mass filter allows only a selected m/z value to be detected) were gathered. A total APCI mass spectrum for methyl salicylate is given in Figure 6.

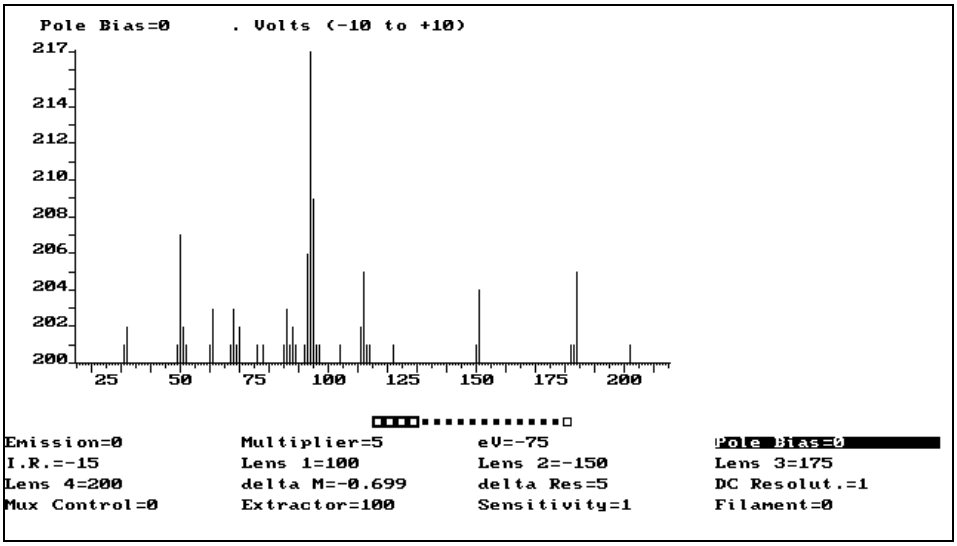

Fig. 6. Total mass spectrum for methyl salicylate (at 10 mg m^{-3})

By using the mass-resolved IMS spectra, it has been clearly demonstrated that ions with m/z 151, 184 and 202 may be assigned to methyl salicylate and that all these ions have the same drift time, corresponding to the second peak in the IMS spectrum (at 8.960 ms - the product ion peak). All the other peaks in the mass spectrum may be assigned to the negative reactant ion species; these are mainly ions of type $(H_2O)_n(CO_2)_mO_2^-$ and $(H_2O)_n(CO_2)_mCO_4^-$.

As a consequence, the ionization chemistry at atmospheric pressure for the target analyte was summarized in Table 1 below.

Table 1

Ionization chemistry for methyl salicylate

Ion species	*Ion identity*	*Reaction type*	*Drift time in IMS spectrum*
m/z 151	$(MSAL - H)^-$	Hydride abstraction (from the phenolic -OH group): $MSAL + O_2^- \longrightarrow (MSAL - H)^- + O_2H$	8.960 ms
m/z 184	$(MSAL)\cdot O_2^-$	Charge transfer reactions: $MSAL + O_2^- \longrightarrow (MSAL)\cdot O_2^-$	8.960 ms
m/z 202	$(MSAL)(H_2O)O_2^-$	Charge transfer with clustering: $MSAL + O_2^- \longrightarrow (MSAL)\cdot O_2^- + H_2O \longrightarrow (MSAL)(H_2O)O_2^-$	8.960 ms

, where MSAL is methyl salicylate molecule.

3. Conclusions

This paper aims to demonstrate the advantages of Ion Mobility Spectrometry and its diversity of applications, including here the detection of a chemical warfare agent simulant for blister agents - methyl salicylate.

Methyl salicylate generates simple ion mobility spectra in the negative mode of operation, which contain only one product ion peak having a drift time of 8.960 milliseconds and a reduced mobility $K_0 = 1.474\ cm^2\ V^{-1}\ s^{-1}$.

One may observe that at the concentration of 10 mg m^{-3} methyl salicylate the reactant ions were preserved, so these measurements fall in the linear range of the IMS response curve (see Figure 2). The limits of detection were not approached, being beyond the scope of this study, but they were previously estimated by other authors to be in the low ppb range - 5 ppb *[12]*; 20 ppb *[13]*; 0.27 mg m^{-3} *[14]*.

Using IMS/MS investigations, it has been found that the ion species that form the unique product ion peak are the following: $(MSAL-H)^-$ with m/z 151; $(MSAL)O_2^-$ with m/z 184, and $(MSAL)(H_2O)O_2^-$ with m/z 202. Therefore, ionization chemistry of this analyte has been elucidated. These findings agree very well with the results of Spangler *[15]*, which observed in the negative mode of operation (by IMS/MS) product ions of hydride abstraction type (m/z 151) and clusters of MSAL with O_2^- and N_2 (m/z 184, 212, 240, and 268).

We are sure that IMS will become very soon a common, widely accepted analytical technique, especially in several particular niches. In fact, it is obvious that the latest trends in IMS field predict a very interesting evolution, especially if the IMS experts and users collaborate to solve the remaining problems.

Acknowledgments

The authors wish to gratefully thank to the company ***Graseby Dynamics Limited - United Kingdom***, for the full suport of this project with both instrumentation and funding (for VBB).

BIBLIOGRAPHY

1 Karasek, F.W., *"The Plasma Chromatograph"*, Res. Dev. 21(3), 34-37 (1970).

2 Cohen, M.J.; Karasek, F.W., *"Plasma Chromatography - A new dimension for gas chromatography and mass spectrometry"*, J. Chromatogr. Sci. 8(6), 330-337 (1970).

3 Bocos-Bintintan, V., *"Spectrometria de mobilitate ionică ",* Editura Presa Universitară Clujeană , Cluj-Napoca (1998).

4 Eiceman, G.A.; Karpas, Z., *"Ion Mobility Spectrometry"*, CRC Press, Boca Raton, FL (1994).

5 Carr, T.W. (Ed.), *"Plasma Chromatography"*, Plenum Press, New York (1984).

6 Bocos-Bintintan, V.; Brittain, A.; Thomas, C.L.P., *"The response of a membrane inlet ion mobility spectrometer to chlorine and the effect of water contamination of the drying media on ion mobility spectrometric responses to chlorine"*, Analyst 126(9), 1539-1544 (2001).

7 Bocos-Bintintan, V.; Brittain, A.H.; Thomas, C.L.P., *"Characterization of the ion mobility spectrometric response to phosgene at room temperature"*, Romanian Journal of Optoelectronics 8(2), 1-12 (2000).

8 Roehl, J., *"Environmental and process applications for ion mobility spectrometry"*, Appl. Spectrosc. Rev. 26(1-2), 1-57 (1991).

9 Bocos-Bintintan, V., *PhD Thesis - "Studies on Phosgene and Chlorine by Ion Mobility Spectrometry and Mass Spectrometry"*, "Babes-Bolyai" University, Cluj-Napoca (2000).

10 Eiceman, G.A.; Snyder, A.P.; Blyth, D.A., *"Monitoring of Airborne Organic Vapors using Ion Mobility Spectrometry"*, Int. J. Environ. Anal. Chem. 38(3), 415-425 (1990).

11 Bollan, H.R.; West, D.J., *"Quantitative Assessment of Ion Mobility Spectrometry and Alternative Technologies in Monitoring Hydrogen Fluoride Vapor in Recycled Atmospheres"*, Proc. of the 5th International Workshop on Ion Mobility Spectrometry, Jackson, Wyoming, Aug. 22-26, 1996, pp. 151-169.

12 Begley, P.; Corbin, R.; Foulger, B.E.; Simmonds, P.G., *"Photoemissive ionization source for ion mobility detectors"*, J. Chromatogr. 588(1-2), 239-249 (1991).

13 Shoff, D.B.; Davis, D.M.; Katzoff, L.; Harden, C.S.; Ewing, R.G., *"Side-by-side comparison of ion mobility spectrometers and surface acoustic wave devices"*, Proc. of the 6th International Workshop on Ion Mobility Spectrometry, Bastei near Dresden, Germany, Aug. 10-14, 1997. In J.I. Baumbach and J. Stach (ed.), "Recent Developments in Ion Mobility Spectrometry", ISIMS (International Society for Ion Mobility Spectrometry), Dortmund, Germany, 1998, ISBN 3-00-003676-8, Pp. 315.

14 Taylor, S.J.; Piper, L.J.; Connor, J.A.; FitzGerald, J.; Adams, J.H.; Harden, C.S.; Shoff, D.B.; Davis, D.M.; Ewing, R.G., *"Design aspects and operational characteristics of the Lightweight Chemical Detector"*, International Journal for Ion Mobility Spectrometry 1(1), 58-63 (1998).

15 Spangler, G.E., *"The Effects of CO_2 on the Negative Reactant Ions of IMS"*, Paper, Proc. 3rd International Workshop on IMS, Galveston, TX, Oct. 16-19, 1994. John H. Cross (Ed.), NASA Conference Publication 3301, pp. 16-33 (1995).

STUDIA UNIVERSITATIS BABEŞ-BOLYAI, CHEMIA, XLVII, 1-2, 2002

Dedicated to Professor Ionel Haiduc
on the occasion of his 65th birthday

REDUCTIVE AMINATION OF METHYL ETHYL KETONE OVER SUPPORTED GROUP VIII NOBLE METAL CATALYSTS

J. BÓDIS[1,2,3] and J. A. LERCHER[1,3]

[1] *Department of Chemical Technology / Catalytic Processes and Materials University of Twente, P.O. Box 217, 7500 AE Enschede, The Netherlands*
Present addresses:
[2] *"Babes-Bolyai" University, Department of Organic Chemistry, str. Arany Janos nr. 11, 3400 Cluj, Romania. E-mail: jbodis@chem.ubbcluj.ro; Fax: 40-(0)64-190818*
[3] *Institut für Technishe Chemie, Technische Universität München, Lichtenberstr. 4, D-85747, Garching bei München, Germany*

ABSTRACT. Reductive amination of methyl ethyl ketone (MEK) with ammonia (at ammonia/MEK molar ratios of ~ 14.5) and hydrogen has been performrd at 50 bar and 323-353 K over graphite and charcoal supported noble metal catalysts. Rhodium and platinum based catalysts showed the highest activity in reductive amination of MEK. The rhodium catalysts had high selectivity towards primary amine (sec-butylamine), while the platinum catalysts towards secondary amine (di-sec-dibutylamine). Tertiary amine (tri-sec-butylamine) was not detected in reaction products. The BET area and metal dispersion was found to have a pronounced influence on activity and selectivity.

Keywords: Reductive amination, Methyl ethyl ketone, Noble metal catalysts

INTRODUCTION

The reductive amination of aldehydes and ketones is an important synthetic route to amines. The reaction proceeds through an intermediately formed imine, hydrogenated with the help of a reducing agent or with molecular hydrogen in presence of a catalyst. Scheme 1 represents a non-exhaustive network of reactions (catalytic and non-catalytic) that could take place during reductive amination.

The addition of ammonia to the carbonyl compound results in aminoalcohol (1). This may be dehydrated to imine, which is subsequently reduced (2-3), or can be directly reduced to the amine (4). The primary amine formed can also behave as an aminating agent for the carbonyl compound, forming Schiff bases, which are reduced to secondary amines (5-6). The addition of a primary amine to imines with subsequent reduction of the adduct also leads to secondary amines (7-8). Secondary amines react similarly with the carbonyl compound (9-10) or with an imine (11-12), forming tertiary amines. The

principal side reaction is the hydrogenolysis reaction of the carbonyl compound involving the formation of an alcohol (13). Apparently, the formation of the primary amine should proceed through steps (1) and (4), but there is evidence that secondary and tertiary amine precursors could be present at concentrations much higher than the amount of secondary and tertiary amine obtained at the end [1]. Thus, the reaction paths leading to the final product and, so, determining the selectivity of a particular catalyst under a set of reaction conditions are not clearly known.

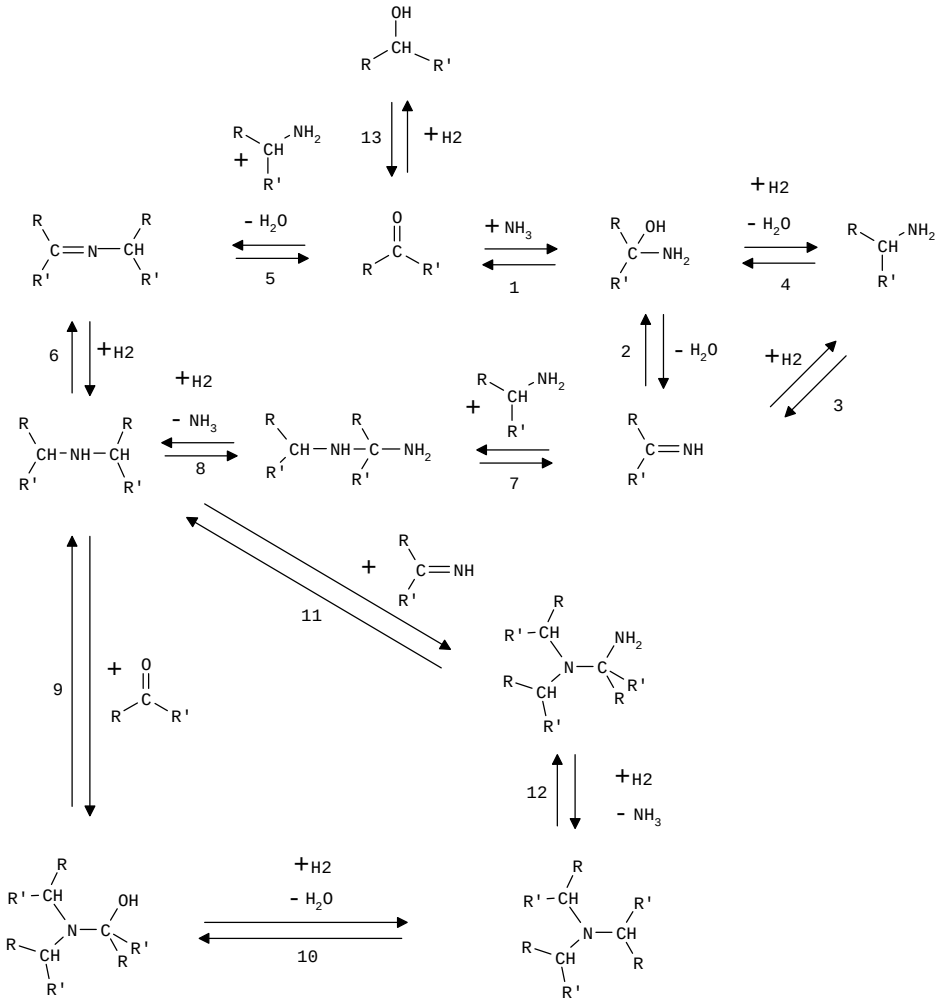

Scheme 1. Reaction pathways in the reductive amination of carbonyl compounds (R, R' = alkyl, aryl, H).

In homogeneous catalysis only a small number of reports [2-5] on the reductive amination of carbonyl compounds exist. Most of them describe complex catalysts [3-5] active in asymmetric reductive amination of prochiral ketones. The main disadvantage of the homogeneous processes is the relatively high value of catalyst loss. This inconvenience could be decreased by using solid catalysts (metal powders or supported metals).

There are numerous reports on the use of supported and unsupported Ni, Co and noble metal catalysts [1,6-14]. Metal sulfides (Re, Fe, Co, Ni, W, Pt, Rh) were also used [15-17] as catalysts in the reductive amination of ketones. The relative inactivity of these catalysts for the hydrogenation of the aromatic ring, ketones, nitriles, esters and other unsaturated functional groups, often permits useful selectivity in case of multifunctional compounds.

Methyl ethyl ketone [18] was chosen as test molecule because of lack of literature information concerning the reductive amination of this substrate with ammonia and hydrogen over supported noble metal catalysts.

EXPERIMENTAL

CATALYSTS: The catalysts tested in the reductive amination of methyl ethyl ketone (MEK) are presented in Table 1 together with some physicochemical characterization data as well. The charcoal supported catalysts contained 55-60% moisture. The quantitative values used for these samples refer to dry material.

Table 1

Catalysts characterization data (metal dispersions were calculated by using n_S values estimated according to literature [19])

Type of catalyst	S_{sp} (m^2/g)	S_M (m^2/g)	Metal location	Dispersion (%)	BET area (m^2/g)
5%Rh/charcoal	950	11.1	Intermediate	50.43	817.8
5%Rh/HSAgraphite	130	9.5	Surface	43.17	94.6
5%Ru/HSAgraphite.	130	8.0	Surface	43.78	41.6
5%Pd/HSAgraphite	130	11.4	Surface	51.10	87.6
5%Pt/HSAgraphite	130	5.0	Surface	40.48	80.1

HSA - high surface area

CATALYSTS TESTING: The reactions were carried out in batch reactors with a volume of about 65 ml. Magnetic stirring at a speed of 1100 rpm was used. The temperature inside the autoclave was measured by a thermocouple mounted on the lid of the autoclave. Weighed amount of catalysts were introduced into the autoclave. In order to assure a well-defined starting time for every reaction, the following experimental procedure was applied:

After addition of methyl ethyl ketone (MEK) and of the solvent (ethanol), the autoclave was flushed with nitrogen to remove the atmospheric oxygen. Ammonia was then added from the liquid ammonia cylinder at room temperature. Then the autoclave was placed in a thermostat bath preset to the reaction temperature. Adding hydrogen and completing fast to the working pressure occurred only after the preformed imine solution reached the desired reaction temperature (t = 0 is set for the time when the final pressure was established).

The progress of reaction in time was evaluated from the hydrogen consumption (added from a well known volume reservoire, V = 11.4 ml), keeping the working pressure in the autoclave constant by regulating a valve manually, or by measuring the hydrogen flow with a flow meter (BROOKS) having the pressure inside the autoclave controlled by a pressure regulator (BROOKS). Liquid sampling was used for monitoring the evolution of products in time.

Reductive amination of methyl ethyl ketone (>99%, Merck) were conducted mostly at 20-50 bar and 80 ˚C. The products were analyzed by using a Hewlett Packard 5890A gas chromatograph equipped with a DB Wax 1701 column and FID detector. Pure sec-butylamine and di-sec-butylamine were used for the identification of the main products in the reaction mixtures. GC/MS analyses were performed in order to identify reaction intermediates. The metal leaching was followed by XRF analysis of the filtered reaction mixtures.

Experiments were done in order to find whether mass transfer rate limitations occurred or not for the highly active catalysts. According to results obtained, mass transfer limitations of hydrogen diffusion from liquid to solid did not influence the measured reaction rates.

RESULTS AND DISCUSSION

In the product mixture resulted during the reductive amination of MEK with ammonia and hydrogen over supported noble metal catalysts we identified sec-butylamine, di-sec-butylamine and 2-butanol. Tri-sec-butylamine was never obtained. According to the analysis results, the reactions occurring in the reactor under the working conditions used (V_{EtOH} = 8 cm^3, n_{MEK} = 0.0222 mol, n_{NH3} = 0.3235 mol, n_{NH3}/n_{MEK} = 14.57, V_{EtOH}/V_{MEK} = 4, p = 50 bar, T = 353 K) are given in Scheme 2.

$$\text{Me-CO-Et} + NH_3 + H_2 \rightarrow \text{Me-CH}(NH_2)\text{-Et} + H_2O$$

$$\text{Me-CO-Et} + \text{Me-CH}(NH_2)\text{-Et} + H_2 \rightarrow \text{Et-(Me)CH-NH-CH(Me)-Et} + H_2O$$

$$\text{Me-CO-Et} + H_2 \rightarrow \text{Me-COH-Et}$$

Scheme 2. Chemical reactions during the reductive amination of MEK.

In order to probe for mass transfer limitations, reductive amination experiments of MEK at different stirring speeds (1100 and 600 rpm), and at different catalysts concentrations were carried out. The experimental conditions and the results obtained for the reductive amination of methyl ethyl ketone on Rh/charcoal and Rh/HSA graphite catalysts are presented in Table 2.

Table 2

Experimental conditions and results for the reductive amination of MEK on charcoal and graphite supported rhodium catalysts at different stirring speeds.

n_M: moles of metal, $n_M = 1.11 \cdot 10^{-4}$ mol, Solvent: EtOH, $V_{EtOH} = 8$ cm^3, $n_{MEK} = 0.0222$ mol (2 cm^3), $n_{MEK}/n_M = 200$, $n_{NH3} = 0.3235$ mol, $n_{NH3}/n_{MEK} = 14.57$, $V_{EtOH}/V_{MEK} = 4$, p = 50 bar, T = 353 K.

Catalyst	t_{react} (min)	X (%)	Y_{pr} (%)	Y_{sec} (%)	$Y_{2\text{-ol}}$ (%)	r_{pr} (mol/mol· h)	r_{sec} (mol/mol· h)	$r_{2\text{-ol}}$ (mol/mol· h)
Rh/HSAgraph								
1100 rpm	60	97.6	85.7	0.4	11.9	171.5	0.7	23.9
600 rpm	65	97.9	84.8	0.7	9.9	169.6	1.3	19.8
600 rpm*	200	82.9	54.3	0.0	1.0	162.7	0.0	3.0
Rh/charcoal								
1100 rpm	8	99.2	98.5	0.4	0.6	1371.3	5.9	13.6
1100 rpm*	40	97.1	92.3	0.9	2.7	1383.8	40.8	12.7
600 rpm*	45	98.4	94.6	0.9	2.8	1261.6	36.8	11.3

X conversion (molar percentage of MEK converted to different products).
Y yield (molar percentage of MEK converted to the corresponding amine).
* $n_{Rh} = 2.22 \cdot 10^{-5}$ mol, $n_{MEK}/n_M = 1000$.

The results (conversions, yields, rates of formation) presented in Table 1 indicate that under the working conditions used, mass transfer limitations are unimportant.

Reductive amination of methyl ethyl ketone was done on the graphite and charcoal supported group VIII noble metal catalysts presented in Table 2. All of the reported experiments were carried out by adding hydrogen only after the preformed imine solution reached the desired reaction temperature. The filtered reaction products obtained on Rh and Pt were colorless, while those resulted on Pd and Ru catalysts were colored yellow. The XRF analysis (Philips PW 1480, wavelength dispersive X-ray fluorescence spectrometer) of colored mixtures indicate the presence of Ru and Pd in the solutions. At a detection limit of 0.002% rhodium was found not to dissolve, but the ruthenium loss of one catalytic cycle was noted to be 3-9 wt.% of the initial metal content.

Fig. 1 illustrates the hydrogen consumption as a function of time for the tested catalysts.

Fig. 1 shows that Rh/charcoal is the most active catalyst, followed by Pt/HSA graphite, Rh/HSA graphite, Ru/HSA graphite while Pd/HSA graphite being the less active catalyst.

The rates of formation of amines (primary and secondary) and 2-butanol normalized per mole of noble metal obtained for the reductive amination of methyl ethyl ketone are presented in Fig. 2.

Fig. 1. Hydrogen consumption versus reaction time during the reductive amination of methyl ethyl ketone on some graphite and charcoal supported group VIII noble metal catalysts. n_M: moles of metal, $n_M = 1.11 \cdot 10^{-4}$, Solvent: EtOH, $V_{EtOH} = 8\ cm^3$, $n_{MEK} = 0.0222$ mol, $n_{MEK}/n_M = 200$, $n_{NH3} = 0.3235$ mol, $n_{NH3}/n_{MEK} = 14.57$, p = 50 bar, T = 353 K.

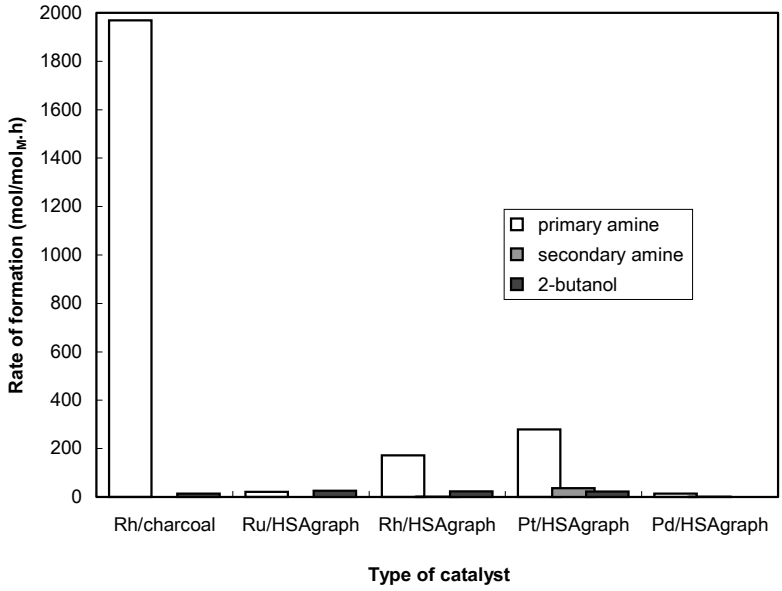

Fig. 2. Rates of formation of the sec-butylamine, di-sec-butylamine and 2-butanol during reductive amination of methyl ethyl ketone on supported group VIII noble metal catalysts. n_M: moles of metal, $n_M = 1.11 \cdot 10^{-4}$, Solvent: EtOH, $V_{EtOH} = 8\ cm^3$, $n_{MEK} = 0.0222$ mol, $n_{MEK}/n_M = 200$, $n_{NH3} = 0.3235$ mol, $n_{NH3}/n_{MEK} = 14.57$, p = 50 bar, T = 353 K.

One mole of Rh supported on charcoal produced ~12 times more sec-butylamine/hour than one mole of Rh supported on graphite. Rh/charcoal catalyst (with high metal dspersion and high BET area) was found to be not only the most active, but also the most selective catalyst. The graphite supported rhodium catalyst is less active and less selective, but in comparison to ruthenium and palladium has higher activity and selectivity. Pt/HSA graphite is an active catalyst, but has lower selectivity towards primary amine than Rh/HSA graphite.

In all the experiments 2-butanol was identified as a reaction product, in case of the Ru/HSA graphite catalysts even being the main component in the product mixture. However, the unwanted hydrogenolysis of MEK can be avoided by decreasing the pressure. Conducting the reductive amination of MEK at 20 bar, only traces of 2-butanol were detected in the product mixtures even by using Ru/HAS graphite as catalyst.

CONCLUSIONS

Among the studied catalysts the Rh and Pt based ones show the highest activity in reductive amination of methyl ethyl ketone. This observation underlines the major role of metal in determining the activity and selectivity of the supported catalysts.

The charcoal appears to be a good catalyst support providing high activity and selectivity for the supported Rh catalyst (having high BET area and high metal dispersion) and being significantly more active compared to Rh/graphite. This emphasizes the important role of the support materials.

The absence of tertiary amines during the reductive amination of methyl ethyl ketone can be attributed to the high sterical hindrance of branched amines.

At higher temperature and pressures (T = 353 K, p = 50 bar), the hydrogenolysis of methyl ethyl ketone to 2-butanol becomes a considerable secondary reaction, especially on graphite supported Ru catalysts.

Rhodium was found not to dissolve, but the XRF analysis indicates a non-negligible leaching of Ru and Pd during the reductive amination of MEK over Ru/HSA graphite and Pd/HSA graphite catalysts.

ACKNOWLEDGEMENT

Financial support from the DSM company is greatly appreciated.

REFERENCES

1. S. Yada, Y. Takagi and M. Hiyamizu, Nippon Kagaku Kaishi, (2) (1995) 107.
2. M.V. Klyuev and M.L. Khidekel, Transition Met. Chem., 5 (1980) 134.
3. C.A. Willoughby and S.L. Buchwald, J. Am. Chem. Soc., 114 (19) (1992) 7562.

4. A. Viso, N.E. Lee and S.L. Buchwald, J. Am. Chem. Soc., 116 (20) (1994) 9373.
5. M.J. Burk, J.P. Martinez, J.E. Feaster and N. Cosford, Tetrahedron, 50 (15) (1994) 4399.
6. M. Freifelder, W.D. Smart and G.R. Stone, J. Org. Chem., 27 (6) (1962) 2209.
7. K.A. Pollart and R.E. Miller, J. Org Chem., 27 (7) (1962) 2392.
8. A.L. Bris, G. Lefebre and F. Coussemant, Bull. Soc. Chim. France, 6 (1964) 1374.
9. A.L. Bris, G. Lefebre and F. Coussemant, Bull. Soc. Chim. France, 7 (1964) 1584.
10. A.L. Bris, G. Lefebre and F. Coussemant, Bull. Soc. Chim. France, 7 (1964) 1594.
11. R.W. White, S.W. King and J.L. O'Brien, Tetrahedron Lett., (39) (1971) 3591.
12. M.V. Klyuev and M.L. Khidekel, Russ. Chem. Rev., 49 (1) (1980) 542.
13. P.L. Mills, D.E. Willis and R.L. Fenton, Ind. Eng. Chem. Res., 27 (7) (1988) 1121.
14. S. Yada and Y. Takagi, Nippon Kagaku Kaishi, (1) (1991) 20.
15. F.S.Dovell and H. Greenfield, J. Org. Chem., 29 (5) (1964) 1265.
16. F.S.Dovell and H. Greenfield, J. Am. Chem. Soc., 87 (12) (1965) 2767.
17. H. Greenfield and F.S.Dovell, J. Org. Chem., 31 (9) (1966) 3053.
18. J. Bodis and J.A. Lercher, Confidential Reports to DSM Company, (1997-1998).
19. J.J.F. Scholten, A.P. Pijpers and A.M.L. Hustings, Catal. Rev.-Sci. Eng., 27 (1) (1985) 151.

STUDIA UNIVERSITATIS BABEŞ-BOLYAI, CHEMIA, XLVII, 1-2, 2002

Dedicated to Professor Ionel Haiduc
on the occasion of his 65th birthday

ADSORPTION OF AMMONIA AND PYRIDINE ON CoAPO-5 SINGLE CRYSTALS STUDIED BY *IN SITU* FT-IR MICRO-SPECTROSCOPY

J. BÓDIS[1,3,4], G. MÜLLER[1], J. KORNATOWSKI[2,4] and J. A. LERCHER[1,4]

[1] *Department of Chemical Technology / Catalytic Processes and Materials University of Twente, P.O. Box 217, 7500 AE Enschede, The Netherlands*
[2] *Institut für Brennstoffchemie und Phys. Chem. Verfahrenstechnik RWTH Aachen, Worringer Weg 1, D-52074 Aachen, Germany*
Present addresses:
[3] *"Babes-Bolyai" University, Department of Organic Chemistry, str. Arany Janos nr. 11, 3400 Cluj, Romania. E-mail: jbodis@chem.ubbcluj.ro; Fax: 40-(0)64-190818*
[4] *Institut für Technishe Chemie, Technische Universität München, Lichtenberstr. 4, D-85747, Garching bei München, Germany*

ABSTRACT. Direct spectroscopic evidence for the existence of Brønsted acid sites in CoAPO-5 single crystal molecular sieves is reported. Compared with unsubstituted $AlPO_4$-5 single crystals, the cobalt substituted samples exhibit well developed bands of isolated bridging hydroxyl groups and a broad absorption band indicating the existence of hydrogen bonded OH groups. Ammonia and pyridine interact with the bridging OH groups. This seems to involve simultaneous interactions with Lewis and Brønsted acid sites. Upon adsorption of pyridine new hydroxyl groups (ν_{OH} = 3682 and 3590 cm^{-1}) were observed in parallel to pyridine bonding to Lewis acid sites. This suggests opening framework metal-oxygen bonds during sorption of pyridine.

Keywords: Cobalt substituted AFI; Single crystals; FT-IR spectroscopy

INTRODUCTION

$AlPO_4$-5 (AFI framework type structure [1,2]) has hexagonal symmetry and contains two parallel one-dimensional channels formed by 12-, and 6-membered rings (see Fig.1a) composed of alternating AlO_4 and PO_4 tetrahedra creating an electrically neutral framework. The larger channels allow sorption of molecules as large as 2,2-dimethylpropane (0.62 nm) [2]. The dominating acid sites observed are terminal P-OH and Al-OH groups with weakly Brønsted acidic character. In order to generate strong acid sites, isomorphous substitution of phosphorous with tetravalent cations (e.g., Si^{4+}, reported first by Lok *et al* [3]) or aluminum with divalent cations (e.g., Mg^{2+}, Mn^{2+}, Fe^{2+}, Co^{2+} and Zn^{2+} [4], Co^{2+} [5]) were performed. Flanigen *et al* [6] reported incorporation of several metal cations leading to combinations of up to six framework cations.

However, direct spectroscopic evidence for the presence of bridging hydroxyl groups (strong Brønsted acids) is scarce for samples with divalent metal cations in the framework. Recent studies by FT-IR microscopy of some metal substituted single crystals [7] showed that upon sorption of pyridine on

bridging hydroxyl groups of SAPO-5, BeAPO-5, MgAPO-5 and CoAPO-5, a new hydroxyl group (ν_{OH} = 3690-3694 cm^{-1}) was formed in parallel to the coordination of pyridine to a strong Lewis acid site. This was interpreted as pyridine cleaving the bond between the oxygen and the metal cation of the bridging OH group [7].

Among the metal substituted aluminophosphate molecular sieves the cobalt substituted ones are the most studied [5, 8-27]. The introduction of a transition metal cation possibly creates redox properties which makes CoAPO a potential catalyst for acid-catalyzed and redox type reactions [5,8-12,15,18,22]. However, the nature of the site allowing the valence change in redox reactions is not defined and the reports are controversial. Bridging OH groups, the direct evidence of Co^{2+} in the framework, could not be found by IR spectroscopy of polycrystalline materials [10,11,15,22]. The present contribution describes an FT-IR micro-spectroscopic study to overcome some of the ambiguities in the characterization of CoAPO-5 by studying large well-defined crystals.

EXPERIMENTAL

For a detailed description of the synthesis of CoAPO-5 see [27]. The crystals were calcined at 780 K for 36 hours in synthetic air and subsequently 108 hours in pure oxygen. The single crystals (Fig.1b) used had a degree of substitution: 2.07 atom%, sorption capacities (at p/ps = 0.8): 13.5 mmol H_2O/mg, 1.19 mmol C_6H_6/mg; average dimensions: 290x40 µm.

Ammonia (99.998%, Union Carbide) and pyridine (99.8%, ALDRICH) were used as probe molecules. The experiments were carried out in a vacuum cell equipped with i.r. transparent windows which was attached to the stage of a BRUKER i.r. microscope coupled to a BRUKER IFS 88 spectrometer.

The externally calcined crystals were introduced in the i.r. cell and heated in vacuum (10^{-6} mbar) or in hydrogen flow (40 cm^3/min) with 10 K/min to 770 K (60 minutes). After cooling in vacuum (10 K/min) to 310 K, spectra of selected crystals were recorded. The sorbates were introduced into the i.r. cell *via* a differentially pumped gas inlet system. The partial pressures (10^{-3} to 1 mbar) were hold constant until sorption/desorption equilibrium was achieved. The sorption was followed *in situ* by time resolved FTIR micro-spectroscopy (1000 scans/spectrum 4 minutes, 4 cm^{-1} spectral resolution). Subsequently, the cell was evacuated (p = 10^{-6} mbar, T = 310 K) and the temperature was increased with 10 K/min to 870 K.

RESULTS AND DISCUSSION

Activated Crystals

The spectra of the crystals activated in vacuum and in hydrogen flow are identical and show bands (Fig.1c) attributed to the stretching vibrations of hydroxyl groups. The absorption band at 3655 cm^{-1} is attributed to OH stretching vibrations of terminal P-OH, Al-OH and/or Co-OH groups, respectively. This assumption is based on analog observations made with other MAPOs [7]. If only free terminal P-OH groups were present, the absorption band should be positioned at around 3670 cm^{-1}.

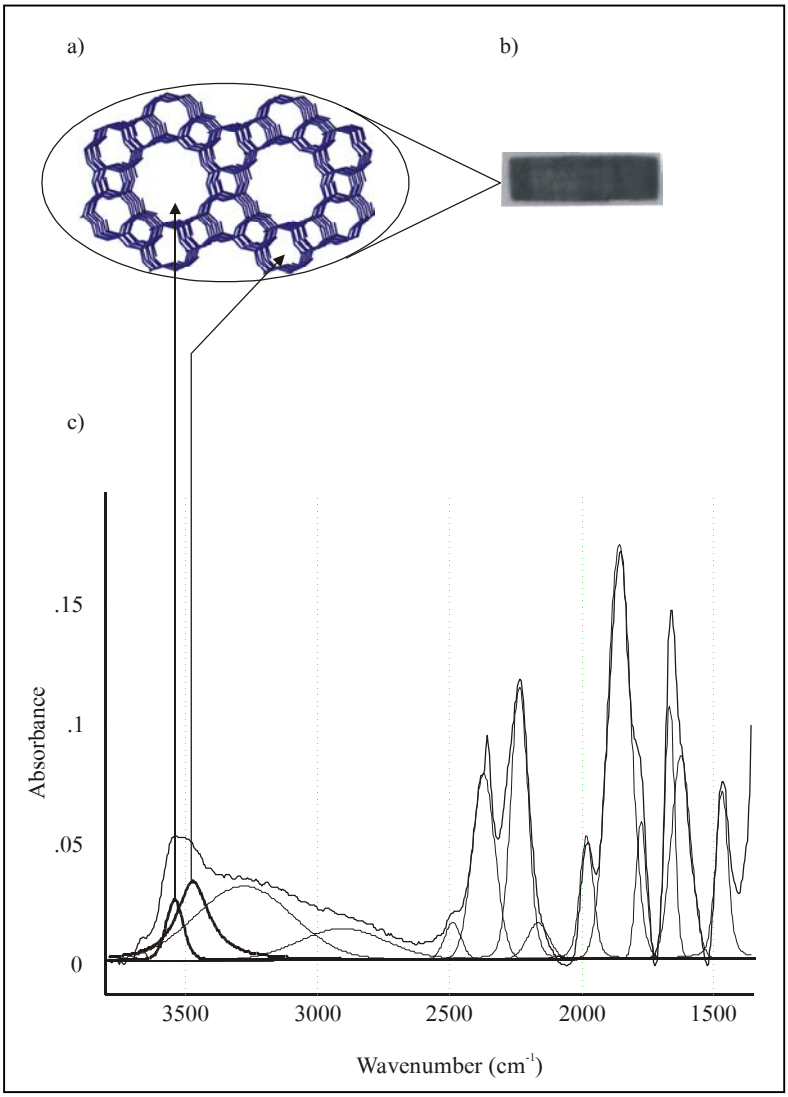

Fig.1: a) Channel systems of AFI, reproduced from the BIOSYM molecular modelling software; b) Optical micrograph of the sample; c) FT-IR spectrum of activated, template free CoAPO-5 single crystal (T = 310 K, p = 10^{-6} mbar)

In analogy to SAPO-5 [7], the band at 3540 cm^{-1} is assigned to the stretching vibrations of bridging OH (Co-OH-P) groups situated in the 12 membered channels, and the band at 3470 cm^{-1} to bridging OH groups in the 6 membered channel system. The presence of bridging OH groups suggests that the activated crystals contain the cobalt ions mainly in the form of Co^{2+}. Even when the calcination was carried out in pure oxygen, the main part of the framework cobalt

remained at that oxidation stage, in agreement with the recent observations on a polycrystalline CoAPO-5 [21]. Further activation in hydrogen flow does not produce a change in the spectral feature, indicating that the extant framework Co^{3+} is not reduced by hydrogen to Co^{2+} even at 770 K. The broad absorption band below 3450 cm^{-1} was assigned to hydrogen bonded hydroxyl groups affiliated with the presence of some debris in the crystal because the absorption band was not affected by any of the molecules adsorbed. In addition, bands were observed in the region below 2500 cm^{-1} (2483shoulder/sh, 2371sh, 2352, 2227, 1975, 1845, 1790sh, 1662, 1603sh, 1450 and 1268 cm^{-1}), which are assigned to overtone and combination vibrations of the lattice.

Sorption of ammonia and pyridine

Ammonia - The difference spectra of adsorbed ammonia (Fig. 2) showed negative i.r. absorption bands in the region of the OH stretching vibrations at 3551 and around 3487 cm^{-1} attributed to the decreasing in intensity of the bridging OH stretching vibrations resulting from the interaction of Co-OH-P groups with ammonia. Increasing equilibration time led to a new asymmetric negative band at around 3655 cm^{-1}, caused probably by the sorption of ammonia on terminal P-OH and Co-OH groups. NH stretching vibrations were detected at 3394, 3284, 3224 and 3190 cm^{-1}. The respective maxima for the NH deformation vibrations were found at 1665, 1618 (assigned to coordinatively bonded ammonia) and at 1445 with a shoulder at 1486 cm^{-1} (assigned to protonated ammonia) [29]. Increasing equilibration time (and hence the coverage), the NH stretching vibrations shifted to lower wavenumbers. Another difference appeared by subtracting the spectrum equilibrated at 10^{-3} mbar with a spectrum at an earlier stage of uptake (Fig. 2). At lower uptake, the two δ_{NH} bands assigned to protonated ammonia had equal intensity, whereas the low frequency δ_{NH} band grew over proportionally with increasing time. Furthermore, two broad absorption bands are observed with their maxima around 2925 and 2723 cm^{-1}, which are assigned to NH stretching vibrations of ammonium ions interacting with the lattice oxygen [30].

Increasing the pressure to 10^{-2} mbar showed only a subtle change in the spectral features of adsorbed ammonia (see Fig. 2). Three bands were observed in the NH stretching region at 3362, 3285 with a shoulder at 3200 cm^{-1}. We did not detect negative bands in the hydroxyl stretching vibration region. This suggests that the accessible acid sites were already completely covered at 10^{-3} mbar. Further increase in pressure led probably to a clustering of ammonia molecules, as indicated by an over proportional growth of the bands at 3362 (ν_{NH}) and at 2750 cm^{-1} (ν_{NH} perturbed by ammonia-ammonia interaction). The final pressure step to 1 mbar caused the appearance of sharp bands of physisorbed ammonia at 3400, 3343, 3302 (ν_{NH}) and 1616 cm^{-1} (δ_{NH}). The relatively broad absorption band with the maximum at 2755 cm^{-1} is attributed to the perturbed NH stretching vibrations of physisorbed ammonia (hydrogen bonding ammonia-ammonia interactions).

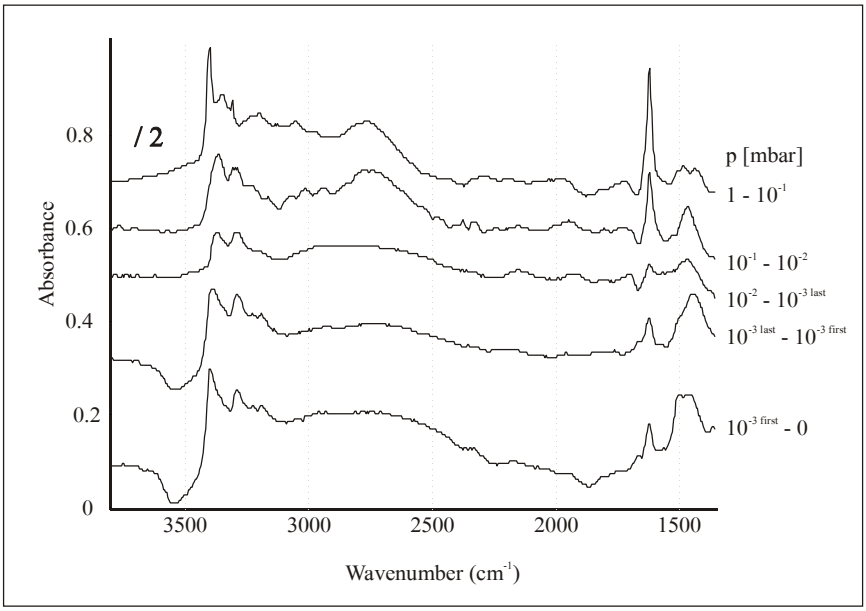

Fig. 2. Difference spectra of ammonia adsorbed on CoAPO-5 at the indicated pressures, T=310 K.

The sorption of ammonia led at low pressures to two pairs of δ_{NH} i.r. absorption bands assigned to coordinatively bonded (1665 and 1618 cm^{-1}) and to protonated molecules (1486 and 1445 cm^{-1}), respectively. We tentatively attribute the high frequency bands of the pairs to ammonia interacting with the acid sites in the constraint environment of the 6-membered pores. Note, that the low frequency bands of these two pairs rose faster in intensity with increasing pressure and equilibration time than the high frequency bands. We speculate this to be caused by the faster transport of ammonia in the large channels compared to the small pore channels.

Because the i.r. absorption bands characteristic for both Lewis bound and protonated ammonia rose in parallel, we suggest that two ammonia molecules are adsorbed per Co-OH-P unit. The first molecule forms a strong coordinative interaction with the cobalt ion, giving rise to the bands close to 1600 cm^{-1}, opening the metal oxygen bond creating a new P-OH group [21]. The proton of the P-OH group is transferred to the second ammonia molecule causing the bands close to 1450 cm^{-1}.

Despite the fact that at 10^{-3} mbar all Brønsted acid sites were covered we still detected absorption bands for both coordinatively bonded and protonated species suggesting a certain mobility of the proton detached from the Brønsted acid sites within the ammonia clusters formed at higher partial pressures.

Evacuation of the system to 10^{-6} mbar led to the desorption of all physisorbed species. The spectrum was comparable to the spectrum of the crystal equilibrated with 10^{-2} mbar of ammonia (see Fig. 2). During TPD the desorption

of ammonia molecules began at around 510 K, and was completed at 710 K. The spectra of the crystal before and after undergoing the experimental procedures were identical.

Pyridine - The strong Brønsted acid sites (Co-OH-P) reach their maximum coverage (approximately a third of the acid sites, estimated from the decrease of the hydroxyl stretching vibrations) at 10^{-2} mbar (Fig. 3). Up to this pressure all absorption bands grew continuously in intensity. Negative bands appeared at 3538 and 3485 cm^{-1}, which are assigned to the stretching vibrations of the strong acidic bridging OH groups interacting with pyridine. The spectral region between 1650 and 1350 cm^{-1} typically used to characterize the adsorption state of pyridine showed the characteristic bands for both coordinatively bonded pyridine to the framework cobalt (1610 and 1449 cm^{-1}) and protonated pyridine (1635 and 1544 cm^{-1}). The presence of protonated pyridine is supported by the absorption bands at 3393 and 3279 cm^{-1} too, which are assigned to ν_{NH} vibrations. The broad band at around 2765 cm^{-1} is assigned to perturbed NH stretching vibrations (i.e., red shifted through interactions with the lattice oxygen atoms).

By increasing the pressure to 10^{-1} mbar (Fig. 3) new i.r. absorption bands appeared at 3682 and 3590 cm^{-1} with an underlying broad absorption band centered around 3180 cm^{-1}. This broad feature is interrupted by negative bands at 3538 and 3485 cm^{-1} of the bridging OH groups involved in the interaction with pyridine. The two new absorption bands at higher wavenumbers (3682 and 3590 cm^{-1}) are assigned to relatively free vibrating hydroxyl groups. In the low wavenumber region the i.r. bands characteristic for coordinatively bound (1610 cm^{-1}) and hydrogen bonded (1576 cm^{-1}) pyridine increased stronger than the absorption band assigned to protonated pyridine. The spectrum at 1 mbar pyridine pressure shows a marginal increase of all bands already observed at 10^{-1} mbar.

Upon evacuation of the system the bands at 1608, 1576 and 1446 cm^{-1} (attributed to physisorbed pyridine) decreased in intensity (Fig. 3). During TPD the i.r. bands of the newly formed hydroxyl groups disappeared around 510 K, whereas desorption of chemisorbed pyridine on Brønsted and Lewis sites was not observed before 550 K. Both protonated and coordinatively bound pyridine were completely removed at 870 K.

With pyridine the interactions are similar to those of the ammonia. Up to a partial pressure of 10^{-2} mbar two pyridine molecules interact per acid site, breaking the cobalt-oxygen bond creating a relatively free vibrating P-OH group which is deprotonated by the second pyridine molecule. This model is supported by the fact, that the absorption bands characteristic for the two different pyridine species rose in parallel. At higher partial pressure two new i.r. bands appeared at 3682 and 3590 cm^{-1}. We suggest that under these conditions the remaining void space does not allow for the pyridine P-OH interaction. These bands are assigned to the P-OH groups created due to the strong coordinative interaction of pyridine leading to the opening of the metal oxygen bond. The appearance of two bands is explained again by the two possible positions of the Co-OH-P

units in the crystal structure (the high frequency band originating from the acid sites in the 12-membered ring channels and the low frequency band stemming from the sites in the 6-membered ring channels).

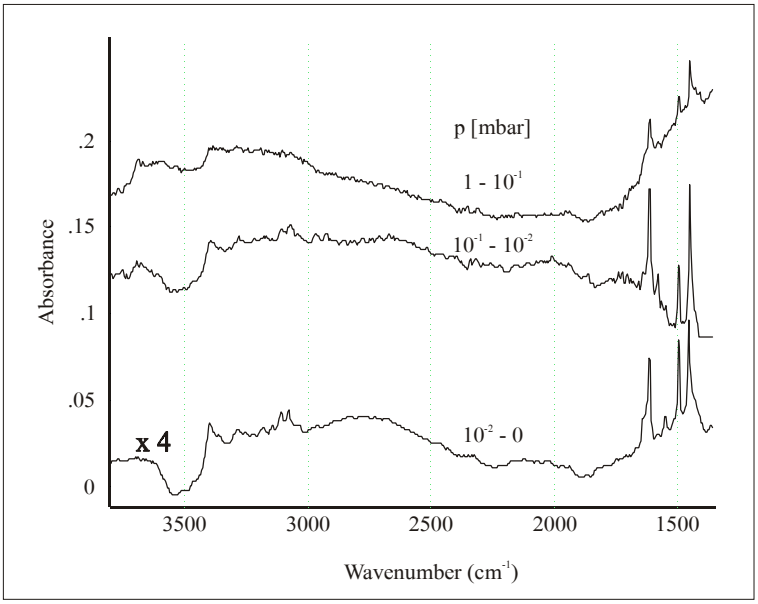

Fig. 3. Difference spectra of pyridine adsorbed on CoAPO-5 at the indicated pressures, T=310 K.

The broad underlying absorption band (3180 cm^{-1}) might be caused by a very weak interaction of some of the newly formed P-OH groups involved in hydrogen bonding to pyridine molecules. This explains also the absorption band characteristic for hydrogen bonded pyridine at 1576 cm^{-1}. The assumption that the appearance of free vibrating P-OH is caused by a steric hindrance at higher partial pressures is supported by the fact that at first upon evacuation and consecutive temperature programmed desorption of pyridine (hence a decrease in the amount of adsorbed pyridine) up to 510 K only the absorption bands characteristic for the newly formed free P-OH groups decreased. The characteristic bands of chemisorbed species (protonated and Lewis bonded) did not decrease in intensity before 550 K.

In the course of pyridine sorption/desorption the intensity of the broad i.r. band ascribed to hydrogen bonded hydroxyl groups attached to extra lattice material decreased. This indicates that some of this material was removed due to experimental procedures.

The spectra of CoAPO-5 recorded before and after the experimental procedures with pyridine was identical with the exception of a decrease of the intensity of the broad absorption band (3000-3450 cm^{-1}) attributed to the hydrogen bonded OH groups attached to extra lattice material.

CONCLUSIONS

CoAPO-5 single crystals contain Brønsted acid sites in both 12-membered and 6-membered channel systems. Even if the calcination of crystals is carried out in air and oxygen, the FT-IR spectra contain the characteristic bands of bridging OH groups suggesting that the main part of framework cobalt ions remain as Co^{2+}.

The adsorption of ammonia and pyridine on CoAPO-5 samples gives proof for the existence of both Brønsted and Lewis acid sites. Due to the parallel increase of the intensity of the respective characteristic IR bands we suggest an adsorption mechanism with two probe molecules interacting with one Co-OH-P unit. The first molecule forms a strong coordinative bond to the cobalt ion and cleaves the metal-oxygen bond creating a P-OH group which binds the second base molecule.

Upon adsorption of pyridine at higher loadings two new, relatively free vibrating P-OH groups (ν_{OH} = 3682 and 3590 cm^{-1}) are formed, the sterical hindrance preventing the interaction of a second pyridine molecule with the newly formed OH groups. In opposite to ammonia, pyridine was unable to access all the Brønsted acid sites; extra framework material deposited in the channel system blocks parts of it for larger molecules.

ACKNOWLEDGEMENT

The financial support of the Christian Doppler Laboratories is greatly appreciated.

REFERENCES

1. S.T. Wilson, B.M. Lok, C.A. Messina, T.R. Cannan and E.M. Flanigen, J. Am. Chem. Soc., 104 (1982) 1146.
2. M. Meier and D.H. Olson, Atlas of Zeolite Structure Types, Butterworth-Heinemann, London/Boston/Singapore/Sydney/Toronto/Wellington, 1992.
3. B.M. Lok, C.A. Messina, R.L. Patton, R.T. Gajek, T.R.Cannan and E.M. Flanigen, J. Am. Chem. Soc., 106 (1984) 6092.
4. C.A. Messina, B.M. Lok and E.M. Flanigen, US Patent 4, 544, 143 (1985); S.T. Wilson and E.M. Flanigen, Eur.Pat. Appl., 132,708, (1985).
5. N.J. Tapp, N.B. Milestone and L.J. Wright, J. Chem Soc., Chem. Commun., (1985) 1801.
6. E.M. Flanigen, B. M. Lok, R.L. Patton and S.T. Wilson, Pure and Appl. Chem., 58 (10) (1986) 1351.
7. G. Muller, J. Bodis, G. Eder Mirth, J. Kornatowski and J.A. Lercher, J. Mol. Structure, 410-411 (1997) 173; G. Müller, J. Bodis, J. Kornatowski and J. A. Lercher, Phys.Chem. Chem. Phys. (PCCP), 1 (1999) 571.
8. R.A. Schoonheydt, R. De Vos, J. Pelgrims and H. Leeman, Stud. Surf. Sci. Catal., 49A (1989) 559.

9. C. Montes, M. E. Davis, B. Murray and M. Narayana, J. Phys. Chem., 94 (1990) 6425.
10. B. Kraushaar-Czarnetzki, W.G.M. Hoogervorst, R.R. Andrea, C.A. Emeis and W.H.J. Stork, Stud. Surf. Sci. Catal., 69 (1991) 231.
11. B. Kraushaar-Czarnetzki, W.G.M. Hoogervorst, R.R. Andrea, C.A. Emeis and W.H.J. Stork, J. Chem. Soc., Faraday Trans., 87 (6) (1991) 891.
12. S. Prasad and I. Balakrishnan, Catal. Lett., 11 (1991) 105.
13. K.J. Chao, S.P. Sheu and H.S. Sheu, J. Chem. Soc., Faraday Trans., 88 (19) (1992) 2949.
14. R.B. Borade and A. Clearfield, Appl. Catal. A: General, 80 (1992)59.
15. M.P.J. Peeters, J.H.C. van Hooff, R.A. Sheldon, V.L. Zhobolenko, L.M. Kustov and V.B. Kazansky, in R. Von Balmoos, J.B. Higgins and M.M.J. Treacy (Eds.), Proceedings of 9th International Zeolite Conference, Montreal 1992, Butterworth-Heinemann, Boston, 1993, vol. 1, p. 651.
16. J. Janchen, M.J. Haanepen, M.P.J. Peeters, J.H.M.C. van Wolput, J.P. Wolthuizen and J.H.C. van Hooff, Stud. Surf. Sci. Catal., 84 (1994) 373.
17. L. Marchese, J. Chen and J. M. Thomas, J. Phys. Chem., 98 (1994) 13350.
18. J. Chen and J.M. Thomas, J. Chem. Soc., Chem. Commun., (1994) 603.
19. J. Janchen, M.P.J. Peeters, J.H.M.C. van Wolput, J.P. Wolthuizen and J.H.C van Hooff, J. Chem. Soc., Faraday Trans., 90 (7) (1994) 1033.
20. J.M. Thomas, G.N. Greaves, G. Sankar, P.A. Wright, J. Chen, A.J. Dent and L. Marchese, Angew. Chem. Int. Ed. Engl., 33 (18) (1994) 1871.
21. U. Lohse, R. Bertram, K. Jancke, I. Kurzawski and B. Parlitz, J. Chem. Soc., Faraday Trans., 91 (7) (1995) 1163.
22. V. Zhobolenko, A. Garforth, L. Clark and J. Dwyer, Stud. Surf. Sci. Catal., 97 (1995) 359.
23. L. Marchese, E. Gianotti, N. Damilano, S. Coluccia and J. M. Thomas, Catal. Lett., 37 (1996) 107.
24. L. Marchese, G. Martra, N. Damilano, S. Coluccia and J. M. Thomas, Stud. Surf. Sci. Catal, 107 (1996) 861.
25. I. Girnus, K. Hoffmann, F. Marlow, J. Caro and G. Doring, Microporous Materials 2 (1994) 537.
26. N. Zabukovec, L. Golic, P. Fajdiga and V. Kaucic, Zeolites 15 (1995) 104.
27. J. Kornatowski, M. Rozwadowski, W.H. Baur, R. Golembiewski, Proc. of Symp. “Characterization and Properties of Zeolitic Materials”, Annual Meeting of the Polish Chemical Society, Torun, Sept. 8-11., 1993, M. Rozwadowski, Ed., N. Copernicus University Press, Torun, (1994) 9.
28. L.J. Bellamy, The Infrared Spectra of complex molecules, 2nd ed., Chapman and Hall, London and New York, 1980.
29. L.H. Little, Infrared Spectra of Adsorbed Species, Academic Press, London, 1966.
30. E.H. Teunissen, R.A. van Santen, A.P.J. Jansen, and F.B. van Duijneveldt, J. Phys. Chem., 99 (1993) 203.

STUDIA UNIVERSITATIS BABEŞ-BOLYAI, CHEMIA, XLVII, 1-2, 2002

Dedicated to Professor Ionel Haiduc on the occasion of his 65th birthday

SYNTHESIS AND STRUCTURAL STUDIES OF SOME METAL COORDINATION COMPOUNDS WITH [1,2,4]-TRIAZOLE DERIVATIVE AS LIGAND

L. OPREAN[1], L.DAVID[2], V. ZAHARIA[1], A.COMSA[1], R. OPREAN[1]

[1] *Faculty of Pharmacy, „Iuliu Haţieganu" University of Medicine and Pharmacy, Emil Isac 13, 3400 Cluj-Napoca, Romania*

[2] *Faculty of Physics, „Babeş-Bolyai" University, Kogă Iniceanu 1, 3400 Cluj-Napoca, Romania*

ABSTRACT. In this paper we report the synthesis and characterization of Co(II), Ni(II), Cu(II), Zn(II) complexes with ethyl-α-[(3-phenyl-[1,2,4]-triazol-5-yl)-thio]-acetoacetate as ligand (L). We have initiated studies of the behavior as ligand of named triazole derivative in methanol and dimethylformamide solutions in different metal-ligand molar ratio. Characterization of all complexes was accomplished by elemental analysis, IR, UV-Vis, ESR spectral studies and magnetic measurements. Correlations of the results obtained from physico-chemical investigations afford the assignment of the most probable structural formulae for the metal complexes. The new complexes are of the type $[ML_2(CH_3COO)_2]$, where M = Co(II), Ni(II) or $[CuL(CH_3COO)_2]$ and $[ZnLNH_3]$. The triazole derivative act as bidentate or tridentate ligand, the Co(II) and Ni(II) complexes have a octahedral geometry and the Cu(II) and Zn(II) complexes have a distorted tetrahedral local symmetry around the metals ions.

1. INTRODUCTION

The chemistry of [1,2,4]-triazole derivatives has been intensively investigated owing to their coordinating capability [1,2], their antibacterial and antifungal properties [3,4], anti-inflammatory activity [5] or others pharmacological activity [6,7]. They easily form chelate compounds with transition metals which also have stronger biological activities, so the coordination chemistry of [1,2,4]-triazole derivatives has been the subject of extensive studies. Taking into consideration these aspects, in this paper we report the synthesis and characterization of Co(II), Ni(II), Cu(II), Zn(II) complexes with ethyl-α-[(3-phenyl-[1,2,4]-triazole-5-yl)-thio]-acetoacetate as ligand (L).

2. EXPERIMENTAL

2.1. Materials and measurements

The ligand was prepared as described in the literature [8]. Metals acetates, zinc chloride and solvents were of chemical reagent grade or analytical grade.

The elemental chemical analysis of the complexes was performed by the classical method. The Ni(II) and Cu(II) ions are determined gravimetrically as $Cu(py)_2(SCN)_2$ and $Ni(dmg)_2$, where py = pyridine and dmg = dimethylglioxime.

The IR spectra were recorded with a FTIR Echinox 55 spectrophotometer in the 4000-400 cm^{-1} range, in KBr pellets.

The electronic absorption spectra in the UV-Vis region (190-900 nm) were recorded with a Perkin Elmer Lambda 15 instrument, in a homogenous suspension of nujol, on a filter paper support.

The polycrystalline powder ESR spectra of Cu(II) complex were obtained at room temperature in the X band (9,4 GHz) using a standard JEOL-JES-3B equipment.

Magnetic susceptibility measurements of Co(II), Ni(II) and Cu(II) complexes were recorded using a horizontal Weiss balance. The values of magnetic moments were determined from the plot of $1/\chi_M$ versus T values (70 – 300K).

2.2. PREPARATION OF COMPLEXES

Synthesis of $[CoL_2(CH_3COO)_2]$ (C_1)

10 ml methanolic solution of $Co(CH_3COO)_2 \cdot 4H_2O$ (0.25 g, 1 mmol) was added to 100 ml methanolic solution of the ligand (0.610 g, 2 mmoles) with continuous stirring at 60℃. After one hour, a pink precipitate was formed. The solid was isolated by filtration, washed with methanol and ethylic ether and dried until constant weight (0.462 g complex, η = 46%). (Found: C 49.27%; H 4.2%; N 9.87%; S 8.21; $C_{32}H_{36}N_6O_{10}S_2$ Co requires: C 48.79%; H 4.5%; N 10.67%; S 8.13%; Co 7.49%)

Synthesis of $[NiL_2(CH_3COO)_2]$ (C_2)

5 ml methanolic solution of $Ni(CH_3COO)_2 \cdot 4H_2O$ (0.25 g, 1 mmol) was added to 100 ml methanolic solution of the ligand (0.610 g, 2 mmoles) with continuous stirring at 60℃. After 40 minutes, a yellow greenish precipitate was formed. The solid was isolated by filtration, washed with methanol and ethylic ether and dried until constant weight (0.401 g complex, η = 51%). (Found: C 48.56%; H 4.1%; N 10.3%; S 8.45%; Ni 8.21% $C_{32}H_{36}N_6O_{10}S_2$ Ni requires: C 48.79%; H 4.5%; N 10.67%; S 8.13%; Ni 7.49%)

Synthesis of $[CuL(CH_3COO)_2]$ (C_3)

50 ml ethanolic (EtOH) solution of $Cu(CH_3COO)_2 \cdot H_2O$ (0.200 g, 1 mmol) was added to the solution of 0.305 g of the ligand (1 mmol) in 50 ml methanol with continuous stirring at 60 °C. After 30 minutes, a dark greenish precipitate was formed. The solid was isolated by filtration, washed with methanol and ethylic ether and dried until constant weight (0.379 g complex, η = 78 %) (Found: C 43.92%; H 4.2%; N 9.28%; S 7.21%; Cu 7.13%; $C_{18}H_{21}N_3OSCu$ requires: C 44.35%; H 4.3%; N 8.6%; S 6.5%; Cu 6.5%)

Synthesis of [ZnLNH$_3$](C$_4$)

0.138 g $ZnCl_2$ (1 mmol) was added with continuous stirring to the solution of 0.305 g of the ligand (1 mmol) in 60 ml methanol at 60℃. Then, 2 ml of concentrated ammonia was added. After two hours of stirring, solution was refluxed for 6 hours. The complex, white solid precipitated, was isolated by filtration, washed with methanol and ethylic ether and dried until constant weight (0.162 g complex, η = 42 %). **(**Found: C 46.81%; H 4.65%; N 14.83%; S 8.64; $C_{15}H_{17}N_4O_3SZn$ requires: C 46.63%; H 4.4%; N 14.5%; S 8.29%; Zn 16.8%).

3. RESULTS AND DISCUSSION

The present ligand L has the capacity of chelation (due to the existence of O, N, S donor atoms in the molecule) in relation to the nature of the metal ion and the anion and to the synthesis conditions (metal - ligand molar ratio, solvent, temperature, pH). In methanol and ethanol solutions the ligand presents a keto-enolic tautomerism peculiar to the structure of the acetoacetic ester, as well a ring-chain tautomerism [9]:

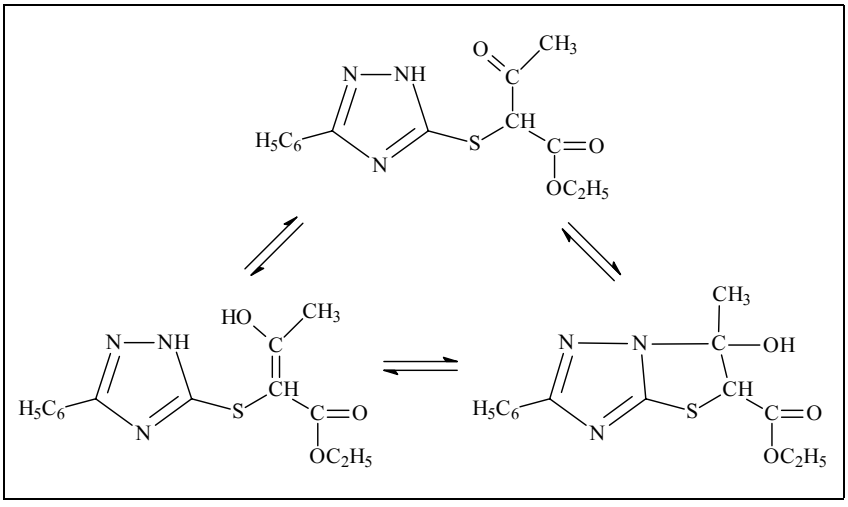

The elemental chemical analyses show that the complexes are of the type $[ML_2(CH_3COO)_2]$, where M = Co(II) and Ni(II), or $[CuL(CH_3COO)_2]$ and $[ZnLNH_3]$. The compounds are microcrystalline powders, sparingly soluble in methanol and ethanol, soluble in warm acetone, dimethyformamide and dimethylsulfoxide. They are air and light stable. The melting point of C_4 is 183 ^oC and the aspect of C_3 shows modifications above 178 ^oC. C_1 and C_2 complexes decompose above 300 ^oC.

3.1. IR Spectra

Information about the coordination mode of the ligands to the metals(II) ions was obtained by comparing the IR spectra of the metallic complexes with the IR spectra of the uncoordinated ligand L (Table 1) and those of the other similar metal complexes [2,4,9-11]. The involvement of the C=O esteric and cetonic group in coordination to the metallic ions is indicated by the shifts (to a lower frequency region, 1700 cm^{-1}, respectively in the 1640-1600 cm^{-1} region) and the shoulder form of the ν(CO) bands in the IR spectra of complexes compared to the ligand. The heterocyclic "C=N" moiety is not involved in the coordination of the metallic ions. This is sustained by the unchanged ν(C=N) triazole vibrations in the IR spectra of Co(II), Ni(II) and Cu(II) complexes compared to the IR spectra of the ligand.

The triazole ring coordinate the Zn(II) ion in C_4 complex through its ^{1}N nitrogen atom after deprotonation, which arises in the lowering of the ν(CN) endocyclic frequency and the increasing of the ν(NN) heterocyclic frequency. The news bands at 3440 cm^{-1} and 1100cm^{-1} in the IR spectra of Zn(II) C_4 complex corresponds to ν(NH) vibrations of the ammonia molecule and, respectively to ν(CO) enol form. These data suggests the enolization of the ligand and the reaction of the enol in deprotonated form [11]. The changes in the IR spectra of Zn(II) complex indicate that the ligand undergoes carbonyl enolization and then coordinate to metal ion through the enolic oxygen atom, triazole ^{1}N nitrogen atom and the ester oxygen atom.

The free acetate ion has characteristic bands at 1580 cm^{-1} (ν_{as}) and 1425 cm^{-1} (ν_s). The coordination of the acetate to the metallic ion is indicated by the complexes new IR bands (1430 - 1495 cm^{-1}).

Table 1

Some IR bands (cm^{-1}) of the ligand and their C_1 – C_4 complexes

Band	L	C_1	C_2	C_3	C_4
ν(NH) ammonia	-	-	-	-	3440 m
ν(CO) esteric	1730 s	1700 b	1700 b	1710 b	1700 b
ν(CO) cetonic	1630 s	1640 b	1640 b	1600 b	1620 b
ν(C=N) triazole	1580 w	1580 w	1580 m	1590 w	1560 w
ν(=NH) triazole	1520 w	1520 w	1520 m	1530 w	1500 w
ν(acetate)	-	1430 m 1490 m	1430 m 1490 m	1445 m 1495 m	-
ν(N-N) triazole	960 m	960 m	960 m	960 w	980 w

w – weak, m – medium, s – strong, b – broad

3.2. Electronic spectra

Information about geometry of complexes was obtained from electronic spectra [12, 13]. The assignment of the bands of the electronic spectra of C_1 – C_3 complexes are set out in Table 2.

Table 2

Electronic spectral data for C_1 – C_3 complexes in nujol suspension (RD)

Complex	ν_{max} [cm^{-1}]	
C_1	ν_1 = 9740	ν_3 = 17880
C_2	ν_1 = 9170	ν_2 = 16950
C_3	ν = 16100	

The reflectance spectrum of Co(II) complex, C_1 shows two bands at 9740 cm^{-1} and 17880 cm^{-1} and a shoulder at about 19260 cm^{-1}. These may arise from $^4T_{2g} \leftarrow {}^4T_{1g}$ (ν_1) and $^4T_{2g} \leftarrow {}^4T_{2g}$ (ν_2) transitions and suggest an octahedral environment around the Co(II) ion.

The RD spectra of Ni(II) complex, C_2, shows two bands at 9170 cm^{-1} and 16950 cm^{-1} assigned to the $^3T_{2g} \leftarrow {}^3A_{2g}$ (ν_1) and $^3T_{1g} \leftarrow {}^3A_{2g}$ (ν_2) transitions of the Ni(II) ion an octahedral stereochemistry. The band corresponding to $^3T_{1g} \leftarrow {}^3A_{2g}$ transition (ν_3 = 19000 – 27000 cm^{-1}) is overlapped with the more intense charge transfer and ligand – to - ligand transitions.

The spectrum of the copper complex displays a broad d – d band at 16100 cm^{-1}. The intense band at 25340 cm^{-1} is assigned to a charge transfer. This data suggest that C_3 has a distorted tetrahedral geometry around the central Cu(II) ion .

3.3. ESR Spectra and magnetic susceptibility measurements

Powder ESR spectrum of the C_3 complex, obtained in the X band at room temperature, contains a broad signal at g = 2.124. The obtained spectra (Fig. 1) are in agreement with a distorted tetrahedral symmetry and a CuO_4 chromophore [12]. For obtaining more information on this system and about the possible interactions between the copper (II) ions, the complex was studies by means of magnetic measurements. The magnetic susceptibility data have been determined for the Co(II) and Ni(II) complexes, the Zn(II) complex are diamagnetic, due to the $3d^{10}$ electronic configuration of Zn(II).

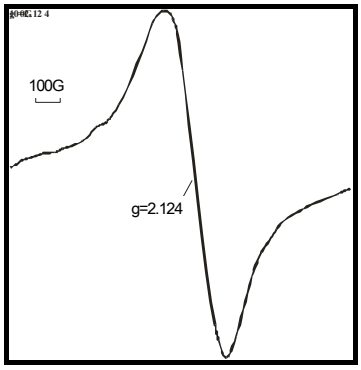

Fig.1 *ESR spectra of theCu(II) C_3 complex*

The magnetic moment of μ_{eff} = 1.94 BM for C_3 indicates the presence of monomeric species and the lack of any interactions between the Cu(II) ions from neighboring molecules (Fig.2) [13].

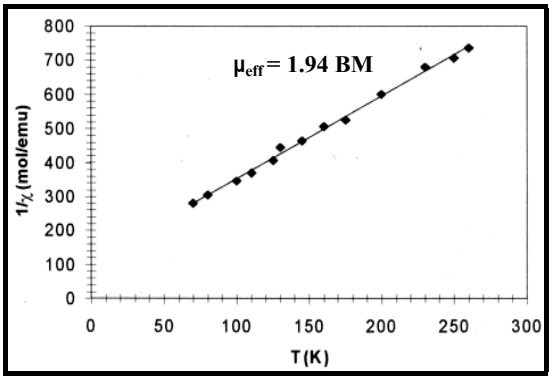

Fig.2 *Temperature dependence of the inverse of the magnetic susceptibility for the C_3 Cu(II) complex*

The magnetic moments obtained for C_1 (μ_{eff} = 4.81 BM) and C_2 (μ_{eff} = 3.20 BM) indicate a octahedral coordination around the Ni(II) ion and, respectively, Co(II) ion [14].

4. CONCLUSION

A correlation of the results obtained from chemical analysis and spectral data afford the assignment of the most probable structural formulae. The ligand L act as tridentate ligand in the Zn(II) complexes, that seams to have a tetrahedral geometry. In the Co(II), Ni(II) and Cu(II) complexes the ligand act as bidentate, with a octahedral geometry around Co(II) and Ni(II) ions and a distorted tetrahedral geometry around the Cu(II) ion. The proposed structures of the complexes are presented in Fig. 4.

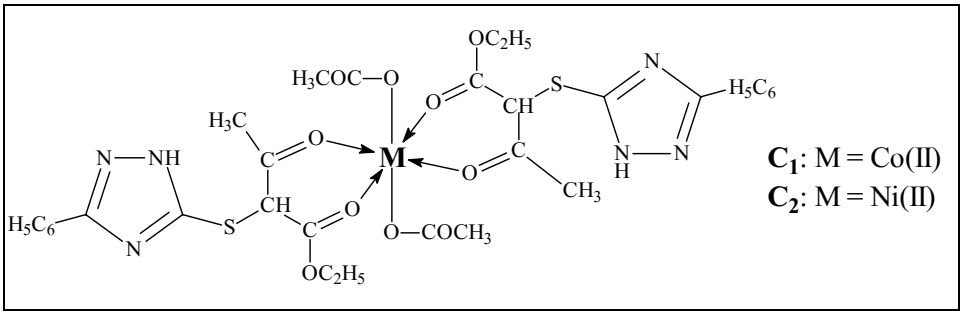

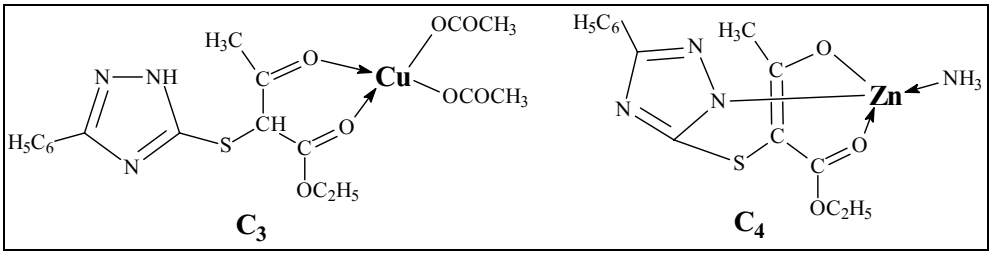

Fig.4 *Proposed structures of the complexes C_1 – C_4*

REFERENCES

1. A.K. Sen, S.N. Dubey and P.J. Squattrito, *Acta Cryst.*, 52, 865 – 868, **1996**.
2. J. G. Haasnoo, *Coord. Chem. Rev.*, **200,** 131 – 185, **2000**.
3. E.Ilhan, N. Ergenc, M. Uzun, D. Kaya, *Arch. Pharm. (Weinheim),* **327,** 825-826, **1994**.
4. A.S. Orabi, M.A. Moneim, E. El–Din Salem and Abd El Fattah *Polish. J. Chem.,* **74,** 1675 – 1683, **1994**.
5. I.H. Hall, R. Simlot, R.A. Izydore, *Arch. Pharm. (Weinheim),***328**, 5 - 10, **1995**.
6. V. Darias, S. Abdala, D. Martin-Herrera, M. Luisa-Tello, S.Vega, *Pharm.,* **53**, 7, 477-481, **1998**.
7. A. Mureşan, M. Palage, *Chimie terapeutică – medicamente utilizate în afecțiuni cardiovasculare,* Ed. Accent, Cluj-Napoca, **2000**.
8. I. Simiti, V. Zaharia, M. Coman, H. Demian, *Arch. Pharm. (Weinheim),* **324,** 49-51, **1991**.
9. I. Simiti, V. Zaharia, H. Demian, and S. Mager, *Studia Univ. Babeş-Bolyai*, XXXIV, **1**, 53-59, **1989**.
10. Nakamoto, *Infrared and Raman Spectra of Inorganic Coordination Compounds*, 3rd, Ed. Wiley, New York **1978**.
11. S. Jayasree and K. K. Aravindakshan, *Polyhedron,* **12**, 1187-1192, **1993**.
12. B.J. Hathaway, in "*Comprehensive Coordination Chemistry*", G. Wilkinson, R. Gillard, J. McCleverty Eds., Pergamon Press, Oxford, **1987**.
13. A.B.P. Lever, in "*Inorganic Electronic Spectroscopy*", Elsevier, New York, **1984**.
14. Drago, S. Russell, *Physical Methods in Chemistry*, W.B. Saunders Company, **1977**.

STUDIA UNIVERSITATIS BABEŞ-BOLYAI, CHEMIA, XLVII, 1-2, 2002

Dedicated to Professor Ionel Haiduc
on the occasion of his 65th birthday

SYNTHESIS AND STEREOCHEMISTRY OF SOME NEW 2,4-SUBSTITUTED-1,3-DIOXANES

ANAMARIA TEREC, LUMINIŢA MUNTEAN, STEFANIA TÖTÖS, NICULINA BOGDAN, CARMEN FLORIAN, D. MĂRGINEANU, S. MAGER and I. GROSU

"Babes-Bolyai" University, Faculty of Chemistry and Chemical Engineering, 11 Arany Janos str., RO-3400, Cluj-Napoca, Romania

ABSTRACT. The stereoselective synthesis and the anancomeric behavior of new 1,3-dioxane derivatives bearing a methyl group at the position 4 and various substituents at position 2 are reported.

INTRODUCTION

The investigations on the stereochemistry of 1,3-dioxane derivatives revealed the high preference of alkyl and aryl groups for the equatorial orientation either at position 2 or at position 4.[1-5] The A-value (free conformational enthalpy) of the same substituent is considerably higher at position 2 than at position 4, but usually in both cases it is high enough to determine the anancomeric behavior of the compound (Table 1, Scheme 1). On the other side due to peculiar rotameric behavior alkyl groups exhibit larger A-value than aromatic substituents (Table 1). It was considered of interest to investigate the conformational and configurational aspects concerning the structure of 1,3-dioxane derivatives bearing a methyl group at position 4 and various aromatic substituents at position 2.

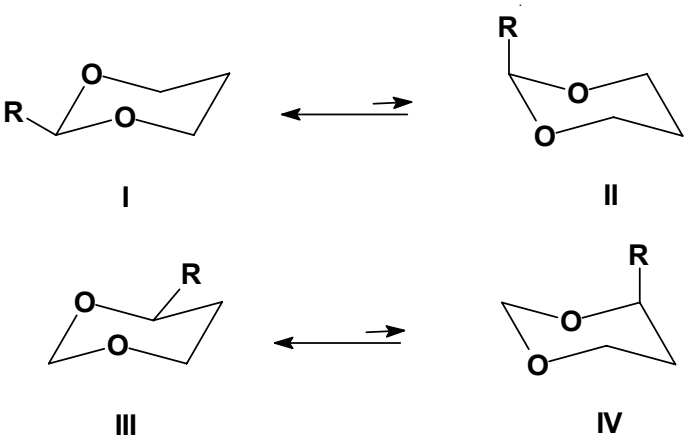

Scheme 1

Table 1.

A-values (kcal/mol) for representative alkyl and aryl groups at positions 2 and 4.

Substituent	A-values			References
	position 2	position 4	ΔA	
Me	3.98	2.90	1.08	6,7
Et	4.04	3.00	1.04	6,8
i-Pr	4.17	3.55	0.62	6,8
Ph	3.12	2.85	0.27	6,8

RESULTS AND DISCUSSIONS

The condensation reaction of racemic 2-methyl-1,3-butanediol with several aromatic aldehyde and ketones leads to 2,4-substituted-1,3-dioxane derivatives (Scheme 2).

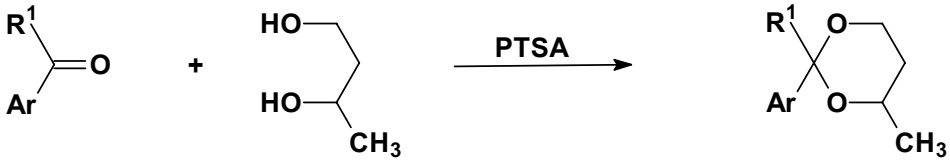

$R^1 = H$	$Ar = C_6H_5$	**1**
$R^1 = H$	$Ar = \beta\text{-}C_{10}H_7$	**2**
$R^1 = CH_3$	$Ar = C_6H_5$	**3**
$R^1 = CH_3$	$Ar = p\text{-}O_2N\text{-}C_6H_4$	**4**
$R^1 = CH_3$	$Ar = o\text{-}O_2N\text{-}C_6H_4$	**5**
$R^1 = CH_3$	$Ar = \alpha\text{-}C_{10}H_7$	**6**
$R^1 = C_2H_5$	$Ar = C_6H_5$	**7**

Scheme 2

All investigated compounds can exhibit *cis* and *trans* isomers (Scheme 3). The acetalisation reaction occurs under equilibrium conditions. *Cis* and *trans* isomers are obtained in ratios reflecting the differences of stability between these isomers. The conformational equilibrium is shifted (as proved by the investigations performed by high resolution NMR spectroscopy and by GC-MS) towards one of the isomers which is more stable and it is obtained as major product being possible its isolation as single compound.

For compounds **1** and **2**, the *cis* isomer can exist in a low energy conformation (V) in which both, the methyl and the aromatic groups at positions 2 and 4 occupy the equatorial positions, while for the *trans* isomer in both conformers (VII and VIII) one of the substituents has to be in an axial orientation and this isomer is of higher energy. Due to the important differences of energy between the configurational isomers of compounds **1** and **2** the acetalisation reaction leads stereoselectively to the *cis* isomer.

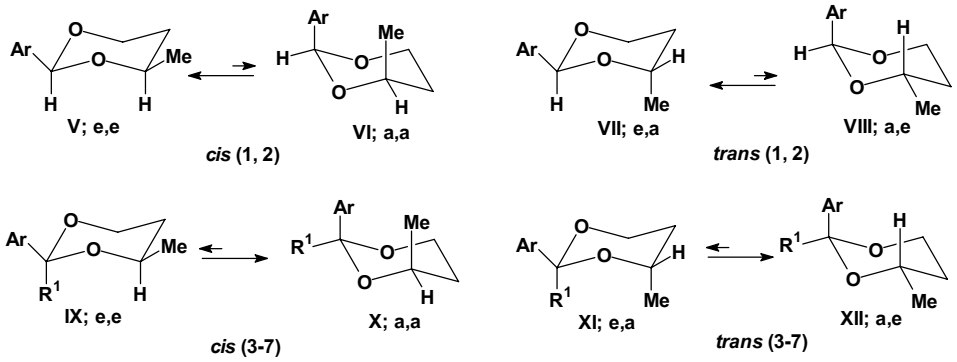

NOTE: Ar is of higest precedence

Scheme 3

The conformational behavior of 1,3-dioxane derivatives bearing alkyl and aryl groups at position 2 was intensively investigated.[9-13] The considerably higher preference of the alkyl group for the equatorial orientation than it can be predicted by comparing the A-values of the two substituents was revealed and the shifting of the conformational equilibrium of 2-alkyl,2-aryl-1,3-dioxanes toward the conformer exhibiting the aromatic substituent in axial orientation was noticed.

For compounds **3**-**7** the *trans* isomer exhibits a conformation (XII) in which the disposition of the substituents is favorable (axial aromatic group at position 2 and equatorial methyl group at position 4), while the conformers of *cis* isomer are of higher energy. Isomers *trans* of compounds **3**-**7** are obtained stereoselectively, the acetalisation reaction undergoing under thermodynamic control.

Compounds **1**-**7** exhibit anancomeric structures the conformational equilibria being shifted towards conformer V (**1** and **2**) or conformer XII (**3**-**7**).

The anancomeric behavior of the compounds determines the recording in the NMR spectra of different signals for the axial and equatorial protons of the 1,3-dioxane ring (Table 2).

Table 2.

NMR data ($CDCl_3$; δ, ppm) for compounds **1**-**7**

Compound	position 6			position 4	
	H-eq	H-ax	$\Delta\delta_{eq-ax}$	H	CH_3
1	3.92	3.48	0.42	3.48	1.10
2	3.99	3.55	0.44	3.56	1.15
3	3.65	3.54	0.09	3.56	1.08
4	3.53	3.17	0.36	3.22	1.03
5	3.53	3.25	0.28	3.32	1.04
6	3.53	3.60	-0.07	3.62	1.14
7	3.65	3.55	0.10	3.58	1.03

As an example the spectrum of compound **5** (Figure 1) exhibit for the axial and equatorial protons at position 6 two different doublet of doublet of doublets a more deshilelded one belonging to the equatorial proton (δ = 3.53 ppm) and another one (δ = 3.25 ppm) overlapped into a doublet of triplets (the geminal and the vicinal axial-axial coupling constants exhibit close values, $^2J_{a\text{-}e} \approx {}^3J_{a\text{-}a}$) pertaining to the axial proton. The axial proton at position 4 exhibit a deshielded doublet of sextets (δ = 3.32 ppm; overlapped doublet of doublet of sextets, in which a coupling constant is two times larger than another one; $^3J_{a\text{-}a} \approx 2x^3J_{H(4)\text{-}Me}$).

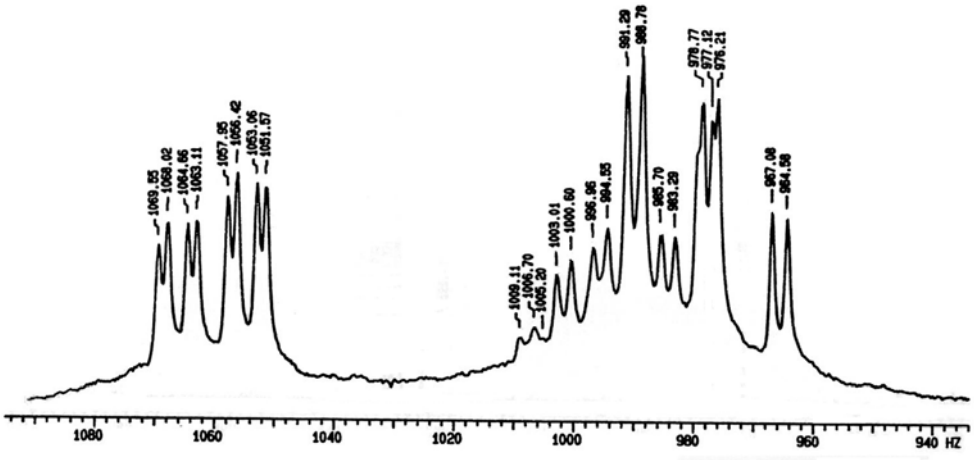

Figure 1. ^{1}H NMR spectrum (fragment) of compound 5.

CONCLUSIONS

The synthesis of 1,3-dioxane derivatives of 1,3-butanediol with aromatic aldehydes leads to *cis* isomers of 2,4-substituted 1,3-dioxane derivatives, while the reaction with alkyl, aryl ketones leads stereoselectively to the isomer exhibiting the reference groups in "*trans*" configuration. The NMR spectra reveal the anancomeric behavior of all investigated compounds and the equatorial preference of the methyl group at position 4.

EXPERIMENTAL

^{1}H and ^{13}C NMR spectra were recorded at *rt*, using $CDCl_3$ as solvent in 5 mm tubes, on a Varian Gemini) Fourier transform NMR spectrometer, equipped with a multinuclear head, operating at 300 MHz for protons and 75 MHz for carbon atoms.

M.ps were measured with Kleinfeld Apotec melting point apparatus and are uncorrected.

2-Phenyl-4-methyl-1,3-dioxane **1**

Liquid, b.p.=79 ℃ (1 mmHg), Yield 75 %. $C_{11}H_{14}O_2$, M=178.23. Found: C, 74.48; H, 8.08; required C, 74.13; H, 7.92. ^{1}H-NMR (C_6D_6) δ 0.84[1H, dddd, $^3J=^3J'$=2.5 Hz; ^2J=12.8 Hz; ^2J=1.4 Hz , 5-H_{eq}], 1.10[3H, d, ^3J=6.2 Hz, 4-CH_3 (eq)], 1.52[1H dddd, $^3J=^3J'$=12.5 Hz; ^2J=12.8 Hz; ^3J=5 Hz , 5-H_{ax}], 3.48[1H, sd* (overlapped ddq), $^3J=^3J'$=12.5 Hz; ^3J=6.2 Hz , 4-H_{ax}; 1H, ddd, ^2J=11.4 Hz; ^3J=12.5 Hz , ^3J=2.5 Hz 6-H_{ax}], 3.92[1H, ddd, ^2J=11.4 Hz; ^3J=5 Hz; ^3J=1.4 Hz 6-H_{eq}], 5.38[1H, s, 2-H_{ax}], 7.20-7.50 [3H aromatic, m, overlapped peaks], 7.70-7.80[2H aromatic, m, overlapped peaks].
^{13}C-NMR (C_6D_6) δ 21.9[4-CH_3 (eq)], 33.1(C^5), 66.9(C^6), 73.2(C^4), 101.3(C^2) 126.7, 128.2, 128.56,140.0 (aromatic carbon atoms).

4-Methyl-2-(β-nafthyl)-1,3-dioxane **2**

Solid, white crystals, m.p.=80-81℃, Yield 58%. $C_{15}H_{16}O_2$, M= 228.29. Found C, 79.16; H, 7.28; required C, 78.92; H, 7.06. ^{1}H-NMR (C_6D_6) δ 0.89 [1H, dddd, $^3J=^3J'$=2.4Hz; ^2J=12.8 Hz; ^3J=1.4 Hz , 5-H_{eq}], 1.15[3H, d, ^3J=6.2 Hz, 4-CH_3 (eq)], 1.58[1H dddd, $^3J=^3J'$=12.4 Hz; ^2J=12.8 Hz; ^3J=5 Hz , 5-H_{ax}], 3.55 [1H, ddd, ^3J=12.6 Hz; ^3J=6.2 Hz; ^3J=2.5 Hz , 6-H_{ax}], 3.56[1H, ddq, ^2J=11.3 Hz; ^3J=12.4 Hz , ^3J=2.5 Hz 4-H_{ax}], 3.99[1H, ddd, ^2J=11.4 Hz; ^3J=5 Hz; ^3J=1.4 Hz 6-H_{eq}], 5.52[1H, s, 2-H_{ax}] 7.10-7.30[2H aromatic,m, overlapped peaks], 7.60-7.70[5H aromatic, m, overlapped peaks], 7.87[1H aromatic, d, ^3J=8.0 Hz], 8.15[1H aromatic, s, α-H]. ^{13}C-NMR (C_6D_6) δ 22.0[4-CH_3 (eq)], 33.2(C^5), 67.0(C^6), 73.3(C^4), 101.6(C^2), 124.9, 126.0, 126.3, 127.5, 127.7, 128.1128.4, 128.7, 133.6, 134.0, 137.4(aromatic carbon atoms).

2-Phenyl-2,4-dimethyl-1,3-dioxane **3**

Solid, white crystals, m.p.=52-53 ℃, Yield 68%. $C_{12}H_{16}O_2$, M= 192.26. Found C, 74.85; H, 8.21; required C, 74.97; H, 8.39. ^{1}H-NMR (C_6D_6) δ 0.73[1H, dddd, $^3J=^3J'$=2.5Hz; ^2J=12.6 Hz; ^3J=1.5 Hz , 5-H_{eq}], 1.08[3H, d, ^3J=6.2 Hz, 4-CH_3 (eq)], 1.53[1H dddd, $^3J=^3J'$=12.4 Hz; ^2J=12.6 Hz; ^3J=5.2 Hz , 5-H_{ax}], 1.6[3H, s, 2-CH_3 (eq)], 3.54 [1H, ddd, ^3J=12.4 Hz; ^3J=6.2 Hz; ^3J=2.5 Hz , 6-H_{ax}], 3.54[1H, ddq, ^2J=11.4 Hz; ^3J=12.4 Hz , ^3J=2.5 Hz 4-H_{ax}], 3.65[1H, ddd, ^2J=11.4 Hz; ^3J=5.2 Hz; ^3J=1.5 Hz 6-H_{eq}], 7.10-7.35 [3H aromatic, m, overlapped peaks], 7.50-7.70[2H aromatic, m, overlapped peaks],.
^{13}C-NMR (C_6D_6) δ 22.1[2-CH_3 (eq)], 33.0[4-CH_3 (eq)], 33.38(C^5), 61.2(C^4), 66.5(C^6), 101.1(C^2) 127.1; 127.6; 128.0; 128.3; 128.9, 142.7 (aromatic carbon atoms).

2,4-dimethyl-2-(p-nitrophenyl)-1,3-dioxane **4**

Solid, white crystals, m.p.=103-104 ℃, Yield 64%. $C_{12}H_{15}NO_4$, M= 237.26. Found C, 60.98; H, 6.15; N, 5.71 required C, 60.75; H, 6.37; N 5.90. ^{1}H-NMR (C_6D_6) δ 0.71[1H, dddd, $^3J=^3J'$=2.45Hz; ^2J=11.6 Hz; ^3J=1.5 Hz, 5-H_{eq}], 1.03[3H, d, ^3J=6.1 Hz, 4-CH_3 (eq)], 1.46[1H dddd, $^3J=^3J'$=12.4 Hz; ^2J=12.9 Hz; ^3J=5.0 Hz,

5-H_{ax}], 1.48[3H, s, 2-CH_3 (eq)] 3.17 [1H, ddd, ^3J=12.4 Hz; ^2J=11.6 Hz; ^3J=2.45 Hz, 6-H_{ax}], 3.22[1H, ddq, ^3J=12.4 Hz , ^3J=6.1 Hz;^3J=2.45 Hz 4-H_{ax}], 3.53[1H, ddd, ^2J=11.6 Hz; ^3J=5.0 Hz; ^3J=1.5 Hz 6-H_{eq}], 7.13[2H, aromatic, d, ^3J=2.83 Hz], 7.85[2H, aromatic, d, ^3J=2.83 Hz].
^{13}C-NMR (C_6D_6) δ 21.9[2-CH_3 (eq)], 32.6[4-CH_3 (eq)], 32.7(C^5), 61.4(C^4), 67.0(C^6), 100.4(C^2) 124.0, 127.8, 128.3, 147.6(aromatic carbon atoms).

2,4-dimethyl-2-(o-nitrophenyl)-1,3-dioxane **5**

Solid, white crystals, m.p.=102-103 ℃, Yield 65%. $C_{12}H_{15}NO_4$, M= 237.26. Found C, 60.58; H, 6.11; N, 5.66 ; required C, 60.75; H, 6.37; N, 5.9. ^{1}H-NMR (C_6D_6) δ 0.57[1H, dddd, ^3J=^3J'=2.5Hz; ^2J=12.8 Hz; ^3J=1.6 Hz , 5-H_{eq}], 1.04[3H, d, ^3J=6.1 Hz, 4-CH_3 (eq)], 1.36[1H dddd, ^3J=^3J'=12.5 Hz; ^2J=12.8 Hz; ^3J=5.2 Hz , 5-H_{ax}], 1.9[3H, s, 2-CH_3 (eq)] 3.25 [1H, ddd, ^3J=12.5 Hz; ^2J=11.5 Hz; ^3J=2.5 Hz , 6-H_{ax}], 3.32[1H, ddq, ^3J=12.5 Hz , ^3J=6.1 Hz;^3J=2.5 Hz 4-H_{ax}], 3.53[1H, ddd, ^2J=11.5 Hz; ^3J=4.9 Hz; ^3J=1.5 Hz 6-H_{eq}], 6.50-7.50[4H aromatic, m, overlapped peaks].^{13}C-NMR (C_6D_6) δ 21.6 [2-CH_3 (eq)], 31.8 [4-CH_3 (eq)], 32.2 (C^5), 61.8 (C^4), 67.9 (C^6), 123.4 (C^2) 127.7, 128.0, 128.3, 128.9, 129.5, 130.5 (aromatic carbon atoms).

2,4-Dimethyl-2-(α-nafthyl)-1,3-dioxane **6**

Solid, white crystals, m.p.=54-56 ℃, Yield 57%. $C_{16}H_{18}O_2$, M= 242.32. Found C, 79.03; H, 7.71; required C, 79.31; H, 7.49. ^{1}H-NMR (C_6D_6) δ 0.77[1H, dddd, ^3J=^3J'=2.5Hz; ^2J=12.6 Hz; ^3J=1.5 Hz , 5-H_{eq}], 1.14[3H, d, ^3J=6.2 Hz, 4-CH_3 (eq)], 1.58[1H dddd, ^3J=^3J'=12.4 Hz; ^2J=12.6 Hz; ^3J=5.2 Hz , 5-H_{ax}], 1.79(3H, s, 2-CH_3), 3.60 [1H, ddd, ^3J=12.4 Hz; ^2J=11.4 Hz; ^3J=2.5 Hz , 6-H_{ax}], 3.62[1H, ddq, ^3J=12.4 Hz , ^3J=6.2 Hz;^3J=2.5 Hz 4-H_{ax}], 3.53[1H, ddd, ^2J=11.4 Hz; ^3J=2.5 Hz; ^3J=1.5 Hz 6-H_{eq}], 7.20-7.80[7H aromatic, m, overlapped peaks]. ^{13}C-NMR (C_6D_6) δ 22.22[2-CH_3 (eq)], 33.09[4-CH_3 (eq)], 33.38(C^5), 61.40(C^4), 66.73(C^6), 101.37(C^2), 124.4, 125.1, 126.3, 126.7, 127.7, 128.4, 129.0, 130.3, 133.4, 140.3.(aromatic carbon atoms).

2-ethyl-2-phenyl-4-methyl-1,3-dioxane **7**

Liquid, b.p.=64-68 ℃ (1 mmHg), Yield 71%. $C_{13}H_{18}O_2$, M=206.29. Found: C, 75.90; H, 9.02; required C, 75.69; H, 8.79. ^{1}H-NMR (C_6D_6) δ 0.73[1H, dddd, ^3J=2.5 Hz; ^2J=12.6 Hz; ^3J=1.4 Hz , 5-H_{eq}], 1.03[3H, t, overlapped peaks ^3J=7.2 Hz(cis), ^3J=7.45 Hz(trans) 2-$\underline{CH_3}$-CH_2-(cis, trans)], 1.08[3H, d, ^3J=6.2 Hz, 4-CH_3 (eq)], 1.97[2H, q, ^3J=7.45 Hz; 2-CH_3-$\underline{CH_2}$-(trans)], 2.43 [2H, q, ^3J=7.2 Hz; 2-CH_3-$\underline{CH_2}$-(cis)], 1.51[1H dddd, ^3J=^3J'=12.4 Hz; ^2J=12.6 Hz; ^3J=5.2 Hz , 5-H_{ax}], 3.55[1H, ddd ^3J=12.4 Hz; ^2J=11.3 Hz; ^3J=2.5 Hz 6-H_{ax}], 3.58[1H, ddq, ^3J=12.4 Hz; ^3J=6.2 Hz; ^3J=2.5 Hz 4-H_{ax}], 3.65[1H, ddd, ^2J=11.3 Hz; ^3J=2.5 Hz; ^3J=1.6 Hz 6-H_{eq}], 7.15-7.30 [3H aromatic, m, overlapped peaks], 7.45-7.55[2H aromatic, m, overlapped peaks].^{13}C-NMR (C_6D_6) δ 7.73[2-CH_3 (ax)], 22.10[2-CH_3 (eq)], 33.25[4-CH_3 (eq)], 38.49(C^5), 61.15(C^4), 66.36(C^6), 102.64(C^2) 127.7, 128.1, 128.6, 132.5, 141.3. (aromatic carbon atoms).

REFERENCES

1. M. J. O. Anteunis, D. Tavernier, F. Borremans, *Heterocycles*, 1976, **4**, 293.
2. F. G. Riddell, "*The Conformational Analysis of Heterocyclic Compounds*", Academic Press, London, 1980, p 74.
3. E. L. Eliel, S. H. Wilen, "*Stereochemistry of Organic Compounds*", Wiley Interscience, New York, 1994, p 745.
4. E. Kleinpeter, *Advances in Heterocyclic Chemistry*, 1998, **69**, 217
5. G. Plé, I. Grosu, S. Mager, M. Darabantu, "*Résonance Magnétique Nucléaire Appliquée à l'Analyse Structurale de Composés Organiques*", Publications de l'Université de Rouen, Rouen, 1999, p 107.
6. F. W. Nader, E. L. Eliel, *J. Am. Chem. Soc*., 1970, **92**, 3050.
7. E. L. Eliel, M. C. Knoeber *J. Am. Chem. Soc*., 1968, **90**, 3444.
8. M. Anteunis, M. Coryn, *Bull. Soc. Chim. Belges*, 1973, 82, 413.
9. S. Mager, I. Grosu, *Studia Univ. "Babes-Bolyai", Chemia*, **1988**, *33*, 47
10. I. Grosu, G. Plé, S. Mager, E. Mesaros, A. Dulau, C. Gego, *Tetrahedron*, 1998, **54**, 2905.
11. I. Grosu, S. Mager, E. Mesaros, G. Plé, *Heterocyclic Commun*., 1998, **4**, 53.
12. I. Grosu, L. Muntean L. Toupet, G. Plé, M. Pop, M. Balog, S. Mager, E. Bogdan, *Monatsh. Chem.,* 2002, **133**, 631.
13. L. Muntean, M. Pop, I Grosu, S. Mager, G. Plé, A. Nan, E. Bogdan, *Rev. Roum. Chim*., 2002, **47**, 121.

STUDIA UNIVERSITATIS BABEŞ-BOLYAI, CHEMIA, XLVII, 1-2, 2002

Dedicated to Professor Ionel Haiduc
on the occasion of his 65th birthday

SYNTHESIS AND STEREOCHEMISTRY OF SOME NEW 1,3-DIOXANE DERIVATIVES OF α, β-UNSATURATED ALDEHYDES

LUMINIŢA MUNTEAN, MIRELA BALOG, CARMEN FLORIAN, ANAMARIA TEREC, I. GROSU, S. MAGER, D.MĂ RGINEANU

"Babes-Bolyai" University, Faculty of Chemistry and Chemical Engineering, 11 Arany Janos str., RO-3400, Cluj-Napoca, Romania

ABSTRACT. The synthesis and the stereochemistry of some new 1,3-dioxane derivatives obtained from α, β-unsaturated aldehydes are discussed. The NMR investigations revealed anancomeric structures and the equatorial orientation of the unsaturated substituent at C^2.

INTRODUCTION

The stereochemistry of 1,3-dioxane derivatives was intensively studied.

The free conformational enthalpy *(A* value) of different groups located at positions 2 and 5 have been measured[1-5] (Table 1).

Table 1.

A values (kcal/mol) for alkyl groups located at positions 2 and 5 of the 1,3-dioxane ring

R	*A*
2-methyl	3.98-4.07
2-ethyl	4.04
2-i-propyl	4.17
2-phenyl	3.12
5-methyl	0.80-0.89

The highest *A* value for the methyl group bound to C^2 shows the capacity of methyl in this position to be a better "holding group" than the methyl located at C^5.

For 1,3-dioxane derivatives bearing alkyl or aryl groups at C^2, the characteristic conformational equilibrium is shifted toward the conformation exhibiting the substituent in equatorial orientation[6-12] (Scheme 2)

It has been considered of interest to study the stereochemistry of some new 1,3-dioxane derivatives obtained from α,β-unsaturated aldehydes and to determine the capacity of the unsaturated substituent at C^2 to be a "holding group" at this position.

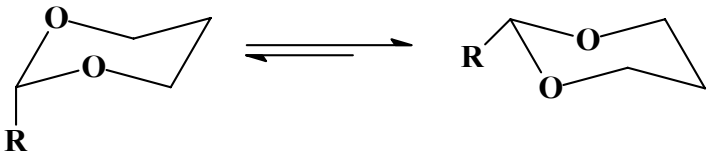

Scheme 2

RESULTS AND DISCUSSIONS

New 1,3-dioxane derivatives have been obtained by the condensation reaction of *trans* α, β- unsaturated aldehydes with the appropiate 1,3-propanediols (Scheme 3).

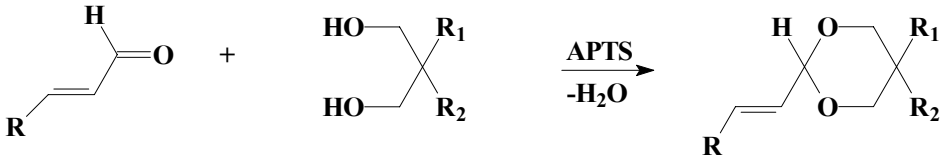

R = CH_3	R_1= H	R_2=CH_3	**1**
R = CH_3	R_1= CH_3	R_2= CH_3	**2**
R = C_6H_5	R_1= H	R_2= H	**3**
R = C_6H_5	R_1= H	R_2= CH_3	**4**
R = C_6H_5	R_1= CH_3	R_2= CH_3	**5**
R = C_6H_5	R_1= $COOC_2H_5$	R_2= $COOC_2H_5$	**6**

Scheme 3

Compounds **2, 3, 5** and **6** exist as unique diastereoisomer. For compounds **1** and **4** two diastereoisomers, *cis* and *trans*, are possible, depending on the relative position of R-CH=CH and R_2 groups located in positions 2 and 5 of the heterocycle (Scheme 4). For the *trans* isomer, the more stable conformer should be **B**, with both R and R_2 substituents in equatorial orientation (R_2 is of highest precedence).

All the investigated compounds exhibit anancomeric structures.

For compounds displaying identical substituents in position 5 (**2, 3, 5** and **6**) the conformational equilibrium is shifted toward the conformer with the substituent at C^2 in equatorial orientation (Scheme 5).

The ^{1}H-NMR spectra of these compounds show different sets of signals for the axial and equatorial protons of the heterocycle and for the protons and carbon atoms of the similar groups located at C^5 (Table 2).

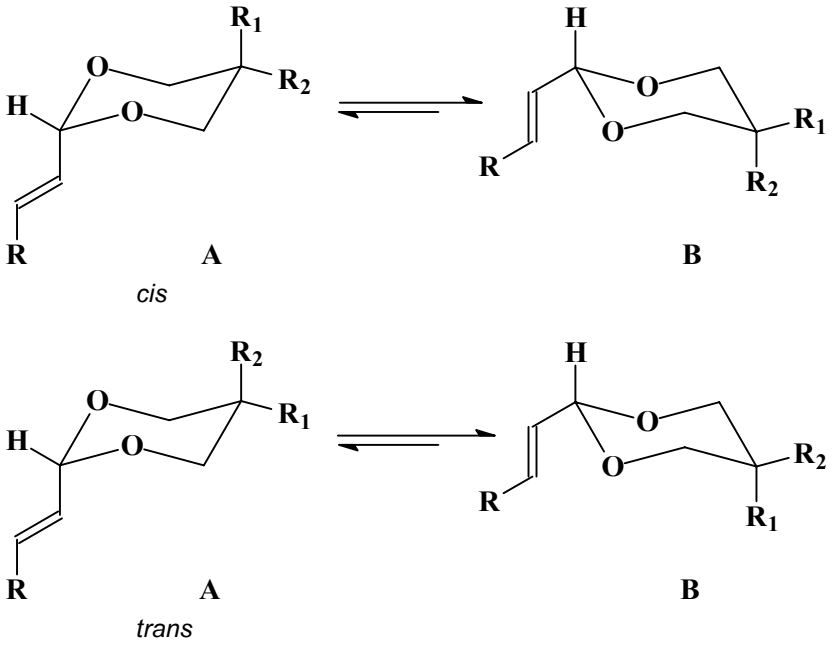

Scheme 4

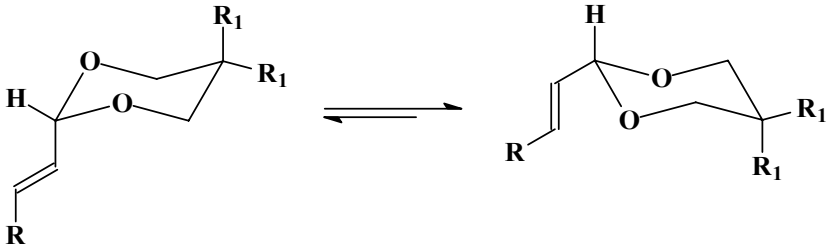

Scheme 5

Table 2.

NMR data (δ, ppm) for the protons of positions 4, 5 and 6 of the 1,3-dioxane ring

Compound	Protons						
	4,6-eq.	4,6-ax.	Δδ	5-CH_3 eq.	5-CH_3 ax.	5-CH_2 eq.	5-CH_2 ax.
1	4.03	3.33	0.70	0.69	-	-	-
2	3.47	3.18	0.29	0.34	1.17	-	-
3	3.87	3.43	0.44	-	-	-	-
4	4.13	3.43	0.70	0.75	-	-	-
5	3.52	3.23	0.29	0.34	1.21	-	-
6	5.06	3.96	1.00	0.80	0.92	3.80	4.05

Compounds **1** and **4** were obtained as a mixture of two diastereoisomers, the *trans* one being the main product. For compound **4** the trans isomer was isolated and characterised.

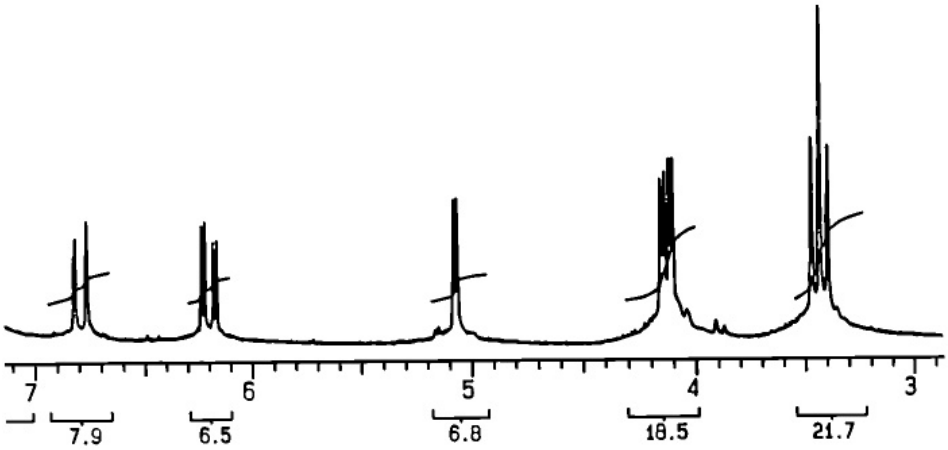

Figure 1

The ^{1}H-NMR spectrum of compound **4** (Figure1) displays different signals for the axial and equatorial protons at positions 4 and 6. The equatorial protons exhibit a doublet of doublet ($\delta_{4,6\text{-eq.}}$= 4.13 ppm, J = 11.5 Hz, J'= 4.6 Hz) due to a large geminal coupling and to a smaller coupling with the axial vicinal proton at position 5. The axial protons exhibit an overlapped doublet of doublet that gives a triplet ($\delta_{4,6\text{-ax.}}$= 3.43 ppm, J = J'= 11.5 Hz) The spectrum also exhibits a doublet for the axial proton located at C^2 ($\delta_{2\text{ -ax.}}$= 5.07 ppm, J = 4.6 Hz), a doublet of doublet for the α-proton of the unsaturated substituent ($\delta_{CH\text{-}\alpha}$ = 6.20 ppm, J = 16.2 Hz, J'= 4.6 Hz) and a doublet for the β-proton ($\delta_{CH\text{-}\beta}$ = 6.79 ppm, J = 16.2 Hz).

The large values of the coupling constants involving the proton at position 5 demonstrate the axial orientation of this proton and the equatorial position of the methyl group at C^5. The values of the chemical shifts of the protons at position 2 and the missing of the characteristic long range coupling with the equatorial protons at positions 4 and 6 show the axial orientation of this proton.

CONCLUSIONS

The NMR investigations of compounds **1-6** bearing an unsaturated substituent at position 2 and one or two methyl groups at the position 5 of the 1,3-dioxanic ring revealed anancomeric structure. The unsaturated substituent located at position 2 prefers the equatorial position, being a good "holding group". In the compounds bearing two different substituents at C^5 (hydrogen and methyl), the methyl group also prefers the equatorial orientation.

EXPERIMENTAL

^{1}H- and ^{13}C-NMR spectra were recorded at room temperature, using $CDCl_3$ or C_6D_6 as solvent, in 5 mm tubes, on a Varian Gemini spectrometer, operating at 300 MHz for protons and at 75 MHz for carbon atoms. Melting points were measured with Electrothermal apparatus and are uncorrected.

New compounds **1-6**, general procedure

Stoechiometric amounts of 1,3-diol and carbonyl compound (0.05 mol) with catalytic amounts of *p*-toluenesulphonic acid (0.05 g) were solved in 100 ml benzene. The mixture were refluxed and the resulted water removed using a Dean-Stark trap. When 80% of the theoretical water was separated, after cooling at room temperature, the catalyst was neutralized (under stirring, 0.5 h) with sodium acetate powder in excess (0.1 g). The reaction mixture was washed twice with 50 ml water. The benzene was removed (after drying with sodium sulphate) and the 1,3-dioxanic compounds were purified by crystallisation or by vacuum distillation.

*5-methyl-2-(1-propenyl]-1,3-dioxane **1**.*
Liquid, b.p.= 50^{0}C (0.1 mm col. Hg). Yield 63.0 %. $C_8H_{14}O_2$, found C 67.39, H 10.02, required C 67.57, H 9.92
^{1}H RMN ($CDCl_3$, δ ppm) 0.69 (1H, d, J = 6.8 Hz, 5-CH_{3eq}), 1.69 (1H, dd, J = 6.6 Hz, J'=1.6 Hz, 2-CH=CH-C$\underline{H}_3$), 2.10 (1H, m, 5-ax), 3.33 (2H, overlapped dd, J = J'= 11.3 Hz, 4,6-H_{ax}), 4.03 (2H, dd, J = 11.3 Hz, J'= 4.6 Hz, 4,6-H_{eq}), 4.81 (1H, d, J = 5.2 Hz, 2-H_{ax}), 5.52 (1H, d, J = 5.2 Hz, J'=1.6 Hz, J''= 15.5 Hz, 2-C$\underline{H}$=CH-CH_3), 5.90 (1H, dq, J = 15.5 Hz, J'= 6.6 Hz, 2-CH=C$\underline{H}$-CH_3)

*5,5-dimethyl-2-(1-propenyl)-1,3-dioxane **2**.*
Liquid, b.p.= 55^{0}C (0.5 mm col.Hg). Yield=58.5 %. $C_9H_{17}O_2$, found C 69.11, H 10.19, required C 69.19, H 10.32
^{1}H RMN (C_6D_6, δ ppm) 0.34 (3H, s, 5-CH_{3eq}), 1.17 (3H, s, 5-CH_{3ax}), 1.50 (3H, ddd, J = .,4 Hz, J'= 1.6 Hz, J"=0.7 Hz, 2-CH=CH-C$\underline{H}_3$), 3.18 (2H, d, J = 11.5 Hz, 4,6-H_{ax}), 3.47 (2H, d, J = 11,5 Hz, 4,6-H_{eq}), 4.68 (1H, dd, J = 4.5 Hz, J'= 0.7 Hz, 2-H_{ax}), 5.78 (1H, m, 2-CH=C$\underline{H}$-CH_3), 5.94 (1H, dq, J = 6.4 Hz, J'= 15.6 Hz, 2-C$\underline{H}$=CH-CH_3), ^{13}C RMN (C_6D_6, δ ppm) 17.64 (2-CH=CH-$\underline{C}H_3$), 21.77 (5-CH_{3eq}), 23.16 (5-CH_{3ax}), 30.00 (C^5), 77.14($C^{4,6}$), 101.37 (C^2), 129.20 (2-$\underline{C}$H=CH-CH_3), 129.60 (2-CH=$\underline{C}$H-CH_3).

*2-[1-(2-phenyl)ethenyl]-1,3-dioxane **3**.*
Liquid, b.p.= 127 – 128^{0}C (0.5 mm col. Hg). Yield 57,0 %. $C_{12}H_{14}O_2$ found C 75.83, H 7.51, required C 75.76, H 7.42
^{1}H RMN (C_6D_6, δ ppm) 0.70 (1H, m, 5-H_{eq}), 1.83 (1H, tq, J $\approx$ J'= 12.5 Hz, J"= 7.6 Hz, 5-H_{ax}), 3.43 (2H, t, J = J =12.5 Hz, 4,6-H_{ax}), 3.87 (2H, dd, J = 12.5 Hz, J'=4.9 Hz, 4,6-H_{eq}), 4.99 (1H, d, J = 3,7 Hz, 2-H_{ax}), 6.38 (1H, dd, J = 2.5 Hz,

J'= 16.2 Hz, 2-C<u>H</u>=CH-C_6H_5), 6.88 (1H, d, J = 16.2 Hz, 2-CH=C<u>H</u>-C_6H_5), 7.0-7.30 (5H, m, aromatic protons) ^{13}C RMN (C_6D_6, δ ppm) 26.11 (C^5), 66.87 ($C^{4,6}$), 101.04(C^2), 127.12, 127.18, 128.10, 128.88, 132.78 (aromatic and vinylic carbon atoms), 136.84 (quaternary aromatic carbon atom).

5-methyl-2-[1-(2-phenyl)ethenyl]-1,3-dioxane ***4****.*
Liquid, b.p.= 140^{0}C (0.1 mm col. Hg). Yield 60.0 %. $C_{13}H_{16}O_2$, found C 76.32, H 7.98, required C 76.44, H 7.90
^{1}H RMN ($CDCl_3$, δ ppm) 0.75 (3H, d, J = 6.5 Hz, 5-CH_{3eq}), 2.18 (1H, m, 5-H_{ax}), 3.43 (2H, overlapped dd, J = J'= 11.5 Hz, 4,6-H_{ax}), 4.13 (2H, dd, J = 11.5 Hz, J'= 4.6 Hz, 4,6-H_{eq}), 6.79 (1H, d, J = 16.2 Hz, 2-CH=C<u>H</u>-C_6H_5), 7.20-7.50 (5H, m, aromatic protons), ^{13}C RMN ($CDCl_3$, δ ppm) 12.43 (5-CH_3), 29.40 (C^5), 73.37 ($C^{4,6}$), 100.47(C^2), 125.59 (2-CH=<u>C</u>H-C_6H_5), 133.40 2-<u>C</u>H=CH-C_6H_5), 126.87, 128.17, 128.56 (aromatic carbon atoms), 136.14 (1 quaternary aromatic carbon atom).

5,5-dimehyl-2-[1-(2-phenyl)ethenyl]-1,3-dioxane ***5***
Solid, m.p.= 55-56^{0}C. Yield 70,0%. $C_{14}H_{18}O_2$, found C 76.89 H 8.25, required C 77.03, H 8.31
^{1}H RMN (C_6D_6, δ ppm) 0.34 (3H, s, 5-CH_{3eq}), 1.21 (3H, s, 5-CH_{3ax}), 3.23 (2H, d, J = 11.1 Hz, 4,6-H_{ax}), 3.52 (2H, dd, J = 11.1 Hz, J'= 1.2 Hz, 4,6-H_{eq}), 4.93 (1H, dd, J = 1.2 Hz, J'= 4,2 Hz, 2-H_{ax}), 6.44 (1H, dd, J = 4.2 Hz, J'=17.2 Hz, 2-C<u>H</u>=CH-C_6H_5), 6.94 (1H, d, J = 17.2 Hz, 2-CH=C<u>H</u>-C_6H_5), 6.98-7.27 (5H, m, aromatic protons) ^{13}C RMN (C_6D_6, δ ppm) 21.75 (5-CH_{3eq}), 23.15 (5-CH_{3ax}), 30.10(C^5), 77.24 ($C^{4,6}$), 101.00 (C^2), 127.15 (2-CH=<u>C</u>H-C_6H_5), 132.98 (2-<u>C</u>H=CH-C_6H_5), 126.98, 128.18, 128.86 (tertiary aromatic carbons), 136.86 (quaternary aromatic carbon atom).

5,5-diethyloxycarbonyl-2-[1-(2-phenyl)ethenyl]-1,3-dioxane ***6***
Liquid, b.p.= 210-211^{0}C (0.5 mm col.Hg). Yield = 61,0%. $C_{18}H_{22}O_6$, found C 64.57, H 6.69, required C 64.66, H 6.63
^{1}H RMN (C_6D_6, δ ppm) 0.80 (3H, t, J = 7.1 Hz, 5-$COOCH_2C$<u>H</u>$_{3eq}$), 0.92 (3H, t, J = 7.1 Hz, 5-$COOCH_2C$<u>H</u>$_{3ax}$), 3.80 (2H, q, J =7.1 Hz, 5-$COOC$<u>H</u>$_2CH_{3eq}$), 3.96 (2H, d, J = 11.5 Hz, 4,6-H_{ax}), 4.05 (2H, q, J = 7.1 Hz, 5-$COOC$<u>H</u>$_2CH_{3ax}$), 4.93 (1H, dd, J = 1.2 Hz, J'= 4.5 Hz, 2-H_{ax}), 5.06 (2H, d, J = 11.5 Hz, 4,6-H_{eq}), 6.27 (1H, dd, J = 4.5 Hz, J'= 16.2 Hz, 2-C<u>H</u>=CH-C_6H_5), 6.80 (1H, d, J = 16.2 Hz, 2-CH=C<u>H</u>-C_6H_5), 7.00-7.30 (5H, m, aromatic protons) ^{13}C RMN (C_6D_6, δ ppm) 13.86 (5-$COOCH_2$<u>C</u>H_{3eq}), 14.00 (5-$COOCH_2$<u>C</u>H_{3ax}), 53.78 (C^5), 61.79 (5-COO<u>C</u>H_2CH_{3eq}), 62.00 (5-COO<u>C</u>H_2CH_{3ax}), 69.64 ($C^{4,6}$), 101.33 (C^2), 125.81 (2-<u>C</u>H=CH-C_6H_5), 133.79 (2-CH=<u>C</u>H-C_6H_5), 127.19, 128.39, 128.83 (tertiary aromatic carbon atoms), 136.46 (quaternary aromatic carbon atom), 167.11 (5-<u>C</u>$OOCH_2CH_{3eq}$), 167.91 (5-<u>C</u>$OOCH_2CH_{3ax}$).

REFERENCES

1. F.W. Nader, E.L. Eliel, *J. Am. Chem. Soc.,* **1970**, 92, 3050
2. K. Pihlaja, S. Luoma, *Acta Chem. Scand*., **1968**, *22*, 2401
3. J. Delmau, J.C. Duplan, M. Davidson, *Tetrahedron*, **1968**, *24*, 3939
4. K. Pihlaja, P. Ayras, *Suomen Kemistilehti*, **1969**, *B42*, 4256
5. F.G. Riddell, M.J.T. Robinson, *Tetrahedron*, **1967**, *23*, 3417
6. E. Kleipeter, *Advanced in Heterocyclic Chemistry*, Academic Press, New-York, **1998**, *69,* 240
7. S. Mager, I. Hopartean, M. Horn, I. Grosu, *Studia Univ. Babes-Bolyai Chemia*, **1979**, *24*, 32
8. S. Mager, I. Grosu, *Studia Univ. Babes-Bolyai Chemia*, **1988**, *33*, 47
9. I. Grosu, S. Mager, G. Ple, N. Ple, A. Toscano, E. Mesaros, R. Martinez, *Liebigs Annalen/Recueil*, **1997**, 2371
10. I. Grosu, S. Mager, L. Toupet, G. Ple, E. Mesaros, A. Mihis, *Acta Chem. Scand.,* **1998**, *52*, 366
11. M. Pop, I. Grosu, G. Ple, S. Mager, L. Muntean, D. Marginean, N. Dinca, *Het. Commun.*, **2002**, *8(1),* 35

STUDIA UNIVERSITATIS BABEŞ-BOLYAI, CHEMIA, XLVII, 1-2, 2002

Dedicated to Professor Ionel Haiduc
on the occasion of his 65th birthday

ELECTRONIC STRUCTURE OF HYPERVALENT ORGANOARSENIC BROMO DERIVATIVES. AN AB INITIO RHF AND DFT-B3LYP INVESTIGATION OF $H_{5-X}AsBr_X$ SYSTEMS

L. SILAGHI-DUMITRESCU and I. SILAGHI-DUMITRESCU*

**Department of Chemistry, Babes-Bolyai University, RO-3400 Cluj-Napoca, Roumania*

ABSTRACT. B3LYP/LACVP* and HF/LACVP* molecular orbital calculations predict trigonal bipyramidal structure for all $H_{5-x}AsBr_x$ (x = 0-5) species and square pyramidal structures for the transition states during the Berry pseudorotation processes. In case of $HAsBr_4$ and H_2AsBr_3 the B3LYP calculations predict lower energies for the isomers with one and respectively two hydrogen atoms in axial positions, in variance with the electronegativity and apicophilicity rules. The homoleptic AsH_5 and $AsBr_5$ are unstable relative to reductive elimination of H_2 or Br_2; H_4AsBr decomposes to AsH_3 and HBr while elimination of Br_2 from H_2AsBr_3 and H_3AsBr_2 is endothermic.

Keywords: arsorane, mixed bromoarsoranes, density functional calculations on stabilities of.

Introduction

Hypervalency is a subject of rather great audience in the last years [1, 2] and in particular, pentacoordinated XY_5 systems have been intensively studied. In this line, hypervalent compounds of phosphorus and arsenic with first to third row substituents have been the subjects of considerable attention in numerous experimental and theoretical approaches. Relatively less is known about arsenic (V) bromine derivatives [3-10] and this paper is devoted to the investigation of electronic structure and energetics of various bromo-substituted arsorane $H_{5-x}AsBr_x$ systems. To have the complete series treated at the same level, the parent AsH_5 molecule has been also considered. The main points addressed here are: a) the geometry of these molecules; b) the geometry and energy of the transition states relating different trigonal bipyramidal (TBP) structures and c) the thermodynamic stability of $H_{5-x}AsBr_x$ toward decomposition to arsenic(III) derivatives.

Computational details

Ab initio molecular orbital calculations have been carried out at the hybrid DFT B3LYP level that uses the Becke's 3-parameter exchange functional [11] with LYP (Lee-Wang-Parr) [12] correlation functionals including both local and nonlocal terms. The LACVP* Los Alamos basis functions used throughout

these calculations include also the Hay-Wadt pseudopotentials [13] for the heavy elements. The DFT calculations have been paralleled by pure HF/LACVP* calculations.

Full geometry optimizations on all TBP based isomers of $H_{5-x}AsBr_x$ and their transition states leading to axial-equatorial ligand exchanges have been carried out until the default convergence criteria from Spartan were achieved (energy convergence criterion = 10^{-6} hartrees; maximum gradient = $4.5x10^{-4}$ hartrees/bohr and maximum displacement criterion = $1.8x10^{-3}$ Å). The nature of all optima has been checked by frequency calculations. All calculations have been done by using the Spartan'02 package [14] run under Windows on a 550 MHz PC.

Results and Discussion

a. Possible structures of $H_{5-x}AsBr_x$

The total energies together with the zero point energies (ZPE) and the ZPE corrected energies of all possible TBP $H_{5-x}AsBr_x$ systems are given in Table 1 and Figure 1 shows the geometry of these species.

Table 1

Energy data on the $H_{5-x}AsBr_x$ TBP systems. The number of axial (ax) and equatorial (eq) bromine atoms are indicated in the first column.

Molecule	Lowest Frequency (cm^{-1})	Total energy (a.u.)	Zero point energy (a.u.)	Zero point corrected energy (a.u)	Method
$AsBr_5$	52.23	-70.6969240	0.0051680	-70.6917560	HF
	43.22	-72.0529615	0.0044923	-72.0484692	B3LYP
$HAsBr_4$ 1ax_3eq	56.51	-58.3260179	0.0142930	-58.3117249	HF
	49.93	-59.4651879	0.0127950	-59.4523929	B3LYP
$HAsBr_4$ 2ax_2eq	56.40	-58.3270696	0.0136093	-58.3134603	HF
	43.14	-59.4636066	0.0121034	-59.4515032	B3LYP
H_2AsBr_3 2ax_1eq	101.07	-45.9564312	0.0220650	-45.9343662	HF
	87.69	-46.8735778	0.0197526	-46.8538252	B3LYP
H_2AsBr_3 3eq	54.04	-45.9530974	0.0215199	-45.9315775	HF
	51.47	-46.8743380	0.0196761	-46.8546619	B3LYP
H_2AsBr_3 1ax_2eq	-*	-	-	-	HF
	-	-	-	-	B3LYP
H_3AsBr_2 3ax	123.87	-33.5845574	0.0301987	-33.5543587	HF
	104.90	-34.2840806	0.0272489	-34.2568317	B3LYP
H_3AsBr_2 1ax_1eq	130.75	-33.5596029	0.0302242	-33.5293787	HF
	121.57	-34.2652664	0.0274752	-34.2377912	B3LYP
H_4AsBr 1ax	167.22	-21.1789109	0.0376838	-21.1412271	HF
	183.98	-21.6664610	0.0341508	-21.6323102	B3LYP
H_4AsBr 1eq	268.97i	-21.1613565	0.0367580	-21.1245985	HF
	195.52i	-21.6572840	0.0338225	-21.6234615	B3LYP
H_5As	568.30	-8.7522733	0.0423085	-8.7099648	HF
	454.47	-9.0336284	0.0388950	-8.9947334	B3LYP

*Isomer not identified during the optimization.

Similar data for the square pyramid (SP) structures are collected in Table 2 and Figure 2. Table 3 contains the barriers to Berry pseudorotation involving the TBP-SP-TBP pathways.

Table 2

Transition state to Berry pseudorotation energies of $H_{5-x}AsBr_x$ systems.

Molecule	Imaginary Frequency cm^{-1}	Total energy (a.u.)	Zero point energy (a.u.)	Corrected total energy (a.u.)	Method
AsBr5	39.87I	-70.6906822	0.0050947	-70.6855875	HF
	28.60I	-72.0489773	0.0044270	-72.0445503	B3LYP
$HAsBr_4$	43.01I	-58.3178037	0.0139424	-58.3038613	HF
4_basal	25.23I	-59.4588934	0.0124890	-59.4464044	B3LYP
$HAsBr_4$	57.64I	-58.3215771	0.0137527	-58.3078244	HF
1_apical_3basal	47.73I	-59.4608190	0.0121974	-59.4486216	B3LYP
H_2AsBr_3	55.46I	-45.9513952	0.0216825	-45.9297127	HF
1_apical_2basal_ opposed	54.49I	-46.8713502	0.0195789	-46.8517713	B3LYP
H_2AsBr_3	43.33I	-45.9430053	0.0224363	-45.920569	HF
3basal	-	-	-	-	B3LYP
H_2AsBr_3	136.65i	-45.9352653	0.0218148	-45.9134505	HF
1apical_2basal_ vicinal	102.19i	-46.8584609	0.0119829	-46.846478	B3LYP
H_3AsBr_2	273.33i	-33.5546274	0.0298991	-33.5247283	HF
2basal_vicinal	170.75i	-34.2633451	0.0272713	-34.2360738	B3LYP
H_3AsBr_2	228.51i	-33.5497591	0.0292154	-33.5205437	HF
1apical_1basal	259.53i	-34.2556442	0.0265063	-34.2291379	B3LYP
H_4AsBr	266.86i	-21.1613628	0.0367468	-21.1246160	HF
1basal	194.66i	-21.6572838	0.0338225	-21.6234613	B3LYP
H_4AsBr	793.85i	-21.1358041	0.0349397	-21.1008644	HF
1apical	842.93i	-21.6273963	0.0321094	-21.5952869	B3LYP
H_5As	408.41i	-8.7483906	0.0416870	-8.7067036	HF
	269.09i	-9.0314574	0.0384169	-8.9930405	B3LYP

There is so far no experimental evidence for the existence of AsH_5, this system has been however the subject of a few theoretical (ab initio) investigations [6, 15, 16]. In accordance with simple VSEPR theory, all these calculations along with those reported here predict that the TBP structure is a minimum on the potential energy surface. The other possible geometry-square pyramid proofs to be a transition state (saddle point) separated by 1.06 kcal/mol (B3LYP) or 2.05 kcal/mol (HF) from the TBP state. These barriers are close to that reported by Trinquier by ab initio valence only SCF+CI calculation: 2.5 kcal/mol) [6] and Moc (2.1 kcal/mol MP4/ECP; 2.2 kcal/mol MP2/AE) [15].

Table 3.

Barriers to Berry pseudorotation in $H_{5-x}AsBr_x$ systems.(kcal/mol)

Molecule	Isomer	Transition state description	Barrier	Method
AsBr5			3.87 2.46	HF B3LYP
$HAsBr_4$	2ax_2eq	4_basal	6.02 3.42	HF B3LYP
	1ax_3eq	1_apical_3_basal	2.45 2.37	HF B3LYP
H_2AsBr_3	2ax_1eq	1_apical_2_basal_vicinal	2.92 1.29	HF B3LYP
	2ax_1eq	3_basal	8.63 -	HF B3LYP
H_3AsBr_2	1ax_1eq	2_basal_vicinal	2.92 1.08	HF B3LYP
	1ax_1eq	1_apical_1_basal	5.54 5.43	HF B3LYP
H_4AsBr	1ax	1_basal	10.42 5.55	HF B3LYP
	1eq	1_apical	14.89 17.68	HF B3LYP
H_5As			2.05 1.06	HF B3LYP

To the best of our knowledge, the trigonal bypiramidal isomers of $H_{5-x}AsBr_x$ (x = 1-4) have not been studied by any theoretical methods and no experimental data on these systems are known.

The hydrogen bond and correlation effect on the binding energies in $H_3As…HBr$ ensemble and in other $H_3E…HX$ complexes was investigated by Hincliffe [17] and Alabart [18].

Optimisations of TBP H_4AsBr, starting from two classes of initial geometries (axial bromine or equatorial bromine) show that bromine prefers the axial position (in agreement with the greater apicophilicity of bromine [19]. The alternative structure with the bromine in the equatorial position is in fact a transition state characterised by one imaginary frequency (see Table 1).

For H_3AsBr_2 two relative arrangement of bromine atoms are possible within a TBP structure: a) with axial and equatorial bromine (1ax1eq in Figure 1) and b) with the Br atoms in axial positions (2ax in Figure 1). At both level of calculations, the (1ax1eq) isomer is found at higher energy (B3LYP: +11.94 kcal/mol, HF: +15.67 kcal/mol). There are two known examples of TBP R_3AsBr_2 systems with bromine in axial positions R = Ph [4, 9]) and R = neo-pentyl [10]. It is interesting to note that R_3AsBr_2 does not adopt always a TBP type structure.

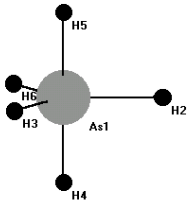

AsH_5

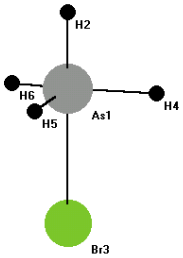

H_4AsBr (ax)

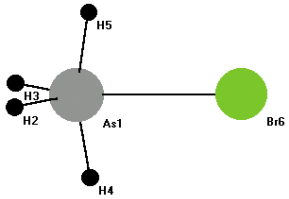

H_4AsBr (eq)

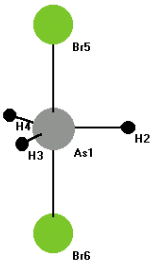

H_3AsBr_2 (2ax)

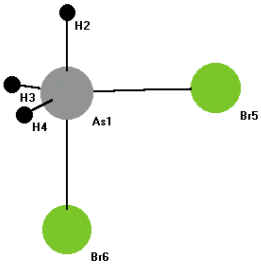

H_3AsBr_2 (1ax1eq)

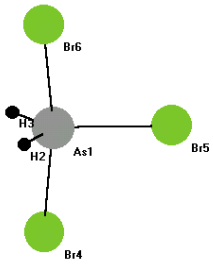

H_2AsBr_3 (2ax1eq)

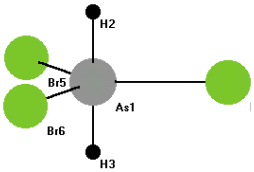

H_2AsBr_3 (3eq)

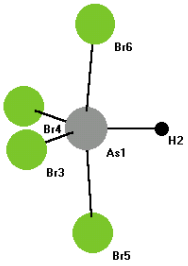

$HAsBr_4$ (2ax2eq)

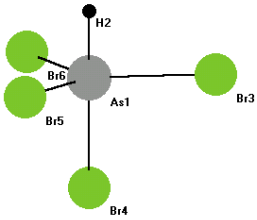

$HAsBr_4$ (1ax3eq)

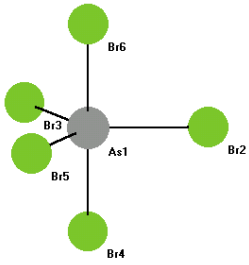

$AsBr_5$

Figure 1. The HF/LACVP* and B3LYP/LACVP* calculated structures of $H_{5-x}AsBr_x$

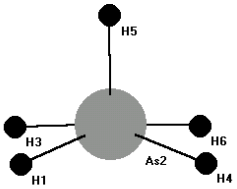

AsH_5

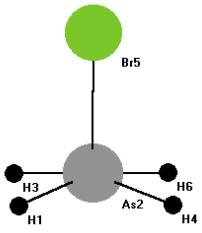

H_4AsBr (1a)

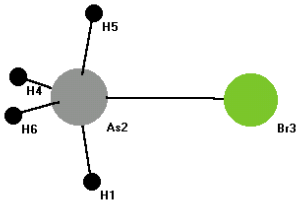

H_4AsBr (1b)

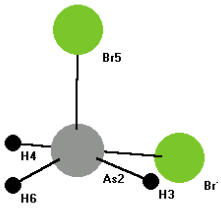

H_3AsBr_2 (1b1a)

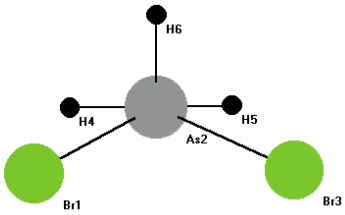

H_3AsBr_2 (2bv)

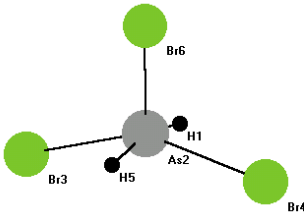

H_2AsBr_3 (2bo1a)

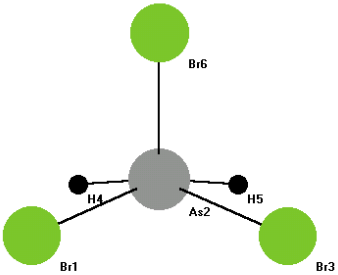

H_2AsBr_3 (2bv1a)

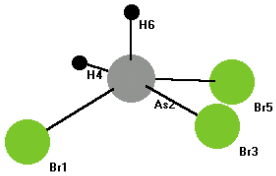

H_2AsBr_3 (3b)

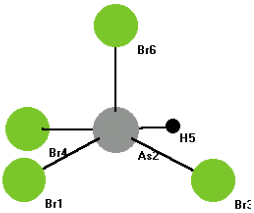

$HAsBr_4$ (3b1a)

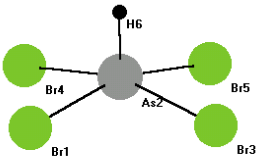

$HAsBr_4$ (4b)

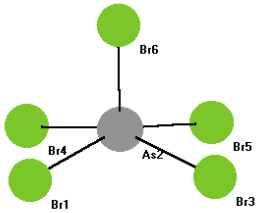

$AsBr_5$

Figure 2. Transition state structures for the Berry pseudorotations of $H_{5-x}AsBr_x$ systems

Thus, the crystal structure of Me_3AsBr_2 is based on an ER_3-X-X tetrahedral arrangement around the arsenic atom [4], which can be also interpreted as an arsonium $ER_3X^+X^-$ salt [5]. This flexibility toward different types of arrangements around the arsenic atoms might be related to the small barrier to pseudorotation for the 1ax1eq isomer (B3LYP 1.08 kcal/mol, HF 2.92 kcal/mol).

H_2AsBr_3 might have the bromine atoms in three different arrangements: all equatorial (3eq in Figure 1), two in equatorial positions (1ax2eq not included in Figure 1) and two in axial positions (2ax1eq in Figure 1). All attempts to optimise the structure of 1ax2eq ended either with 3eq or with 2ax1eq (depending on the exact starting geometry), so we could not locate at this level of calculations a genuine 1ax2eq isomer.

At the B3LYP level 2ax1eq is higher by 0.52 kcal/mol while at the HF, the order is reversed (3eq higher by 1.74 kcal/mol). Since the barrier to pseudorotation converting the 2ax1eq isomer to the 3eq isomer is relatively small (B3LYP1.29 kcal/mol; HF 2.92 kcal/mol, see Table 3) this species is rather flexible.

There is only one known representative of the R_2AsBr_3 class (R = Ph) and this has a TBP structure with two bromine atoms in axial positions [8].

For $HAsBr_4$ the B3LYP results again predict that the isomer with two axial bromine atoms (2ax2eq) is higher in energy by 0.57 kcal/mol (B3LYP) than the 1ax3eq isomer. Such discrepancies between the prediction based on electronegativity rules or apicophilicity of the substituents have been discussed earlier [20]. Thus, higher-level calculations are required, in order to confirm this deviation from the order predicted by the apicophilicity of bromine.

According to the present calculations and in agreement with previous reported results [3] $AsBr_5$ adopts a TBP structure while the SP structure is a transition state during the Berry pseudorotation process. The barrier to pseudorotation is estimated to 2.46kcal/mol (B3LYP).

b. Thermodynamic considerations. Table 4 lists the calculated enthalpies of the decomposition reactions of all $H_{5-x}AsBr_x$.

Table 4.

Calculated Enthalpies of Decomposition Reactions of $H_{5-x}AsBr_x$

Molecule	ΔH (Kcal/mol)	
$AsBr5 = AsBr_3+Br_3$	-15.15 -8.65	HF B3LYP
$HAsBr_4 = AsBr_3 + HBr$ 1ax_3eq	-32.62 -26.75	HF B3LYP
$HAsBr_4 = AsBr3 + HBr$ 2ax_2eq	-31.53 -27.30	HF B3LYP
$HAsBr_4 = HAsBr_2 + Br_2$ 1ax_3eq	-3.46 3.84	HF B3LYP

Molecule	ΔH (Kcal/mol)	
$HAsBr_4 = HAsBr_2 + Br_2$	-2.38	HF
2ax_2eq	3.28	B3LYP
$H_2AsBr_3 = AsBr_3 + H_2$	-22.68	HF
2ax_1eq	-32.09	B3LYP
$H_2AsBr_3 = AsBr_3 + H_2$	-24.43	HF
3eq	-31.56	B3LYP
$H_2AsBr_3 = HAsBr_2 + HBr$	-19.28	HF
2ax_1eq	-15.80	B3LYP
$H_2AsBr_3 = HAsBr_2 + HBr$	-21.03	HF
3eq	-15.08	B3LYP
$H_2AsBr_3 = H_2AsBr + Br_2$	10.08	HF
2ax_1eq	12.71	B3LYP
$H_2AsBr_3 = H_2AsBr + Br_2$	8.32	HF
3eq	13.24	B3LYP
$H_3AsBr_2 = HAsBr_2 + H_2$	-10.98	HF
2ax	-20.16	B3LYP
$H_3AsBr_2 = HAsBr_2 + H_2$	-26.65	HF
1ax_1eq	-32.11	B3LYP
$H_3AsBr_2 = H_2AsBr + HBr$	-7.37	HF
2ax	-5.96	B3LYP
$H_3AsBr_2 = H_2AsBr + HBr$	-23.04	HF
1ax_1eq	-17.90	B3LYP
$H_3AsBr_2 = H_3As + Br_2$	21.48	HF
2ax	19.61	B3LYP
$H_3AsBr_2 = H_3As + Br_2$	5.81	HF
1ax_1eq	7.65	B3LYP
$H_4AsBr = H_3As + HBr$	-16.76	HF
ax	-16.33	B3LYP
$H_4AsBr = H_2AsBr + H_2$	-19.88	HF
ax	-27.58	B3LYP
$H_5As = H_3As + H_2$	-40.64	HF
	-46.16	B3LYP
	-58.6	Ref. 6

$AsBr_5$ is thermodynamically unstable relative to $AsBr_3 + Br_2$ like is the chlorine analog [21]. The instability of AsH_5 relative to AsH_3 and H_2 is even more accentuated. Note also that the elimination of HBr or H_2 from $H_{5-x}AsBr_x$ (x = 1-4) is constantly highly exothermic while decomposition to Br_2 (x = 2-4) and the corresponding As(III) species is endothermic. These data suggest, that the simultaneous presence of hydrogen and bromine induces a relative stabilization of the As(V) derivatives compared to the homoleptic AsH_5 or $AsBr_5$. Thus, it might be speculated that even the existence of the above-cited R_2AsBr_3 and R_3AsBr_2 derivatives is a consequence of this kind of stabilization.

Acknowledgement. This paper was supported by grant CNCSIS no. 274C/2002.

REFERENCES

1. Kin-yo Akiba and (editor), *Chemistry of Hypervalent Compounds*. 1998: Wiley-VCH.
2. G.P. Kostikova, D.V. Korolkov, and Y.P. Kostikov*, Uspekhi Khimii*, **1997***, 66,* 307.
3. J. Breidung, and W. Thiel,. *J. Comput. Chem.*, **1992**. *13,* 165.
4. N. Bricklebank, S.M. Godfrey, H.P.Lane, C.A. McAuliffe, R.G.Pritchard, J.-M. Moreno, *J.Chem.Soc., Dalton Trans.*, **1995**, 3873.
5. H.C. Wang, E.J. Gaffney, C.R. Dybowski, and A.L. Rheingold, J.Organomet.Chem., **1996**, ***512***, 21.
6. G. Trinquier, J-P. Daudey, G.Caruana, and Y. Madaule, *J.Amer.Chem.Soc.*, **1984**, *106*, 4794.
7. D.J. Sutor, and F.R. Harper, *Acta Crystallogr.*, **1959**, *12*, 585.
8. L. Silaghi-Dumitrescu, I. Silaghi-Dumitrescu, R.Silaghi-Dumitrescu, I. Haiduc, A.J. Blake, and D.B. Sowerby, *Rev.Soc.Quim.Mex.*, **2000**, *44*, 134.
9. B. Neumuller, S. Chitsaz, and K. Dehnicke, *Z.Naturforsch.*, **1999**, *B54*, 1611.
10. J.C. Pazik, and C. George, *Organometallics*, **1989**, *8*, 482.
11. A.D. Becke, *J.Chem.Phys.*, **1993**, *98*, 5648.
12. C. Lee, W. Yang, and R.G.Parr, *Phys.Rev.*, **1988**, *37B*, 785.
13. P.J. Hay, and W.K. Wadt, *J.Chem.Phys.*, 1985, *82*, 299.
14. Spartan'02, Wavefunction, Inc., Irvine, C.A.
15. J. Moc, and K. Morokuma, *J.Amer.Chem.Soc.*, **1995**, *117*, 11790.
16. J. Breidung, W. Thiel, and A. Komornicki, *Inorg.Chem.*, **1991** *30*, 1067.
17. A.Hinchliffe, *J.Mol.Struct. (THEOCHEM)*, **1985**, *22*, 201.
18. J.R. Alabart, and R. Caballol, *Chem.Phys. Lett.*, **1987**, *141*, 334.
19. J.A.Deiters, R.R. Holmes, and J.M. Holmes, *J.Amer.Chem.Soc.*, **1988**, *110*, 7672.
20. H. Oberhammer, J. Grobe, and D. Le Van, Inorg. Chem., **1982**, *21*, 275.
21. K. Seppelt, *Angew.Chem. Int.Ed.Engl.*, **1976**, *15*, 377.

Dedicated to Professor Ionel Haiduc on the occasion of his 65th birthday

RECENZII - BOOK REVIEWS

Planar Chromatography A Retrospective View for the Third Millennium, Ed. Sz. Nyiredy, Springer, Budapest, 2001, 614 p.

A book has a monographic character and the material is systematized on domains as follow: 1. A contemporary view of the kinetic theory of planar chromatography (C.F. Poole); 2. Adsorbents in thin-layer chromatography (T. Kowalska); 3. Optimization of the mobile phase (A.M. Siouffi and M. Abbou); 4. Modern TLC chambers (T.H. Dzido); 5. The different modes of development (B. Szabady); 6. Multidimensional planar chromatography (Sz. Nyiredy); 7. Modern sample application methods (T. Omori); 8. Overpressured-layer chromatography (optimum performance laminar chromatography) (OPLC) (E. Tyihak and E. Mincsovics); 9. Rotation planar chromatography (Sz. Nyiredy); 10. Electroosmotically driven TLC (J.Z. Rozylo and I. Malinowska); 11. Displacement chromatography and its application using a planar stationary phase (H. Kalasz and M. Báthori); 12. Planar chromatography and densitometry (W. Dammertz and E. Reich); 13. Planar chromatography and IR (I.O.C. Rager and K.-A. Kovar); 14. Planar chromatography with mass spectrometric detection (K.L. Busch); 15. Practical aspects of ion-pair thin-layer chromatography (I.D. Wilson); 16. Application of planar chromatography and digital autoradiography in metabolism research (I. Kleibovich); 17. Photoacoustics and photothermy in planar chromatography (I. Vovk and G. Močnik); 18. Validation of planar chromatographic procedures (K. Ferenczi-Fodor, Z. Végh, A. Nagy-Turák, B. Renger and M. Zeller); 19. Quantitative analysis in TLC and HPTLC (S. Ebel); 20. Possibilities of preparative planar chormatography (Sz. Nyiredy); 21. Pre- and post-chromatographic derivatization (G. Cîmpan); 22. Documentation in thin-layer chromatography (E. Hahn-Deinstrop); 23. Image analysis (I. Vovk, M. Prošek and R.E. Kaiser); 24. Detection of microbiologically active compounds (L. Botz, S. Nagy and B. Kocsis); 25. Chiral separations by TLC (L. Lepri, M. Del Bubba and A. Cincinelli); 26. Planar chromatography in medicinal plant research (Sz. Nyiredy and K. Glowniak); 27. Thin-layer chromatography in environmental analysis (J. Sherma); 28. Planar chromatography in pharmaceutical practice (K. Ferenczi-Fodor, Z. Végh and B. Renger); 29. Future possibilities and dreams of planar liquid chromatography (R.E. Kaiser).

Each chapter contains personal research results obtained by the authors with their teams from institutes or research groups, which have as fundamental concern the reported issue.

Theoretical and practical aspects of thin-layer chromatography (TLC) are presented in this book.

More than 1700 literature references were quoted.

The book is very interesting for liquid chromatography specialists as well as researchers, which use TLC.

C.P. I Dr. C. MĂ RUȚOIU